INDUCTION HEATING
Coil and System Design

P. G. SIMPSON

McGRAW-HILL

INDUCTION HEATING
Coil and System Design

P. G. SIMPSON
B.Sc., A.M.A.I.E.E., A.M.I.E.E.

McGRAW-HILL BOOK COMPANY, INC.
New York Toronto London
1960

INDUCTION HEATING

 Library of Congress Catalog Card Number: 60-6983

57421

PREFACE

Induction heating has been utilized successfully for a number of years as an extremely useful production tool, and can now be considered to have graduated from the various arts and sciences on which it is based into a practical engineering subject. Therefore, although fundamental electromagnetic and heat-flow theory are discussed briefly in this book, they are mentioned only as a basis for formulas from which practical designs can be developed.

Basic induction heating theory is covered by existing literature, but little mention is made of systematic coil and system design. The main purpose of this book is to outline a design procedure for coils, power systems, and generating equipment intended for typical applications. Stress is placed on economy as well as on technical conditions. Design engineers should always bear in mind that equipment meeting ideal requirements often does not meet the budget of a potential customer.

While induction heating users should be gradually brought to see the desirability of higher-quality equipment, the basic fact remains that these users consider low initial and running costs as important as quality.

Other types of heating often compete with induction heating, particularly industrial furnaces of the electric-resistance, gas, and oil-fired types. Induction heating should be used only when its advantages can be fully realized. These advantages are considerable and include fast heating, high power densities, accurate time and temperature control, and clean operating conditions. Induction heating has an almost innate ability to become part of automatic processes. When these factors are taken into account running costs are usually lower than those of other available methods.

Typical processes are described. They include low-frequency through-heating, accurate surface hardening, localized metal joining and annealing at higher frequencies, and high-speed tin reflow. Coil and system designs are given for typical applications in these fields.

Methods and data have been collected from work carried out in the Industrial Electronics Division of the Westinghouse Electric Corporation, the High Frequency Heating Laboratory of the General Electric Company of England, and the Industrial Electronics Laboratory, Redifon Ltd.,

England. The author is indebted to his colleagues in these companies, and in particular to Mr. R. M. Baker of Westinghouse Corporation, and Mr. E. W. Rogers and Mr. M. T. Elvy, both of Redifon Ltd., for their invaluable help in proofreading and for their many helpful suggestions.

P. G. Simpson
Haywards Heath
Sussex, England

CONTENTS

CHAPTER 1

THEORY OF INDUCTION HEATING

The main utilization of induction heating, a relatively recent process, centers around its unique properties. By making use of the skin-effect phenomenon found when a rapidly alternating current flows in a metallic workpiece, which concentrates the current near the surface, a highly selective heating source is created in the metal surface itself. Advantage is taken of this phenomenon and of the remarkable fact of electromagnetic induction, discovered by Michael Faraday, the true father of induction heating, and the result is a heat method requiring no external heating but using the piece to be heated as its own heat source. The method also requires no physical contact with the energy source, the induction coil. Further properties include the ability to select the heated depth by choice of frequency, accurate location of the heated area by coil-coupling design, and high power concentrations or densities.

To utilize fully all these basic properties by selecting heat-treatment processes suitable for induction techniques, and then to design complete equipment to carry them out, several steps must be followed.

First, the required process specifications must be compared with basic induction properties. The rest of this chapter outlines the electromagnetic effects in a workpiece carrying an induced electric current, and the resultant current distribution and power absorbed. The next chapter covers the heat and temperature effects of the induced current and describes the temperature distributions for different frequencies, metals, and work shapes. Armed with this knowledge, prospective users and designers can select or reject induction heating as a means of meeting the specifications.

Second, the particular type of induction heating most suited to the specification must be determined and a broad outline of the complete application developed. Chapter 3 covers most of the applications current in industry today and gives examples of each type of application, together with its production specifications.

Third, after the suitability of induction heating and the best method for its application have been determined, the coil and power system have to be designed. Chapter 4 gives detailed methods for the design of coils for typical

applications. The remaining chapters describe in some detail the design of complete power systems for each of the three main frequency divisions (supply, machine alternator, and radio-frequency generator) and various auxiliary equipments. Some metallurgical considerations are discussed in Chap. 2.

The approach to many induction heating problems combines a basically engineering approach with an intuitive know-how. This combination usually comes with practical experience. It could almost be said that no induction heating coil or system can be designed without a feel for the right coil shape, power frequency, and heat properties of the metal to be treated.

The action of induction heating might be compared to flame hardening, if the invisible effect of the magnetic field is taken into account. For instance, the higher frequencies from radio-frequency (r-f) generators (200,000 cycles and higher) usually give a very intense, fast, and local heat pattern. This can be compared to the effect of a small and concentrated high-temperature gas flame. Alternatively, a more diffuse and slower heating effect with a deeper heat penetration results from motor-generator frequencies (1,000 to 10,000 cycles). This is similar to the effect of a large widespread gas flame.

The first equation, Eq. (1-1), illustrates this action mathematically. It relates the depth of current penetration δ into the metal from the surface near the coil to the frequency f of the power. As the frequency increases, so the current depth decreases, and therefore the current remains localized near the coil. A similar contrast can also be achieved at any one frequency by the design of the coil. A single-turn coil can be made to concentrate the current into a small area. Large areas are usually heated by a multi-turn coil.

Equations (1-1) and (1-67) also highlight another feature, the relation between the current depth δ and the physical properties of the heated metal. The most important of these properties are the magnetic permeability μ and the electrical resistivity ρ. It is soon obvious in induction heating that steel heats up faster and better than nonferrous metals. The main reason is that most steels are magnetic, with high values of permeability. Nearly all nonferrous metals are nonmagnetic, with a value of 1 for permeability μ. Therefore, from Eq. (1-1), the current depth in steel should be small; this is seen in practice. Similarly, Eq. (1-67) shows that for steel, the power input will be higher than for nonferrous metals.

A basic feature of coil design is the importance of the product of coil turns N_c and current I_c, the "ampere-turns." The greatest power loading into the workpiece is achieved with the highest magnetic field or greatest number of ampere-turns $I_c N_c$; this is seen in Eq. (1-5). As the number of coil turns is often limited by the physical area of the workpiece, it is obvious that the higher the coil current, the greater the power loaded into the metal. Most

r-f generators are constant-current devices, so that this value is relatively fixed, unless a current transformer is used to step up current. Occasionally, the coil current may be increased by adding power-factor capacitors across the coil, as illustrated in Chap. 5. Motor generators may be considered as constant-voltage devices, so that the coil current is largely determined by the coil design itself, or by the use of current transformers.

When considering power input to the workpiece, various losses must be taken into account. If the time required for the treatment is long or the temperature is high, then the heat losses will be large and extra power must be allowed for. Figure 2-9 indicates that the radiation losses rise steeply as the temperature increases. Some of these losses can be reduced by lining the inside of the coil with thermal-insulating materials, such as asbestos or ceramics. In practice, losses of this type are mainly found in through-heating and melting at machine frequencies and supply-line frequencies (60 cycles). Most other types of heat-treatment, such as hardening and brazing, occur too quickly for excessive radiation and convection losses. One type of loss—the resistive loss caused by the current in the coil itself—is inevitable in any coil. Nearly all coils are wound of copper and are water-cooled, and the greater the power and current required for application, the greater the loss. Equation (4-28) indicates the various factors affecting the coil resistance and therefore its copper loss. The resistance increases with turns per inch N_c/l_c, turns N_c, coil diameter d_c, frequency f, and the resistivity of the coil material ρ. This means that a coil with a small number of turns in a given length, wound with a small-diameter and low-resistivity material, such as copper, and operating at a low frequency, will result in the minimum losses. However, greater power inputs result from high frequencies, so the designer has to compromise between the most efficient type and the shape, power requirements, etc., of the material heated. In general, greater coil efficiencies (taking into account power loading into the metal) are achieved at higher frequencies and larger diameters. Figure 2-16 gives some comparative efficiencies.

The efficiency and cost of the different types of power systems vary considerably, but as a rule of thumb, 50 to 60 per cent can be taken as the ratio of useful power in the load to power drawn from the supply. Cost of equipment per kilowatt rises with frequency. This can be expected, as higher-power r-f components are usually expensive.

Summarizing, these points should be considered when using induction heating:

1. Frequency selection for the required treatment
2. Coil design to give the best heat pattern and highest degree of efficiency
3. System design to minimize losses

The solid cylindrical shape is used as a basis for most of the design

formulas in this book, as it has a convenient geometry for theoretical analysis and is the most widely encountered shape in induction heating practices. However, hollow cylinders and rectangular slabs are also treated in some detail, and some applications of proximity-heated surfaces are described. The cgs system is used in all derivations of formulas because of ease of conversion to the fps system of practical units. These practical units are used in all design methods.

1-1. BASIC TRANSFORMER EQUATIONS

The ideal coil and workpiece and the current distribution are shown in Fig. 1-1.

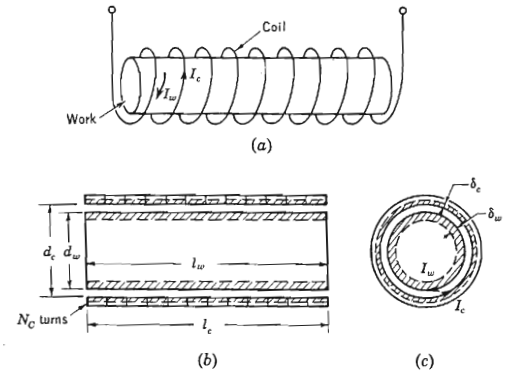

FIG. 1-1. Current depth in an ideal workpiece.

The symbols used are given below:

I_c = coil current, amp
I_w = work current, amp
δ_c = equivalent current depth for coil, cm
δ_w = equivalent current depth for work, cm
d_w = work outer diameter, cm
d_c = coil inner diameter, cm
l_w = work length, cm
E_c = coil terminal voltage, volts
R_w = work resistance, ohms

f = frequency of I_c and I_w, cps
ρ_w = work resistivity, microhm-cm
ρ_c = coil resistivity, microhm-cm
μ_w = work permeability
N_c = coil turns
P_w = work power, kw
P_c = coil-power loss, kw
R_c = coil resistance, ohms

Most induction heating problems involve the derivation of the coil ampere-turns and volts per turn, given the work power (from production rate and temperature requirements). From these results are obtained the coil turns, volts, and current that can be matched to available power supplies. The total coil power, including all losses as well as work power, gives a complete specification for the power supply.

This section is concerned only with the power dissipations due to resistances and does not take into account any reactive volt-amperes (var) due to reactances. These are secondary to the main process, as they do not contribute to the heating effect by I^2R losses; however, because they are inevitable in any transformer circuit they are developed later in this chapter and in Chap. 4.

The flux is assumed to be perfectly linear axially through the turns of the coil windings and workpiece, so that end effect, flux variations, and flux leakages are neglected. While the actual current distribution in the work and coil is a complex function, approximating to an exponential drop in value, as explained later, it is represented here by an equivalent depth. This is defined as

$$\delta = \frac{1}{2\pi}\sqrt{\frac{\rho}{\mu f}} \quad \text{cm} \tag{1-1}$$

It is the depth of the equivalent d-c direct current and is defined as the depth at which the current density is 36.7 per cent of its surface value. The derivation is given later.

On the basis of these assumptions and Fig. 1-1, the ampere-turns relation between coil and work is

$$I_c N_c = I_w \qquad \text{amp-turns} \tag{1-2}$$

The work is the short-circuited secondary of the transformer and has unity turns.

The work resistance is obviously the resistance of the equivalent current path of cross section $\delta_w l_w$ and length πd_w (approximately). Therefore its value is given by

$$R_w = \frac{\rho_w \pi d_w \times 10^{-6}}{\delta_w l_w} \qquad \text{ohm} \tag{1-3}$$

The power induced into the work is found by substituting Eqs. (1-2) and (1-3) in

$$P_w = I_w^2 R_w \times 10^{-3} \quad \text{kw}$$

$$P_w = \frac{I_c^2 N_c^2 \rho_w \pi\, d_w \times 10^{-6} 10^{-3}}{\delta_w\, l_w} \tag{1-4}$$

Therefore

$$P_w = \frac{I_c^2 N_c^2 \rho_w \pi\, d_w \times 10^{-9}}{\delta_w\, l_w} \quad \text{kw} \tag{1-5}$$

It is assumed that the current depths in coil and work are small compared with their diameters.

The coil loss is given from

$$P_c = I_c^2 R_c \times 10^{-3} \quad \text{kw} \tag{1-6}$$

and its effective resistance is seen to be

$$R_c = \frac{\rho_c \pi\, d_c\, N_c^2 \times 10^{-6}}{\delta_c\, l_c} \quad \text{ohm} \tag{1-7}$$

This is derived in the same way as Eq. (1-3), but the resistance is increased by the increase in path length $\pi\, d_c\, N_c$ and is increased also by the decrease in cross section $\delta_c\, l_c / N_c$, giving a total factor of N_c^2 increase over a one-turn coil. Substituting Eq. (1-7) in Eq. (1-6)

$$P_c = \frac{I_c^2 N_c^2 \rho_c \pi\, d_c \times 10^{-9}}{\delta_c\, l_c} \quad \text{kw} \tag{1-8}$$

Therefore the coil ampere-turns can be obtained from Eq. (1-5) and in turn inserted in Eq. (1-8) to give the loss in coil windings. This gives the total coil power required for a given work power from

$$P_{ct} = P_c + P_w \quad \text{kw} \tag{1-9}$$

These are the fundamental induction heating equations; they give the coil ampere-turns and the total power required to produce a specified power into the work. All other effects are "losses" (resistive or reactive); they require extra power or voltage and will be dealt with later. Although these formulas are approximate, they give some indication of the power requirements for most applications and can always be used as a check on the more accurate formulas.

1-2. DIFFERENTIAL EQUATION FOR A SOLID CYLINDER

The external energy source in induction heating is the magnetizing force of field intensity. For this reason it is of great importance to determine how

this field intensity is distributed throughout the work. The field intensity, created by the alternating current, in turn induces the heating current in the work, which bears a direct relation to it. Therefore, the distribution of magnetic field intensity gives a direct indication of the distribution of heat and temperature gradient in the workpiece.

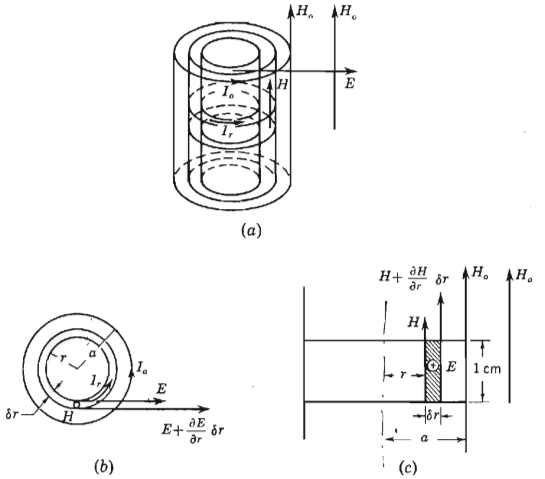

FIG. 1-2. Magnetic and electric field intensities in a solid cylinder.

It is assumed in Fig. 1-2 that the instantaneous field intensity surrounding the work is independent of distance from the work and is not affected by its presence.

All vector quantities are indicated by boldface notation, e.g., $\boldsymbol{\phi}$, and are instantaneous values. The units used in the derivation are the electromagnetic units unless otherwise stated.

List of Symbols

a = radius of work, cm
d_w = diameter of work, cm
r = radius of shell inside work, cm ($r < a$)
$\mathbf{H}_o$ = magnetic field intensity surrounding work, oersteds

$\mathbf{E}$ = electric field intensity inside work at r, abvolt per cm
ρ = work resistivity (assumed constant), abohm-cm
μ = work permeability (assumed constant), gauss per oersted
μ_o = free-space permeability ($\mu_o = 1$), gauss per oersted
$\boldsymbol{\phi}_r$ = magnetic flux inside shell at r, maxwells
A_r = cross-sectional area of shell at r, sq cm
A_w = cross-sectional area of work described by a, sq cm
δr = thickness of shell at r ($\delta r \gg r$), cm
$\mathbf{I}_r$ = current density at shell radius r, abamp per sq cm
$\mathbf{I}_a$ = surface current density, abamp per sq cm
R_r = resistance at r to $\mathbf{I}_r$, abohm
l_w = length of work, cm

Therefore the electromotive force (emf) induced as a result of the varying magnetic intensity $\mathbf{H}$ at r, given by $\mathbf{E}2\pi r$, will result in a current $\mathbf{I}$, where

$$\mathbf{I} = \frac{\mathbf{E}2\pi r}{R_r}$$

The resistance R_r of unit length of the shell to $\mathbf{I}_r$ is given from

$$R_r = \frac{\rho 2\pi r}{\delta r} \tag{1-10}$$

Therefore,

$$\mathbf{I} = \frac{\mathbf{E}2\pi r}{\rho 2\pi r/\delta r} = \frac{\mathbf{E}\delta r}{\rho} \tag{1-11}$$

The current flow through the shaded area $\delta r 1$ of Fig. 1-2*c* will therefore be of density

$$\mathbf{I}_r = \frac{\mathbf{E}}{\rho} \tag{1-12}$$

The line integral of magnetic field intensity around any closed loop surrounding a current is given from

$$\mathbf{I} = \frac{1}{4\pi} \oint \mathbf{H}\, ds \tag{1-13}$$

Therefore, by taking the line integral around the shaded area in Fig. 1-2*c*,

$$\mathbf{I} = \frac{1}{4\pi}\left[\mathbf{H} - \left(\mathbf{H} + \frac{\partial \mathbf{H}}{\partial r}\,\delta r\right)\right] = -\frac{1}{4\pi}\,\delta \mathbf{H} \tag{1-14}$$

and the current density is

$$\mathbf{I}_r = -\frac{1}{4\pi}\frac{\partial \mathbf{H}}{\partial r} \tag{1-15}$$

Equating Eqs. (1-12) and (1-15),

$$\frac{\partial \mathbf{H}}{\partial r} = -\frac{4\pi \mathbf{E}}{\rho} \tag{1-16}$$

Also the integral of electric field intensity around any closed loop surrounding a magnetic flux is given by

$$\oint \mathbf{E}\, ds = -\frac{d\phi}{dt} \tag{1-17}$$

If ϕ_r is the total flux in the ring, then

$$\phi_r = \mu \mathbf{H} A_r \tag{1-17a}$$

and if it is assumed that $\mathbf{H}$ is a sinusoidal function, then

$$\frac{d\phi_r}{dt} = \mu A_r \frac{d\mathbf{H}}{dt} = jw\mu \mathbf{H} 2\pi r\, \delta r \tag{1-18}$$

and Eq. (1-17) may be written

$$\left(\mathbf{E} + \frac{\partial \mathbf{E}}{\partial r}\delta r\right)2\pi(r + \delta r) - \mathbf{E}2\pi r = -jw\mu 2\pi r\, \delta r \mathbf{H} \tag{1-19}$$

as ϕ_r is the difference between the flux inside $r + \delta r$ and that inside r, linked by the difference between the two emf's in Eq. (1-19).

$$\text{Therefore} \quad 2\pi \mathbf{E}\, \delta r + 2\pi r \frac{\partial \mathbf{E}}{\partial r}\delta r + 2\pi \frac{\partial \mathbf{E}}{\partial r}\delta r^2 = -jw\mu 2\pi r\, \delta r \mathbf{H} \tag{1-19a}$$

Neglecting the very small term δr^2,

$$\frac{\partial \mathbf{E}}{\partial r} + \frac{\mathbf{E}}{r} = -jw\mu \mathbf{H} \tag{1-20}$$

Combining Eqs. (1-16) and (1-20) and changing to differentials

$$\frac{d^2\mathbf{H}}{dr^2} + \frac{1}{r}\frac{d\mathbf{H}}{dr} - \frac{j\mathbf{H}w\mu 4\pi}{\rho} = 0 \tag{1-21}$$

Let

$$k^2 = \frac{4\pi w\mu}{\rho} = \frac{8\pi^2 f\mu}{\rho} \tag{1-22}$$

Therefore Eq. (1-21) becomes

$$\frac{d^2\mathbf{H}}{dr^2} + \frac{1}{r}\frac{d\mathbf{H}}{dr} - k^2 j\mathbf{H} = 0 \tag{1-23}$$

This is the fundamental equation for the distribution of magnetic field intensity $\mathbf{H}$; its solution gives the value of $\mathbf{H}$ at any point inside the work and therefore the current density $\mathbf{I}_r$. The equation is solved by the use of Bessel functions (1). The standard general solution for Eq. (1-23) is

$$\mathbf{H} = AI_o(kr\sqrt{j}) + BK_o(kr\sqrt{j}) \tag{1-23a}$$

where for small values of kr,

$$I_o(kr\sqrt{j}) = 1 + \frac{j(kr)^2}{2^2} - \frac{(kr/2)^4}{2!^2} - \frac{j(kr/2)^6}{3!^2}\cdots \tag{1-24}$$

and $$K_o(kr\sqrt{j}) = I_o(kr\sqrt{j})\,(\log 2 - \gamma - \log kr) + \frac{j(kr)^2}{2^2}$$

$$- \left(1 + \frac{1}{2}\right)\frac{(kr/2)^4}{2!^2} - j\left(1 + \frac{1}{2} + \frac{1}{3}\right)\frac{(kr/2)^6}{3!^2}\cdots \tag{1-25}$$

When kr is large

$$I_o(kr\sqrt{j}) = \frac{e^{kr\sqrt{j}}}{\sqrt{2kr\sqrt{j}}}\left[1 + \frac{1^2}{8kr\sqrt{j}} + j\frac{(1^2)(3^2)}{2!(8kr)^2} + j\frac{(1^2)(3^2)(5^2)}{3!(8kr\sqrt{j})^3} + \cdots\right] \tag{1-26}$$

and $$K_o(kr\sqrt{j}) = e^{-kr\sqrt{j}}\sqrt{\frac{\pi}{2kr\sqrt{j}}}\left[1 - \frac{1^2}{8kr\sqrt{j}} + j\frac{(1^2)(3)^2}{2!(8kr)^2}\right.$$

$$\left. - j\frac{(1^2)(3^2)(5^2)}{3!(8kr\sqrt{j})^3} + \cdots\right] \tag{1-27}$$

These expressions are simplified by separating real and imaginary terms in Eqs. (1-24) and (1-25) and defining the results as below.

$$I_o(kr\sqrt{j}) = \text{ber } kr + j\,\text{bei } kr \tag{1-28}$$

$$K_o(kr\sqrt{j}) = \text{ker } kr + j\,\text{kei } kr \tag{1-29}$$

Therefore, for example, in Eq. (1-28),

$$\text{ber } kr = 1 - \frac{(kr/2)^4}{(2!)^2} + \frac{(kr/2)^8}{(4!)^2} - \cdots \tag{1-30}$$

$$\text{bei } kr = \frac{(kr)^2}{(2)^2} - \frac{(kr/2)^6}{(3!)^2} + \frac{(kr/2)^{10}}{(5!)^2}\cdots \tag{1-31}$$

Useful derivatives of Eqs. (1-28) and (1-29) are

$$\text{bei}'\, kr = \frac{k}{r}\int r \,\text{ber}\, kr\, dr \tag{1-32}$$

$$\text{ber}'\, kr = -\frac{k}{r}\int r \,\text{bei}\, kr\, dr \tag{1-33}$$

$$\text{kei}'\, kr = \frac{k}{r}\int r \,\text{ker}\, kr\, dr \tag{1-34}$$

$$\text{ker}'\, kr = -\frac{k}{r}\int r \,\text{kei}\, kr\, dr \tag{1-35}$$

The values of the ber, bei, ker, and kei functions and their derivations have been tabled (2–4), and the results will be used later in the solutions of Eq. (1-23) and other equations. Useful values are given in Appendix A.

Now in the case of a solid cylinder, the magnetic field density is obviously not infinite in value at the center of the work, i.e., when $r = 0$, $\mathbf{H}$, given by Eq. (1-23), is not infinite. In Eq. (1-25), when $r = 0$, $\log kr$ is infinite and $K_o(kr\sqrt{j})$ is infinite; therefore B in Eq. (1-23*a*) must be zero and the solution reduces to

$$\mathbf{H} = AI_o(kr\sqrt{j}) \tag{1-36}$$

Therefore

$$\mathbf{H} = A(\text{ber}\, kr + j\,\text{bei}\, kr) \tag{1-37}$$

from Eq. (1-28).

At the surface of the work, where $r = a$, $\mathbf{H} = \mathbf{H}_o$

Therefore,

$$\mathbf{H}_o = A(\text{ber}\, ka + j\,\text{bei}\, ka) \tag{1-38}$$

and Eq. (1-37) becomes

$$\frac{\mathbf{H}}{\mathbf{H}_o} = \frac{\text{ber}\, kr + j\,\text{bei}\, kr}{\text{ber}\, ka + j\,\text{bei}\, ka} \tag{1-39}$$

Now, from Eqs. (1-15) and (1-37),

$$\mathbf{I}_r = -\frac{Ak}{4\pi}(\text{ber}'\, kr + j\,\text{bei}'\, kr) \tag{1-40}$$

$$\mathbf{I}_a = -\frac{Ak}{4\pi}(\text{ber}'\, ka + j\,\text{bei}'\, ka) \tag{1-41}$$

$$\frac{\mathbf{I}_r}{\mathbf{I}_a} = \frac{\text{ber}'\, kr + j\,\text{bei}'\, kr}{\text{ber}'\, ka + j\,\text{bei}'\, ka} \tag{1-42}$$

$$\left|\frac{I_r}{I_a}\right| = \frac{\sqrt{\text{ber}'^2\, kr + \text{bei}'^2\, kr}}{\sqrt{\text{ber}'^2\, ka + \text{bei}'^2\, ka}} \tag{1-43}$$

Figure 1-3 shows this ratio for different values of ka. For example, if the current distribution is required in a cylinder, the curves can be used, as in the following examples:

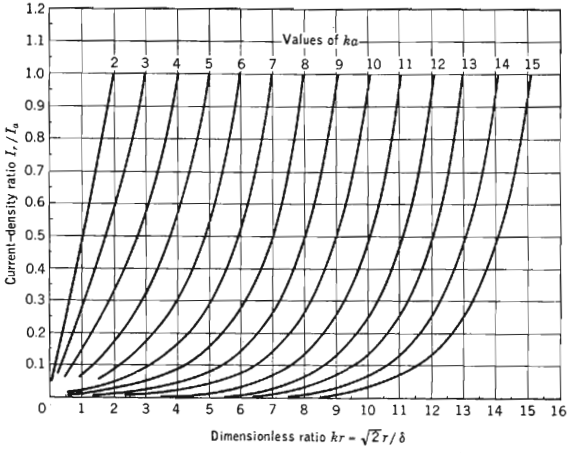

FIG. 1-3. Current-density distribution in a solid cylinder.

Example 1-1

Metal ..... Steel
Frequency, f ..... 60 cps
Resistivity, ρ ..... 100 microhm-cm $= 10^5$ abohm-cm
Permeability, μ ..... 800 gauss per oersted
Radius, a ..... 0.25 in. = 0.635 cm

From Eq. (1-22)

$$k = \frac{(2)(\pi)(2)^{1/4}(60)^{1/4}(8)^{1/4}(10^2)^{1/4}}{(10^4)^{1/4}(10)^{1/4}} = 6.15$$

Therefore, $ka = 6.15 \times 0.635 = 3.91$

Approximating to the $ka = 4$ curve in Fig. 1-3, the current distribution can easily be evaluated, as a function of radius r, as k is now fixed. It can be noticed that the current density has dropped to half its surface value at a radius of 2.8/4, or 70 per cent of the work radius. From the curve it is seen

that at this low frequency, the skin effect is not so pronounced, as the 50 per cent current point is found 30 per cent in from the surface.

Example 1-2

Metal ..... Stainless steel
Current frequency, f ..... 450,000 cps
Resistivity, ρ ..... 100 microhm-cm $= 10^5$ abohm-cm
Permeability, μ ..... 1.0 gauss per oersted
Radius, a ..... 0.25 in. $= 0.635$ cm

From Eq. (1-22),

$$k = \frac{(2)(\pi)(2)^{1/2}(45)^{1/2}(10^4)^{1/2}}{(10^4)^{1/2}(10)^{1/2}} = 18.8$$

$$ka = 18.8 \times 0.635 = 11.9$$

When the $ka = 12$ curve in Fig. 1-3 is used, the current distribution is seen to differ considerably from the $ka = 4$ curve in the previous example. This is mainly because of the much higher frequency, and results in a pronounced skin effect. For example, the current density drops to half its surface value at 92 per cent of the work radius (11/12), or 8 per cent in from the surface.

Many examples can be simply derived by approximating Eq. (1-42) when the value of kr is large, i.e., when either the frequency of the induced current or the work radius at the point considered is large. The Bessel functions can be written under these conditions as

$$\text{ber } kr = \frac{e^{kr/\sqrt{2}}}{\sqrt{2\pi\, kr}} \cos\left(\frac{kr}{\sqrt{2}} - \frac{\pi}{8}\right) \tag{1-44}$$

$$\text{bei } kr = \frac{e^{kr/\sqrt{2}}}{\sqrt{2\pi\, kr}} \sin\left(\frac{kr}{\sqrt{2}} - \frac{\pi}{8}\right) \tag{1-45}$$

$$\text{ber}' kr = \frac{e^{kr/\sqrt{2}}}{\sqrt{2\pi\, kr}} \cos\left(\frac{kr}{\sqrt{2}} + \frac{\pi}{8}\right) \tag{1-46}$$

$$\text{bei}' kr = \frac{e^{kr/\sqrt{2}}}{\sqrt{2\pi\, kr}} \sin\left(\frac{kr}{\sqrt{2}} + \frac{\pi}{8}\right) \tag{1-47}$$

Therefore Eq. (1-42) reduces to

$$\frac{\mathbf{I}_r}{\mathbf{I}_a} = \left[\sqrt{\frac{2\pi\, ka}{2\pi\, kr}}\, e^{(k/\sqrt{2})(r-a)}\right] \times \left[\frac{\cos(kr/\sqrt{2} + \pi/8) + j \sin(kr/\sqrt{2} + \pi/8)}{\cos(ka/\sqrt{2} + \pi/8) + j \sin(ka/\sqrt{2} + \pi/8)}\right] \tag{1-48}$$

This indicates that at a depth x where

$$x = a - r \tag{1-49}$$

the phase of the current density has been retarded by $(k/\sqrt{2})(a - r)$. The phase will be reversed completely when

$$x = \frac{\sqrt{2}\,\pi}{k} \tag{1-50}$$

As a and r both become very large, Eq. (1-48) further reduces to

$$\frac{I_r}{I_a} = e^{-kx/\sqrt{2}} = e^{-x/\delta} \tag{1-51}$$

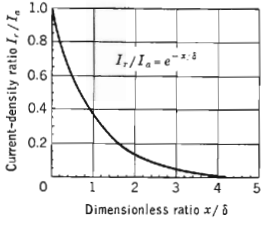

FIG. 1-4. Current-density distribution —approximate function.

This is plotted in Fig. 1-4; it can be seen that when $x = \sqrt{2}/k$, i.e., $x = \delta$ where, from Eq. (1-22),

$$k = \sqrt{2}(2)\pi\sqrt{\frac{\mu f}{\rho}} = \frac{\sqrt{2}}{\delta} \tag{1-52}$$

Therefore, $I_r = (1/e)I_a$, i.e., I_r is reduced 36.7 per cent of its surface value. This is the "equivalent current depth" mentioned in the initial section.

By a similar analysis

$$H_r = H_0 e^{-x/\delta} \tag{1-53}$$

The current depth δ is given from Eq. (1-52) by

$$\delta = \frac{1}{2\pi}\sqrt{\frac{\rho}{\mu f}} \quad \text{cm}$$

It is interesting to use this curve to derive the distribution of the current density in the previous example.

Example 1-3

Let $k = 6.15$, as in Example 1-1.
From Eq. (1-52),

$$\delta = \frac{\sqrt{2}}{k} = \frac{2^{1/4}}{6.15} = 0.23 \text{ cm}$$

At 30 per cent from the surface, $x = (0.7 \times 0.635) = 0.444$ cm.

Therefore

$$\frac{x}{\delta} = \frac{0.444}{0.23} = 1.93$$

From Fig. 1-4, at $x/\delta = 1.93$, the current density is 15 per cent of the surface value, whereas at the same value of x (70 per cent of the radius $a = 0.444$) and on the basis of Fig. 1-3, the current density is just 50 per cent. The difference lies in the fact that Fig. 1-3 is based on the accurate formula in Eq. (1-43), which takes into account the effects of the current flow from the opposite side of the cylinder, whereas Fig. 1-4 is based on the approximation in Eq. (1-51), which assumes no effect from the current on the opposite side, i.e., an infinite plane effect.

In later power calculations the accurate expressions will always be used, as considerable error in power requirements can obviously result if incorrect current distributions are used. However, Fig. 1-4 can be used with reasonable accuracy when $\delta < \frac{1}{5}a$, i.e., the current depth is less than one-fifth of the radius.

1-3. TOTAL FLUX AND POWER IN A SOLID CYLINDER

The *total* flux Φ_{tr} inside the area enclosed by the ring at r, Fig. 1-2*b*, is given by integrating Eq. (1-17*a*).

$$\Phi_{tr} = \int_0^r \mu \mathbf{H}_r 2\pi r \, dr = 2\pi\mu \int_0^r A(\text{ber } kr + j \text{ bei } kr) r \, dr \tag{1-54}$$

From Eqs. (1-32) and (1-33), Eq. (1-54) can be reduced to

$$\Phi_{tr} = \frac{2\pi\mu A r}{k} (\text{bei}' \, kr - j \, \text{ber}' \, kr) \tag{1-55}$$

Substituting for A from Eq. (1-38),

$$\Phi_{tr} = \frac{2\pi\mu \mathbf{H}_o r}{k} \frac{\text{bei}' \, kr - j \, \text{ber}' \, kr}{\text{ber } ka + j \, \text{bei } ka} \tag{1-56}$$

At $r = a$, $\Phi_{tr} = \Phi_a$, where Φ_a is the total flux inside the work.

Therefore,
$$\Phi_a = \frac{2\pi\mu \mathbf{H}_o a}{k} \frac{\text{bei}' \, ka - j \, \text{ber}' \, ka}{\text{ber } ka + j \, \text{bei } ka} \tag{1-57}$$

This can be simplified to

$$\Phi_a = \mu \mathbf{H}_o A_w (P - jQ) = \Phi_p - j\Phi_q \tag{1-58}$$

where
$$P = \frac{2}{ka} \frac{\text{bei}' \, ka \, \text{ber } ka - \text{ber}' \, ka \, \text{bei } ka}{\text{ber}^2 \, ka + \text{bei}^2 \, ka} \tag{1-59}$$

and
$$Q = \frac{2}{ka} \frac{\text{bei}' \, ka \, \text{bei } ka + \text{ber}' \, ka \, \text{ber } ka}{\text{ber}^2 \, ka + \text{bei}^2 \, ka} \tag{1-60}$$

These expressions are extremely useful and will be used later in coil calculations (5). They are plotted in Fig. 1-5, as functions of d/δ where

$$\frac{d}{\delta} = \frac{2\,ak}{\sqrt{2}} = \sqrt{2}\,ka \tag{1-61}$$

because this ratio is commonly used in induction heating calculations. It

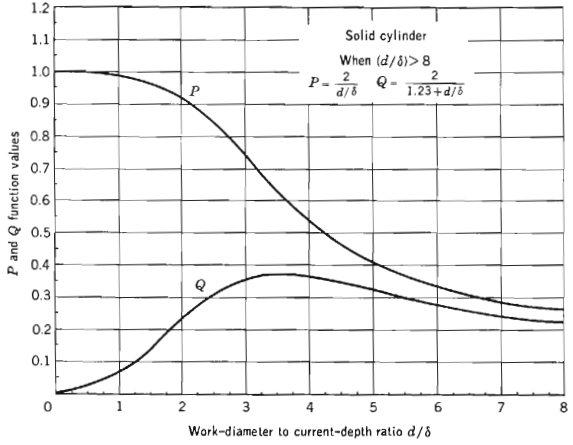

FIG. 1-5. P and Q functions—solid cylinder.

can be seen from the values of the functions in Eqs. (1-59) and (1-60) that when $d/\delta > 8$,

$$P \rightarrow \frac{2}{d/\delta} \quad \text{and} \quad Q \rightarrow \frac{2}{1.23 + d/\delta}$$

and these values may be used.

The heat generated in the solid cylinder can be derived by considering the total current flowing in the shell of width δr in 1 cm of work length. This is given by Fig. 1-2*c*.

$$\mathbf{I}_{tr} = \mathbf{I}_r\,\delta r \tag{1-62}$$

The resistance of the shell is given by Eq. (1-10); therefore the power or heat dissipation lost is

$$\mathbf{I}_{tr}^2 R_r = \mathbf{I}_r^2 2\pi\rho r\,\delta r \tag{1-63}$$

Using Eq. (1-40) and integrating over the complete radius, the power lost

per centimeter length is

$$P_1 = \int_0^a \frac{|A|^2 k^2 \rho}{8\pi^2} (\text{ber}'^2\, kr + \text{bei}'^2\, kr)\pi r\, dr \qquad (1\text{-}64)$$

Utilizing Eqs. (1-32) and (1-33) and simplifying the Bessel functions (1)

$$P_1 = \frac{|A|^2 \rho\, ka}{8\pi} (\text{ber}\, ka\, \text{ber}'\, ka + \text{bei}\, ka\, \text{bei}'\, ka) \qquad (1\text{-}65)$$

With the value of $|A|$ obtained from Eq. (1-38),

$$P_w = \frac{H_o^2 \rho k a l_w}{8\pi} \frac{\text{ber}\, ka\, \text{ber}'\, ka + \text{bei}\, ka\, \text{bei}'\, ka}{\text{ber}^2\, ka + \text{bei}^2\, ka} \quad \text{ergs/sec} \qquad (1\text{-}66)$$

for the work of length l_w cm. By using Eqs. (1-22) and (1-60) and converting to watts,*

$$P_w = 2.5 f H_o^2 l_w \mu A_w Q \times 10^{-8} \quad \text{watt} \qquad (1\text{-}67)$$

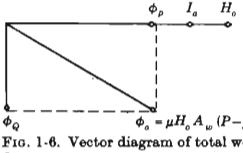

FIG. 1-6. Vector diagram of total work flux.

The surface magnetic intensity is always assumed to be the reference vector with zero phase angle; the relative phase angles of the flux and current in the work are shown in Fig. 1-6. In most induction heating applications P_w is given. In the following example, the surface magnetic intensity is derived for a through-heating application.

Example 1-4

Metal	Aluminum
Current frequency, f	60 cps
Resistivity, ρ	5.7 microhm-cm $= 5.7 \times 10^3$ abohm-cm
Required work power, P_w	100 kw $= 10^5$ watts
Permeability, μ	1.0
Diameter, d_w	3.0 in. $= 7.6$ cm
Length, l_w	20 in. $= 50.8$ cm

From Eq. (1-1) the "current depth" is

$$\delta = \frac{1}{2\pi}\sqrt{\frac{\rho}{\mu f}} = \frac{(57)^{1/4}(10^2)^{1/4}}{(2)(\pi)(1)^{1/4}(60)^{1/4}} = 1.54 \text{ cm}$$

Therefore

$$\frac{d_w}{\delta} = \frac{7.6}{1.54} = 4.94$$

* A factor of 2 has been introduced into Eq. (1-67) because the P and Q curves have been plotted as functions of the work diameter d instead of the radius a.

From Fig. 1-5, for $d/\delta = 4.94$, $Q = 0.32$. Using Eq. (1-67),

$$H_o^2 = \frac{P_w \times 10^8}{2.5 f l_w \mu A_w Q} = \frac{(10^5)(10^8)(4)}{(2.5)(60)(50.8)(1)(\pi)(7.6)^2(0.32)}$$

$$= 0.9 \times 10^8$$

Therefore $H_o = 9{,}500$ oersteds

For a constant diameter, the optimum frequency can be determined from Eq. (1-67) for maximum power density. Rewriting Eq. (1-67),

$$P_{cc} = 2.5 f H_o^2 \mu Q \times 10^{-8} \text{ watt/cu cm} \qquad (1\text{-}67a)$$

From Fig. 1-5 the maximum value of Q occurs at a value of d/δ given by 3.5. In the above example, at a frequency of 60 cps, the current depth δ was given as 1.54 cm.

Therefore $d_{opt} = \delta \times 3.5 = 1.54 \times 3.5 = 5.4$ cm

Therefore for 60-cycle aluminum heating, the work diameter for maximum power input will be 5.4 cm or 2.1 in. However, as will be seen later, this method for evaluating the optimum diameter does not necessarily give the correct value, because of other variables.

1-4. POWER AND FLUX INDUCED IN A WIDE RECTANGULAR SLAB

By using an analysis similar to that in the preceding section, the differential equation for the field distribution in a rectangular slab can be derived, assuming the width w to be large compared with the thickness t.

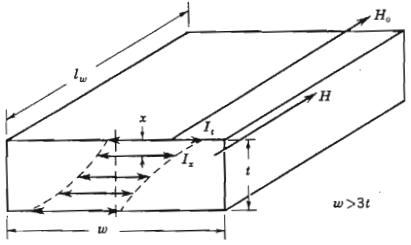

FIG. 1-7. Wide rectangular induction-heated slab.

It is apparent from Fig. 1-7 that the assumption that $w \gg t$ also includes a negligible edge effect at the extremities of the width w. If the slab is thin, i.e., t is small, the current distribution will be somewhat like that in Fig. 1-7,

where the magnetic intensity on one side of the slab actually induces some current in the other half. As in the case of the cylindrical workpiece, this current will tend to oppose the stronger current induced by the closer magnetic field. The effect will be seen in the solution to the equation. The equation for distribution of the magnetic field intensity is

$$\frac{d^2\mathbf{H}}{dx^2} - jk\mathbf{H} = 0 \tag{1-68}$$

where

$$k^2 = \frac{8\pi^2 f\mu}{\rho} = \frac{2}{\delta^2} \tag{1-69}$$

The current-density distribution is given by a similar expression

$$\frac{d^2\mathbf{I}_r}{dx^2} - jk\mathbf{I}_r = 0 \tag{1-70}$$

The solution is

$$\mathbf{I}_r/\mathbf{I}_i = \frac{\cosh k\sqrt{jx}}{\cosh k\sqrt{jt/2}} \tag{1-71}$$

Total flux in the slab is obtained by the expression in Eq. (1-58), but here

$$P = \frac{1}{kt}\frac{\sinh kt + \sin kt}{\cosh kt + \cos kt} \tag{1-72}$$

$$Q = \frac{1}{kt}\frac{\sinh kt - \sin kt}{\cosh kt + \cos kt} \tag{1-73}$$

These functions are plotted in Fig. 1-8. The total power absorbed is given by Eq. (1-67), where A_w is now given by

$$A_w = wt \tag{1-74}$$

An example will illustrate the surface magnetic intensity required, given the power in the work.

Example 1-5

Metal ..... Steel
Required power, P_w ..... 50 kw $= 5 \times 10^4$ watts
Current frequency, f ..... 3,000 cps
Resistivity, ρ ..... 100 microhm-cm $= 10^5$ abohm-cm
Permeability (assumed constant), μ ..... 10^3 gauss per oersted
Width, w ..... 5 in. $= 12.7$ cm
Thickness, t ..... $\frac{1}{4}$ in. $= 0.635$ cm
Length, l_w ..... 10 in. $= 25.4$ cm

It is required to find the peak magnetizing field H_o, in oersteds. From Eq. (1-1), the equivalent current depth is

$$\delta = \frac{1}{2\pi}\sqrt{\frac{\rho}{\mu f}} = \frac{(10^5)^{1/4}}{(2)(\pi)(10^3)^{1/2}(3)^{1/2}(10^3)^{1/4}} = 0.029 \text{ cm}$$

Refer to Fig. 1-8. Now $t/\delta = 0.63/\delta = 22$; as this is greater than 8, the

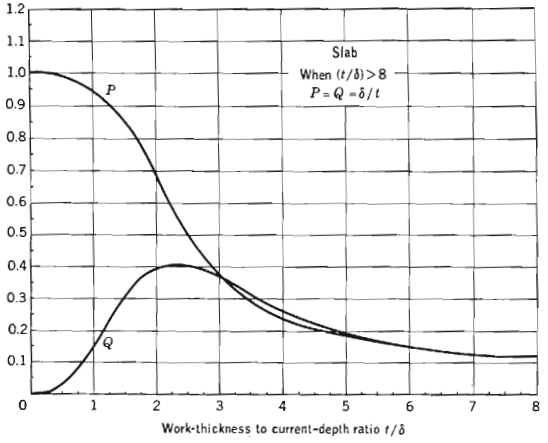

FIG. 1-8. P and Q functions—solid slab.

approximation $P = Q = \delta/t$ can be used, i.e., $Q = 0.0455$. Therefore, from Eq. (1-67),

$$H_o^2 = \frac{(5)(10^4)(10^8)}{(2.50)(3)(10^3)(25.4)(10^3)(12.7)(0.635)(0.0455)}$$

$$= 7.15 \times 10^4$$

Therefore $H_o = 267$ oersteds

It should be noted that in this example, as in the previous steel example, the permeability is assumed constant. This is not true in practice, as it is a function of the magnetic field intensity surrounding the work and the degree of magnetic saturation. It is usually assumed that most induction-heated steels saturate at about 32,400 gauss. Therefore the permeability is given by

$$\mu = 1 + \frac{32{,}400}{H_o} \tag{1-75}$$

The value of 1 is included because at a very high value of H_o, μ must assume the value of free-space permeability, i.e., unity. The value of H_o can now no longer be obtained from

$$H_o = \frac{P_w \times 10^8}{2.5 f l_w \mu A_w Q} \tag{1-76}$$

as Q, a function of μ, is therefore also a function of H_o. The only way to

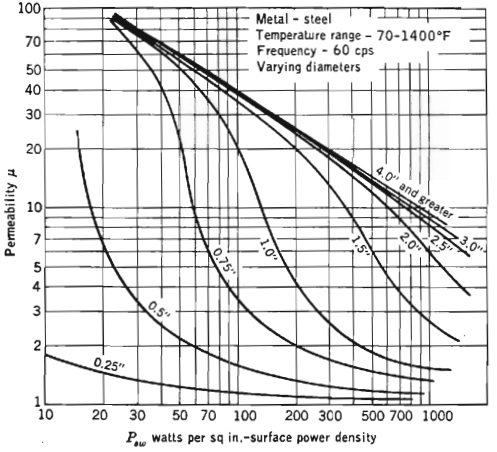

FIG. 1-9. Permeability vs. work-surface power density.

determine μ is to utilize curves of surface power density against permeability. An example of the cylindrical case is given in Fig. 1-9; at the frequency selected, diameters of 4 in. and larger result in a straight line, because the skin effect becomes negligible in comparison with the diameter and becomes a constant.

When the width w approaches the thickness t, the above formulas no longer apply. In the case of a square cross section where $w = t$, the cylindrical formulas can be used with a value of the radius a given by

$$a = \frac{2w}{\pi} \quad \text{cm} \tag{1-77}$$

1-5. POWER INDUCED IN HOLLOW CYLINDERS AND OTHER MISCELLANEOUS SHAPES

The differential equation of a hollow cylindrical workpiece is the same as that for a solid cylinder, i.e., Eq. (1-23). However, the boundary conditions will obviously be different.

In the case where the wall thickness t is small compared with the radius a and the current penetration depth δ, uniform current density can be

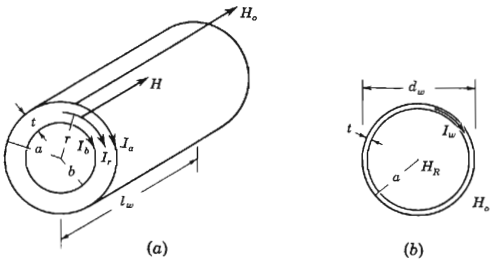

FIG. 1-10. Induction-heated hollow cylinder.

assumed across t (Fig. 1-10*b*). Therefore the total resultant field intensity $\mathbf{H}_R$ inside the shell is the vector sum of the external field $\mathbf{H}_o$ and $\mathbf{H}_w$, resulting from the induced current $\mathbf{I}_w$. As the shell is assumed to be negligibly thin, this intensity is assumed to be constant across the work area A_w bounded by the perimeter $2\pi a$. The vector equation for $\mathbf{H}_r$ is therefore

$$\mathbf{H}_R = \mathbf{H}_o + \mathbf{H}_w \qquad \text{oersteds} \tag{1-78}$$

Now from Eq. (1-13),

$$\oint \mathbf{H}_w \, ds = 4\pi \mathbf{I}_w$$

Therefore, as $\mathbf{H}_w$ is assumed to be constant along the work length (disregarding end effects),

$$\mathbf{I}_w = \frac{\mathbf{H}_w l_w}{4\pi} \tag{1-78a}$$

From Eq. (1-17)

$$\oint \mathbf{E} \, ds = -\frac{d\boldsymbol{\Phi}_R}{dt} = -A_w \frac{d\mathbf{H}_R}{dt}$$

Assuming $\mathbf{E}$ to be constant around the shell,

$$\oint \mathbf{E}\, ds = \mathbf{E} 2\pi a = \mathbf{E}_w = -A_w \frac{d\mathbf{H}_R}{dt} \tag{1-79}$$

If $\mathbf{H}_R$ is assumed to be sinusoidal,

$$\frac{d\mathbf{H}_R}{dt} = jw\mathbf{H}_R$$

Therefore,
$$\mathbf{E}_w = -jwA_w\mathbf{H}_R = -jw\boldsymbol{\Phi}_R \tag{1-80}$$

Therefore the flux leads the voltage by $\pi/2$. The resistance of the shell to $\mathbf{I}_R$ is given by

$$R_w = \frac{\rho\pi 2a}{l_w t} \tag{1-81}$$

Therefore, $\mathbf{I}_w$ is obtained from

$$\mathbf{I}_w = \frac{\mathbf{E}_w}{R_w} = -\frac{jA_w\mathbf{H}_R w l_w t}{\rho\pi 2a} \tag{1-82}$$

Equating Eqs. (1-82) and (1-78*a*),

$$\mathbf{H}_w = -\frac{\mathbf{H}_R 2jA_w wt}{\rho a} \tag{1-83}$$

From Eqs. (1-83) and (1-78),

$$\mathbf{H}_o = \mathbf{H}_R\left(1 + \frac{2jA_w wt}{\rho a}\right) \tag{1-84}$$

If
$$\gamma = \frac{2A_w wt}{\rho a} = \frac{2\pi^2 df t}{\rho} \tag{1-85}$$

$$\mathbf{H}_o = \mathbf{H}_R(1 + j\gamma)$$

Therefore,
$$\mathbf{H}_R = \mathbf{H}_o\left(\frac{1 - j\gamma}{1 + \gamma^2}\right) \tag{1-86}$$

If
$$P = \frac{1}{1 + \gamma^2} \quad \text{and} \quad Q = \frac{\gamma}{1 + \gamma^2} \tag{1-87}$$

$$\mathbf{H}_R = \mathbf{H}_o(P - jQ)$$

$$\boldsymbol{\Phi}_w = \mathbf{H}_o A_w(P - jQ) \tag{1-88}$$

This is identical to Eq. (1-58), except that the permeability is obviously assumed to be that of the free space inside the work, i.e., $\mu = 1$.

The formulas are reasonably accurate when the work is nonmagnetic and the current depth is greater than three times the wall thickness, i.e.,

$$\delta > 3t \tag{1-89}$$

The power equation Eq. (1-67) can be used provided it is remembered that A_w is the total cross section bounded by the outer diameter of the work, i.e., d_w cm.

The P and Q curves are plotted on Fig. 1-11 and an example is given below:

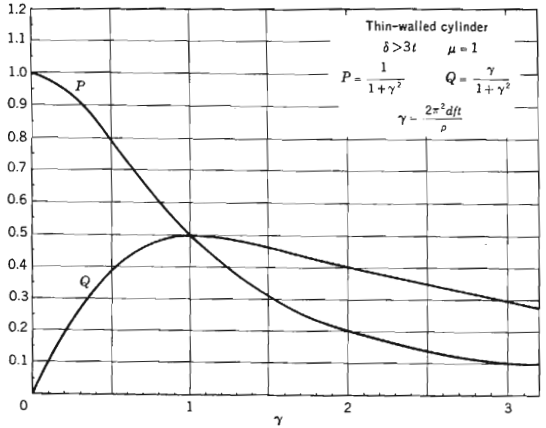

FIG. 1-11. P and Q functions—thin-walled cylinder.

Example 1-6

Metal	Stainless steel
Required power, P_w	5 kw = 5×10^3 watts
Current frequency, f	3,000 cps
Resistivity, ρ	120 microhm = 1.2×10^5 abohm-cm
Permeability, μ	1 gauss per oersted
Wall thickness, t	0.125 in. = 0.318 cm
Work diameter, d_w	3 in. = 7.6 cm
Work length, l_w	8 in. = 20.3 cm

It is required to find the surface magnetizing force necessary to induce the required power into the work.

From Eq. (1-1) the current depth is

$$\delta = \frac{l}{2\pi}\sqrt{\frac{\rho}{\mu f}} = \frac{(1.2)^{1/2}(10^4)^{1/2}(10)^{1/2}}{(2)(\pi)(30)^{1/2}(10^2)^{1/2}} = 1.05 \text{ cm}$$

As $3t = 3 \times 0.318 = 0.955$, and $\delta = 1.05$, a "thin-walled" formula can be used. From Eq. (1-85),

$$\gamma = \frac{2\pi^2 \, dft}{\rho} = \frac{(2)(\pi)^2(7.6)(3{,}000)(0.318)}{(1.2)(10^5)} = 1.2$$

From Fig. 1-11, $Q = 0.45$. Using Eq. (1-67),

$$H_o^2 = \frac{P_w \times 10^8}{2.5 f l_w \mu A_w Q} = \frac{(5)(10)^3(10)^8}{(2.5)(3{,}000)(20.3)(\pi)(3.8)^2(0.45)}$$

$$= 16.0 \times 10^4$$

Therefore, $H_o = 400$ oersteds

In the case where $t > \delta/3$, a more accurate formula must be used, because the current density is not reasonably constant across the wall thickness. The differential equation is the same as in the solid case.

$$\frac{d^2\mathbf{H}}{dr^2} + \frac{1}{r}\frac{d\mathbf{H}}{dr} - k^2 j\mathbf{H} = 0 \qquad (1\text{-}23)$$

However, the boundary conditions are affected by the hollow center. In the general solution

$$\mathbf{H} = AI_o(kr\sqrt{j}) + BK_o(kr\sqrt{j}) \qquad (1\text{-}23a)$$

The term B was assumed to be zero in the solid cylindrical case, i.e., when $r = 0$. But in the hollow cylinder, the boundary is at $r = b$, so the full expression in Eq. (1-23a) has to be used. By an analysis somewhat similar to that in the solid cylindrical case, but including the inner boundary condition $r = b$ for the work inside diameter ID

$$P - jQ = \frac{2}{ka}\left[\frac{(\text{bei}'\, ka - j\,\text{ber}'\, ka) + c(\text{kei}'\, ka - j\,\text{ker}'\, ka)}{(\text{ber}\, ka + j\,\text{bei}\, ka) + c(\text{ker}\, ka + j\,\text{kei}\, ka)}\right] \qquad (1\text{-}90)$$

$$\text{where } c = \frac{(\text{ber}\, ka + j\,\text{bei}\, ka) - (2\mu/ka)(\text{bei}'\, ka - j\,\text{ber}'\, ka)}{(\text{ker}\, ka + j\,\text{kei}\, ka) - (2\mu/ka)(\text{kei}'\, ka - j\,\text{ker}'\, ka)} \qquad (1\text{-}91)$$

Simplifying and rationalizing the above,

$$P = \frac{2}{ka}\left(\frac{cd + ef}{d^2 + f^2}\right) \qquad (1\text{-}92)$$

$$Q = \frac{2}{ka}\left(\frac{cf - de}{d^2 + f^2}\right) \qquad (1\text{-}93)$$

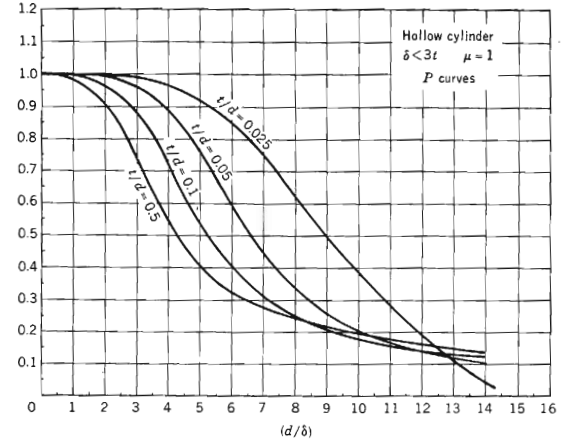

FIG. 1-12. P functions—hollow cylinder.

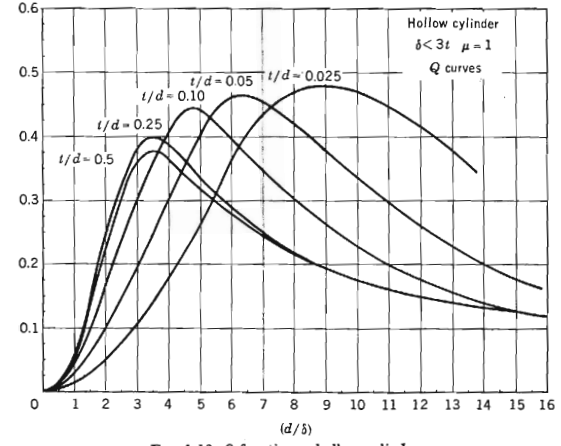

FIG. 1-13. Q functions—hollow cylinder.

where $c = (\text{bei}' ka - \alpha \text{ kei}' ka - \beta \text{ ker}' ka)$

$d = (\text{ber } ka - \alpha \text{ ber } ka + \beta \text{ kei } ka)$

$e = (\alpha \text{ ker}' ka - \beta \text{ kei}' ka - \text{ber}' ka)$

$f = (\text{bei } ka - \alpha \text{ kei } ka - \beta \text{ ker } ka)$

and

$$\alpha = \frac{(\text{ker } kb - 2\mu/kb \text{ kei}' kb)(\text{ber } kb - 2\mu/kb \text{ bei}' kb)}{(\text{ker } kb - 2\mu/kb \text{ kei}' kb)^2 + (\text{kei } kb + 2\mu/kb \text{ ker}' kb)^2} + \frac{(\text{bei } kb + 2\mu/kb \text{ ber}' kb)(\text{kei } kb + 2\mu/kb \text{ ker}' kb)}{(\text{ker } kb - 2\mu/kb \text{ kei}' kb)^2 + (\text{kei } kb + 2\mu/kb \text{ ker}' kb)^2}$$

$$\beta = \frac{(\text{bei } kb + 2\mu/kb \text{ ber}' kb)(\text{ker } kb - 2\mu/kb \text{ kei}' kb)}{(\text{ker } kb - 2\mu/kb \text{ kei}' kb)^2 + (\text{kei } kb + 2\mu/kb \text{ ker}' kb)^2} - \frac{(\text{ber } kb - 2\mu/kb \text{ bei}' kb)(\text{kei } kb + 2\mu/kb \text{ ker}' kb)}{(\text{ker } kb - 2\mu/kb \text{ kei}' kb)^2 + (\text{kei } kb + 2\mu/kb \text{ ker}' kb)^2}$$

Curves of the functions in Eqs. (1-92) and (1-93) are shown in Figs. 1-12 and 1-13. As the cylinder-wall thickness is no longer negligible, it is shown as a third variable and the curves are plotted for varying ratios of t/d. An example is given in which the workpiece of Example 1-6 is heated at 10,000 cps.

Example 1-7

Metal	Stainless steel
Required power, P_w	5 kw $= 5 \times 10^3$ watts
Current frequency, f	10,000 cps
Resistivity, ρ	120 microhm-cm $= 1.2 \times 10^5$ abohm-cm
Permeability, μ	1 gauss per oersted
Wall thickness, t	0.125 in. $= 0.318$ cm
Work diameter, d_w	3 in. $= 7.6$ cm
Work length, l_w	8 in. $= 20.3$ cm

$$\delta = \frac{1}{2\pi}\sqrt{\frac{\rho}{\mu f}} = \frac{(1.2)^{1/2}(10^4)^{1/2}(10)^{1/2}}{(2)(\pi)(10^4)^{1/2}} = 0.55 \text{ cm}$$

$$3t = 3 \times 0.318 = 0.955$$

Therefore, the "thin-walled" curves in Fig. 1-11 cannot be used, and the hollow-cylinder curves in Fig. 1-13 must be used, as δ is not greater than $3t$. Now

$$\frac{d}{\delta} = 7.6/0.55 = 13.9$$

and

$$\frac{t}{d} = 0.318/7.6 = 0.042$$

Therefore, from the curve $t/d = 0.05$, $Q = 0.225$.
From Eq. (1-67)

$$H_o^2 = \frac{P_w \times 10^8}{2.5 f l_w A_w Q \mu} = \frac{(5)(10^3)(10^8)}{(2.5)(10^4)(20.3)(\pi)(3.8)^2(0.225)}$$

$$= 9.55 \times 10^4$$

Therefore, $H_o = 309$ oersteds

It is interesting that considerably less magnetizing field is required for the same workpiece if a higher frequency is used.

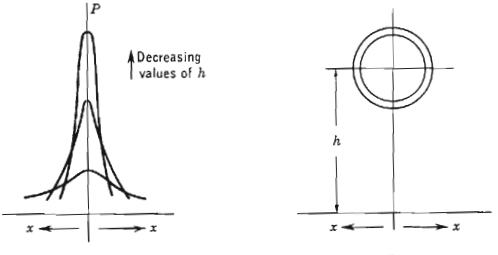

(a) (b)

FIG. 1-14. Power distribution in a flat plane from single-conductor proximity heating.

Proximity heating can only be approximated quantitatively, as many variables exist, but some idea of power input can be obtained from (5)

$$P = \frac{l_w I_c^2}{h} \sqrt{\mu f \rho} \times 10^{-9} \quad \text{watt} \tag{1-94}$$

where l_w = work length, cm
I_c = conductor current, amp
h = distance between conductor center line and sheet, cm
and ρ, f, and μ are as before.

Figure 1-14*a* shows the effect of bringing the conductor close to the work, i.e., decreasing h.

In general, proximity heating effects are utilized to produce a closely defined heat pattern rather than a given amount of power. This, combined with the difficulty of calculating the magnetizing field, usually results in a coil design determined purely by the shape and dimensions of the pattern required. However, some quantitative idea of the flux pattern can be obtained using equipotential methods; this is discussed in Chap. 4.

1-6. SUMMARY AND RELATIONS TO APPLICATIONS

It is interesting to compare the simple transformer equation for induced power in a long cylinder, Eq. (1-5), with Eq. (1-67), using the approximation for Q when d/δ is large, i.e., $Q = 2\delta/d$.

$$P_w = 2.5fH_o^2 l_w \mu A_w Q \times 10^{-8} \quad \text{watt} \tag{1-67}$$

Therefore $$P_w = \frac{5fH_o^2 l_w \mu A_w \delta}{d_w} \quad \text{watt}$$

Now for a long solenoid, the peak magnetic intensity is given from

$$H_o = \frac{0.4\pi N_c I_c \sqrt{2}}{l_w} \quad \text{oersteds} \tag{1-95}$$

Therefore $$P_w = \frac{0.4f\,\delta\pi^3 N_c^2 I_c^2 \mu \times 10^{-8}}{l_w}$$

But from Eq. (1-53)

$$\mu f = \frac{\rho}{4\pi^2 \delta^2}$$

Therefore $$P_w = \frac{N_c^2 I_c^2 \rho\pi\, d \times 10^{-9}}{\delta\, l_w} \quad \text{watt}$$

Now Eq. (1-5) is

$$P_w = \frac{N_c^2 I_c^2 \rho_w \pi\, d_w \times 10^{-9}}{\delta_w\, l_w} \quad \text{kw} \tag{1-5}$$

Remembering that in Eq. (1-5) ρ_w is in microhm centimeters, and ρ abohms $= \rho_w \times 10^3$ microhms, and converting to watts

$$P_w = \frac{N_c^2 I_c^2 \rho\pi\, d_w \times 10^{-12} \cdot 10^3}{\delta_w\, l_w}$$

Therefore these equations are identical, proving Eq. (1-67) and making it clear that it should be used only for small-diameter pieces where $d/\delta < 8$. This is also true for all shapes, and illustrates that the fundamental phenomenon of induction heating is nothing more than a simple transformer action.

Chapter 4 will outline complete design procedures by which coils to produce the required magnetic intensity are designed around the application specification. Typical applications and specifications are given in Chap. 3. The complete system, including coil ampere-turns, volts per turn, power input, power factor, etc., centers around the coil, which in turn is designed solely to produce the required power input or heat pattern in the work.

CHAPTER 2

HEAT AND METALLURGICAL EFFECTS

2-1. HEAT CONDUCTION IN INDUCTION HEATING

The major cause of the special type of conduction of heat usually encountered in induction heating is the skin effect. This results in heat being generated *inside* the surface of the metal, the amount falling off exponentially toward the center of the piece, just as current drops toward the center (Fig. 1-4). In general, the power generated (or the heating effect) falls off from the surface about three to four times as rapidly as the current effect. For example, if at a certain depth the current had dropped to three-quarters of its surface value, the quantity of heat or power generated would be about one-quarter of its surface value. Therefore, in any consideration of induction heating applications, this relation between heat depth and current depth should always be remembered.

In through-heating for forging, the best type of current would be direct current as it would evenly heat the whole workpiece. As this is impossible using induction principles, the lowest frequency should be used, consistent with avoiding flux cancellation, as pointed out in Chap. 1. This results in the deepest current and heat penetration and means that the heat must conduct along the shortest distance to attain uniform temperature distribution. However, for surface hardening the heat must be localized only at the surface, and the skin depth should therefore be small. This means a high-frequency current generating heat only near the surface.

Another important factor is time. Most production lines using induction heating equipment require high production rates and short heating times. This helps in surface heating, as heat conduction away from the surface is minimized. For through-heating the heat must be conducted to the center of the piece and must be generated without overheating and perhaps melting the surface. Fortunately, nearly all metals that are surface-heated are steel alloys, in which low heat conductivity reduces heat flow from the surface. Most through-heating is done with nonferrous metals of high heat conductivity, which assists in heat flow to the center. Considerable through-heating is also carried out on steel, and other low-conductivity metals are receiving attention in this application of induction heating. In these

instances, time has to be increased or a soak chamber used between heats to equalize cross-sectional temperatures.

The major factors in heat and temperature distribution are therefore seen to be current depth, time, and heat conductivity. The basic induction

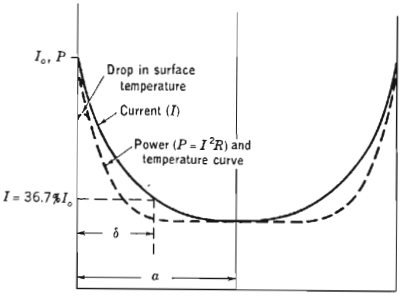

(*a*) Low-frequency heating of cylinder

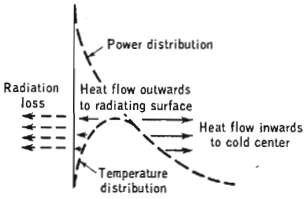

(*b*) Surface effect of radiation loss

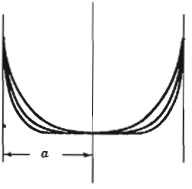

(*c*) High-frequency heating of cylinder

FIG. 2-1. Temperature distributions in induction heating.

heating equation, Eq. (1-1), shows that current depth is a function of frequency, resistivity, and permeability. However, for surface hardening, the heat must be localized only at the surface; therefore the skin depth should be small. This means a high-frequency current generating heat near the surface only.

The characteristic physical properties of the metal (emissivity, resistivity, thermal conductivity, and permeability) play a large part in induction heating. Figure 2-1 shows the typical effects of induction heating at low

and high frequencies. But during the heating process most of these properties change in value, so it is useful to know their relationship to temperature. In general, the resistivity increases with temperature in nearly all metals, which increases the current depth. This is advantageous in through-heating, as the heating effect (or power generated) penetrates further, resulting

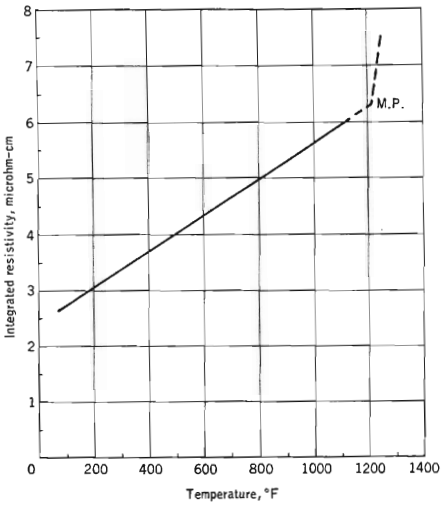

FIG. 2-2. Integrated resistivity vs. temperature—pure aluminum (integrated from room temperature, 70°F).

in a more uniform temperature distribution. Usually this increase in resistivity is linear with temperature rise, so the average or integrated resistivity between room temperature and the final required temperature can be used to derive a reasonably approximate value for the average current depth.

Figure 2-2 shows the integrated resistivity of pure aluminum; Fig. 2-3 gives that of common steel alloys. Similar curves for other metals commonly encountered in induction heating are given in Appendix B. These will be used later in calculating coil and system requirements for different applications and can be used as references for calculations of depth of current penetration.

Example 2-1

Find the *average* depth of current penetration δ in. for the following cases: (*a*) 0.44 per cent carbon steel heated to 1400°F at 960 cps with a magnetizing field of 1,000 oersteds; (*b*) pure aluminum heated to 1000°F at 60 cps.

(*a*) From Fig. 2-3, the integrated resistivity for 0.44 per cent steel to 1400°F is 54 microhm-cm. From Fig. 2-3*A*, the depth is seen to be 0.085 in. (column *D*). It is interesting that if the steel were nonmagnetic, the depth would be 0.5 in. (from column *B*).

(*b*) From Fig. 2-2, the integrated resistivity is 5.7 microhm-cm for pure aluminum. Using Fig. 2-3*A*, one finds the depth to be 0.61 in. (from column *B*).

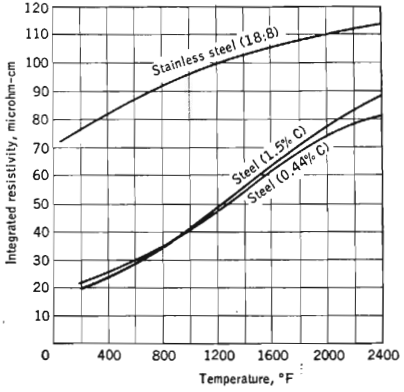

FIG. 2-3. Integrated resistivity vs. temperature—steel alloys (integrated from room temperature, 70°F).

The first example illustrates that greater heat uniformity will result from induction heating steel above the Curie point in the nonmagnetic temperature range. Unfortunately, in this range, cancellation of flux occurs, with resultant loss in power transfer and efficiency. In practice, small bars of nonmagnetic steel can not be heated with the same efficiency as magnetic steel bars of the same diameter. This is illustrated in Chap. 3, which describes selection of frequency for varying diameters.

Thermal-conductivity values usually rise with temperature, which assists in through-heating applications, as the higher the temperature, the more even is its distribution across a workpiece. One exception is steel thermal

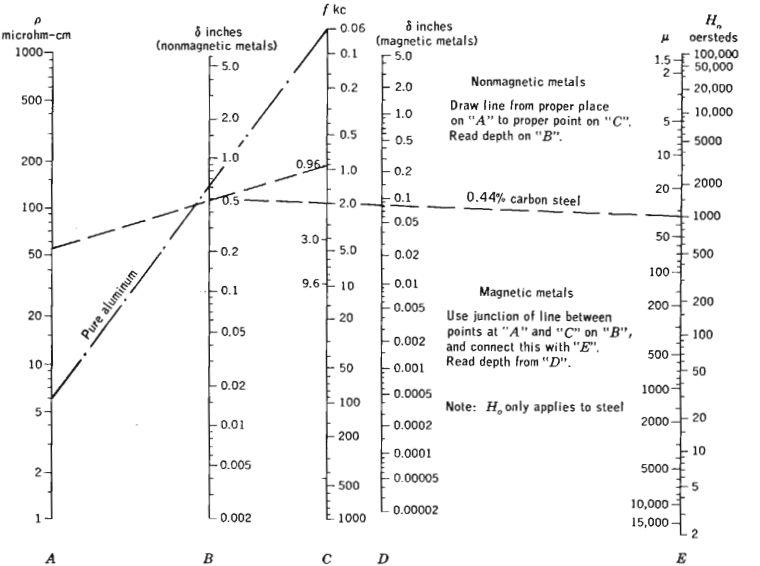

FIG. 2-3A. Depth-of-current-penetration nomograph.

conductivity, which falls with temperature. Considerable surface heating is carried out with steel, and this property is advantageous because it tends to slow down heat conduction to the center of the piece. Figure 2-4 shows some typical variations of thermal conductivity with temperature for

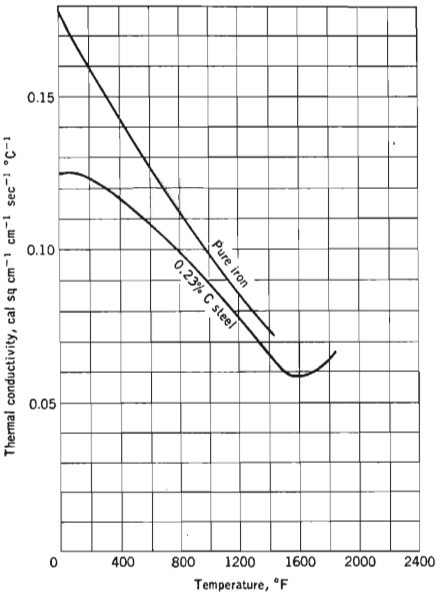

FIG. 2-4. Thermal conductivity vs. temperature—iron and steel.

various metals. Even if the nonferrous alloys rise in thermal conductivity, the values are very low compared with that of steel, so that even temperatures are generally achieved.

2-2. TEMPERATURE DISTRIBUTION IN A BUSBAR

The heat flow across a current-carrying busbar is of some importance in determining the dimensions of the bar when water-cooled. Figure 2-5 shows

a busbar of width 1 in. and thickness t in., water-cooled along one edge and carrying a current I amp. By considering the heat flow across the bus to the water-cooled edge, held at θ_c°C, one can derive the following expression for

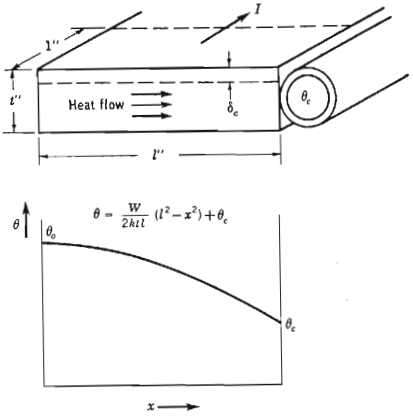

FIG. 2-5. Temperature drop across a water-cooled busbar.

the temperature at any point X from the hot edge:

$$\theta^\circ = \frac{W}{2ktl}(l^2 - x^2) + \theta_c \tag{2-1}$$

where θ° = temperature at x in., °C
W = heat in 1 in. of bus due to I, watts
I = current along bus, amp
k = thermal conductivity, watts in.$^{-1}$ °C^{-1}
t = bus thickness, in.
l = bus width, in.
θ_c = temperature of coolant, °C

To find the temperature θ_o at the hot edge, let $x = 0$.

$$\theta_o = \frac{Wl}{2kt} + \theta_c \tag{2-2}$$

Example 2-2

Given a busbar with the following current and frequency:

Material ..... copper
Width, l ..... 5 in.
Current, I ..... 2,000 amp
Frequency, f ..... 200,000 cps
Coolant temperature, θ_c ..... 15°C
Thermal conductivity, k ..... 10 watts in.$^{-1}$ °C^{-1}
Resistivity, ρ ..... 2×10^{-6} ohm-cm

To find the necessary thickness t, in., to keep the temperature rise $\theta_o - \theta_c$ across the bus to 25°C, assume the current is flowing in a depth δ_c (equivalent current depth).

The resistance per in. is given from

$$R/\text{in.} = \frac{\rho}{l\,\delta_c} = \frac{(2)(10)^{-6}(200{,}000)^{\frac{1}{2}}}{(5)(1.98)(2)^{\frac{1}{2}}}$$

$$= 25.3 \times 10^{-6} \text{ ohm/in.}$$

The expression for δ_c is derived from Eq. (1-1).

Therefore the loss per inch is given from

$$W = I^2R/\text{in.} = (2{,}000)^2(25.3)(10)^{-6}$$

$$= 101.2 \text{ watts/in.}$$

Rewriting Eq. (2-2),

$$t = \frac{Wl}{(\theta_o - \theta_c)2k}$$

$$= \frac{(101.2)(5)}{(2)(10)(25)} = 1.012 \text{ in.}$$

This is the necessary thickness to keep the temperature drop down to 25°C, which is considered good practice.

2-3. THE METALLURGY OF STEEL

Magnetic steel has certain properties over and above those of other metals and these are very important in induction heating. Chief among these properties is permeability, which varies considerably with temperature. Equation (1-1) shows the effect of this change of permeability on the current depth; Eq. (1-67) illustrates how the power input to the work is also a function of permeability. In general, the permeability becomes unity at

temperatures between 1275 and 1600°F, depending on the intensity of the magnetizing field and the alloy content of the steel.

Hopkinson (55) showed that for very weak fields, the permeability actually rises, whereas in strong fields it falls off rapidly at 1400 to 1475°F to about one-hundredth of its value. Nickel has the same effect at about 600°F (55). The following table gives the magnetic change points of common metals (61).

TABLE 2-1. MAGNETIC CHANGE POINTS

Metal	*Temperature, °F*
Iron	1420
Cobalt	2105
Nickel	680
Nickel-iron (30 Ni–70 Fe)	160
Permalloy (78 Ni–22 Fe)	1020
Nickel-copper (Thermalloy, Thermoperm)	50–160
Carbon steel (medium)	1330

This critical temperature is called the Curie point, in honor of the pioneer of much of the work on magnetization (56). Molybdenum and silicon in steel increase the Curie point; manganese and nickel decrease it.

At this stage it is advisable to consider the iron-carbon diagram, as both magnetic and hardening effects can be estimated from it. Figure 2-6 shows a simplified form with the various transformation lines. The line *PSO* divides the two crystalline structures of the basic or pure iron, ferrite. Below *PSO*, ferrite is a body-centered cubic lattice (*bcc*) with eight corner atoms and one in the lattice center. This structure results in a magnetic material. Above *PSO* (or the Ac_1 line) the ferrite starts to be transformed to a face-centered cubic lattice (*fcc*) with eight corner atoms and six face-centered atoms, or a total of fourteen. This is a more compact lattice and therefore the steel shrinks in volume. Between the Ac_1 and the Ac_3 lines, steel with less than 0.83 per cent carbon is a mixture of the transformed ferrite (austenite), which is nonmagnetic, and ferrite. Above the Ac_3 line, all the ferrite has been transformed to austenite and the steel is nonmagnetic. This line is the "critical line," and the temperature at which it occurs is a function of the carbon content.

Below the Ac_1 line the diagram indicates that steel has two components, pearlite and ferrite. The ferrite-austenite transformation is explained above. Pearlite is a mixture of ferrite and cementite, the cementite being ferrite and carbon in layers. What happens below the Ac_1 line is that carbon is incompatible with iron at these temperatures and will dissolve in it only up to 0.008 per cent. Above the AC_1 line the cementite (or iron carbide) starts to go into solution with the transformed ferrite lattice structure

(austenite). This structure *is* compatible with carbon. Therefore, the pearlite content (cementite and ferrite) decreases and the austenite increases in temperature until the Ac_3 line is reached, where all the pearlite has been transformed into austenite. This is called a "solid solution."

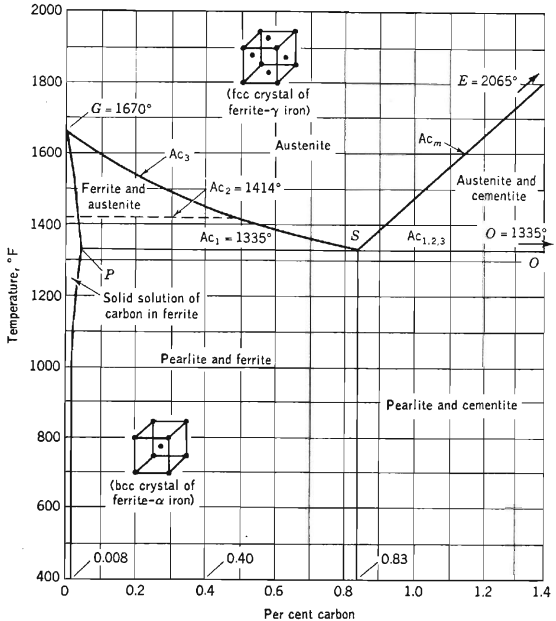

FIG. 2-6. Iron-carbon equilibrium diagram. (*From "ASM Metals Handbook,"* 1947.)

If the steel is allowed to cool, exactly the same process occurs in reverse. Some of the austenite reverts to ferrite below the Ac_3 line. Below the Ac_1 line all the austenite has changed, and the main constituents are pearlite (the dissolved atoms of carbon solidifying out of solution to form cementite) and ferrite.

Two other points should be noted from Fig. 2-6. At the 0.83 per cent carbon line, the steel is in a eutectoid state. This means that when the point

S is reached, the Ac_3 and Ac_1 lines must meet and the transformation from pearlite to austenite is instantaneous, with no intermediate or partial solution state. It also implies that the optimum combination of ferrite and cementite, as pearlite, is at 0.83 per cent carbon. Above this percentage the excess carbon forms extra cementite; below it the lack of carbon results in pure iron or ferrite.

The mechanics of hardening are not fully explained by the iron-carbon diagram; time is also a very important variable. As shown above, if the steel is allowed to cool slowly, the transformations occur exactly in reverse; the cold steel is structurally the same as in its original state before heating. If this cooling rate is sufficiently increased by a quench, such as a water or oil spray, the transformation is completely different. Below the Ac_1 line the carbon does not separate out as pearlite but is retained in solution until about 450°F. Then a new transformation occurs and the carbon comes rapidly out of solution to form a new substance, martensite, a thin, hard, crystalline structure in which the crystals interlock to form a hard steel. With higher carbon content, the number of martensite crystals increases and the steel becomes harder. Therefore, by referring to Fig. 2-6, one can obtain the correct hardening temperature if 50 to 150°F is added to the Ac_3-line temperature. For example, a 0.4 per cent carbon steel should be heated to 1500 to 1600°F for complete hardening (57). The effects on hardening of the addition of different metals in steel alloys will be discussed later.

As one of the main advantages of induction heating is the very rapid speed of power input and temperature rise, steels which have rapid solution rates are most suitable. These include nearly all heat-treatment steels except "high-speed" steels containing high percentages of chromium and tungsten. Another advantage of this rapid heating rate is that considerable overheating of the surface above the critical temperature can be tolerated without deterioration, because grain growth is small during the short times involved. Surface temperatures as high as 400°F above the critical temperature are not uncommon (64). This often leads to greater surface hardness.

Times of 1 sec or less are not unusual in some applications, and plain carbon steel (1045) has been heated to hardening temperature in 0.3 to 0.5 sec.

A brief description of magnetization will be useful in understanding induction heating processes. Most materials can be divided into three magnetic classifications (58). The first group is paramagnetic and has unbalanced electron orbits which produce a magnetic moment. This results in the production of thermal energy in a magnetizing field; the material has a

permeability slightly greater than unity. Examples are aluminum and platinum. The second group, classified as ferromagnetic, contains three metals, iron, nickel, and cobalt, which have magnetic permeability values many times greater than unity. The third group, called diamagnetic, has balanced electron orbits, with the resultant magnetic moment of zero. A magnetizing field will not affect the magnetic moment of the complete atom but will exert some influence on each electron orbit. This results in permeability values slightly less than unity. Examples are copper, gold, and

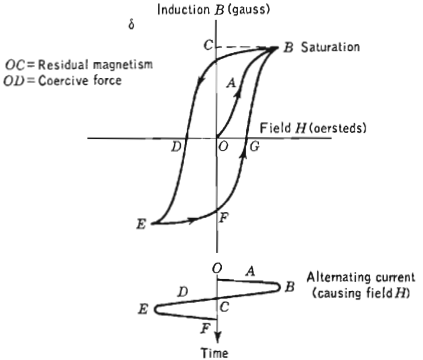

FIG. 2-7. Hysteresis curve.

bismuth. For the purposes of induction heating, all materials are said to have unity permeability except the ferromagnetic group.

When the magnetizing field is large and alternating (typical induction heating conditions), the ferromagnetic materials go through a cycle of magnetization. Most of the early work on this phenomena was carried out by Sir J. J. Ewing (59), who named the time lag encountered between induction and magnetic field *hysteresis*. Figure 2-7 illustrates a typical hysteresis curve, with the cycle starting at 0 and progressing through B (saturation point), C (point of zero field and residual magnetism), D (negative field required to reduce the magnetism to 0), and E (equivalent point to B). An approximate value for B, the saturation flux density, is usually given as 18,000 gauss for induction heating steels. In practice this is multiplied by 1.8 to give Eq. (1-75) (60). Hence the effective flux is 32,400 gauss. This value gives good results in practical coil designs and is used to plot Fig. 1-9.

2-4. SPECIFIC HEAT EFFECTS

Specific heat properties are utilized mainly in through-heating, where the total heat requirements can be accurately calculated. The quickest way to use the average specific heat over a certain temperature range is to convert it to pounds per kilowatthour. Figure 2-8 illustrates the pounds per kilo-

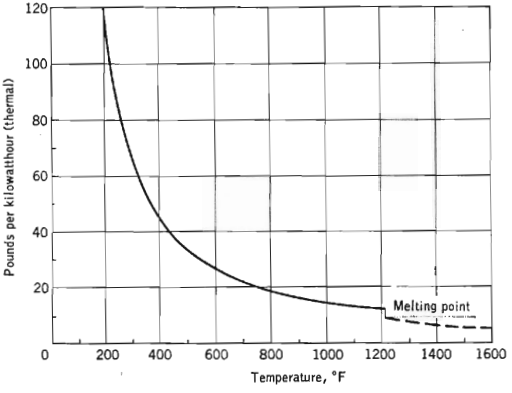

FIG. 2-8. Pounds per kilowatthour vs. temperature—aluminum (room temperature, 70°F).

watthour of aluminum; Appendix B contains the equivalent curves for other metals encountered in through-heating.

The definition of pounds per kilowatthour (lb per kwhr) is as follows:

$$\text{lb/kwhr} = \frac{3{,}413}{s\,\Delta\theta} \tag{2-3}$$

where $\Delta\theta$ = temperature rise, °F

s = average specific heat over $\Delta\theta$

The thermal, or useful, power required to raise the temperature by $\Delta\theta$ is obtained from

$$P_t = \frac{\text{lb/hr}}{\text{lb/kwhr}} \tag{2-3a}$$

Example 2-3

Find the power input to heat aluminum billets from room temperature to 1050°F at a production rate of 5,000 lb per hr.

Assume room temperature to be 70°F.

From Fig. 2-8, the pounds per kilowatthour to 1050°F are 14. As a production rate of 5,000 lb per hr is required, the power input to the billets must be:

$$\text{Power} = 5{,}000/14 = 357 \text{ kw}$$

from Eq. (2-3*a*).

2-5. HEAT RADIATION AND CONVECTION

Heat lost by radiation can play an important part in the slower forms of induction heating at high temperatures. Temperatures below about 1500 to 1600°F usually result in very little loss in most metals totally enclosed in the solenoid type of heating coils. Above these temperatures, losses become significant, especially in the through-heating of steel to temperatures in the region of 2400°F for forging. Most of these losses are conducted through the coil liner and removed by the coil cooling water.

For surface heating for hardening and joining, losses are usually radiated to the open air, and therefore the ambient temperature is lower than in a totally enclosed solenoid coil with an insulating liner. The heating rates are usually fast in these cases so that the energy loss is small.

The radiation loss is given by

$$P_R = 37\, e[T_s^4 - T_A^4]10^{-12} \qquad \text{watt/sq in.} \qquad (2\text{-}4)$$

where e = emissivity coefficient of the surface

T_s = surface temperature, °K ($T_s = \frac{5}{9}$°F + 255.4)

T_A = ambient temperature, °K ($T_A = \frac{5}{9}$°F + 255.4)

Figure 2-9 shows a set of curves for typical metals. These figures are based on a normal surface on the commercial type of workpiece. With temperature rise, many of the surfaces oxidize, which will usually increase the value of e and, therefore, of radiation losses. For instance, copper may vary in the value of e from 0.03 for a polished surface to 0.70 for a heavily oxidized surface (60).

From these considerations it can be seen that it is very difficult to calculate accurately the radiation losses to be expected in induction heating. In general, for surface hardening where power inputs usually have values of over 10 kw per sq in. and temperatures are about 1600 to 1800°F at the surface, the radiation loss to free air is less than 100 watts per sq in., or 1 per cent. Such a loss can be safely disregarded.

For through-heating of steel and other metals up to 2400°F, power inputs

are usually smaller; they may vary between 200 and 500 watts per sq in. Most coils are well insulated with liners so that the effective power lost in radiation from the work surface through the coil liner, averaged between room temperature and 2400°F, is usually about 25 watts per sq in. This is

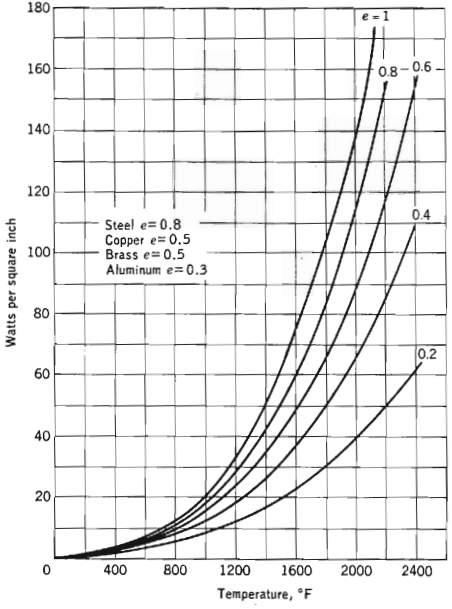

FIG. 2-9. Radiation losses.

not a negligible amount and should be calculated for the whole work-surface area. The coil liners used in through-heating will be described in detail in Chap. 4. Most of them vary in thickness between $\frac{3}{16}$ and 1 in. or more, and consist of either a metal inner shell and refractory felt or a cast, or a rammed solid refractory shell with steel rails. These materials act as good muffles and keep the heat inside the coil (the temperature drop radially across the total liner may be as high as 500 to 1000°F).

At this point, a temperature-conversion chart between degrees Fahrenheit

and centigrade, together with data on the color of steel at different temperatures, will often be useful (Fig. 2-10). It is seen that most hardening radiation colors occur between cherry red and light red (1400 to 1600°F); this empirical rule is often reasonably accurate for induction hardening.

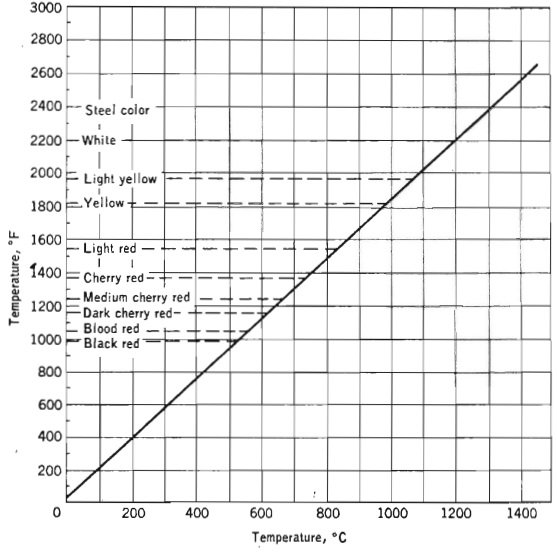

FIG. 2-10. Radiation color and temperature-conversion chart.

Convection losses are usually minute in induction heating, especially in surface hardening, where the power densities are very high. A good approximation is

$$P_{con} = 4.55(\Delta\theta)^{5/4}10^{-4} \quad \text{watt/sq in.} \tag{2-5}$$

where $\Delta\theta$ = temperature rise above ambient, °F

Example 2-4

Calculate the convection loss at 1800°F for an induction-hardened steel rod 1 in. in diameter, heated for a 2-in. length. Assume room temperature of 70°F.

$$P_{con} = (4.55)(1{,}730)^{5/4}(10)^{-4} = 9.45 \text{ watts/sq in.}$$

Therefore P_{con} (total) $= (9.45)(\pi)(1)(2) = 59$ watts

As most hardening power densities are of the order of 10 kw per sq in., 9.45 watts is a negligible proportion of the input.

2-6. TEMPERATURE DISTRIBUTION IN INDUCTION THROUGH-HEATING

While temperature distribution is important in surface heating as a factor in determining hardness depth, it affects the metal near the surface only. In through-heating the heating specifications usually include a maximum value of surface-to-center temperature differential. The heat flow to the center of the workpiece and the temperature distribution throughout the cross section should therefore always be determined. This fundamental difference between surface- and through-heating requirements is obvious when the forging, forming, and extruding processes following the heating are considered. Uniformity of product and die life are probably affected more by the evenness of temperature than by any other factor.

In general, the easiest ways to ensure the minimum temperature differential are to heat very slowly or to allow the work to soak out in a muffle or soak chamber. These methods are sometimes used, but in most induction heating systems, two of the prime requirements are fast production rates and minimum floor area. These requirements often eliminate the possibility of an extra soak chamber or of slow heating rates.

These considerations show the need for analyzing in some detail the actual temperature distribution in typical through-heating conditions. The mathematical steps used to derive the following equations are given in the various references and only the equations are quoted.

The classical heat-flow equation for the temperature θ_r°C at any radius r cm in a cylinder of radius a cm is given by the following expression (62):

$$\theta_r = \frac{P_o a}{k_c}\left[\frac{2kt}{a^2} + \frac{r^2}{2a^2} - \frac{1}{4} - 2\sum_{1}^{\infty} e^{-\frac{k\beta^2 t}{a^2}} \frac{J_o(\beta r/a)}{2J_o(\beta)}\right] \tag{2-6}$$

where θ_r = temperature (or temperature difference), °C
P_o = surface power density, cal sec^{-1} sq cm^{-1}
a = radius of cylinder, cm
k_c = thermal conductivity, cal sec^{-1} cm^{-1} °C^{-1}
k = thermal diffusivity, sq cm per sec ($k = k_c/\gamma_c$)
c = specific heat, cal gm^{-1} °C^{-1}
t = time, sec
r = radius (variable), cm
β_n = positive roots of $J_1(\beta) = 0$
$J_o(x)$ = Bessel's function of first kind and zero order
γ = density, gm per cu cm

This expression may be simplified by using the dimensionless function T, where

$$T = \frac{kt}{a^2} \tag{2-7}$$

and making T greater than 0.25. The summation becomes zero and Eq. (2-6) reduces to

$$\theta_r = \frac{P_o a}{k_c}\left(2T + \frac{r^2}{2a^2} - \frac{1}{4}\right) \tag{2-8}$$

Figure 2-11 shows Eq. (2-6) plotted for $\theta_r/(P_o a/k_c)$ as a function of r/a for different values of T. It is seen that up to $T = 0.25$, the heat flow is in a transient state, with the surface rising faster than the center. Above this

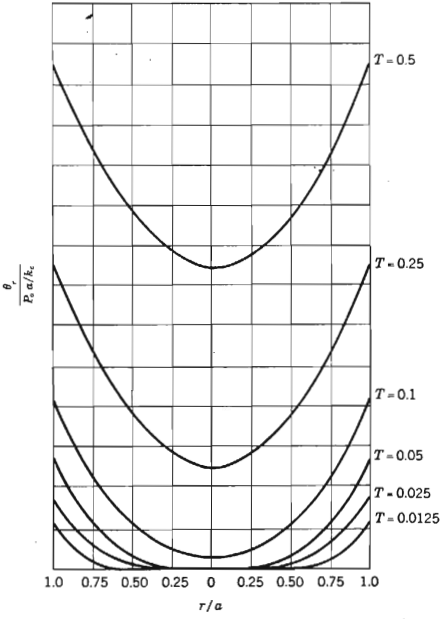

FIG. 2-11. Temperature-distribution curves—surface power input.

value, all points on the radius rise at the same value and a "steady-state" condition is achieved, assuming that all other values in Eq. (2-6) remain constant (63).

Equation (2-8) can be used to determine the temperature difference between surface θ_s and center θ_c after the steady-state condition has been reached, by using the values of $r/a = 1$ and $r/a = 0$.

Therefore
$$\theta_s = \frac{P_o a}{k_c}(2T + \tfrac{1}{4}) \tag{2-9}$$

and
$$\theta_c = \frac{P_o a}{k_c}(2T - \tfrac{1}{4}) \tag{2-10}$$

Therefore
$$\theta_s - \theta_c = \frac{P_o a}{2k_c} \tag{2-11}$$

This is simply the temperature drop across a slab of thickness $a/2$ with a surface power-density input of P_o and is quite accurate for most large diameters. However, all these equations are based on the assumption that radiation losses are negligible and that the heat is generated at the surface. Corrections have to be made for both factors.

2-7. EFFECT OF CURRENT DEPTH

The correction for finite current depth, and therefore for power generation inside the surface, is contained in the following equation (63):

$$\theta_r - \theta_c = \frac{P_o a}{2k_c}\left[\frac{r^2}{a^2} - \frac{1}{k_2}\left(\frac{X(k_2 r/a) - 1}{Z(k_2)}\right)\right] \tag{2-12}$$

where $X(k_2 r/a) = \text{ber}^2\,(k_2 r/a) + \text{bei}^2\,(k_2 r/a)$
$Z(k_2) = \text{ber}\,k_2\,\text{ber}'\,k_2 + \text{bei}\,k_2\,\text{bei}'\,k_2$
$k_2 = k_1 a$

Here k_1 is a function of current depth δ, where

$$k_1 = \frac{\sqrt{2}}{\delta} = \sqrt{\frac{8\pi^2 \mu f \times 10^{-3}}{\rho}} \tag{2-13}$$

where μ = permeability
f = frequency, cps
ρ = resistivity, microhm-cm

Equation (2-12) is plotted in Fig. 2-12 with $\theta - \theta_c/(P_c a/2k_c)$ as a function of r/a for different values of a/δ. It should be realized that Eq. (2-12) is based on the assumption that sufficient time t_1 has elapsed so that all points

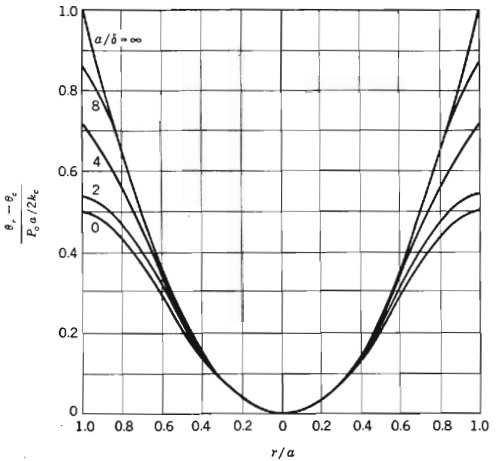

FIG. 2-12. Temperature-distribution curves—finite current depth.

on the radius are rising at a uniform rate, i.e., $T \geqslant 0.25$ in Eq. (2-7). The time t for this value of T is given by (63):

$$T = \frac{kt_1}{a^2} = \frac{k_c t}{\gamma c a^2} \qquad \geqslant 0.25 \tag{2-13a}$$

Therefore

$$t = \frac{\gamma c a^2}{4k_c} \tag{2-14}$$

Comparing Figs. 2-11 and 2-12, the result of a finite current depth δ can be seen to be a considerable change in distribution. The surface temperature is lowered in all cases except where $a/\delta = \infty$, i.e., $\delta = 0$ or $a \to \infty$.

The opposite extreme, where $a/\delta \to 0$, would obviously produce an infinitely small efficiency of power transfer, as the radius would be negligible compared with the current depth. From Chap. 1 this is seen to produce a

complete flux cancellation. From a practical viewpoint the value of $a/\delta > 1.5$ is usually used.

As before, Eq. (2-12) is used to determine the surface-to-center temperature differential by using a value of 1 for r/a.

$$\theta_s - \theta_c = \frac{P_a a}{2k_c}\left[1 - \frac{1}{k_2}\frac{X(k_2) - 1}{Z(k_2)}\right] \tag{2-15}$$

Equation (2-15) is corrected for radiation losses by the following equation:

$$\theta_s - \theta_c = \frac{P_n a}{2k_c}\left\{1 - \left[\frac{1}{P_n/P_a}\right]\left[\frac{1}{k_2}\right]\left[\frac{X(k_2) - 1}{Z(k_2)}\right]\right\} \tag{2-16}$$

where P_a = *total* power input, cal sec^{-1} sq cm^{-1}

P_n = *net* or effective power input (after radiation), cal sec^{-1} sq cm^{-1}

Radiation losses are therefore the difference between total power and net power inputs. The factor P_n/P_a will always be less than unity; therefore the value of the surface-to-center differential $(\theta_s - \theta_c)$ is reduced, as expected. When the radiation losses are negligibly small, $P_n/P_a \rightarrow 1$ and $P_n \rightarrow P_a$. Equation (2-16) then gives the same results as Eq. (2-15).

Converting Eqs. (2-13*a*) and (2-16) into practical units or fps,

$$\theta_s - \theta_c = \frac{0.084 P_n a}{k_c} F(P_n/P_a, k_2) \tag{2-17}$$

where $\theta_s - \theta_c$ = surface-to-center differential, °F

P_n = net power input, watts per sq in.

a = radius, in.

k_c = thermal conductivity, cal sec^{-1} cm^{-1} $°\text{C}^{-1}$

γ = lb per cu in.

The units of thermal conductivity are retained as values in tables and are usually expressed in these units. Appendix C contains a table of conversion factors for these and other units.

The correction factor $F(P_n/P_a, k_2)$ is given from

$$F(P_n/P_a, k_2) = 1 - \left[\frac{1}{P_n/P_a}\right]\left[\frac{1}{k_2}\right]\left[\frac{X(k_2) - 1}{Z(k_2)}\right] \tag{2-18}$$

This is plotted on Fig. 2-13 for different values of the ratio of radius to current depth a/δ. At large values of the radius a, the function tends to unity value and Eq. (2-17) becomes the simple equation of heat conduction

across a slab of thickness $a/2$ (assuming no radiation). The ratio a/δ is given by

$$\frac{a}{\delta} = \frac{a}{1.98}\sqrt{\frac{\mu f}{\rho}} \tag{2-18a}$$

Finally, the temperature distribution throughout the radius can be determined by taking the generalized version of Eq. (2-16).

$$\theta_r - \theta_c = \frac{P_n a}{2k_c}\left[\frac{r^2}{a^2} - \left[\frac{1}{P_n/P_a}\right]\left[\frac{1}{k_2}\right]\left[\frac{X(k_2 r/a) - 1}{Z(k_2)}\right]\right] \tag{2-19}$$

Figure 2-14 illustrates a typical set of temperature-distribution curves for the values shown when a steel billet 8 in. in diameter is heated up to forging

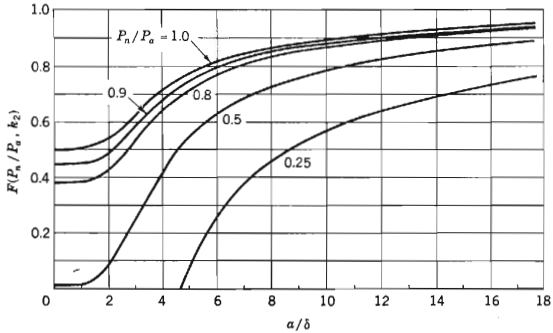

FIG. 2-13. Radiation correction factors.

temperatures. Comparing these curves with Fig. 2-12, for the curve of $a/\delta = 2$, the effect of radiation loss is immediate. It is obvious from Fig. 2-14 that at the surface, when $r/a = 1$, values of 0.25 or less for P_n/P_a will result in negative values for the surface temperature.

From Fig. 2-9, at about 2000°F the radiation to free air from steel would be about 120 watts per sq in. Assuming a total power input of 240 watts per sq in., this gives a value of $P_n/P_a = 0.5$. Figure 2-14 then shows that a negligible surface-to-center differential exists. With most through-heating coils, the thermal liner insulation reduces the radiation to about half that of free space. In this example, the resultant radiation would be 60 watts per sq in. Typical power inputs may range up to 500 watts per sq in. This

results in $P_n/P_a = (500 - 60)/500 = 0.88$. From Fig. 2-14, this shows about a 20 per cent difference between the differential calculated with and without radiation correction.

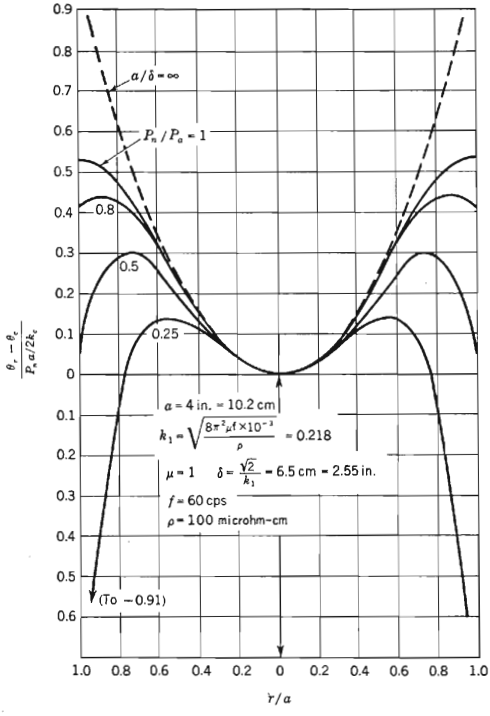

FIG. 2-14. Temperature distribution in a steel billet heated to 2100°F.

Example 2-5

Calculate the temperature differential in a cylindrical aluminum billet, given the following specifications:

Metal ..... Aluminum
Required *average* temperature, θ ..... 900°F

Production rate	4,000 lb per hr (during heating)
Radius, a	4 in.
Thermal conductivity at θ, k_c	0.38 cal cm^{-1} sec^{-1} $°C^{-1}$
Length, l	30 in.
Density, γ	0.097 lb per cu in.
Specific heat at θ, c	0.257
Permeability, μ	1
Frequency, f	60 cps
Resistivity at θ, ρ	8.4 microhm-cm
Assumed room temperature, θ_o	70°F

First, the time of heating t is determined from the mass of the billet M and the required production rate.

$$M = \pi a^2 l \gamma$$

$$= (\pi)(4)^2(30)(0.097) = 145 \text{ lb}$$

Therefore $$t = \frac{M \times 3{,}600}{\text{lb/hr}} = \frac{145 \times 3{,}600}{(4{,}000)} = 131 \text{ sec}$$

Then the factor T is derived from Eq. (2-13a):

$$T = (5.6)(10)^{-3} \frac{k_c t}{\gamma c a^2} = \frac{(0.38)(131)(5.6)(10)^{-3}}{(0.097)(0.257)(4)^2}$$

$$= 0.7$$

This value of T is greater than 0.25; therefore the steady-state heating time has been reached and Eq. (2-17) can be used. It is interesting to evaluate the time at which the conditions change from transient to steady-state. Using Eq. (2-13a) and the value of 0.25 for T,

$$t = \frac{T \gamma c a^2}{(5.6)(10)^{-3} k_c}$$

$$= \frac{(0.25)(0.097)(0.257)(4)^2}{(5.6)(10)^{-3}(0.38)} = 48.2 \text{ sec}$$

Therefore, up to 48.2 sec, the heating is in a transient state with the surface rising faster than the center.

The next step is to determine the net or useful thermal power density into the work. Using Eq. (2-3a) and Fig. 2-8,

$$P_t = \frac{4{,}000}{16} = 250 \text{ kw}$$

where P_t is the thermal power required.

The net power density is

$$P_n = \frac{P_t \times 10^3}{\text{surface area}} = \frac{P_t \times 10^3}{2\pi al}$$

$$= \frac{(250)(10)^3}{(2)(\pi)(4)(30)} = 330 \text{ watts/sq in.}$$

In order to use Fig. 2-13 to determine the value of $F(P_n/P_a, k_2)$, the ratio a/δ must be derived from Eq. (2-18*a*).

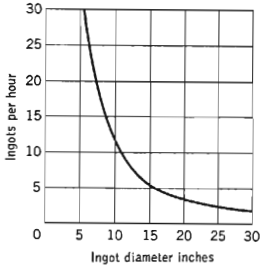

FIG. 2-15. Rates of through-heating for aluminum billets.

$$\frac{a}{\delta} = \frac{(4)(1)^{1/2}(60)^{1/2}}{(1.98)(8.4)^{1/2}} = 5.4$$

Radiation at $\theta = 900°\text{F}$ can be found from Fig. 2-9. This is

$$P_r = 5 \text{ watts/sq in.}$$

Therefore the total power-density input is P_a

$$P_a = P_n + P_r = 330 + 5$$
$$= 335 \text{ watts/sq in.}$$

The ratio P_n/P_a is

$$\frac{P_n}{P_a} = \frac{330}{335} = 0.985$$

Using the curve of $P_n/P_a = 1.0$ from Fig. 2-13, the value of $F(P_a/P_n, k_2)$ is 0.8, at $a/\delta = 5.4$.

Finally, Eq. (2-17) is used to determine the actual differential.

$$\theta_s - \theta_c = \frac{(0.084)(330)(4)(0.8)}{(0.38)} = 233°\text{F}$$

One result of through-heating with induction methods is that the high power input often results in high surface-to-center differentials, in some cases up to 200 to 300°F. This can produce considerable stress effects on the cross section of the billet; in some cases cracking has been observed. No accurate relation between differential and excessive stress has been established, but a rule of thumb of 50°F maximum per radial inch for nonferrous metals is reasonably accurate. Typical rates for aluminum heating, based on a final temperature of about 900°F, averaged from surface to center, are shown in Fig. 2-15 (21).

2-8. TEMPERATURE DISTRIBUTION IN INDUCTION SURFACE HARDENING AND HEATING

Here the problem is exactly the reverse of that in through-heating. The surface has to be brought up to and beyond the hardening temperature (the

Ac_3 line—Fig. 2-6) and quenched before any significant amount of heat flows in to the center. Therefore, the heating rate or power input is much higher. The transient condition usually occurs and the surface rises much faster than the center.

Figure 2-15*A* shows the relation between the ratio of temperature θ_x inside a distance x to the surface temperature θ_s, and the time t, distance x, and

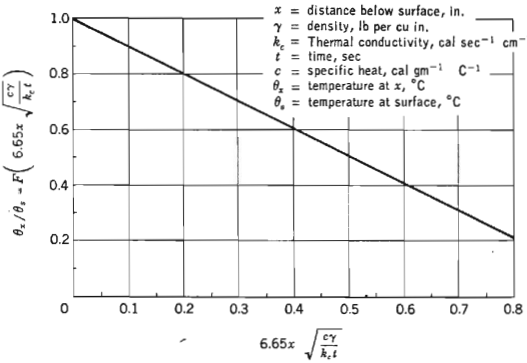

FIG. 2-15*A*. Temperature distribution below a surface raised to and maintained at a temperature θ_s.

physical properties of the metal. An example will illustrate how an approximation to the heating time can be made on the basis of certain assumptions.

Example 2-6

Metal	Steel
Hardened depth, x	0.03 in.
Critical temperature at x, θ_x	1500°F
Assumed surface temperature, θ_s	1700°F
Density, γ	0.283 lb per cu in.
Thermal conductivity at θ_x, k_c	0.06 cal cm^{-1} sec^{-1} $°C^{-1}$
Specific heat at θ_x, c	0.165 cal gm^{-1} $°C^{-1}$

To find the time t sec to bring the material at a depth x in. to a temperature of θ_x°F, assuming the surface is brought suddenly to a temperature θ_s°F and maintained at θ_s°F,

$$\frac{\theta_x}{\theta_o} = \frac{1{,}500}{1{,}700} = 0.88$$

From Fig. 2-15*A*, this gives a value of 0.1 on the x axis; therefore

$$6.65x\sqrt{\frac{c\gamma}{k_c t}} = \frac{(6.65)(0.03)(0.165)^{1/2}(0.283)^{1/2}}{(0.06)^{1/2}(t)^{1/2}} = 0.1$$

$$t = \frac{(6.65)^2(0.03)^2(0.165)(0.283)}{(0.1)(0.06)} = 0.31 \text{ sec}$$

Considerable work has been done by Losinsky (7) and others on the relationships between heat or power inputs, hardened depths, heat times, and frequencies. These factors are all interdependent; they also depend on whether the heating cycle is very rapid or allows some time for heat conduction. The rapid cycle allows just sufficient time to heat the hardened depth required, whereas the heat-conduction cycle allows some heat to flow inwards from the surface.

The heat-conduction cycle is usually carried out with high frequencies and results in heating about three times the actual hardened depth required. This is the preferred type, as the transition between hardened surface and soft core is more gradual than in the rapid cycle. Power densities are somewhat lower and heating times longer, allowing greater accuracy in time control.

Other factors affecting the hardened depth include the steel and its treatment prior to hardening, the quench type and material, and the coil design. A good induction steel is 1045 (0.45 per cent carbon) and the hardened depth usually decreases in value from a prior treatment of annealing (deep cases), normalizing (medium cases), or hardening and tempering (shallow cases). Therefore, the ideal prior treatment is hardening and tempering; a 1048 steel with a 0.030-in. case can be hardened to 757 Vickers Pyramid Number 30 on the surface with prior hardening and tempering. The same steel will result in only 550 Vickers Pyramid Number 30 with a prior treatment of normalizing, and 530 Vickers Pyramid Number 30 if previously annealed. In practice a normalized treatment prior to hardening results in a good hardness structure for the deeper cases. This is the usual induction heating method. A closely coupled coil will give the most uniform hardened depth of the minimum value. Coil designs are discussed in some detail in Chap. 4.

Figure 3-22 summarizes Losinsky's work, carried out mainly on a single-shot basis. Scanning curves on the basis of practical results are given in Figs. 3-23, 3-24, and 3-24*A*. In general, these curves illustrate the various factors influencing hardened depth.

Frequency is usually selected to give the optimum range of case depths. Table 2-2 illustrates frequencies most used in practice to obtain different hardened depths on bars of various diameters.

The preferred frequencies are given first, with alternatives in parentheses.

TABLE 2-2. SELECTION OF POWER SOURCE AND FREQUENCY FOR VARIOUS APPLICATIONS OF INDUCTION HARDENING (65)

Hardened depth, in.	Diameter of bar, in.	Frequencies used in practice, cps
0.015–0.050	¼–1	450,000
0.050–0.100	¼–⅝	450,000 (9,600)
	⅝–1	9,600; 450,000
	1–2	9,600 (3,000; 450,000)
	Over 2	9,600 (3,000)
0.100–0.200	¾–2	9,600; 3,000
	2–4	3,000 (960; 3,000)
	Over 4	960 (3,000)

As two other major factors, power density and heat time, also affect hardened depth, these frequency choices are arbitrary. In general, the lower frequency alternative of a choice of two or more can often be used with a higher power density. Referring to Figs. 3-23 and 3-24, it is seen that the same hardened case depth can be achieved at a lower frequency by using a higher power density, given the same time in the coil. For example, a case of 0.100 in. can be obtained at 9,600 cps, using 11 kw per sq in. in 2 sec. In the same time (2 sec), the same case depth requires 14 kw per sq in. at 3,000 cps.

Energy transfer is always more efficient at higher frequencies; Fig. 2-16 illustrates the relation for the four major frequencies (65). But as r-f generators for 500,000 cps are less efficient from input to coil output than motor-generator sets, the difference in over-all efficiency from line to bar is often small. As pointed out in Chap. 3, a consistent figure of 50 to 55 per cent efficiency (supply line to work), can be expected for all induction heating frequencies (except steel heated below the Curie point). It is often possible to obtain higher power densities more economically using machine-frequency equipment in preference to r-f generators.

The major factor is the case depths available at each frequency range; some depths are available only at radio frequencies. Power selection methods are described fully in Chap. 3, and surface-heating coils are covered in Chap. 4.

2-9. QUENCHES AND QUENCHING

The process of hardening, or the formation of martensite from austenite, is critically controlled by the rate of cooling. Natural quenching, or cooling, is rarely fast enough, even considering the rapid heating and shallow heated

depths resulting from induction heating. Nearly all hardening has to be achieved with forced quenches, using water, oil, brine, or forced air; water is used most often. The types of quench include spray, agitated-bath, or a

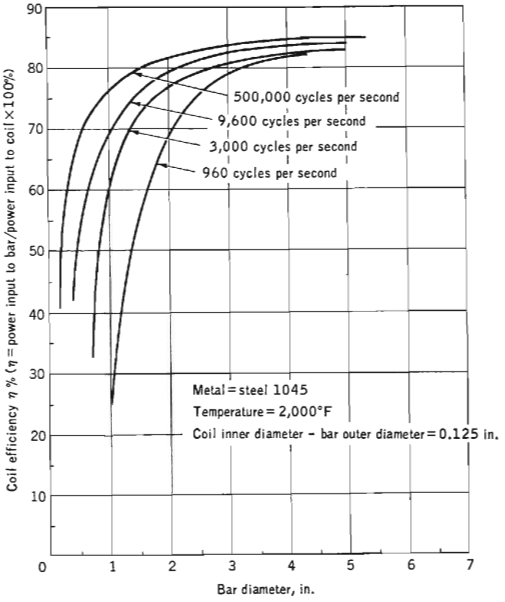

FIG. 2-16. Coil efficiencies for bar hardening at different frequencies.

combination of these two. Some steels, including the SAE 3100, 4100, and 52000 series, require a small delay time between shutting off power and quenching, to complete the process of carbide solution. The need for this delay has been eliminated in quenching steels in the SAE 1000 and 1300 series. Other factors affecting hardness include quenching time and the pressure, velocity, and direction of the quenching medium.

Figure 2-17 illustrates the six basic types of quenches used in induction hardening. Figure 2-17*a* and *b* shows the scanning quench, with the flat-surface type in *a* and the circular type in *b*. Either the work or the coil and

quench can scan according to the best mechanical layout. Angle of incidence is very important; experience has shown that up to 50° must be used. This allows the sprays to wash the surface with an even film of water or oil,

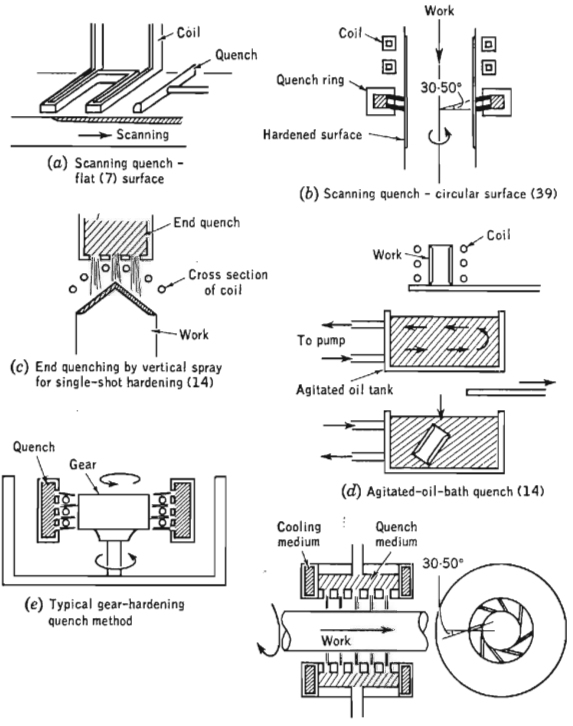

FIG. 2-17. Types of quenches used in induction heating.

resulting in an even depth of hardness and eliminating local overhardened spots. In both cases, a short distance is allowed between the time the work leaves the coil and the time it enters the quench. With accurate control of

the scanning speed, this distance results in an accurately controlled delay time for completing the carbide solutioning mentioned before. Nearly all shaft-hardening methods use the scanning quench shown in *b*, with the shaft itself rotating as well as traveling. End hardening is achieved by using a spray through the coil, as shown in *c*. A typical agitated-bath quench is illustrated in *d*; the work is statically heated, then dropped into the bath. This simple method is very effective and economical in small-part hardening and is also used for gear hardening. The coil can also be located inside the bath. In some cases the work is manually dropped into the coil when the operator judges that the temperature is high enough (39).

Figure 2-17*e* shows a "static" quench where the work remains in the coil after heating, the quench medium being sprayed in between the coil turns. This method is often used in gear hardening, with the gear rotating during heating and quenching to achieve full uniformity. Care should always be taken to drill the spray holes at an angle to the radius between 30 and 50°, as in the scanning case. A very useful combination of coil and quench is shown in Fig. 2-17*f*, where the coil structure includes channels containing the quench medium, which is forced out through spray holes on the inner coil face. This is particularly suited to single-shot or static hardening where it is desirable to reduce the delay time to a minimum. The heat can be turned off and the quench applied almost instantaneously.

The quench medium is determined by the steel and work shape. Water is used most often; it is suitable for low-alloy and carbon steels and for cast iron with straight shapes (shafts, flat surfaces, etc.). Oils, such as Sinclair Quenchol 521, are usually recommended for high-carbon steels and higher-hardness surfaces, and also for parts with nonuniform sections. Brine is used occasionally for steels of low hardenability, and air can be used for stainless steels. Air is also used in the form of compressed air sprayed through quench rings for small areas on alloy steels where the heat flow away from the area after heating is fast enough to quench the steel (65). In all cases of spray quenching, great care should be taken to maintain sufficient pressure at all points around the surface of the quench face to ensure even quenching.

Quenches are usually supplied from separate self-circulating systems with heat exchangers, pumps, temperature and flow controls, etc. Oil systems in particular should be adequately cooled, as fire hazards from the fine spray around the hot work are always present. A maximum temperature of 150°F is usually recommended. If a complete film can cover the work, or if it can be completely submerged, flash fires can be reduced.

Quenching cracks are sometimes encountered; the following precautions should always be taken: (1) minimize cracked pieces prior to treatment; (2) heat uniformly; (3) quench at the lowest acceptable temperature and as slowly as possible, consistent with required hardness; (4) cool and

quench uniformly; (5) eliminate sharp angles, uneven cross sections, etc. (67). Tempering immediately after quenching is also helpful in reducing cracking.

Carbon content in the steel hardened affects the possibilities of cracking. As a general rule, a maximum carbon content of about 0.44 per cent is recommended for water-quenched plain carbon steels. Higher carbon contents usually require oil, and pieces having splines, flanges, or sharp changes in shape should be of lower carbon content to reduce cracking at the sharp angles. Other characteristics known to affect the amount of cracking include coarse surface machining, seams, and surface defects.

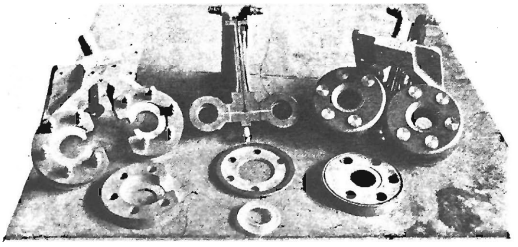

FIG. 2-18. Typical coil and quench assembly for scanning hardening of shafts. (*Westinghouse Electric Corp.*)

Tempered martensite spirals are occasionally produced during shaft hardening by scanning methods, with the shaft rotating as well as moving axially. These spirals result in soft areas and lack of uniformity of surface hardening. The causes include incorrect drilling of the angle of quench spray holes and subsequent prequenching, misalignment of the quench ring or shaft, distorted shafts, uneven quench pressure around the perimeter, and low quench pressure. In addition to correcting these faults, taking care to drill the holes at 45° to the radius, one can reduce the spirals by increasing the speed of rotation of the shaft.

When the quench ring is separate from the coil but mounted close to it, risk of induction heating is present. The ring is then made of nonmetallic material such as Micarta or another plastic.

Figure 2-18 shows the construction of a typical coil and quench for a scanning assembly used to harden automobile axle shafts. The use of plastic materials, in order to reduce induction heating of the quench itself, is clearly illustrated. The rugged nature of the whole assembly is typical of industrial design. This design corresponds to that shown in Fig. 2-17*b*.

A gear-hardening quench is seen in Fig. 2-19, illustrating the design of Fig. 2-17*e*. This is almost an agitated-bath type. Another example of a gear-hardening quench is shown in Fig. 3-25, and an agitated-bath quench can be seen in Fig. 3-26.

The importance of time in quenching is fully illustrated by isothermal transformation diagrams. The derivation and use of these curves are fully described in the literature (68) and will be only briefly mentioned here. The basis of the curves is that when steel is held in the austenitic state at any

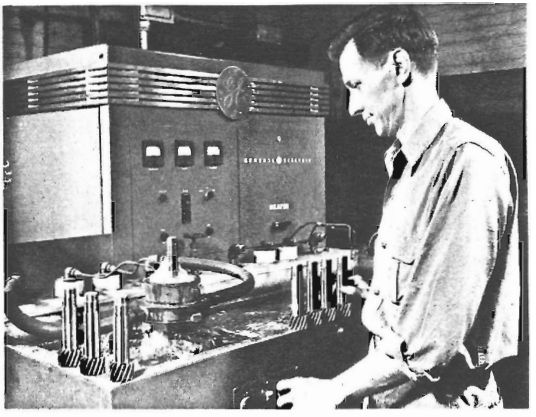

FIG. 2-19. Gear-hardening coil and quench. (*General Electric Corp.*)

temperature below the Ac_3 line, it is unstable and will transform in time until the amount of austenite is reduced to zero. In Fig. 2-19*A*, the top curve shows the extent of this transformation at 700°F, where the austenite content falls from 100 to 0 per cent between 30 and 250 sec. These curves are repeated for different temperatures, and the corresponding points for 0, 50, and 100 per cent transformation are plotted in the form of isothermal transformation lines, as shown on the lower curve in Fig. 2-19*A*. These are known as *S* curves; their shape is a function of the composition and grain size of the austenite. In general, an increase in either carbon or alloy content or grain size moves the nose of the curves to the right, i.e., retards transformation. This retardation is called the reaction rate and results in greater steel hardenability.

The main use of the curves is to select a quenching time short enough to miss the nose of the S curve during temperature drop. For instance, in the curve shown in Fig. 2-19A, the time required to drop the temperature from 1400°F (a typical hardening temperature) to 1000°F is shown as about 1 sec. This is the desired quench time, as it misses the S-curve nose.

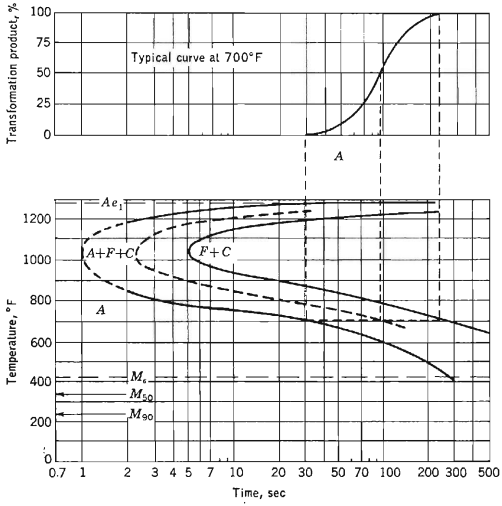

FIG. 2-19A. Typical isothermal transformation diagram.

Other information in the isothermal diagram is given by the lines M_s, M_{50}, M_{90}, and M_f, which indicate the temperatures at which martensite forms in various degrees, M_s indicating the beginning of martensite formation; M_{50} and M_{90}, the 50 and 90 per cent martensite-content temperatures; and M_f the completion of martensite formation. The letters A (austenite), F (ferrite), and C (carbide) indicate the phase state of the steel after it has been austenitized, then quenched and held isothermally within the time-temperature limits of the field. The Ae_1 line corresponds approximately to the Ac_1 line but actually represents the equilibrium transformation temperature. Above this line, austenite is partially unstable and will in time be transformed in part. As austenite is always present in this region, the line

representing *completion* of transformation can never enter it. Below this line, austenite is completely unstable and in time will be transformed entirely to ferrite and carbide.

2-10. EXAMPLES OF TEMPERATURE DISTRIBUTION AND HARDNESS PATTERNS IN SURFACE HEATING AND THROUGH-HEATING

The theory of induction heating temperature distribution was fully explained in Sec. 2-8. The case of magnetic steel is further complicated by the fact that in induction heating the surface may rise above the Curie point before the rest of the workpiece. The fact that power input was proportional to permeability in Eq. (1-67) indicates that the surface power input or heating rate will decrease as the Curie point is reached. At some point in from the surface, the temperature will still be below the Curie point, the steel will be magnetic, and the flux will be at a maximum. The flux increases from the center toward the surface and concentrates at the most magnetic cross sections. At this point the power input will be at a higher rate than at the surface and a "magnetic wave," illustrated in Fig. 2-20, is thought to appear (24). The wave is seen to move inwards from the surface with time until all of the billet is above the Curie point and the steel is nonmagnetic. At this time the distribution follows the conventional pattern described in Sec. 2-3.

It should also be noted that the equivalent depth of current penetration is greater in the nonmagnetic case and the slope of heat generated, proportional to current squared, is not so steep. This is immediately apparent from Eq. (1-1), where the current depth is seen to be proportional to the inverse square of the permeability. Also the nomograph in Fig. 2-3*A* gives an example of 0.44 carbon steel. Below Curie, this would have a current depth of less than 0.1 in. at 60 cps; above Curie the depth increases to 0.5 in.

A typical time-and-temperature curve for a steel billet is shown in Fig. 2-21, with the temperatures at the surface, at the center, and at the mid-point plotted against time of heating. Below Curie point the current depth is small and the surface temperature much higher than the temperature at the other two points. As the surface reaches the Curie temperature, its heating rate drops; a drop in the rate for the mid-point follows, and then the rate for the center drops. The billet is now entirely nonmagnetic and power input is proportionately lower, giving a lower heating rate.

The power input and current are also shown on the same illustration. The initial dip in the power and current curve is thought to be due to the sharp increase in resistivity of the steel and the resistance of the current path, which is at first shallow. This would decrease power drain. As the current

depth increases with time, the cross-sectional area of the current path increases faster than the resistivity, resulting in a net drop in resistance to the current, which increases, increasing power while the steel is magnetic. At the Curie point, power drops, as explained. Current rises as the current-path resistance drops, with permeability becoming unity; then it settles at a steady value as the current depth remains reasonably constant.

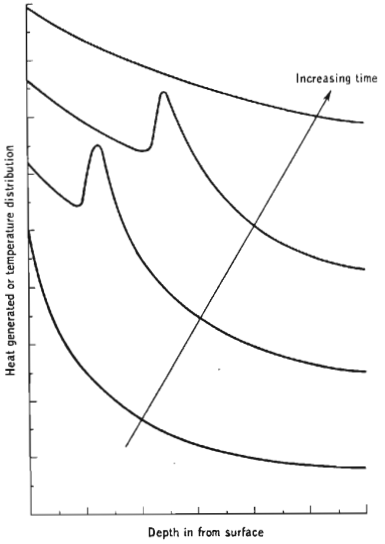

FIG. 2-20. Heating effect in magnetic steel.

Considerable work has been done on steel through-heating, especially at low frequencies (24). Although most of this type of heating is at present experimental, use of low frequencies is expected to increase. Installations already in operation are mainly dual-frequency types, with a supply frequency of 60 cps used to heat the steel billets up to the Curie point (1300 to 1400°F) and motor-generator frequencies of 960 cps heating up to forging temperatures (2200 to 2400°F). Chapter 3 illustrates some of these applications.

Nonferrous induction billet heating, in particular aluminum heating, is widely accepted as a standard heating method. Chapter 3 describes several installations of this type; it is seen that the various time-temperature relations and the temperature distribution in the billet are very important. Figure 2-22 shows a typical nonferrous heat cycle. The transient state during t_t corresponds to the curves for $T < 0.25$ in Fig. 2-11. The steady-state time t_s corresponds to the curves for $T > 0.25$ in Fig. 2-11. The actual temperature differential during t_s is the result of the finite depth of current, as shown in Fig. 2-1, and the radiation loss, as illustrated in Fig. 2-13.

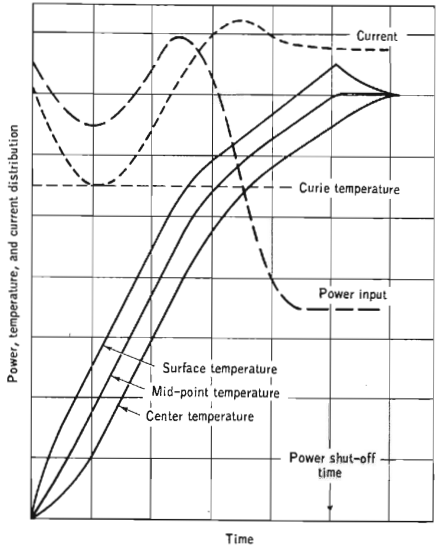

FIG. 2-21. Typical temperature distribution and induced power in a steel billet.

The final average temperature, shown as θ_a in Fig. 2-22, is the result of a fall in the surface temperature θ_s, due to radiation losses, and a rise in the center temperature θ_c to equalize with the surface. This is the required temperature of the billet for its forming or extrusion operation, with some allowances made for over-all cooling between the time the billet leaves the heating coils and the time it is formed or extruded. Usually this cooling

rate is slow and all parts of the billet fall in temperature evenly, as in curve A. Occasionally the surface radiation is greater than the heat flow to the center and the two temperatures cross over, with a negative differential, as in curve B. This is equivalent to the curves for $P_n/P_a < 0.5$ in Fig. 2-14.

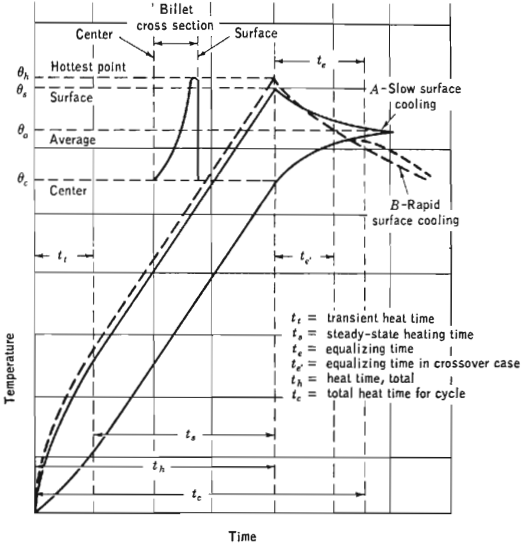

FIG. 2-22. Typical heat cycle in nonferrous through-heating.

From Fig. 2-22, it is seen that considerable care is required to derive the actual temperature conditions, in particular when the heating process is controlled by some form of surface-temperature measurement. Also the importance of overheating is illustrated by the cross-sectional temperature distribution shown. The hottest point, θ_h, is actually a little way in from the surface, and in cases of aluminum overheating a ring of partially melted metal can often be seen, about ½ in. below the surface. Therefore in calculating heat input, care should always be taken to ensure that θ_h is sufficiently below the melting point of the metal heated. Also, as previously mentioned, the surface-to-center differential, $\theta_s - \theta_c$, should not set up stresses which could crack the metal.

In practice, the measured temperature distribution, obtained experimentally by embedding chromel-alumel thermocouples, corresponds fairly closely to the calculated results. The difference between the hottest point and the surface temperature is often small, and is usually negligible shortly after the heat time has elapsed, even in metals of low thermal conductivity. Occasionally it is possible to measure the temperature distribution at the end surface of a billet; this is sometimes done in billet heaters.

The effect of phase junctions in three-phase coils and the design of coils to result in given temperature differentials and heating rates are described fully in Chap. 4.

2-11. TYPICAL INDUCTION HARDENING STEELS

The basis of selection of induction hardening steels is similar but not identical to that of choosing steels hardened by other methods. Increase in carbon content for plain carbon steels results in increased hardenability. For instance, 0.2 per cent carbon steel, or 1020 steel, will harden only to Rockwell 48C, but 0.45 per cent, or 1045, steel will result in Rockwell 60C. Additions of alloying agents such as chromium, nickel, molybdenum, tungsten, etc., by moving the nose of the S curve to the right, result in greater hardenability.

For example, in through-hardening, a plain carbon steel requires a rapid rate of cooling or quenching to avoid the nose of the S curve and therefore to avoid softening. Layers below the quenched surface, which are more slowly cooled because of delays in heat conduction, are likely to soften owing to incomplete martensite transformation. Even in surface hardening, heat conducted to the surface from the center of the piece often tends to slow down the cooling. This produces the same effect, with formation of pearlite causing a softer surface. If a more drastic quench than oil is used, distortion is often excessive. Therefore, by adding only small percentages of these alloying agents, oil quenching can be used to minimize distortion. At the same time the required hardness can be achieved.

Another reason for alloy addition is to improve engineering strength of the steel in terms of tensile, yield, impact, and fatigue properties. This improved strength enables the desired hardness to be obtained.

The property of surface heating by induction considerably influences the choice of steel. The problem of incomplete transformation below the surface does not occur, because only the surface layers have been heated. Also the fast rate of heating of the surface often means that a fast quench can be used without risk of distortion due to internal stresses. The center of the piece therefore retains its initial strength, as it has not been heated or hardened at all. These two effects mean that a plain carbon steel can often be

substituted for a more expensive alloy steel previously hardened by through-heating methods.

Another reason for preferring plain carbon steels for induction hardening is that in general they go into solution faster and at lower temperatures than alloy steels. This means that a shorter heating time can be used, with less loss of heat to the center and with increased production rates. A further reason is that a water quench, which is more economical than an oil quench, can often be used. The only reason for using an alloy steel is to produce a hardened piece with an unusually high core strength.

The amounts of carbon and alloy content suitable for induction surface hardening are given below in order of preference:

C = 0.35–0.60 per cent
C = 0.30–0.40 per cent, Mn = 0.6–1.9 per cent
C = 0.30–0.45 per cent, Ni = 3.0–5.0 per cent
C = 0.35–0.45 per cent, Ni = 0.46–0.7 per cent, Cr = 0.3–0.6 per cent
C = 0.35–0.45 per cent, Ni = 1.5–3.5 per cent, Mo = 0.25 per cent
C = 0.35–0.45 per cent, Cr = 1.0 per cent, Mn = 0.6–1.2 per cent

Examples are SAE steels 1040, 1050, 1340, 2345, 3140, and 4640.

Previous heat-treatment of the steels is also of great importance, primarily because of the short heating times encountered in most induction heating processes. This time is not long enough to allow coarse or heterogeneous grained steel to diffuse evenly. Free ferrite usually remains after treatment, causing localized soft areas. Annealed, spheroidized, and similar pretreatments should always be avoided where possible. The most desirable pretreatment is normalizing, which results in an evenly distributed fine pearlite structure.

CHAPTER 3

INDUCTION HEATING APPLICATIONS

3-1. CLASSIFICATION OF APPLICATIONS

As production lines in the past became more automatic and longer, the need grew for a flexible but precise method of heat-treatment. Accurate control of temperature, minimum size, and low cost were also required. In fact, a method was needed that would replace the large, immobile, and costly gas, oil, and resistance furnaces then in use for various heat-treatments. The suitability of various types of induction heating methods for such heat-treatments of metals in production processes is now firmly established (16, 23).

One of the first applications was in the metal-melting industry, when Northrup and others developed spark-gap oscillators in conjunction with a coreless induction furnace (6). In later work lower frequencies, down to 1,000 cps, were used, but the applications were still mainly for melting processes.

During World War II large through-heating equipment was installed, mainly for bomb and shell-nose annealing in quantity, and for through-heating shell bar stock for forging. Through-heating by the lower machine frequencies (960 and 3,000 cps) and supply-line frequencies (50 and 60 cps) has now become standard for such applications (22, 24, 25).

The use of the skin-effect phenomena for surface heating and hardening has only been developed to any degree during the last 15 years. The availability of reliable industrial-type high-frequency power sources, such as r-f electronic oscillators and motor-generator sets, has been one reason for the rapid growth of this type of induction heating. Probably steel surface hardening has been the major use of these higher frequencies. Applications include continuous hardening of bar stock and rails (7–11), single-shot hardening of gear teeth (12–15), internal-diameter hardening (7), and a wide variety of methods for surface hardening of miscellaneous parts (17–20).

Aluminum and other nonferrous heating for extrusions (20, 21) is also an accepted industrial method.

Localized heating for joining, using brazing and soft-soldering techniques, has already been developed rapidly, mainly in parallel-to-surface hardening,

as the same type of electronic r-f generators and motor generators is often used for both applications (26, 28). Both continuous (27) and single-shot methods (29) are used. A specialized type of welding for joining or seaming pipes is often used in conjunction with induction heating for high-speed production (30–32).

From this summary, three major types of induction heating emerge, as well as some miscellaneous applications. These methods are based on the available power supplies and frequencies and utilize the natural advantages of each frequency. They are briefly outlined below, together with some miscellaneous classifications, and then each type of heating is described in detail as far as applications and choice of equipment are concerned. The matching system between coil or coils and the supply line are covered in Chaps. 5, 6, and 7, and some of the systems accompanying the following applications are described in detail.

Through-heating for Forging, Forming, Etc.

Through-heating requires low-frequency power sources of considerable magnitude, as the current depth is inversely proportional to the square root of the frequency [see Eq. (1-1)] and production rates for most forming, forging, and annealing operations in terms of pounds per hour of metal are usually high. Power sources of line frequencies (25, 50, and 60 cps) and the lower machine frequencies (960 and 3,000 cps) possess both these characteristics. They also possess the advantages of being relatively cheap in terms of price per kilowatt for initial and running costs, and of being simple to maintain. Occasionally two frequencies are combined in a "dual-frequency" installation. The lower frequency heats steel up to the Curie point (22). At this temperature, the steel becomes nonmagnetic ($\mu = 1$) and at the lower frequency, the current penetration would become excessive and flux cancellation would occur. [See Eq. (1-1) and P and Q curves.] Therefore, a higher frequency is used between Curie temperature (approximately 1400°F) and forging temperature (2100 to 2400°F).

Localized Heating for Joining

Joining operations such as brazing, soft soldering, and welding usually require a highly concentrated and accurate type of heating. Also the power source should be capable of being instantaneously and repeatedly switched, as well as closely controlled and regulated, as the heat times for many joining applications are short. Both through-heating and surface heating are suitable, depending on the size of the piece and the locality of the joint. The higher machine frequencies (3,000 and 9,600 cps) and lower radio frequencies (400 to 500 kc) satisfy most of these requirements. Power requirements are usually not so high as for through-heating.

Surface Heating for Hardening

This type of application primarily requires the higher frequencies, as hardened skin depths and therefore current-penetration depths are usually small. Power-level control and accuracy requirements are very important, as in joining, and the power sources should lend themselves to automatic control. The same frequencies are often used in surface hardening as in joining, i.e., 3,000 and 9,600 cps and 400 to 500 kc.

Miscellaneous Applications

Besides having the three major uses described above, induction heating is often suitable for other applications requiring highly concentrated, shallow-depth heating, localized heating, a high degree of power control and accuracy, or deep-penetration heating. These applications include quality-alloy melting furnaces, semiconductor crystal growing and refining, high-speed bright tin reflowing, vacuum-tube degassing, shrinking and straightening, rubber-to-metal debonding, cable-sheathing, etc.

3-2. THROUGH-HEATING

Nearly all through-heating applications and systems can be divided into two types, depending on the method of power control. The first type is based on a time-controlled heat cycle in which the work is loaded into the equipment, heated, and ejected (manually or automatically) on the basis of a time cycle which results in a constant production rate. The time cycle is chosen to result in the heating of the work to the correct temperature for the subsequent operation. This method is ideally suited to forging operations with a high production rate, where small variations in final temperature are not too critical and the forging can be carried out continuously. It is used in most automatic ferrous induction forging lines, where final temperatures are usually in the range of 2100 to 2400°F and variations of ± 50°F can often be tolerated. The coils are energized continuously, with no power switching.

The second type, in which temperature is used to control power, can only be considered semiautomatic. This method is used where the final billet temperature is more critical but where the billet may not be required when it is up to temperature. One major application is in the nonferrous forming and forging industry. Another use of this system is in the annealing of large ferrous workpieces which cannot be handled automatically by the time-controlled method. Usually only a few billets are heated in one machine as against ten or more in the time-controlled method; it is sometimes called

"single-shot" to distinguish it from the "progressive" or time-controlled type.

Occasionally a temperature check is used on a time-controlled system, and billets that are out of limits are rejected for reheat.

Steel heating up to the Curie temperature results in special problems. One, mentioned already, is the change from magnetic to nonmagnetic condition and the resulting drop in value of permeability μ, which causes large changes in current penetration (22). This same change causes wide differences in coil impedances for static heating, as the reactive component, based on the inductance of the loaded coil, is constantly changing. In machine-frequency systems it is not uncommon to have to switch in coil-tuning capacitors during the heat cycle in order to prevent a serious mismatch and overloading of the generator. Other problems include strong electromagnetic forces acting on load, and vibration effects similar to those from loose transformer cores.

3-3. TYPICAL APPLICATIONS

Figure 3-1 shows a dual-frequency through-heating line of coils (22). The process involves heating 3½-in. round-cornered square steel billets for forging into 105-mm shells at a temperature of 2150°F. Each machine has a production rate of 480 billets an hour. The frequencies used are 60 cps to the Curie point and 960 cps (motor-generator sets) up to forging temperature. The parts are automatically loaded, fed through, and ejected; therefore the equipment is time-controlled. Any pieces below the required temperature are rejected via signals fed from radiation pyrometers, which are sited on the outfeed end. Six of these machines in one installation heat a total of 40 tons of billets an hour, using approximately 13,600 kw of power.

A smaller static or "single-shot" machine is shown in Fig. 3-2. This type of heating involves loading the work and heating it up to a certain temperature, at which point it is either automatically ejected or left with power being cycled on and off. In either case, temperature is the controlling source. The work in this case is steel bars of various sizes and lengths, and the frequency is either 3 or 10 kc, by motor generators. The total capacity supplying one plant with induction heating power for these installations is about 5,000 kw. The heated bars are forged into various tractor parts.

Another example of the use of the dual-frequency effect is given in reference 22. Here bar stock up to 1½ in. in diameter is heated to Curie temperature in the first two of three coils with 3 kc power and then up to forging temperature (2350°F) with 10 kc. The bar is then cut and formed into nuts; the production rate from the final press is 4,200 blanks per hour. Temperature is controlled and recorded via a Rayotube and control

instruments. Here the process is a combination of time and temperature control; both the rate of feed-through and the generator power determine the temperature.

Hollow workpieces may also be advantageously heated with induction heating, especially if the optimum frequency is chosen for the wall thickness

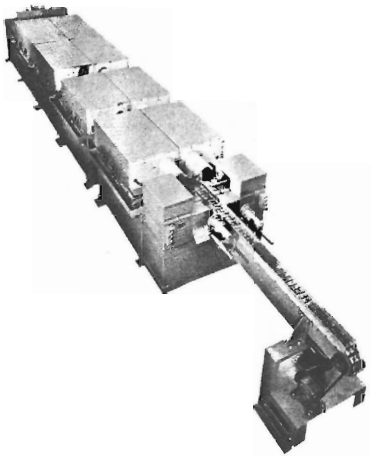

FIG. 3-1. Dual-frequency through-heating (60 and 960 cps) of 3¼-in., round-cornered square steel billets, 8½ in. long, to 2150°F forging temperature. (*Westinghouse Electric Corp.*)

concerned. A large installation, consisting of 5,000 kw of 960-cps power, is used in one ordnance plant for heating 155-mm and 8-in. rough-turned hollow-steel pieces to forging temperature for hot-press nosing into shells (33). The temperature is graded from 2175°F at the hot end to 750°F some 9 to 12 in. away. The heat cycle is 53 sec for the 155-mm shell. Figure 3-3 shows one of the coils and a shell after heating and prior to being loaded onto a conveyor belt. Figure 3-4 illustrates another form of hollow-cylinder heating. This is essentially time-controlled, as the piece is heated in a fixed time of 22 sec to 1350°F for annealing. Use is made of iron cores to improve flux concentration and reduce external reluctance to flux. This in turn improves coil efficiency.

An ingenious combination of the use of the electromagnetic force of traction and the muffle-furnace principle is utilized in a multipurpose 60-cps installation, shown in Fig. 3-5 (34). Here three hollow-steel pipes are heated directly by induction heating and maintained at annealing temperature. Variously shaped workpieces are loaded by gravity into the pipes, where they are both induction-heated by the flux inside the pipe and heated by

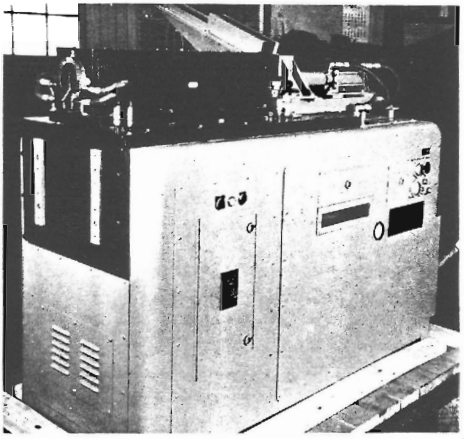

FIG. 3-2. Machine-frequency bar-heating unit for tractor parts.

radiant heat from the muffle for annealing and stress-relieving effect. While below Curie temperature, the pieces are attracted into the coil magnetically, and the force is sufficient to push the foregoing line all the way through. The exit pieces are up to and above Curie temperature and therefore are not attracted back into the coil. Coils with between one and five pipes are used and it is claimed that pieces that normally cannot be heated by line frequency because of their small diameter can be raised to as high as 2350°F at production rates of 2,000 lb per hr.

These examples are just a few of the many applications of induction heating in the steel-forming and -forging industry. Efficiencies of 5 to 8 lb per kwhr can be realized for steel heated to forging temperatures and higher efficiencies (8 to 14 lb per kwhr) for annealing processes (Fig. 3-5*A*). Virtually complete automation can often be achieved.

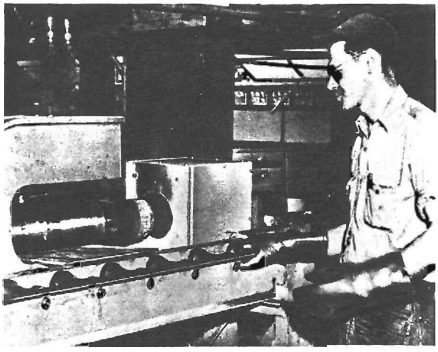

FIG. 3-3. Heating for shell nosing by 960-cps power. (*Westinghouse Electric Corp.*)

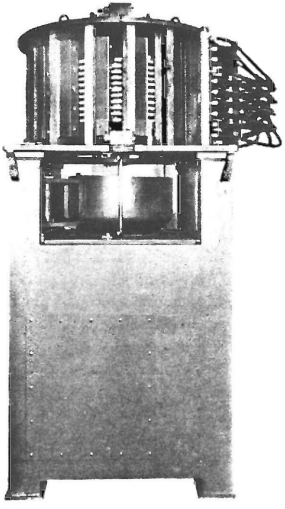

FIG. 3-4. Annealing of gas cylinders by 60-cycle power. A 400-kw installation using iron cores. (*Westinghouse Electric Corp.*)

Nonferrous billet heating is another fairly recent use of induction heating. The metal most widely heated is aluminum at the supply-line frequency of 60 cps, probably because of the phenomenal growth of the aluminum extrusion industry (20). A typical unit is shown in Fig. 3-6; the process is usually temperature-controlled (54). The billets are hand-loaded onto the gravity ramp and automatically fed into the coil. The number of billets in

FIG. 3-5. Muffle induction coil heating steel billets for annealing. (*Mullins Co.*)

the coil heated at any one time may vary from three to as many as ten, and the process is a continuous one in which a cold billet entering the coil travels along it in stages, being heated at each stage, until at the last stage it achieves the final temperature. Unlike most of the ferrous cases, this process is usually temperature-controlled, power being pulsed on and off to maintain the exit billet at temperature until required by the press operator. The temperature is sensed by prod thermocouples impinging on the surface of the billet. Figure 3-7 shows a six-unit installation of this type of heater for an air force heavy-press program.

These two illustrations show the versatility of induction heating, in which one heater can treat a variety of diameters and lengths at a number of

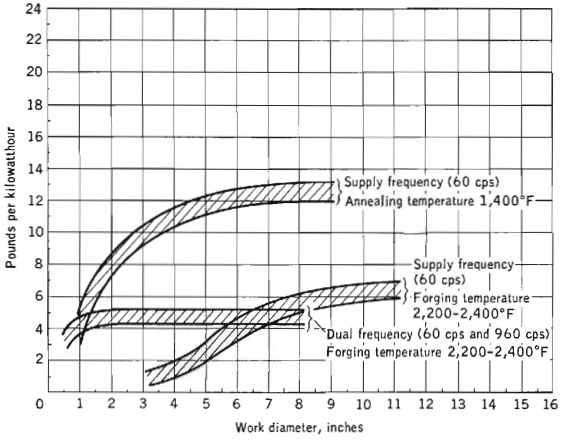

FIG. 3-5*A*. System pounds per kilowatthour—steel.

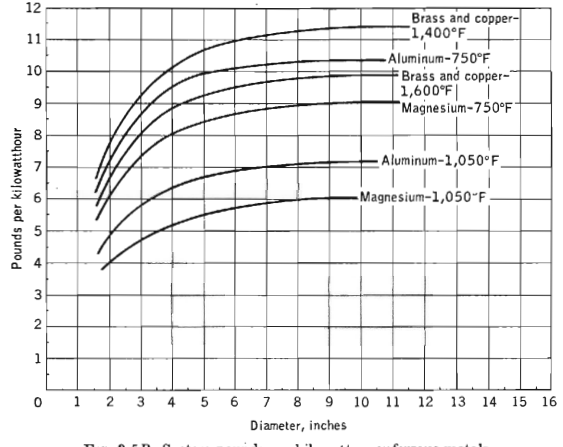

FIG. 3-5*B*. System pounds per kilowatt—nonferrous metals.

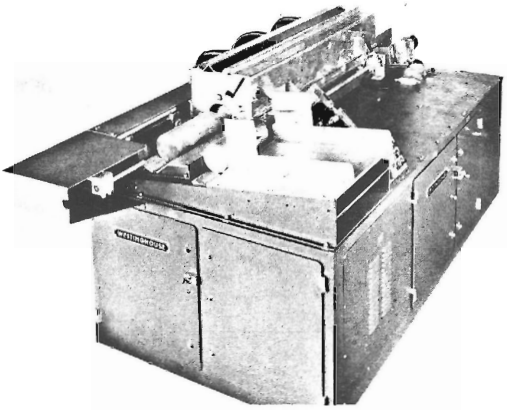

FIG. 3-6. 60-cycle aluminum through-heating at 5,000 lb per hr to 950°F by an 800-kw billet heater. (*Westinghouse Electric Corp.*)

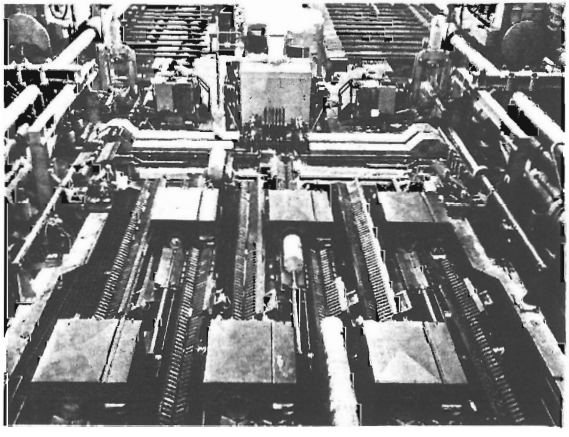

FIG. 3-7. Large 60-cycle aluminum heating installation. Billets up to 26 in. in diameter and 65 in. long can be heated to 850°F. (*Kaiser Aluminum and Chemical Co.*)

different production rates and temperatures. Production efficiencies vary between 6 and 11 lb per kwhr to extruding temperatures ranging between 750 and 1050°F (Fig. 3-5*B*). The efficiency increases with increasing diameters as well as lower temperatures, as flux cancellation effects at lower diameters require higher induced currents and therefore higher losses in the coil, resulting in lower efficiencies. It has been estimated that approximately 200 aluminum billet heaters are now in operation, with a combined capacity of nearly 100,000 kw of power.

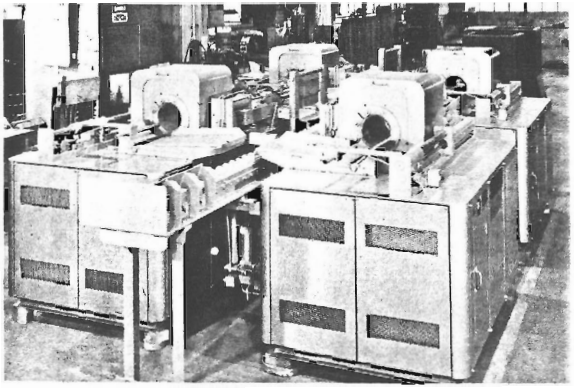

FIG. 3-8. Four 500-kw 60-cycle brass and copper-alloy billet heaters for billets 7 in. in diameter and 15 in. in length. (*Magnathermic Corp.*)

Other nonferrous metals now being induction through-heated include brass, copper, and magnesium (36) and stainless steel (24). The total number of installations heating these metals is not large at present, mainly because of the somewhat experimental state of the extrusion art. However, advances are being made rapidly (Fig. 3-8). The brass-heating installation is similar in principle to the aluminum heaters but because of the higher temperatures required (1400 to 1600°F), closer control is needed. Also the coils are single-phase, to result in even temperature distribution, as three-phase coils occasionally tend to result in "cold areas" at the phase functions owing to flux cancellations. This point is explained fully in the next chapter on coil design. Efficiencies for most low-resistivity metals (copper, brass, magnesium, etc.) tend to be the same as for aluminum. One of the first

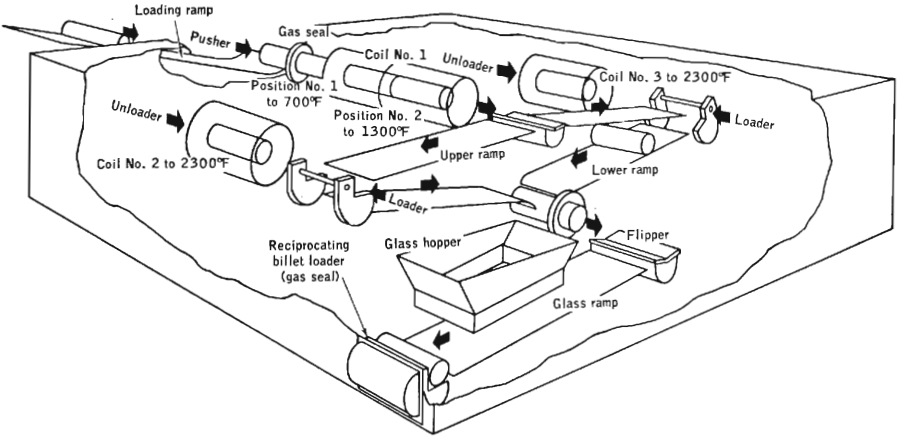

FIG. 3-9. Carbon steel heating to 2300°F in a helium atmosphere using 60-cycle power. (*Jones and Laughlin.*)

stainless steel extrusion installations put into production utilizes 60 cps single-phase coils of vertical design. One reason for this method of vertical heating is that high-temperature coils require ceramic liners, which can be better protected from damage from the heavy billets by vertical loading.

One factor often guiding the heating of billets is that of protective atmospheres. Conventional furnaces have the advantage of being able to supply reducing atmospheres for oxide prevention in conjunction with the heating required. Induction systems usually heat up at a fast enough rate to reduce oxidation to a minimum on the smaller diameters, but when larger pieces are heated, requiring larger heat and soak times, atmosphere protection is an advantage. Figure 3-9 shows an interesting installation in which helium is used to prevent oxidation during steel heating for hot extrusion (35). Several experimental induction heating (in atmosphere) units are proposed at the time of writing for titanium and uranium.

3-4. LOCALIZED HEATING FOR JOINING

The main subdivisions of metal joining are brazing, soldering, and welding. Because of the very fast heating rates realizable with induction heating, oxidation and distortion are both minimized in all three processes and costs reduced to below those of conventional methods.

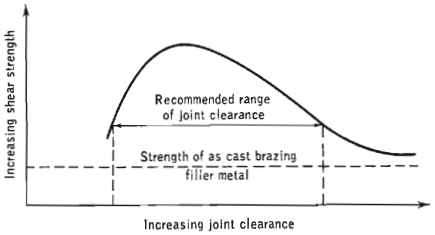

FIG. 3-10. Optimum joint-clearance curve for filler brazing metal.

Prior to the actual heating, some consideration should be given to the design and assembly of various types of joints encountered (37). One of the first factors is the strength of the filler material. Each material has an optimum strength, depending on the joint clearance, and curves for the particular material, such as Fig. 3-10, should be consulted. The various basic joints are shown in Fig. 3-11; Fig. 3-12 illustrates some adaptations of these joints to different shapes. Often it is possible to improve the overall strength and design of the finished product by redesigning it to utilize

fully the advantages of metal joining. Figure 3-13 shows some improved designs using brazed joints.

The usual method in induction heating is to use preforms of the joining or filler metal. This allows semiautomatic operation of the process. Figure 3-14 illustrates typical preform applications and the results, with good

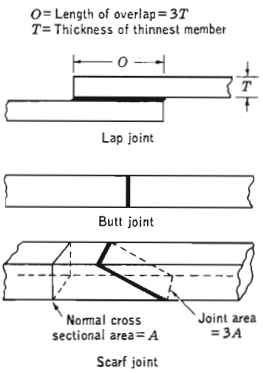

FIG. 3-11. Basic brazing joints (lap, butt, and scarf.)

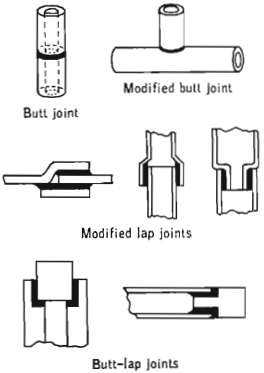

FIG. 3-12. Modified brazing joints.

penetration. Self-jigging joints, as shown in Fig. 3-15, are the most economical for induction heating where the process is manual.

Table 3-1 (40) lists the silver-brazing alloys in common use, together with the recommended flow temperatures (38).

Soft solders are given in Table 3-2, together with composition and melting range (39).

One widely used induction brazing method is carbide tool tipping. Figure 3-16 illustrates a typical manually operated jig. It has been found that the most economical and flexible process for tool tipping uses manual methods, because of the large variations in size, heat time, etc. The brazing alloy is usually of the type which flows between 1250 to 1450°F and is placed in the form of a flat shim between tip and shank. Best results are obtained if pressure is applied during heating or immediately afterwards. Coils usually either completely enclose the end of the tool (closed) or couple to part of the tip (open).

Using a 6-kw heater and an open coil, heating times vary from about 8 sec

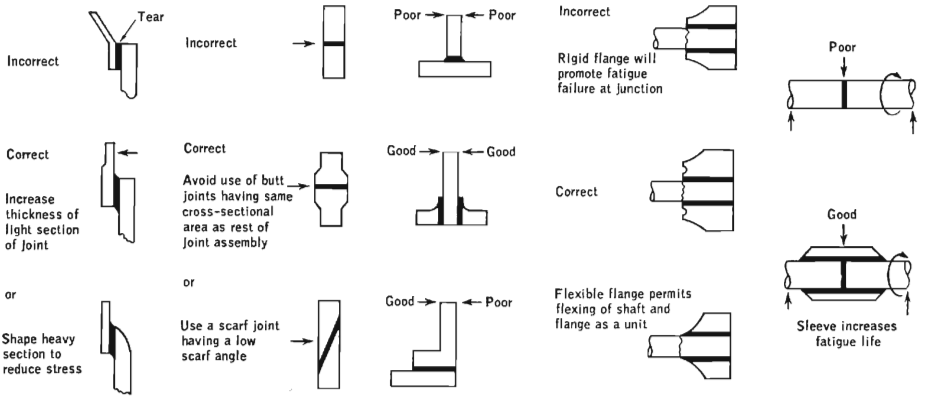

FIG. 3-13. Correct design of joints reduces stress concentrations and fatigue failures.

TABLE 3-1. INDUCTION HEATING OF SILVER-BRAZING ALLOYS

Grade	Chemical composition, per cent					Melting point, °F	Flow point, °F
	Silver	Copper	Zinc	Cadmium	Phosphorus		
1	10	52	38	...	...	1510	1600
2	20	45	30	5	...	1430	1500
3	30	38	32	...	...	1370	1410
4	40	36	24	...	...	1330	1445
5	45	30	25	...	...	1250	1370
6	50	34	16	...	...	1280	1425
7	60	25	15	...	...	1260	1325
8	70	20	10	...	...	1335	1390
9	72	28	...	...	...	1435	1435
10	80	16	4	...	...	1360	1460
11	15	80	...	...	5	1190	1300
12	50	15.5	16.5	18	...	1160	1175

TABLE 3-2. INDUCTION HEATING OF SOFT SOLDERS

Chemical composition, per cent						Melting range	
Tin	Antimony	Bismuth	Lead	Silver	Cadmium	Solidus, °F	Liquidus, °F
51.2	...	...	30.6	...	18.2	292	292
43.1	...	56.9	...	...	...	280	280
25.0	...	50.0	25.0	...	...	205	208
15.5	...	52.5	32.0	...	...	205	205
12.5	...	50.0	25.0	...	12.5	158	162
95.0	5	...	...	...	...	456	467
5.0	4	...	91.0	2.5	...	462	537
...	...	...	97.5	...	...	579	579

(½ by ½ in. shank) to 35 sec (1¼ by 1¼ in. shank). For larger shanks a closed coil is used and a heater of the same rating will heat in times varying from 40 sec (1½ by 1½ in.) to about 60 sec (1¾ by 1¾ in.).

Large tools have been tipped and hardened in one operation, using a 15-kw generator and copper as a brazing material, heated to about 2100°F. The time for this operation is about 1½ min for a 1½- by 1½-in. shank (39).

Other brazing examples, both semiautomatic, are shown in Figs. 3-17 and 3-18 (16), where the nature of the operation lends itself to mass production.

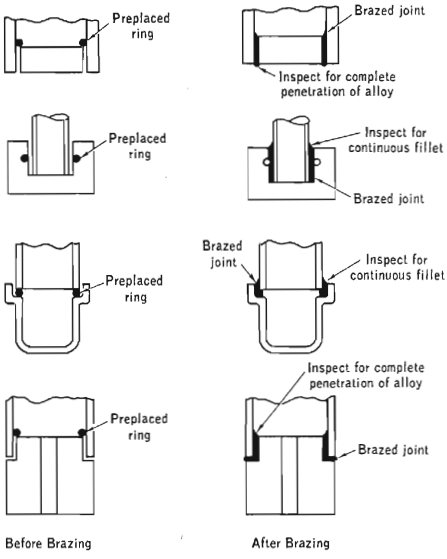

FIG. 3-14. Preplacement of filler metal.

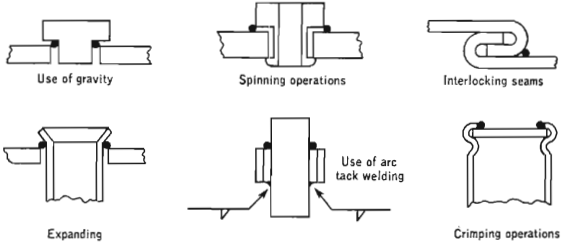

FIG. 3-15. Self-jigging brazed joints.

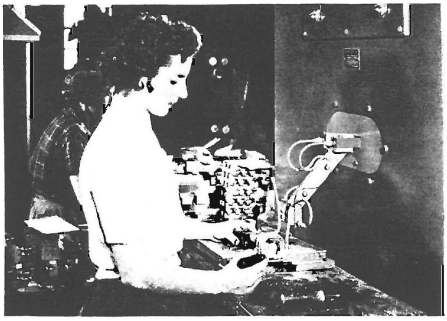

FIG. 3-16. Carbide tool tipping at 530 kc. (*Metro Tool and Gage Co.*)

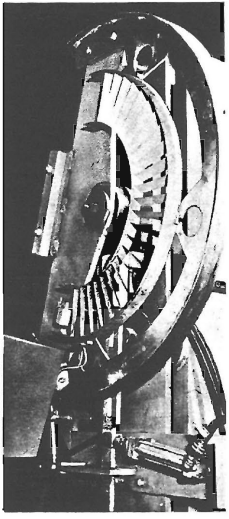

FIG. 3-17. R-F semiautomatic brazing of jet-engine turbine blades. (*Westinghouse Electric Corp.*)

The two-position method shown in Fig. 3-18 is often utilized in brazing operations where one position is being loaded while the other is heating. In this case the excess flux is automatically washed away immediately after cooling, resulting in a semiclean part.

Savings in brazing material are often achieved, as shown in Fig. 3-19, when induction heating replaces torch methods. Figure 3-20 shows a multiposition station where the work is assembled, heated, cleaned, and removed on a circular work-handling production line.

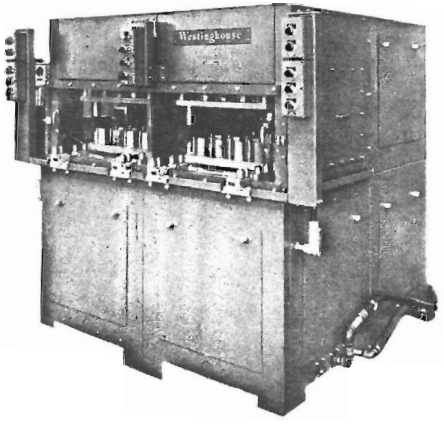

FIG. 3-18. Two-position semiautomatic 105-mm shell-nose-plug brazing at 10 kc. (*Westinghouse Electric Corp.*)

Many other applications of induction brazing are currently in use, particularly in the automotive field (40) and in the manufacture of refrigerators, twist drills, etc. Stainless steel brazing is now accepted in the aircraft industry; it is particularly suited to induction methods, as the temperature required is often below that of the oxidation point.

Soft soldering is another process highly suitable for induction heating either in manual or automatic assemblies. The solder is available in various forms, such as wire, foil, ribbon, washers, powder, and paint. It can be obtained cored or plain. Some available solders leave a noncorrosive colored deposit for identification purposes. As in brazing, the gap between parts to

be soldered is important; allowing it to be too large because of differences in expansion, etc., will cause a lowering of the joint strength. For example, 9,000 lb per sq in. can be achieved with a gap of 0.002 in., but this is decreased to 3,000 lb per sq in. when the gap opens to 0.008 in. (39).

Figure 3-21 illustrates a typical automatic operation involving induction soft soldering. Although these units employ generators of 10- and 20-kw

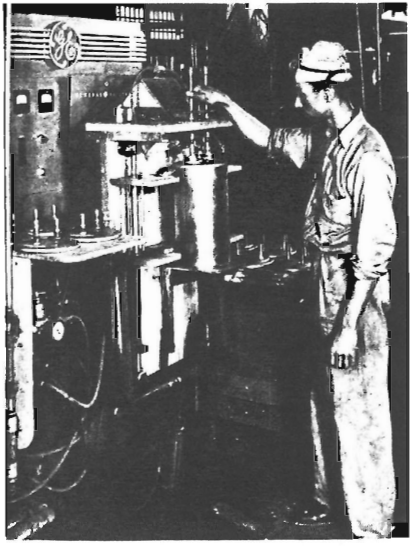

FIG. 3-19. Stainless-steel nipple brazing, using a 20-kw 530-kc r-f generator. (*Vacuum Can Co.*)

ratings, often smaller sets are the most economical for hand-loaded assemblies. A typical range of power for most smaller applications is 6 to 10 kw. Other applications include continuous soft-solder seam joining of tin cans, plumbing joint soldering, electric motor end-plate soldering, etc.

Continuous seam welding has been the subject of considerable development work (42). High operating rates have been achieved; in one continuous seam-welding installation 250 ft per min of tubing between ½ to 2 in. in diameter is continuously welded. Diameters of up to 30 in. have

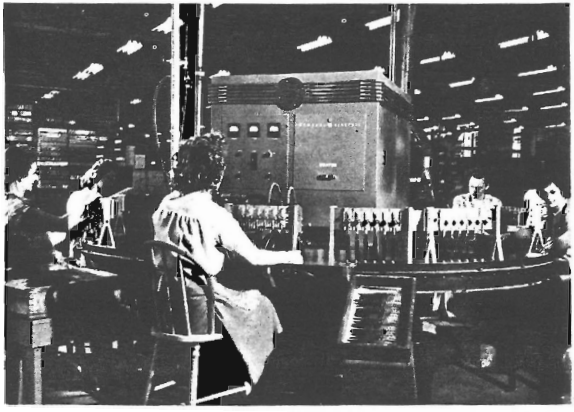

FIG. 3-20. Batch production of knife-handle brazing at a r-f power of 530 kc. (*Oneida Ltd.*)

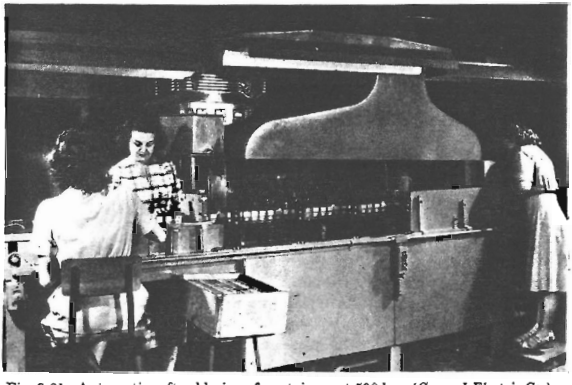

Fig. 3-21. Automatic soft soldering of containers at 530 kc. (*General Electric Co.*)

been joined, and both nonferrous and ferrous tubes have been welded (23). Usually the method consists of heating edges of partially formed strips and pressing the edges together, also under heat. Power consumed varies between 50 to 150 kwhr per ton of tubing (41). Sometimes the strip is preheated to Curie temperature by longitudinal flux.

Pressure welding is occasionally used together with induction heating. A typical application is in the manufacture of heavy farm and road machinery. Welds are uniform and the process results in a 5:1 decrease in cost and 30 per cent increase in production.

Often considerable savings are effected by the use of induction brazing to replace the machining of the solid piece. The strength is improved and the labor and materials involved are reduced.

3-5. SURFACE HEATING FOR HARDENING

Induction hardening has been one of the most widely utilized methods of induction heating. One reason is the advantage of using heat generated in the same locality as the required hardness and at a rate fast enough to prevent conduction away from this area.

The metallurgical and heat-flow effects were discussed in the previous chapter, and details of hardening coils will be given in the next chapter. This section will cover the relationship between the required hardness depths and the other variables, such as power density, time, frequency, etc.

Figure 3-22 relates these variables from calculations made by Losinsky (7). It is simplified to include the currently available frequencies and is based on hardening temperatures between 1550 and 1650°F. The great majority of hardness depths required vary between 0.01 and 0.20 in. Therefore from the curves it is obvious that 450 kc is the only frequency to cover this range fully; in fact, this is the most widely used frequency. The motor-generator frequencies of 3 and 10 kc will cover the deeper cases of over 0.05 in. and are used mainly for large power application.

Simple conclusions that can be drawn from these curves are useful in qualitatively evaluating a hardening application. These are as follows:

1. The shallower case depths require higher frequencies for a given time and power density.

2. Given a fixed frequency, the shallower case depths are achieved by shorter times and higher power densities.

The major subdivisions of hardening depend on the movement of the piece and are static or single-shot and progressive. Static methods are used mainly on small pieces which can be either hand or mechanically loaded into the coil. The area to be hardened is small enough so that the power input can achieve the required hardness depth in one shot. The progressive

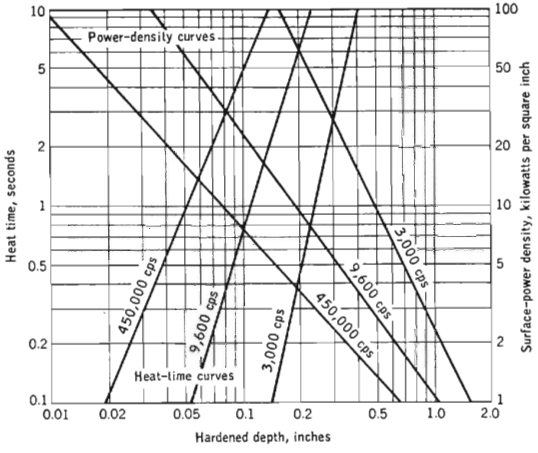

FIG. 3-22. Hardening curves.

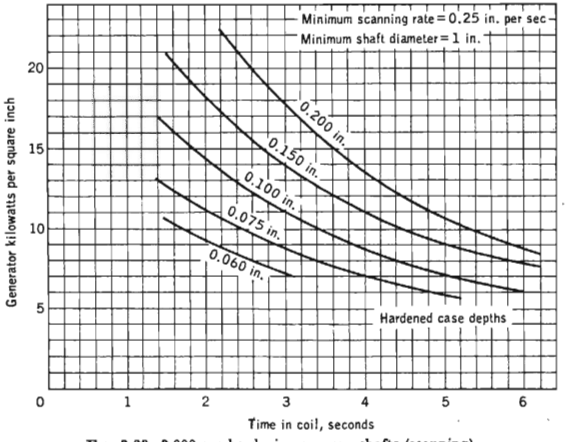

FIG. 3-23. 3,000-cps hardening curves—shafts (scanning).

method consists of scanning the piece, such as a bar, through the coil, which heats only a small area at a time. It is used on pieces too large in surface area for static heating. They are nearly always automatically fed through the coil.

The power and frequency required for a particular application are functions of production rate, surface area to be hardened, case depth, and heat

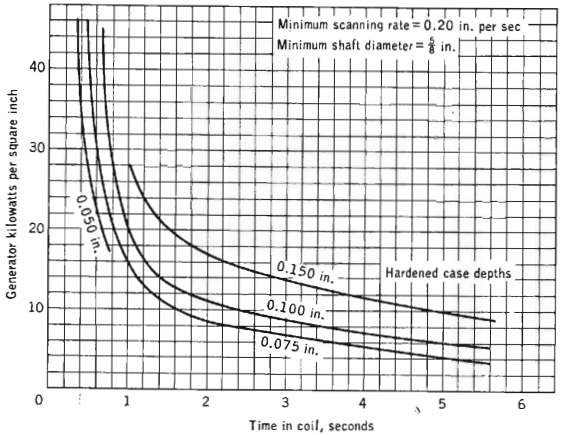

FIG. 3-24. 9,600-cps hardening curves—shafts (scanning).

losses (coil loss, radiation, and conduction). To a lesser extent, they are also functions of type of steel and required hardness, but these do not usually vary so much as the other parameters.

In the case of scanning methods, Figs. 3-23 and 3-24 give approximate relations between the actual generator power and the case-depth requirements. The depths given represent the distance in from the surface to the bend or knee of the hardness curve at the point where hardness starts to fall rapidly. This may vary from 50 to 80 per cent of the actual heated depth and depends on the metallurgy of the metal. In this case the steel used for the curves was a plain carbon (0.45 per cent carbon) type. Minimum speeds and diameters are given on the curves; results were obtained with a single-turn work coil and a current transformer. A minimum density of 20 kw per sq in. is recommended at 9,600 cps for shafts between $\frac{5}{8}$ and $\frac{7}{8}$ in. in

diameter. The most efficient parts of the curves, on the steepest slopes, should be used wherever possible. The points on the steep sections correspond to the calculated curves of Losinsky given in Fig. 3-22.

Coil losses have been allowed for, and the scanning speed can be calculated as in the example below.

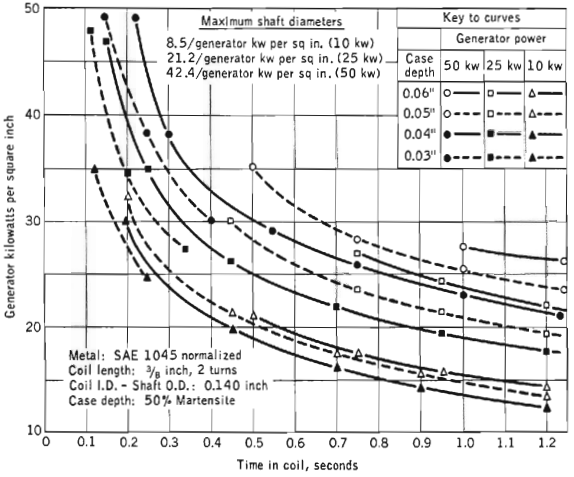

FIG. 3-24*A*. 450 kc/sec hardening curves—shafts (scanning).

Example 3-1

Shaft diameter	1 in.
Required hardened case depth	0.100 in.
Available generator	50 kw
Available coil length	1 in.

Therefore the shaft area heated at any one time is given by

$$\text{Area} = (\pi)(1)(1) = 3.14 \text{ sq in.}$$

As the generator is 50 kw power output, the "generator kw per sq in." is

$$50/3.14 = 16 \text{ kw per sq in.}$$

From the 3,000-cps curve, this gives 1.6 sec in the coil and from the 9,000-cps,

this would be 1.2 sec in the coil. Therefore, the scanning rates as determined by the two frequencies are:

$$3{,}000\text{-cps scanning rate} = 1/1.6 = 0.625 \text{ in./sec}$$

$$9{,}600\text{-cps scanning rate} = 1/1.2 = 0.833 \text{ in./sec}$$

This illustrates that for shallower cases, the higher frequency is preferable.

By doubling the generator size and coil length, the same power density is obtained, given the same time in the coil for the heated area. As this is now doubled, the scanning speed is doubled and the production rate increased accordingly.

Although the range of possible variables is considerable, certain generalizations can be stated as a result of industry practice and the conclusions reached on the preceding curves. Most energy inputs to the work surface for case depths between 0.075 and 0.150 in. run between 20 and 40 kwsec per sq in. The actual minimum case-depth–frequency relationship has been standardized with the following values (43):

Frequency, cps	*Minimum case depth, in.*
3,000	0.060
9,600	0.040
450,000	0.020

It also appears from the previous example that the same case depths can often be achieved at more than one frequency. They depend mainly on the hardened material, its condition, the shape of the piece, and the frequency. There are also minimum diameters that can be effectively hardened at any frequency. For instance, pieces 0.10 in. in diameter could probably never be heated fast enough to provide an effective case.

In choosing power and time, the practical factor of control should always be considered. For example, in the previous case, 29 kwsec per sq in. was required. If the surface area to be treated is about 3.0 sq in., 87 kw is required at the work, probably necessitating at least a 100-kw 10-kc generator, if a heating time of 1 sec is chosen. This time-power combination is very difficult to control. However, if for the same case depth of 0.10 in. a time of 2 sec is chosen, only 43.5 kw is required; this time is easier to control.

Quenches were discussed in detail in Chap. 2, but an example is given in Fig. 3-25, which shows a typical gear-hardening coil-quench combination, with the coil surrounding the gear and producing a deep case following the contour of the teeth. After heat has been applied, the outer quench ring sprays the whole of the gear, resembling an agitated-bath quench more than a direct spray.

Parts suitable for induction hardening are shown in Figs. 3-26 through

FIG. 3-25. Gear hardening by induction heating. (*Cleereman Machine Tool Co.*)

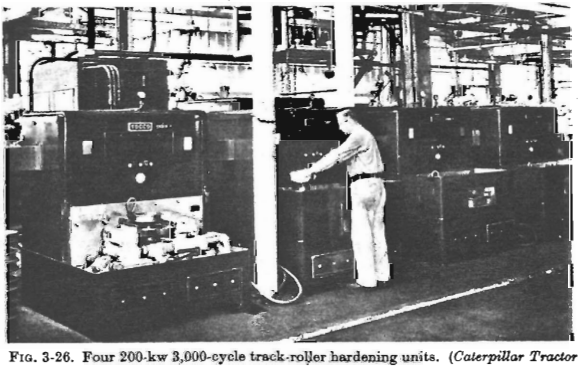

FIG. 3-26. Four 200-kw 3,000-cycle track-roller hardening units. (*Caterpillar Tractor Co.*)

FIG. 3-27. Gear-tooth hardening at varying depths. (*Westinghouse Electric Corp.*)

FIG. 3-28. Hardening the inside and sidewalls of steel cartridge cases at motor-generator frequencies. (*Westinghouse Electric Corp.*)

FIG. 3-29. A section blade on a farm mower being hardened by r-f heating.

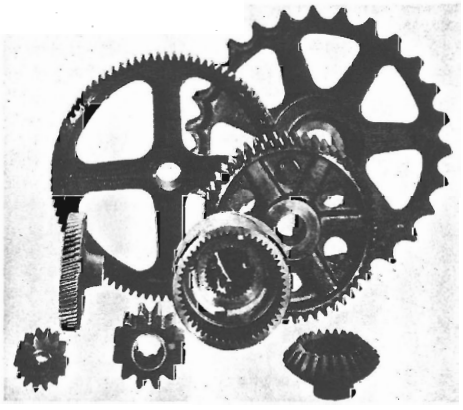

FIG. 3-30. Miscellaneous r-f induction-hardened gears. (*Magnathermic Corp.*)

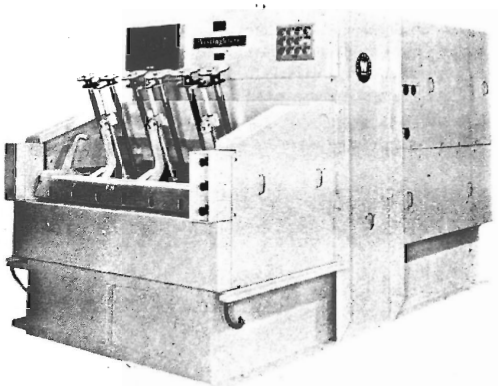

FIG. 3-31. Automobile rear-axle shafts being hardened at 3,000 cps. (*Westinghouse Electric Corp.*)

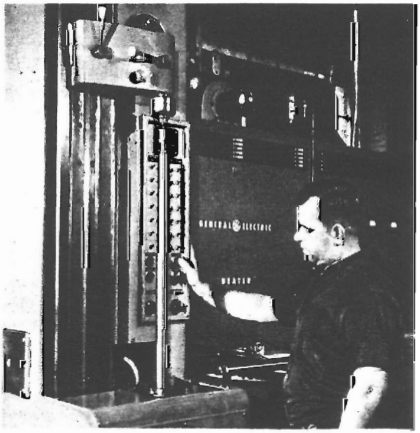

FIG. 3-32. Twister-roll hardening at 530 kc in a textile machinery plant. (*Whitin Machine Works.*)

3-30. These represent only a small fraction of the various shapes suitable for hardening, which range from needles to tractor gears of 3 to 4 ft or more in diameter and shafts of 20 ft in length. Most suitable, however, are the smaller pieces as they are adaptable to automatic handling, which usually obtains the greatest degree of efficiency from the equipment as it utilizes the power for the greatest percentage of time.

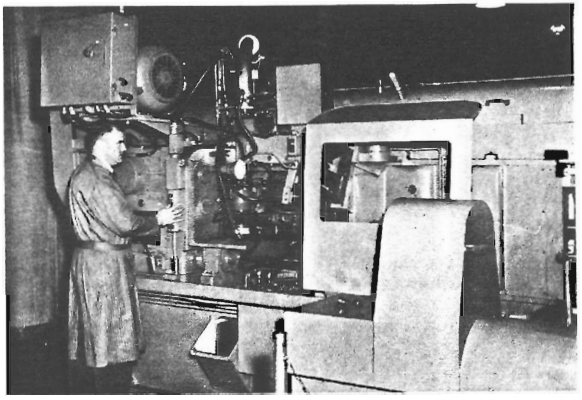

FIG. 3-33. Combined hardening and machining of automobile trunnion cups. (*Mechanics Universal Joint Corp.*)

Gears are highly adaptable to induction methods (13). A typical section is shown in Fig. 3-27, which illustrates the precise control and distortion-free results. In this case, previous methods involved selective carbonizing, with protective copper plating, and often produced distortion. Using only 20 kw of power and heating one tooth at a time, the gears were completed with minimum costs. The smaller gears are often heated in a large coil, as shown in Fig. 3-26. Here the hardness pattern will not be so shallow as in Fig. 3-27 but will follow the gear-teeth outline only approximately. Occasionally two frequencies are used, the lower frequency through-heating the teeth for a preheat and the higher frequency for the hardening process. The gear is rotated during both these heating stages and is lowered from one coil to the other. The result is a deep transition zone which tapers the hardness gradually from the surface and gives considerable strength and a hard surface.

Examples of shaft hardening are shown in Figs. 3-31 and 3-32; it is seen that a variety of frequencies may be used (49). The automobile axles and crankshafts usually require deep case depths and therefore use 3,000 cps.

An interesting example of a combined heat-treat and machining process is shown in Fig. 3-33, where the workpiece is machined and hardened on one unit. The coil is built into the machine and supplied from a remote generator via a transmission line.

Other parts suitable for induction hardening include knife blades, pliers, lathe beds, push rods, tappets, rocker arms, valvestems, etc. (Fig. 3-30)(50).

3-6. MELTING FURNACES

As pointed out earlier, melting was one of the first applications of induction heating and is still a very active field. Basically the system employs a crucible rammed with a refractory in the case of large melts, and surrounded by a heavy copper coil, usually tapped. The low-resistivity metals will not result in sufficient I^2R loss alone and are often indirectly heated by a graphite crucible. Incidental stray-induced losses in metal surrounding the coil are minimized, and the magnetizing field is concentrated in some cases by using external cores of transformer-type laminations.

Furnaces are either the pot hearth, used for higher-frequency melting, or the submerged-resistor type, powered from lower-frequency sources (44, 48). An example of the pot type is the Ajax-Northrup furnace, which is open and can be poured clean. The submerged-resistor type depends on a "heel" of metal in the lower part of the furnace, to complete a high current circuit on starting up, and therefore cannot be poured clean. However, it can be operated directly off the line. Examples of this type of low-frequency furnace are the Ajax-Wyatt and the Ajax-Tama-Wyatt furnaces, which have melting channels in their lower sections. The molten metal rises through the remainder of the metal, melting and stirring simultaneously.

The low-frequency furnaces are used for copper, zinc, aluminum, and cast-iron melting and alloying. High-frequency types are mainly used for steels, carbides, nickel, etc.

Although high-capacity steel induction furnaces up to 10 tons or more and of 1,200-kw capacity have been built, most applications in the high-quality alloy industries use lower-capacity furnaces. Carbides, brass, bronze, alnico, cupronickel, nickel-silver, aluminum, as well as quality steel alloys are some of the metals involved in current installations. The stirring action of many furnaces is used to assist in the homogeneity required for high-quality results.

The copper alloys and copper can be melted at between 8 and 10 lb per kwhr and poured at rates up to 6 tons an hour. Nearly all wrought-brass

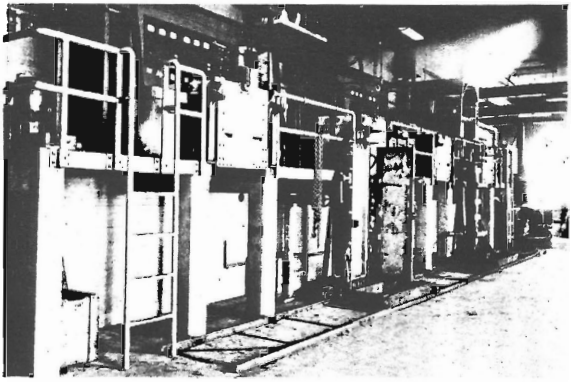

FIG. 3-34. Melting coinage metal at 960 cps, using three 250-kw furnaces. (*U.S. Mint, Denver.*)

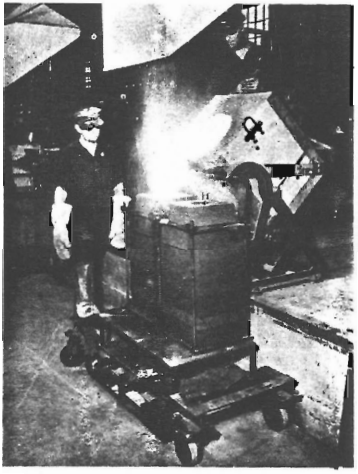

FIG. 3-35. Pouring Alnico magnet material melted by induction heating. (*General Electric Co.*)

alloys are now melted in induction furnaces. Zinc and its alloys have melting rates of about 20 lb per kwhr, and furnaces for these metals run up to 10 tons in capacity. Aluminum alloys are often melted in the Ajax-Tama-Wyatt type of furnace, and rates of 5 lb per kwhr are common, with pouring rates up to 2½ tons per hour. Recently cast iron has been successfully cast at rates of 1,200 lb per hr (44).

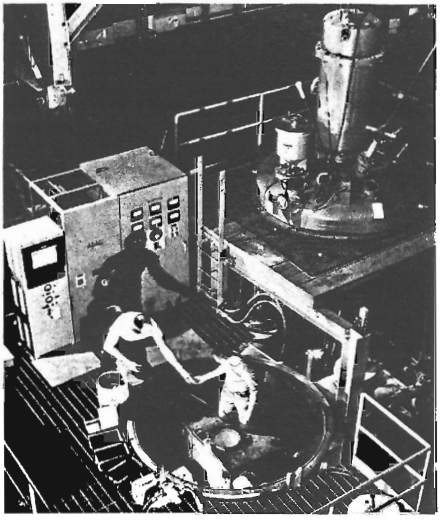

FIG. 3-36. Vacuum induction melting of high-purity alloys at 700 kw, 960 cps. (*Westinghouse Electric Corp.*)

Cast shapes include billets, wire, sheet, strip, plate, and forgings. The power sources usually consist of motor-generator sets in the 960- to 3,000-cps range, spark-gap converters of up to 20 kc, and supply frequencies (50 and 60 cps). Occasionally radio-frequency generators are used in the 400- to 500-kc range for small-scale work such as gold melting.

Examples of precision alloy casting are shown in Figs. 3-34 and 3-35 (16). In each case the alloy melted requires a high degree of consistency and accuracy in its proportion of elements, and induction melting offers the best method of control. It is interesting to note that in the U.S. Mint installation

shown in Fig. 3-34, the existing motor-generator sets were preceded by the older spark-gap converters. As mentioned at the beginning of this chapter, the spark-gap generator and its application for coreless furnaces were among the first uses of industrial induction heating.

Because of the rapid rate of heating, oxidation is minimized and contamination from coke-oven gases eliminated. Recent developments indicate

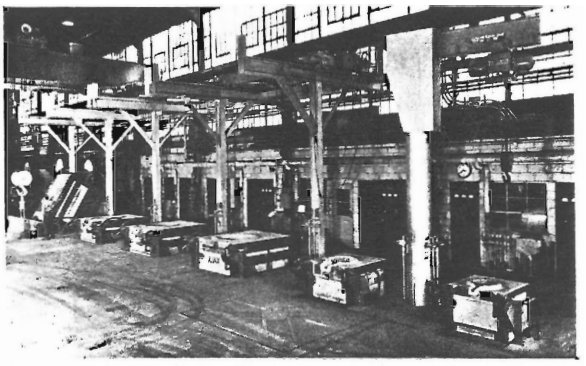

FIG. 3-37. A large-scale steel-melting induction-furnace installation. (*Sandusky Foundry and Machine Co.*)

that further purity to a degree hitherto unobtainable may be obtained by vacuum induction melting (45, 46) (Fig. 3-36).

An interesting type of casting used for intricate parts, and sometimes for pieces difficult to cast in the conventional way, is centrifugal casting, which employs a refractory mold, formed from a wax replica of the required piece. The mold is filled with the molten metal and rotated on an arm so that the centrifugal action ensures excellent filling and an accurate duplication of the original. Although the process is usually used for small charges, it has been used for gun-barrel casting and for heavy-roll production (Fig. 3-37).

Occasionally the stirring properties of induction heating are utilized to upgrade the quality of steel cast from a conventional electric-arc furnace (47). Coils are mounted beneath the furnace and are excited at the very low frequency of 1.4 cps from a single-phase, commutator, 250-kva generator. The resultant rotating magnetic field in the steel causes a slow stirring action, which reduces or eliminates impurities and considerably improves the quality of the alloy.

3-7. MISCELLANEOUS APPLICATIONS

Because all other methods of vacuum tube degassing were partially or completely unsuccessful, one of the earliest applications of induction heating was in this field. It was also an ideal method in an automatic assembly; Fig. 3-38 illustrates such an installation. Low power and high *KVA* are usually required, because of the very poor coupling between coil and "getter"; radio frequencies are usually used.

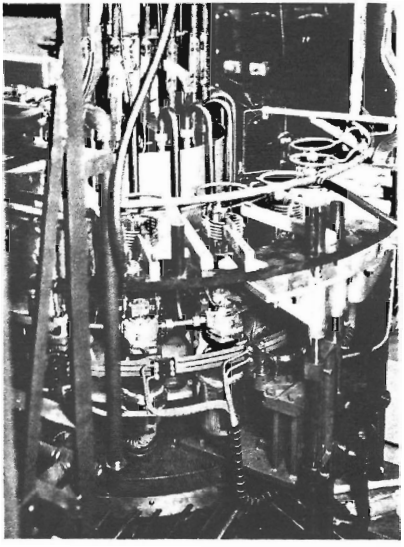

FIG. 3-38. Degassing of vacuum tubes by r-f heating.

An interesting use of transverse flux heating is the annealing and heat-treatment of nonferrous metals (51, 52). Transverse flux is applied to either side of a strip by a series of pole pieces arranged with alternating magnetic poles, as shown in Fig. 3-39*a*. The flux is then transverse or perpendicular to the moving strip, and the current circulates around the strip, as in Fig. 3-39*b*. As the strip is moving, the areas of high current concentration underneath the coils in the slots scan the strip, giving high power but

uniform heat. Owing to this high power density, the necessary heat can be obtained in a few feet of strip; 100 ft or more is required in conventional furnaces. Frequencies between 60 and 10,000 cps are used; metals treated include aluminum, brass, copper, magnesium, and steel above the Curie temperature. The top and bottom pole structures are varied laterally to the movement of strip to accommodate different widths. Strip thicknesses

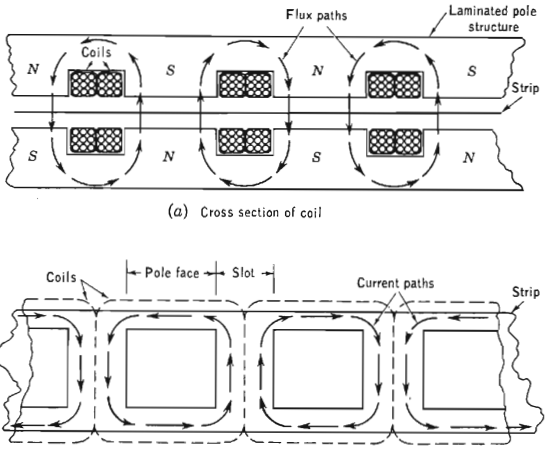

(*a*) Cross section of coil

(*b*) Plan view of coil

FIG. 3-39. Transverse flux heating.

between 0.002 and 0.010 in. can be heated with 9,600 cps, and 60 cps will heat thicknesses between 0.016 and 0.080 in.

Strip heating with conventional longitudinal flux obtained with rectangular coils surrounding the moving strip is used for bright tin reflow (53). Radio frequencies between 100 and 500 kc are used, at high power levels; Fig. 3-40 shows a typical installation.

Occasionally two more heat-treatments are combined in one machine, which simultaneously hardens and anneals shafts at a high production rate. Four parts are loaded, heated and sprayed for hardening, and finally given a short heat for drawing or annealing.

Induction heating is used for shrink fitting, localized expansion being

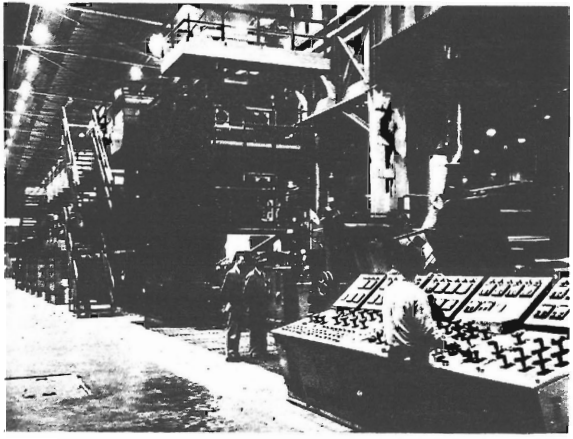

FIG. 3-40. A 2,400-kw 150-kc bright reflowing line for electrolytically deposited tin. (*Westinghouse Electric Corp.*)

FIG. 3-41. Silicon and germanium crystal growing, using 450-kc r-f generators. (*Texas Instruments, Inc.*)

achieved by internal coupling of holes. Internal coils are used, and the power is supplied from r-f generators.

The semiconductor crystal-growing industry has utilized a considerable number of r-f generators. During the various stages of preparing semiconductors, induction heating is used for fusion of the metal powder (silicon or germanium), crystal growing, and zone refining of the finished crystal. The advantages of fast response time, accurate control, and clean operating conditions are well suited to these applications. Frequencies are usually in the 300- to 400-kc range, but 4 Mc is being tried experimentally for silicon, as this semiconductor requires preheating at the lower frequencies. Protective atmospheres or vacuum techniques are used; the coil coupling is therefore necessarily loose because of the need of inserting gas-containing vessels between coil and work. Therefore the generator KVA must be very high for the high Q circuits encountered (Fig. 3-41).

The numerous miscellaneous uses of induction heating include plastic-wire stripping, bonding and debonding of rubber to metal, and removing vacuum-tube bases. Fusing plastic parts by the insertion of a thin wire between the two plastic surfaces is achieved by heating the wire with r-f induction, which then locally melts and fuses the surfaces. Many curing and drying processes, such as paint drying, plastic surfacing, etc., are rapidly accomplished.

3-8. SELECTION OF POWER SYSTEMS FOR INDUCTION HEATING

The selection of the appropriate power system to give the optimum results is very important. Usually the two main guiding factors are current penetration and economics, but often other considerations must also be weighed. For instance, many localized heating applications can be achieved only by radio frequencies, because accurate localization is obtained at these frequencies. The actual heat depth here is relatively unimportant, and although lower-frequency motor-generator equipment might be cheaper, r-f generators are the only logical choice. Usually most smaller localized heating applications involve r-f frequencies and generators, and the larger jobs use motor-generator sets, usually at 9,600 cps.

Hardening is governed by the hardened depth required and bar diameter. The various hardening charts in this chapter and following chapters illustrate the available ranges. As a general rule, the following subdivisions apply in practice:

Frequency	*Case depth, in.*
3,000 cps	0.100–0.250
9,600 cps	0.080–0.120
450 kc	0.030–0.090

Through-heating applications are not quite so critical from the frequency standpoint and economical considerations are as important as frequency choice. Occasionally two frequencies are used for steel heating, as pointed out previously.

Table 3-3 lists the diameters and frequencies used in practice for steel

TABLE 3-3. STEEL THROUGH-HEATING FREQUENCIES FOR FORGING (2300°F)

Bar diameter, in.	Frequencies used in practice, cps	
	Below Curie point	Above Curie point
0–¼	450,000	450,000
¼–½	3,000	9,600
½–1	960	9,600
1–1½	960	3,000 and 9,600
1½–2	60	960 and 3,000
2–6	60	960
6 and over	60	60

through-heating (35). Considerable overlap often occurs as other considerations, such as the possible use of the equipment for other applications, influence the choice.

The nonferrous metals with high electrical resistivities (stainless steel, nickel, titanium, etc.) approximate closely to steel above Curie point, and the same approximate frequency divisions apply. For the lower-resistivity metals (aluminum, brass, copper, magnesium, etc.), the current depth is shallower and therefore the same frequencies can heat smaller diameters. Typical frequency-diameter applications are shown in Table 3-4.

TABLE 3-4. LOW-RESISTIVITY NONFERROUS METAL HEATING

Bar diameter, in.	*Frequencies used in practice, cps*
0–¼	450,000
¼–1	9,600 and 3,000
1–3	960
3 and over	60

Power input varies as the square root of frequency; therefore it would be expected that efficiency would increase as the frequency increases. This is generally true, but the equipment necessary to generate the higher frequencies usually has a lower over-all efficiency, counteracting this advantage. For instance, at 450 kc, a coil efficiency of 80 per cent or better may be expected for steel heating to Curie, but the electronic r-f generator would have an over-all efficiency from line to work of only about 50 to 55 per cent.

A line supply-frequency coil may be only 55 per cent efficient for nonferrous heating, but as no frequency conversion is required, the over-all line-to-work efficiency would be about 50 per cent. Motor-generator frequencies usually result in coils of 70 per cent efficiency for steel, but as the rotating equipment itself usually has an efficiency of only 70 to 80 per cent, the over-all line-to-work efficiency is again about 50 to 55 per cent. From these figures it appears that for nearly all induction heating equipment, a useful efficiency of 50 to 55 per cent may be realized for most metals. Steel below Curie point results in slightly higher figures, about 55 to 70 per cent. Therefore, the running costs in terms of line kilowatthours are about the same for most systems, but maintenance costs are usually a little higher for r-f generators. Line-frequency equipment has very low maintenance costs.

Each case should be considered in the light of its particular features, as will be detailed in the three chapters on the three basic systems used in induction heating (radio-frequency, machine-frequency, and supply-frequency).

Economic factors will also be considered in detail in these chapters. General rules can be applied to comparisons of frequency systems, however, and one generalization is that higher frequencies usually result in higher costs per output of kilowatts. Motor generators cost from $60 to $100 per kilowatt output, and r-f generators cost between $300 and $600 per kilowatt output. These prices do not include auxiliary equipment such as transformers, capacitors, control stations, coils, etc., and work-handling machinery. In general, the cost per kilowatt decreases with higher-power equipment in a square-root relationship. For instance, a fourfold increase in generator power results in approximately twice the cost. Line-supply-frequency equipment costs only between $50 and $75 per kilowatt output, including coil, work-handling machinery, etc., and is obviously more economical in initial cost, as no frequency conversion is required.

CHAPTER 4

COIL DESIGN

4-1. GENERAL PRINCIPLES AND METHODS OF COIL DESIGN

Methods of induction heating coil design can be classified as either calculated or purely practical. In general the slower types of through-heating (heating for extrusion, forging, etc.) require multiturn solenoid coils which can often be designed with little or no prior experience. The faster types of surface or proximity heating (heating for hardening, brazing, soldering, etc.) are usually carried out with single-turn coils or coils with few turns. These are either based purely on the shape of the workpiece and the area to be heated or, in the case of scanning hardening, they are often derived from empirical curves.

In most cases the calculated coils use fixed-voltage power sources, such as the line voltage (460 volts) in supply-frequency heating or the generator voltage (400 or 800 volts) in motor-generator heating. Transformers are sometimes used, but in general the coils are designed to a given or preferred voltage. This is a relatively simple procedure because of the variations possible in the large number of coil turns. In other words, the coil is matched to both application and power source.

The proximity, or shaped, coils are usually of very low impedance values and nearly always have to be matched by a transformer. The coils are primarily designed to heat the area required in the application; matching, usually to an r-f or motor-generator source, follows afterwards. In some cases the r-f generator is provided with an infinitely variable matching r-f transformer to give optimum output for a wide range of coil impedances.

The purpose of this chapter is to provide design methods and simple calculations which result in coils for nearly all types of induction heating. The slower forms of through-heating solenoid coils are primarily based on Chap. 1. Equations are quoted and not derived, and systematic procedures are outlined. The faster forms of proximity hardening coils, both single-shot and scanning, will be derived from empirical curves. Some of these methods are illustrated in Chap. 3. Coils based purely on the shape and size of the required heated area and workpiece are designed from practical considerations.

The first step in nearly all induction heating applications is to consider the frequency and amount of power required for the process. The application usually specifies a production rate, a workpiece with its dimensions and metallic content, and a temperature rise. In through-heating the production rate is usually given as either pounds per hour or billets per hour. Most other applications specify pieces per hour required. Metallic content includes alloy composition and prior heat-treatment. Temperature rise is usually given directly in the case of through-heating, joining, etc. In the case of surface heating for hardening, the required hardness depth is usually specified. This in turn is a direct function of temperature rise and depth of current penetration, i.e., amount of heat required.

Therefore, in all cases the thermal power, defined as the useful power raising the work temperature, can be derived. The various power losses from the workpiece due to radiation, conduction, and convection can be calculated as shown in Chap. 2. The sum of these losses and the thermal power in the work represents the total work power. The surface area of the work into which this power is induced, and therefore the power density, is determined by several factors. In the case of through-heating, a maximum surface-to-center temperature differential is usually specified and this provides a maximum value for the power density. As it is always more economical to build a short-length work coil, this value is also taken as the operating figure, and the coil length and work-surface area are derived accordingly.

For surface hardening, as seen in Figs. 3-22 through 3-24, the "generator power density" is determined from the required hardness depth, given the frequency. The work area is usually specified directly; therefore the work power is obtained from these two factors. For joining, the metal surrounding the joint usually has to be heated; in general the workpiece to one side of the joint is heated first to draw the joining alloy into the joint. The total volume of metal heated can be approximated from heat-conduction and current-depth calculations. The work power is derived from heating time or production rate, and the power density is incidental to the required heated surface area. This procedure is also adapted for single-shot hardening, and quite often the actual area heated in both hardening and joining applications is determined experimentally. In some cases the power can only be determined experimentally, and the coil is designed on the basis of purely practical considerations. If the required application is achieved successfully, then the generator power is noted and this figure is used directly as a basis for the selection of a generator for the final installation.

When the total power into the work, the area to be heated, and therefore the surface power density from the application requirements have been derived, the coil is then designed. A good guide to the main factors is given

in Eq. (1-5). Rewriting this to give surface power density,

$$P_{sw} = \frac{I_c^2 N_c^2 \rho_w \times 10^{-9}}{\delta_w l_w} \tag{4-1}$$

where P_{sw} = surface power density into the work, kw per sq cm
I_c = coil current, amp
N_c = coil turns
l_w = heated work length, cm
ρ_w = average work resistivity over temperature rise, microhm-cm
δ_w = current depth, cm [see Eq. (1-1)]
l_c = coil length, cm (assumed equal to l_w)

As the work resistivity and current depth are primarily determined from the physical properties and the chosen frequency, the main variables are coil current, turns, and length. This fundamental relationship between surface power density and ampere-turns per centimeter or per inch is the basis of all coil design. All the following methods will produce a coil the physical dimensions of which are largely dictated by work shape. The current and turns, and therefore voltage, will be based on work power density and on matching requirements to the frequency source. Even coils designed purely from experimental tests can be checked by this basic equation.

Problems connected with matching will be covered in Chaps. 5, 6, and 7, but the impedance of the power source should always be kept in mind. This is particularly important if the maximum power available from the source is to be used. For instance, a motor generator may be rated at 100 kw with either a 400-volt, 250-amp or a 200-volt, 500-amp output. From the coil design, suppose that 5,000 amp-turns are required. If 50 turns are selected, only 100 amp will be drawn with the highest voltage (400), so that 40 kw will be the maximum power. Therefore, 10 turns with the 200-volt output and 20 turns with the 400-volt output should be used, as these values give the correct current (500 and 250 amp, respectively) and the maximum available power. If only one turn can be used (as in a hardening application), the coil current is 5,000 amp and a current transformer is required. For the 200-volt-output generator the turns ratio would be 5,000:500, or 10:1.

In practice the power factor of the coil has to be corrected to unity (in the case of motor-generator frequencies) and to between 75 and 90 per cent lagging in supply frequencies. Therefore these values of currents are for the circulating current in the parallel tuned circuit between the correction capacitors and the coil (or between the coil and the transformer). In most r-f generators the coil (and transformer if used) is tuned by an internal capacitance, so that the output current is also the coil current. Occasionally, extra capacitors are added across the coil to boost KVA when the coupling is poor and the work nonferrous. The necessary power-factor correction

methods are described in full in the relevant chapters on the three main systems.

4-2. APPLICATION SPECIFICATIONS FOR DESIGN

The following outline summarizes all previous descriptions of the various types of induction heating. The main steps involved in choosing the coil requirements are listed, together with symbols. The final results will be used in designing the coil to the work specifications.

A. Billet Through-heating for Forming, Forging, Extruding, Etc.

1. *Application specifications:*

Metal composition	
Production rate	lb per hour
Temperature rise required, averaged over billet cross section	$\Delta\theta$, °F(θ_o–θ)
Maximum allowable surface-to-center temperature differential	θ_s–θ_c, °F
Mass of billet	M, lb
Billet length	l_w, in.
Billet outer diameter	d_w, in.
Billet inner diameter (if hollow)	ID_w, in.
Billet width (if rectangular)	w_w, in.
Billet thickness (if rectangular)	t_w, in.
Metal density	γ, lb per cu in.
Metal resistivity, averaged over $\Delta\theta$	ρ_w, microhm-cm
Maximum allowable temperature differential along billet length	θ_l, °F
Metal specific heat averaged over $\Delta\theta$, or metal pounds per kilowatthour over $\Delta\theta$	s, or lb per kwhr, respectively
Metal thermal conductivity over $\Delta\theta$	kcal sq cm^{-1} $°C^{-1}$ sec^{-1}
Surface emissivity over $\Delta\theta$	e

2. *Choose frequency f, cps, and calculate depth of current penetration δ_w, in.* Section 3-8 outlines the methods used to select the frequency. The current depth is given by

$$\delta = \frac{1}{2\pi}\sqrt{\frac{\rho}{\mu f}} \quad \text{cm} \tag{4-2}$$

The nomograph in Fig. 2-3*A* enables this equation to be solved quickly except in the case of magnetic steel, where the value of permeability is unknown. However, if it is assumed that μ will vary, approximately, between 15 and 25, some indication is possible for δ_w at this stage.

3. *Determine surface power losses P_r, watts per sq in.* The main source of losses is radiation. If it is assumed that the greater part of the work in most through-heating applications is inside the coil, a general rule is that the radiation is reduced to about 25 per cent of its free-space value. From the considerations in Sec. 2-5, the curves shown in Fig. 2-9 may be used, and the values reduced by 25 per cent. As an approximation, most nonferrous metals heated to extruding temperature lose between 5 to 10 watts per sq in. in a coil, averaged over their heating cycles. Steel heated to forging temperatures may lose 15 to 25 watts per sq in.

4. *Calculated thermal power P_t, kw, required in the work.* Section 2-4 shows that it is simpler to use the value of thermal pounds per kilowatthour, and curves of this property plotted against the temperature are given for common metals in Appendix B. The thermal power in kilowatts is then given from Eq. (2-3*a*).

$$P_t = \frac{\text{production rate in lb/hr}}{\text{lb/kwhr}} \tag{2-3a}$$

An important consideration in heating the ends of bars for forging is the extension of heating beyond the required length to be forged. The temperature will fall off toward the cold end, but a certain amount of power is required over and above the value of P_t to maintain this gradient.

This extension is given in Fig. 4-1 as a function of heating time. It can be seen that for steel, even a 7-sec heat time can produce $\frac{1}{4}$ in. of extended heated metal. The power to heat the extra mass must always be accounted for.

5. *Determine total work length l_w, in., to be heated to give maximum allowable value of surface-to-center temperature differential $\theta_s - \theta_c$, °F.* The net surface power-density input as a function of the surface-to-center temperature differential is given in Eq. (2-17), with the thermal conductivity and the radius. Unfortunately it is complicated by the correction factor $F(P_n/P_a, k_2)$, which is also a function of the net power density.

$$P_n = \frac{(\theta_s - \theta_c)k_c}{0.084\, F(P_n/P_a, k_2)a} \qquad \text{watts/sq in.} \tag{4-3}$$

where k_c = thermal conductivity, cal sec^{-1} cm^{-1} $°\text{C}^{-1}$
P_n = net surface power density, watts per sq in.
P_a = total surface power density, including radiation loss, watts per sq in.
$F(P_n/P_a, k_2)$ = correction factor given in Fig. 2-13
a = work radius ($d_w/2$), in.
δ_w = current depth, in.
$k_2 = \sqrt{2\delta_w a}$

If it is assumed that P_n/P_a is approximately 0.9, i.e., radiation losses are reasonably small, then the factor $F(P_n/P_a, k_2)$ can be read off from Fig. 2-13, and P_n derived as above. It should be remembered that the value of temperature differential $\theta_s - \theta_c$ is related to the actual temperature distribution as shown in Fig. 2-14. Therefore the section of billet a little way in from the surface may be higher in temperature than the surface itself.

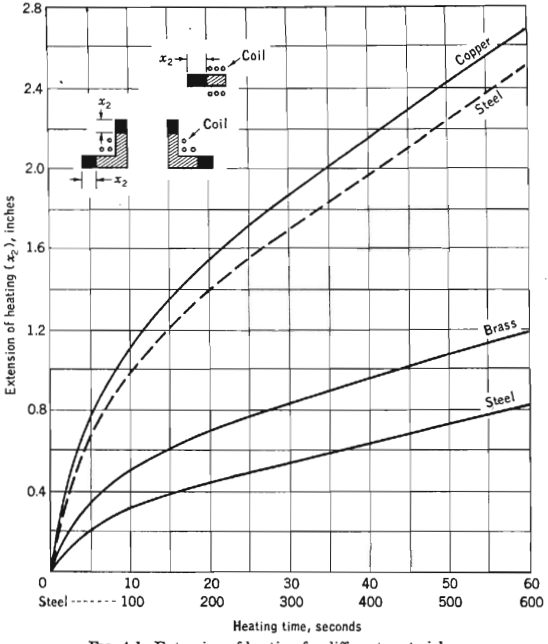

FIG. 4-1. Extension of heating for different materials.

As the maximum net surface power density P_n and the net thermal power P_t have been derived, the minimum surface area to be heated can be calculated by

$$A_s = \frac{P_t \times 10^3}{P_n} \quad \text{sq in.} \tag{4-4}$$

The minimum length is given from

$$l_w = \frac{A_s}{\pi d_w} \quad \text{in.} \tag{4-5}$$

This length is the shortest total work length that can be heated consistent with keeping the surface-to-center differential at its maximum allowable value.

6. *Derive total work power P_w, kw, and work-surface power density P_a.* The total work power is obviously the sum of the radiation power loss (obtained from the radiation density loss and work area) and the thermal power. The work-surface power density is this total power divided by the area A_s, sq in., to be heated. Figure 1-9 can be used, in the case of steel heating at 60 cps, to check the assumed permeability in item 2, above.

7. *Estimate the coil dimensions: l_c, in.; d_c, in.; w_c, in.; or t_c, in.* The effective diameter for coil calculations is usually taken as the inside diameter of the windings. In the case of steel heating up to the Curie point at supply frequencies, it will be taken as the mean of the outer and inner diameters of the windings. This is because in most cases of magnetic steel heating, the cheaper construction of multiple layers of copper tubing can be used. The current required is less than in the nonferrous and nonmagnetic steel coils, and therefore the low-loss solid-copper windings used in these coils are not required.

The inner diameter or dimension of a through-heating coil usually depends on the weight and temperature of the billet and the distortional and dimensional tolerances. The method of feed-through will also determine the diameter. As a general guide, Table 4-1 gives some indication of practical diameters for through-heating coils. The construction will be detailed

TABLE 4-1. RECOMMENDED AIR GAPS FOR THROUGH-HEATING COILS

	Frequency f									
	60 cps			1 kc		3 kc		10 kc		450 kc
Temperature of billet, θ°F	1000	1600	2300	1600	2300	1600	2300	1600	2300	2300
Air gap x in. for d_w = 0–2½ in.	1	1	2	2	2½	2	2½	2	2½	¼–1
Air gap x in. for d_w = 2½–5 in.	1	1½	2	2½	3					
Air gap x in. for d_w = 5–10 in.	1	1½	3½	3	3½					

later in this chapter. The air gap is defined as the difference between coil inner dimension (diameter, width, or length) and work outer dimension.

The length of coil windings depends largely on the chosen method of work handling and the metal heated. In most steel installations, where the production rate is high, the coils are often separated. The resulting cold areas have a negligible effect on the temperature distribution, as usually a sufficiently large number of billets is progressing through the tunnel of coils to spread out and cancel the heatless zones. Therefore, the length of each coil is determined mainly by available power supplies and the maximum length allowed for each line of coils. In most nonferrous installations, the billet dimensions are larger than those of steel billets, and each heating unit has only one coil, with no gap along its length. Therefore, by adding 1 to 3 in. to the minimum work length, the coil length can be estimated closely enough for electrical calculation purposes.

The seven steps above have resulted in the following values for coil calculations:

Frequency ..... f, cps
Current depth in work ..... δ_w, in.
Surface power-density losses ..... P_r, watts per sq in.
Thermal power required ..... P_t, kw
Total work power required ..... P_w, kw
Minimum work length to be heated ..... l_w, in.
Coil inner dimensions ..... d_c, in. (or w_c and t_c, in.)
Coil length ..... l_c, in.

B. Localized Heating for Brazing, Soldering, and Welding

1. *Application specifications:*

Metal or metals to be joined .....
Joining alloy (if specified) .....
Flow or melting temperature of joining alloy ..... °F
Dimensions and shape of workpiece .....
Areas to be joined .....
Areas that must not be heated over a certain temperature (if any) .....
Production rate ..... Pieces per hour
Heat time ..... t, min
Specific heat or thermal pounds per kilowatthour integrated over temperature ..... s, or lb per kwhr
Density of metals heated ..... γ, lb per cu in.

In general, the steps prior to designing a coil for metal joining are not so logical as those for through-heating, as most of the variables are fixed by the

factors above. Usually the power required is determined by experiments and the equipment is based on the results. However, certain guides, outlined below, can be applied. There is no particular sequence to the steps.

2. *Choose the frequency of the power supply.* Most soldering, brazing, and welding applications at the smaller workpieces are carried out at radio frequencies (400 to 500 kc), because of the fast rate of power input and the ability to localize the heat to small areas at these frequencies. The larger ferrous brazing applications are also carried out at machine frequencies (3 and 10 kc), particularly where high production rates are required. In general, nonferrous soldering and brazing is possible only using radio frequencies.

One advantage of machine-frequency soldering and brazing is that the number of volts per turn of the coil and the number of volts from coil to work are much smaller than in r-f joining. This is important where volatile flux is used, as it often tends to short out turns or to cause an arc between coil and work at radio frequencies.

3. *Determine the mass of metal to be heated M, lb.* The minimum amount of the workpiece should be heated consistent with the area of the joint, but heat losses play a large part in joining. If one cross section is heavier than the other, more power should be applied to the heavier section to prevent overheating of the lighter part. If one part is steel and the other nonferrous, the coil should be coupled closer to the nonferrous part, as power input, a function of coupling, is greater for steel. If both parts are steel a smaller area should be heated, as power input is greater and the temperature of the joint will reach the solder or brazing alloy flow temperature quicker for nonferrous parts. Steel-heating coils can therefore be of a smaller number of turns. To avoid softening, etc., areas which have had prior heat-treatment, such as hardening, should not be heated. If the work has sharp edges, heating must be slower and more metal must be heated, to prevent burning of the edges.

Current depth may sometimes determine the depth of metal heated in large pieces. Usually, however, heat conduction inward is the major factor for depth.

From these considerations and the extension of heating effects shown in Fig. 4-1, some idea of the total mass of metal to be heated can be derived.

4. *Calculate the power input P_t, kw.* Usually the time required for each joining operation is a function of the various factors mentioned above. Therefore as the mass of metal to be heated, the average temperature required, and the time are fixed, the power input can be determined approximately from

$$P_t = \frac{Ms\ \Delta\theta}{t} 17.6 \qquad \text{watts} \tag{4-6}$$

where M = mass of metal to be heated, lb
$\Delta\theta$ = temperature rise, °F
s = specific heat, integrated over $\Delta\theta$, cal gm^{-1} $°C^{-1}$
t = heat time, min

While this value is approximate and usually has to be checked experimentally, it gives some indication of the power per piece. Figures 4-2 and 4-3 illustrate typical r-f power densities.

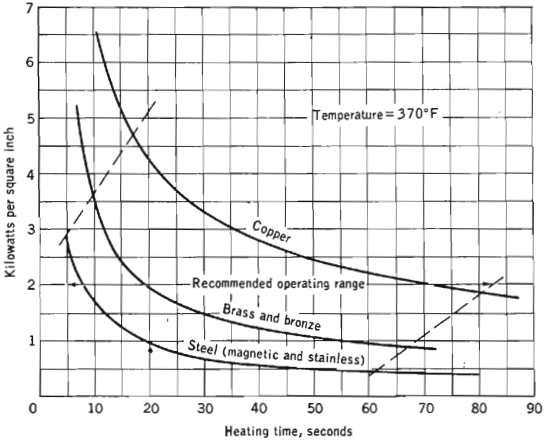

FIG. 4-2. R-F generator rating power density for soft soldering.

5. *Estimate radiation losses* P_r. For soldering applications these are small and can be neglected. For brazing and welding, approximately 10 per cent of the thermal power can be used as a guide.

6. *Determine number of coils or number of pieces per coil.* If the production rate requires a shorter heat time than that estimated above, then either two or more coils are required, or more than one piece should be heated in a coil. Chapter 3 shows a number of applications in which several coils are connected in series to achieve a high production rate.

7. *Select the most suitable brazing or soldering alloy.* If this is not specified, a suitable alloy should be chosen from tables such as those in Sec. 3-4. In

general, the silver-copper-zinc-cadmium alloy is most suitable for induction brazing (69), because of its low flow temperature. Tin-lead-cadmium soft solders are usually used for soldering.

8. *Select the location of the joining alloy.* Figures 3-11 to 3-15 illustrate typical joints and locations of the joining alloy.

9. *Determine coil dimensions.* From all the above considerations, the shape of the coil (or coils) can be estimated. In general, clearances of $\frac{1}{16}$

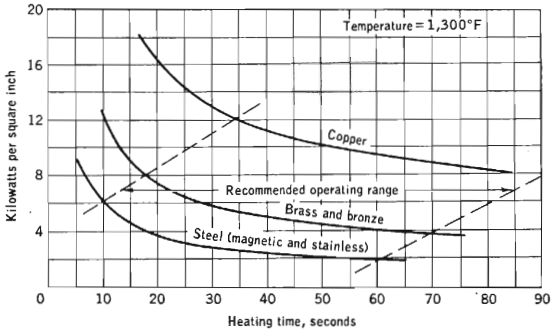

FIG. 4-3. R-F generator rating (power density) for silver soldering.

to $\frac{1}{4}$ in. are practical for most r-f brazing and soldering coils. Figure 4-4 shows some typical coils illustrating some of the above points. There are, however, such a large variety of possible shapes that clearance usually becomes a matter of experience when the coil dimensions are being considered.

The nine steps above should result in the following factors:

Power frequency	f, cps
Mass of metal to be heated	M, lb
Thermal power input	P_t, kw
Radiation losses	P_r, kw
Number of coils or pieces per coil	
Brazing or soldering alloy	
Location of joining alloy	
Coil dimensions and shape	
Work-surface power density	P_a, watts per sq in.

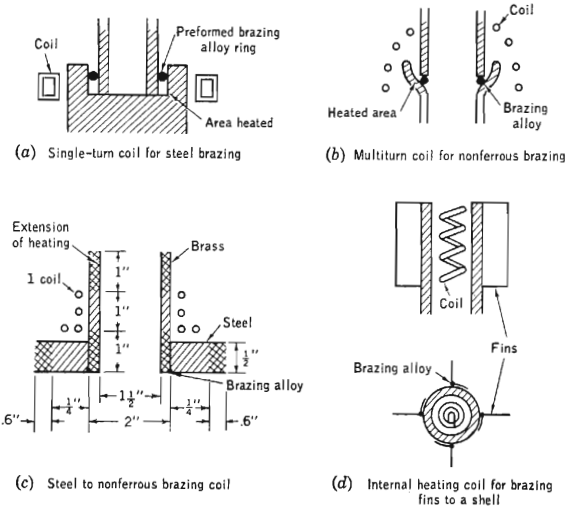

FIG. 4-4. Typical induction brazing and soldering coil shapes.

C. Surface Heating for Hardening

1. *Application specifications:*

Metal alloy composition and prior treatment, if any
Production rate ..... lb per hr or pieces per hr
Mass of workpiece to be heated ..... M, lb
Case depth required ..... d_h, in.
Dimensions of workpiece:
  Outer diameter ..... d_w, in.
  Length to be heated ..... l_w, in.
Area to be hardened ..... A_w, sq in.

2. *Choose the power-supply frequency.* Several variables affect the choice of frequency; they are discussed in detail in Sec. 3-8. The major factors are hardened case depth required, shape of the workpiece, production rate, and

the importance of localization. The frequencies used, in general, are as follows:

Frequency	*Hardened case depth*
3,000 cps	0.100–0.250 in.
9,600 cps	0.080–0.120 in.
450 kc	0.030–0.090 in.

Small workpieces or small areas to be hardened are usually treated at 450 kc, but scanning hardening is done at all frequencies. Owing to the availability of higher powers from motor generators, the faster production rates in scanning usually follow 3 and 9.6 kc, particularly when the workpiece is large. The curves and examples in Sec. 3-5 give the best guide to frequency selection for scanning hardening. Gears are occasionally preheated at a low frequency and hardened at a higher frequency.

3. *Select the method of hardening.* Nearly all small pieces are hardened by single-shot methods, with the coil designed to heat the complete area to be hardened. This also applies to small areas to be hardened on larger pieces. In general, areas up to 3 sq in. are hardened by this method.

Shafts, axles, etc., with reasonably constant diameters or surfaces, are scanned through the coil. Gears are usually rotated inside large coils if deep cases can be tolerated. Large gears are often hardened by scanning each tooth separately.

4. *Determine the area to be heated A_w, sq in.* This is directly determined from the specifications for single-shot hardening, as the hardened and heated areas are almost identical. Selective quenching can occasionally be used to harden part of a heated area where stray heating is inevitable.

Scanning hardening is a somewhat different problem. Chapter 3 contains scanning curves for the three main frequencies (Figs. 3-23, 3-24, and 3-24*A*). With the case depth and frequency already fixed, and the work diameter given, the only variables are power density and time in the coil. These depend directly on coil length and generator size. Most coils are single-turn and vary between ½ and 2 in. long. By fixing a suitable generator, the surface area is determined from the generator kilowatts per square inch, and the coil length from the area and bar diameter. The generator size and coil length can be varied to obtain the best conditions.

5. *Estimate the power density $P_a w$ per sq in., total power P_w, kw, and time required t, sec.* Most single-shot applications at 450 kc require ½ to 1½ sec. For scanning hardening the time can be estimated from the curves, given the frequency, case depth, and generator power density.

The power follows from the power density and the area to be hardened. In single-shot cases 10 to 30 kw per sq in. covers most applications. For scanning, the power density is already established, together with the generator power, from item 4, above.

6. *Select the coil dimensions.* Single-shot hardening coils are coupled as closely as possible to the work surface to be hardened. The turns are kept to a minimum and the area of the coil corresponds closely to that of the area to be hardened. Air gaps between windings and work vary from 0.030 in. upwards, depending on the accuracy of the locating fixtures and the condition of the work surface.

Scanning coils occasionally have to allow a somewhat larger air gap because of work distortions and tolerances. Practical gaps range from 0.040 to 0.120 in.

As the coil area in both single-shot and scanning hardening is already fixed, the inner dimension completes the total dimensions necessary to design the complete coil.

The five steps have resulted in the following information:

Power frequency	f, cps
Method of hardening	
Work area to be heated and hardened	A_w, sq in.
Power density at work	P_a, kw per sq in.
Generator power density	P_g, kw per sq in.
Work power	P_w, kw
Heating time	t, sec
Coil dimensions	

4-3. EXAMPLES OF APPLICATION SPECIFICATIONS

The following examples are typical of industrial requirements and will be used as the basis for coil designs in later sections.

A. Billet Through-heating

Example 4-1.

1. *Application specifications:*

Metal alloy composition	Aluminum 2SO (commercially pure)
Production rate	5,000 lb per hr
Temperature rise (averaged over billet cross section), $\Delta\theta$	880°F (70 to 950°F)
Maximum surface-to-center temperature differential, $\theta_s - \theta_c$	100°F
Mass of each billet, M	55 lb
Billet length, l'_w	20 in.
Billet diameter, d_w	6 in.
Metal density, γ	0.097 lb per cu in.
Metal resistivity, ρ	5.45 microhm-cm

Maximum allowable temperature differential along length, θ_l ..... 15°F
Metal pounds per kilowatthour over $\Delta\theta$. 16.2 lb per kwhr
Metal thermal conductivity over $\Delta\theta$, k_c . 0.38 cal cm^{-1} sec^{-1} $°C^{-1}$
Surface emissivity over θ, P_r..... 5 watts per sq in.

2. *Frequency f, cps, and current depth δ, in.* From Fig. 2-3*A*, and if a frequency of 60 cps is selected, the current depth δ, in., is given as 0.6 in. As the radius is 3 in., which is greater than 3×0.6 or 1.8 in., this frequency is satisfactory. Section 3-8 confirms this.

3. *Surface-power losses $P_r w$ per sq in.* From Fig. 2-9, for a value of $\epsilon = 0.3$ averaged over 70 to 950°F, the radiation loss can be taken as 5 watts per sq in.

4. *Thermal power required P_t, kw.* Using Eq. (2-3),

$$P_t = \frac{5{,}000}{16.2} = 308.6 \text{ kw}$$

5. *Minimum work length l_w, in., for surface-to-center differential $\theta_s - \theta_c$, °F.* The correction factor $F(P_a/P_n, k_2)$ in Fig. 2-13 is a function of a/δ.

$$\frac{a}{\delta} = \frac{d_w}{2\delta} = \frac{6}{2 \times 0.6} = 5$$

Assuming that $P_n/P_a > 0.9$, i.e., that radiation losses are less than 10 per cent, the value of $F(P_a/P_n, k_2)$ is approximately 0.75, from Fig. 2-13.

Using Eq. (4-3),

$$P_n = \frac{(100)(0.38)}{(0.084)(0.75)(3)} = 200 \text{ watts/sq in.}$$

The minimum heated surface area is obtained from Eq. (4-4).

$$A_s = \frac{308.6 \times 10^3}{200} = 1{,}543 \text{ sq in.}$$

The minimum length l_w is given by Eq. (4-5).

$$l_w = \frac{1{,}543}{\pi \times 6} = 82 \text{ in.}$$

As each billet length is 20 in., the nearest multiple is 80 in., which is close enough to the minimum value calculated. The work surface heated will be:

$$A_s = (\pi)(d_w)(l_w) = (\pi)(6)(80) = 1{,}500 \text{ sq in.}$$

This means that four billets, each 55 lb, will be heated together in the coil. As the production rate is 5,000 lb per hr, the number of billets heated per hour is given by

$$\text{Billets per hour} = \frac{5{,}000}{4 \times 55} = 22.5$$

The curve of Fig. 2-15 recommends a maximum rate of 25 billets per hour for a 6-in. diameter, so this rate is below the maximum figure. The heating per billet is the inverse of 22.5, i.e.,

$$t_h = 60/22.5 = 2.67 \text{ min}$$

6. *Total work power P_w, kw, and work-surface power density P_a, watts per sq in.* The thermal net power density is

$$P_n = \frac{P_t}{A_s} = \frac{308.6 \times 10^3}{1{,}500} = 206 \text{ watts/sq in.}$$

The total power density is

$$P_a = P_n + P_t = 206 + 5 = 211 \text{ watts/sq in.}$$

Therefore the work power must be

$$P_w = (211)(\pi)(80)(6)(10^{-3}) = 316 \text{ kw}$$

7. *Coil dimensions (l_c, in.; d_c, in.).* From Table 4-1, the recommended air gap is 1 in. Therefore, the inner diameter of the coil windings is

$$d_c = d_w + 1 = 7 \text{ in.}$$

The coil length is approximately 2 in. longer than the total work length; therefore in this case

$$l_c = 80 + 2 = 82 \text{ in.}$$

Example 4-2

1. *Application specifications:*

Metal alloy and composition	0.44 per cent C steel
Production rate	1,900 lb per hr
Temperature rise, $\Delta\theta$	2300°F
Maximum temperature differential, $\theta_s - \theta_c$	150°F
Mass per billet, M	5.28 lb
Billet length, l_w	3.75 in.
Billet diameter, d_w	2.5 in.
Metal density, γ	0.283 lb per cu in.
Metal resistivity, 70–1400°F, ρ_w	54 microhm-cm
Metal resistivity, 1400–2300°F, ρ_w	117 microhm-cm
Metal pounds per kilowatthour, 70–2300°F	9.5 lb per kwhr
Metal pounds per kilowatthour, 70–1400°F	16 lb per kwhr
Metal thermal conductivity, 70–2300°F, k_c	0.10 cal cm^{-1} sec^{-1} $°C^{-1}$
Surface emissivity averaged over $\Delta\theta$, ϵ	120 watts per sq in.

2. *Frequency f, cps.* From Table 3-3, a suitable combination of frequencies is 60 cps below the Curie point and 960 cps above. This is in fact a typical dual-frequency application. Figure 2-3*A* enables the current depth to be determined in both magnetic and nonmagnetic cases. Below Curie at 60 cps it is approximately 0.5 in., and above Curie at 960 cps it is about 0.7 in.

3. *Surface power losses P_s, watts per sq in.* Below Curie, Fig. 2-9 indicates approximately 10 watts per sq in. Although the coil will effectively reduce this, it is usually retained, as it will include safety factors. Above the Curie point, an average figure of 100 watts per sq in. would be the free-space radiation. This is usually halved to 50 watts per sq in., as the coils are designed with greater thermal insulation.

4. *Thermal power required, P_t, kw.* The total thermal power to heat to 2300°F is, from Eq. (2-3*a*),

$$P_{t(2300)} = 1{,}900/9.5 = 200 \text{ kw}$$

The power to heat to 1400°F is given by

$$P_{t(1400)} = 1{,}900/16 = 119 \text{ kw}$$

Therefore the 960 cps power must be the difference, or 81 kw.

5. *Minimum work length l_w, in., for specified surface-to-center temperature differential $\theta_s - \theta_c$, °F.* In steel heating it is difficult to estimate accurately the temperature differential below the Curie point. Section 2-6 and Fig. 2-21 indicate the effect of the variables. In practice, the time and heated work length are approximately the same below and above the Curie point. Therefore by calculating the length above Curie, and allowing a safety factor, the length below Curie can be approximated.

The ratio a/δ_w or $d_w/2\delta_w$ above Curie is

$$\frac{d_w}{2\delta_w} = \frac{2.5}{2 \times 0.7} = 1.8$$

If it is assumed that the radiation is about 20 per cent of the total power input between 1400 and 2300°F, Fig. 2-13 shows a value of 0.4 for $F(P_a/P_n, k_2)$ on the curve of $P_n/P_a = 0.8$. Using Eq. (4-3),

$$P_n = \frac{(150)(0.10)}{(0.084)(0.4)(1.25)} = 357 \text{ watts/sq in.}$$

Equation (4-4) gives the minimum heated surface area.

$$A_s = \frac{81 \times 10^3}{357} = 226 \text{ sq in.}$$

The minimum length is then

$$l_w = \frac{226}{\pi \times 2.5} = 28.8 \text{ in.}$$

As the billet is small compared with this value, it need not be adjusted to be a multiple of the billet length.

6. *Total work power P_w, kw, work-surface power density P_a, watts per sq in., and permeability, μ_w.* Below Curie, if the same coil length and heated surface area are assumed, the net thermal power density is

$$P_n = \frac{119 \times 10^3}{226} = 525 \text{ watts/sq in.}$$

The total surface power density is

$$P_a = P_n + P_r = 525 + 10 = 535 \text{ watts/sq in.}$$

Above Curie, the total surface power density is

$$P_a = P_n + P_r = 357 + 50 = 407 \text{ watts/sq in.}$$

Therefore the total work-power values are

$$P_w = P_a A_s \times 10^{-3} = (535)(226)(10^{-3}) = 121 \text{ kw (70–1400°F)}$$
$$= P_a A_s \times 10^{-3} = (407)(226)(10^{-3}) = 96 \text{ kw (1400–2300°F)}$$

From Fig. 1-9, the permeability at 535 watts per sq in. for a 2.5-in. diameter is given as 12.

7. *Coil dimensions* (l_c, *in.*; d_c, *in.*) *and heating time* t_h, *min.* If air gaps of $1\frac{1}{2}$ and 3 in. are selected for the 60- and 960-cps coils, respectively, the inner dimensions of the coil windings are:

$$d_c = 2.5 + 1.5 = 4 \text{ in. (70–1400°F)}$$
$$= 2.5 + 3.0 = 5.5 \text{ in. (1400–2300°F)}$$

The billets will be fed continuously through the two coils but the coils will be separated. The effective coil lengths can be taken to be the same as the total billet length. As each billet is 3.75 in. long, the number of billets per coil is

$$\text{Billets/hr/coil} = \frac{1{,}900 \times 3.75}{28.8 \times 5.28} = 46.8$$

The time for each billet in *both* coils is

$$t_h = 60/46.8 \times 2 = 2.57 \text{ min}$$

and in each coil it is 1.29 min.

It is interesting to compare these figures with the formulas given by May (66).

$$t_h = 25\, d_w^2 \quad \text{sec}$$

where t_h = heating time per billet, sec
d_w = work diameter, in.

Also
$$P = 3.2 + 0.16\, d_w \quad \text{kw/in. of billet} \tag{4-7}$$

where P = power input per inch of billet.

Substituting the work diameter of 2.5 in. in the above equation,

$$t_h = \frac{25 \times 2.5^2}{60} = 2.6 \text{ min}$$

This compares with 2.57 min calculated above. In Eq. (4-7),

$$P = 3.2 + (0.16 \times 2.5) = 3.6 \text{ kw/in.}$$

As each coil is 28.8 in. long, the power into the billets for both coils would be

$$P'_w = (28.8)(2)(3.6) = 207 \text{ kw}$$

In fact the total power calculated above is

$$P'_w = 121 + 96 = 217 \text{ kw}$$

Therefore these two equations can be used as a useful check.

The coil lengths can be taken as approximately 4 in. over the total billet lengths, in this case

$$l_c = 28.8 + 4.2 \cong 33 \text{ in.}$$

B. Heating for Joining

Example 4-3

1. *Application specifications:*

Metals to be joined	Steel and brass
Dimensions and shape of work	See Fig. 4-4c
Joining alloy	Silver solder (silver-copper-zinc-cadmium)
Flow temperature	1175°F (approximate)
Production rate	90 pieces per hour
Heat time (100 per cent duty cycle)	40 sec
Density	0.283 lb per cu in. (steel)
	0.3 lb per cu in. (brass)
Specific heat over 1200°F	0.145 (steel)
	0.1045 (brass)

2. *Power-supply frequency.* Because of the nonferrous component, 400 to 500 kc should be used.

3. *Mass of metal heated.* Assume the coil dimensions are as shown in Fig. 4-4c. From Fig. 4-1, the extensions of heating for a 40-sec heat time are 1.0 in. (brass) and 0.6 in. (steel). Therefore the total masses of metal heated are

$$M \text{ (brass)} = \pi(1^2 - 0.75^2)(1.0 + 2.0)(0.3) = 1.25 \text{ lb}$$
$$M \text{ (steel)} = \pi[(1.25 + 0.6)^2 - 1^2](0.5)(0.283) = 1.07 \text{ lb}$$

4. *Power input required.* Using Eq. (4-6),

$$P_t \text{ (brass)} = \frac{(1.25)(0.1045)(1{,}200)(17.6)}{(0.33)(10^3)} = 8.4 \text{ kw}$$

$$P_t \text{ (steel)} = \frac{(1.07)(0.145)(1{,}200)(17.6)}{(0.33)(10^3)} = 9.8 \text{ kw}$$

Allowing 10 per cent radiation losses,

$$P_w \text{ (brass)} = 8.84 \text{ kw}$$
$$P_w \text{ (steel)} = 10.78 \text{ kw}$$

Therefore P_w (total) = 19.62 kw

These figures can also be checked against those derived from Fig. 4-3. The cross-sectional area of the brass workpiece is 1.37 sq in., and that of the steel piece is 3.14 sq in. With a 40-sec heating time, the brass curve requires 5 kw per sq in. and the steel curve 2.4 kw per sq in. Therefore the power inputs are

$$P_g \text{ (brass)} = 5.0 \times 1.37 = 6.85 \text{ kw}$$
$$P_g \text{ (steel)} = 2.4 \times 3.14 = 7.53 \text{ kw}$$
$$P_g \text{ (total)} = 14.38 \text{ kw}$$

This differs from the calculated result mainly because of the arbitrary heated areas chosen. As the curves have been proved in practice, they should be used in preference to the calculated figures. They also give the generator power directly.

5. *Coil dimensions and shape.* As the curves indicate that less power is required, the coil can be reduced in dimensions by approximately the ratios of the powers. For example, the length of the coil coupled to the brass could be reduced to about 0.8 in., and the length coupled to the steel reduced to about 0.2 in.

C. Heating for Hardening

Example 4-4

1. *Application specifications—single-shot:*

Metal	Steel
Production rate	3,600 pieces per hour
Case depth required	0.040 in.
Dimensions of workpiece	0.5-in. diameter, 1 in. long
Area to be hardened	Cylindrical surface
Handling time	0.5 sec

2. *Power-supply frequency.* The total production time is obviously 1/3,600 or 1 sec. With the allowed handling time of 0.5 sec, the heating time is 0.5 sec. It is obvious from Figs. 3-23, 3-24, and 3-24*A* that only 450 kc will harden in this time. This is confirmed by the hardness depth required.

3. *Method of hardening.* Pieces of this size are nearly always hardened by single-shot methods.

4. *Surface area heated.* As all the cylindrical surface has to be hardened, the heated area is

$$A_w = (\pi)(0.5)(1.0) = 1.57 \text{ sq in.}$$

5. *Power and time.* From Fig. 3-24*A*, the heating time, in the coil, of 0.5 sec could be achieved by 19 kw per sq in. with a 10-kw generator, 24 kw per sq in. with a 25-kw generator, or 30 kw per sq in. with a 50-kw generator. Both the 10- and 25-kw generators would be insufficient, as the total required powers of $19 \times 1.57 = 29.8$ kw and $24 \times 1.57 = 38$ kw are in excess of the generator powers.

The 50-kw generator would be sufficient, as the total power is $30 \times 1.57 = 47$ kw.

6. *Coil dimensions.* The coil length would correspond to the heated length, 1 in. The coil inner diameter, from Fig. 3-24*A*, would be

$$ID_c = 0.5 + 0.14 = 0.64 \text{ in.}$$

Example 4-5

1. *Application specification—shaft scanning:*

Metal	Steel
Production rate	1 shaft per min
Mass of shaft	24 lb
Case depth required	0.1 in.
Dimensions of shaft:	
Diameter	1.5 ± 0.010 in.
Length	48 in.
Area to be hardened	Complete 48-in. length

2. *Power-supply frequency and power required.* The case depth of 0.1 in. can be achieved by either 3,000 or 9,600 cps. Therefore the heating time must determine the choice of frequency. Allowing 12 sec for loading and unloading time, the heating time for each shaft is 60 − 12, or 48, sec. The scanning rate is

$$v = \tfrac{48}{48} \text{ or } 1 \text{ in./sec}$$

If a coil 1 in. long is chosen, the heating time in the coil is 1 sec. From Fig. 3-24, the 0.100-in. curve gives a "generator kw per sq in." of 20 at 9,600 cps.

As the heated area is

$$A_w = \pi \times 1.5 = 4.72 \text{ sq in.}$$

the generator power required is

$$P_g = 4.72 \times 20 = 94.4 \text{ kw}$$

This could be achieved by a 100-kw 9,600-cps generator.

Figure 3-23 indicates that 1 sec is too short for 3,000 cps. But if a 2-in.-long coil is used, the heating time becomes 2 sec, which is within the range of the curves. The curve for 0.100 in. at 2 sec gives a power density of 14.5 "generator kw per sq in." As the heated area is now doubled, the total power required is

$$P_g = (2)(4.72)(14.5) = 137 \text{ kw}$$

This would require a 150-kw 3,000-cps generator.

The choice is therefore the 100-kw 9,600-cps generator for economic reasons.

3. *Coil dimensions.* The length is 1 in. The inner diameter is determined by the amount of distortion. In this case, the total distortion is 0.020 in., so a practical air gap would be 0.070 in. The coil inner diameter is

$$ID_c = 1.5 + 0.07 = 1.57 \text{ in.}$$

A single- or two-turn coil would be suitable.

4-4. APPROXIMATE COIL-DESIGN METHOD

This method is a fast and reasonably accurate means of determining the major coil variables of power, voltage, current, and turns. The coil power factor, efficiency, and copper loss are also determined. The method applies primarily to multiturn solenoid coils but can be used, with modifications, for almost any coil.

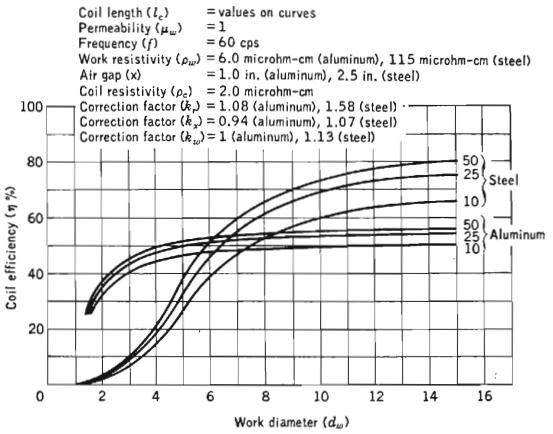

FIG. 4-5. Coil efficiency vs. work diameter for aluminum (70 to 1000°F) and steel (1400 to 2300°F).

The basis of the method is the use of design curves for efficiency, power factor, and reflected impedance per turns squared. These curves can be calculated from equations given in a later section; some examples are given in Figs. 4-5 to 4-10.

The curves are primarily theoretical but are corrected by correction factors based on practical tests. The coil efficiency is defined as

$$\eta = \frac{P_w \times 10^2}{P_o} \quad \text{per cent} \tag{4-8}$$

where η = coil efficiency, per cent
P_w = total power into work, including radiation losses, kw
P_o = total power at coil terminals, including coil losses, kw

Coil length (l_c) = values on curves
Permeability (μ_w) = values on curves
Frequency (f) = 60 cps
Work resistivity (ρ_w) = 54 microhm-cm
Air gap (x) = 1.5 in.
Coil resistivity (ρ_c) = 2.0 microhm-cm
Correction factor (k_r) = 2.37
Correction factor (k_x) = 0.87 (d_w<3 in.), 0.94 (d_w>3 in.)
Correction factor (k_w) = 0.54 (d_w<3 in.), 0.81 (d_w>3 in.)

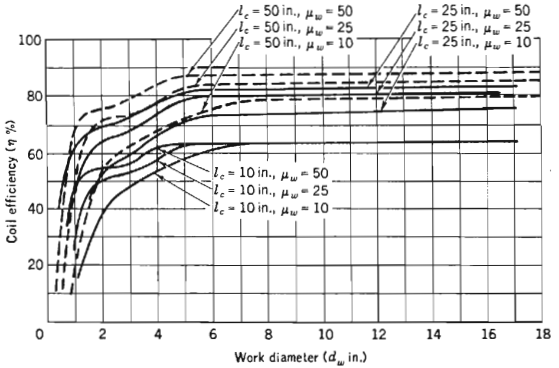

FIG. 4-6. Coil efficiency vs. work diameter for steel (70 to 1400°F).

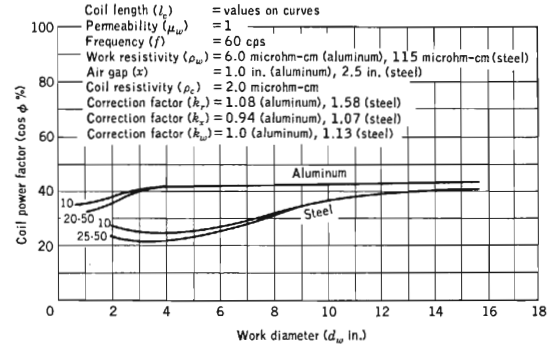

FIG. 4-7. Coil power factor vs. work diameter for aluminum (70 to 1000°F) and steel (1400 to 2300°F).

The coil power factor is defined as

$$\cos \phi = \frac{P_o \times 10^2}{KVA_c} = \frac{P_o \times 10^5}{E_c I_c} \quad \text{per cent} \tag{4-9}$$

where KVA_c = coil kilovolt-amperes at terminals
E_c = coil voltage at terminals, volts
I_c = coil current, amp

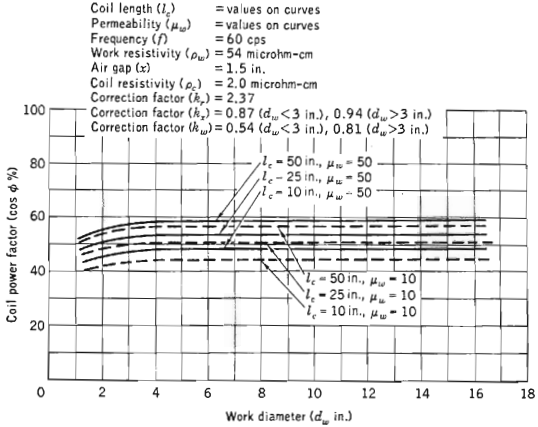

FIG. 4-8. Coil power factor vs. work diameter for steel (70 to 1400°F).

The coil impedance per turn squared is defined as

$$\frac{Z'}{N_c^2} = \frac{KVA_c \times 10^3}{(I_c N_c)^2} = \frac{E_c}{N_c} \frac{10^{-3}}{KVA_c} \tag{4-10}$$

This last term will be explained more fully later; it is a useful definition for the impedance of a coil of one turn.

A systematic design procedure is now possible, using these curves and the application specifications prepared as outlined in Sec. 4-2.

1. *Summarize application specifications:*

Total work power, P_w ..... kw
Temperature rise, $\Delta\theta$ ..... θ_o–θ°F
Work diameter, d_w ..... in.
Work resistivity over $\Delta\theta$, ρ_w ..... microhm-cm

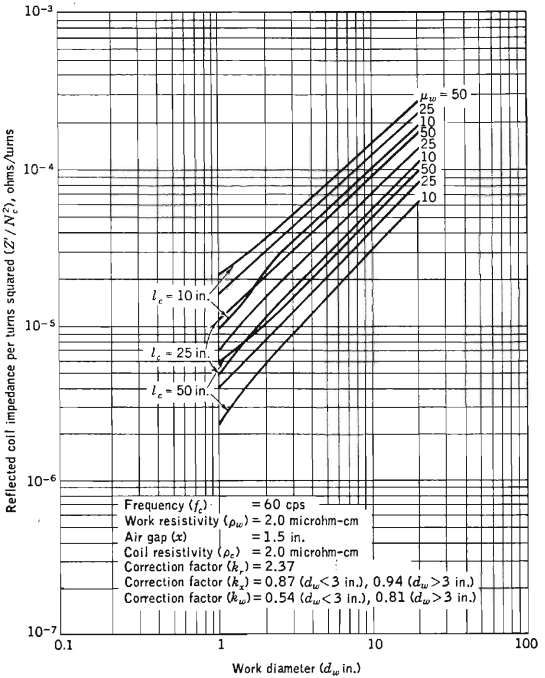

FIG. 4-9. Coil reflected impedance per turns squared vs. work diameter for steel (70 to 1400°F).

Mass of work in coil, M ..... lb
Coil length, l_c ..... in.
Coil inner diameter, d_c ..... in.
or coil inner width, W_c ..... in.
and coil inner thickness, t_c ..... in.
Air gap ($d_c - d_w$), x ..... in.
Frequency, f ..... cps
Preferred coil voltage, E_c ..... volts
Work permeability, μ_w .....

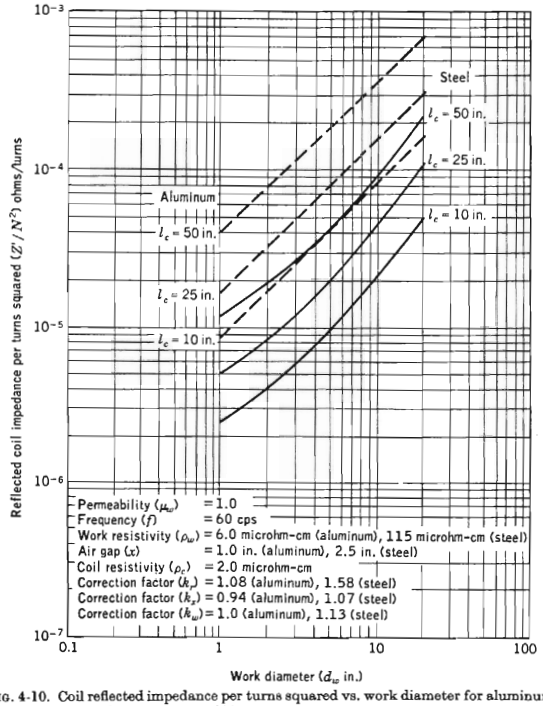

FIG. 4-10. Coil reflected impedance per turns squared vs. work diameter for aluminum (70 to 1000°F) and steel (1400 to 2300°F).

2. *Determine coil efficiency* η, *per cent, power factor* $\cos \phi$, *per cent, and impedance per turns squared* Z'/N_c^2. These are read directly from the curves for the diameter of work.

3. *Derive coil power* P_o *and coil* KVA. Equations (4-8) and (4-9) are utilized to obtain these values.

4. *Obtain coil volts per turn* E_c/N_c *and ampere-turns* I_cN_c. Equation (4-10), in both forms, is used for these values.

5. *Derive coil volts* E_c, *turns* N_c, *and current* I_c. The volts and turns depend to a large degree on the available supply voltage and the available widths of

coil conductors. If a generator frequency or the line supply is being utilized directly, then the volts are fixed. If transformers can be used, then the turns and volts can be selected to give the best compromise.

The current is derived from the ampere-turns and the selected turns.

6. *Calculate the coil copper loss P_c and cooling water required GPM_c.* The copper loss must be the total coil power less the work power.

$$P_c = P_o - P_w \quad \text{kw} \tag{4-11}$$

The cooling water is

$$GPM_c = \frac{P_c}{0.147 \times \Delta\theta_c} \quad \text{gpm} \tag{4-12}$$

where P_c = coil copper loss, kw

$\Delta\theta_c$ = specified cooling-water temperature rise, °F

In general, $\Delta\theta_c$ is 40°F maximum, with the upper temperature of the coil outlet water fixed at 130°F. Below this figure, moisture tends to condense on the windings, which could cause electrical breakdown.

Example 4-6

Design the coil required for the application specifications, derived in Example 4-2, for heating steel to Curie temperatures.

1. *Application specifications:*

Total work power, P_w	121 kw
Temperature rise, $\Delta\theta$	70–1400°F
Work diameter, d_w	2.5 in.
Work resistivity over $\Delta\theta$, ρ_w	54 microhm-cm
Mass of work in coil, M	40.66 lb
Coil length, l_c	28.8 in.
Coil inner diameter, d_c	4 in.
Air gap, x	1.5 in.
Frequency, f	60 cps
Preferred coil voltage, E_c	440 volts
Work permeability, μ_w	12

2. *Coil efficiency, power factor, and impedance per turn squared.* From Fig. 4-6, the values for the given constants are very similar to those above. If the curve is selected for $l_c = 25$ in. and $\mu_w = 10$, the coil efficiency is given as

$$\eta_c = 56 \text{ per cent}$$

It is interesting that with a larger value of μ_w, i.e., a lower surface power density and a larger coil, the efficiency would be considerably improved.

Using Fig. 4-8, as above, the coil power factor is

$$\cos\phi = 49 \text{ per cent}$$

From Fig. 4-9, the coil impedance per turn squared is

$$\frac{Z'}{N_c^2} = 1.4 \times 10^{-5} \text{ ohm per turn squared}$$

3. *Coil power or KVA_c.* From Eqs. (4-8) and (4-9)

$$P_o = (121 \times 10^2)/56 = 216 \text{ kw}$$
$$KVA_c = (216 \times 10^2)/49 = 450$$

4. *Coil volts per turn and ampere-turns.* Using Eq. (4-10),

$$\frac{E_c}{N_c} = \left[\left(\frac{Z'}{N_c^2}\right)(KVA_c)10^3\right]^{1/2}$$
$$= [(1.4)(10^{-5})(450)(10^3)]^{1/2}$$
$$= 2.5 \text{ volts/turn}$$

$$I_c N_c = \frac{KVA_c \times 10^3}{Z'/N_c^2}$$
$$= \left(\frac{450 \times 10^3}{1.4 \times 10^{-5}}\right)^{1/2}$$
$$= 179{,}000 \text{ amp-turns}$$

5. *Coil volts, turns, and current.* The preferred coil voltage is 440 volts from the supply line. Therefore the turns are given from

$$N_c = 440/2.5 = 176 \text{ turns}$$

As the coil length is 28.8 in., or approximately 29 in., the pitch of the coil is

$$29/176 = 0.165 \text{ in./turn}$$

The coil current is

$$I_c = 179{,}000/176 = 1{,}020 \text{ amp}$$

As one layer of windings would have to use only $\frac{1}{8}$ in. tube and this is obviously insufficient copper for 1,020 amp, a better choice is three layers, using tubing $\frac{3}{8}$ in. in diameter. Each layer would consist of $176\frac{2}{3}$ or 59 turns, with a pitch of $29\frac{1}{59}$ or 0.49 in. per turn. This allows ample space for the Fiberglas sleeving used on these coils, which is usually 0.03 in. thick.

6. *Coil copper loss and cooling water.* From Eq. (4-11),

$$P_c = 216 - 121 = 95 \text{ kw}$$

Therefore the minimum cooling water is obtained, using Eq. (4-12) and assuming a rise of 40°F.

$$GPM_c = 95/(0.147 \times 40) = 16.2 \text{ gpm}$$

4-5. EQUIVALENT CIRCUIT COIL-DESIGN METHOD

The basis for this method of coil design is the reduction of the induction heating coil and workpiece to their equivalent resistances and inductances. This is the same procedure as the reduction of a transformer to its equivalent

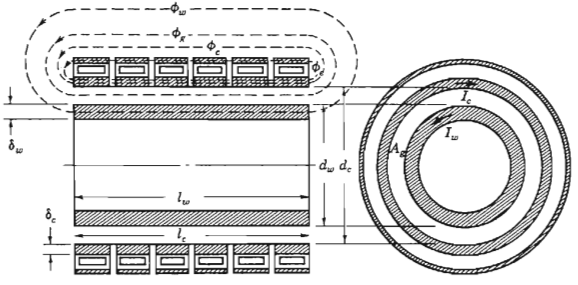

(*a*) Flux and current paths in a coil

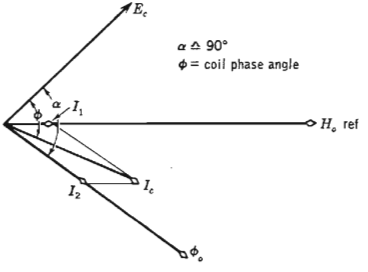

(*b*) Vector diagram for a short coil

FIG. 4-11. Flux paths and vector diagram for a solenoid coil.

circuit, where the various flux paths are represented in terms of inductances, and the losses, including the load, represented as resistances. The equations have been fully derived in reference 62 and will only be summarized here.

Figure 1-1*b* illustrated the current paths in an ideal solenoid work coil, and Fig. 4-11*a* shows the distribution of flux which induces the currents.

The fluxes through the work ϕ_w, coil ϕ_c, and air gap ϕ_g are given as follows:

$$\phi_c = \frac{k_r p_c \delta_c}{2} H_o(1 - j) \qquad \text{maxwells} \tag{4-13}$$

$$\phi_w = \mu_w A_w H_o(P - jQ) \qquad \text{maxwells} \tag{4-14}$$

$$\phi_g = H_o A_g \qquad \text{maxwells} \tag{4-15}$$

where k_r = coil resistance correction factor (usually between 1.0 and 1.5)
p_c = inside coil perimeter, cm
δ_c = current depth in coil, cm
H_o = peak magnetizing field in air gap, oersteds
μ_w = work permeability
P, Q = correction factors (see Chap. 1)
A_w = cross-sectional work area, sq cm
A_g = cross-sectional air-gap area, sq cm

Equation (4-14) was derived as Eq. (1-58).

Using the basic relationship,

$$\text{Magnetomotive force (MMF)} = \text{reluctance} \times \text{flux}$$

the total MMF generated in the coil is used up as follows:

$$0.4\pi N_c \mathbf{I}_c \sqrt{2} = H_o l_c + R_e \boldsymbol{\Phi}_o \tag{4-16}$$

where N_c = coil turns
l_c = coil length, cm
$\mathbf{I}_c$ = coil current, amp
R_e = reluctance of external flux path
$\boldsymbol{\Phi}_o$ = total flux linking the coil, oersteds

The MMF drop inside the coil is $H_o l_c$, and outside the coil it is $R_e \boldsymbol{\Phi}_o$. In along coil, R_e tends to zero and all the MMF is dropped internally.

Rewriting Eq. (4-16),

$$\mathbf{I}_c = \frac{H_o l_c}{0.4\pi N_c \sqrt{2}} + \frac{R_e \boldsymbol{\Phi}_o}{0.4\pi N_c \sqrt{2}} \tag{4-17}$$

or

$$\mathbf{I}_c = I_1 + \mathbf{I}_2 \tag{4-18}$$

This is best represented by the vector diagram shown in Fig. 4-11*b*. In the case of a long or ideal coil, $\mathbf{I}_2$ would be zero and I_1 would equal $\mathbf{I}_c$.

The field intensity H_o in the air gap is established by the coil voltage, given by the familiar transformer equation,

$$\mathbf{E}_c = j\sqrt{2} f N_c \boldsymbol{\Phi}_o \times 10^{-8} \tag{4-19}$$

If Eqs. (4-18) and (4-19) are compared, it is obvious that the equivalent circuit consists of two impedances, Z_1 and Z_2, in parallel. Their values are given by dividing $\mathbf{E}_c$ by $\mathbf{I}_c$.

$$Z_1 = \frac{0.8\pi f N_c^2 \times 10^{-8}}{l_c} \left(\frac{j\boldsymbol{\phi}_o}{H_o}\right) \tag{4-20}$$

$$Z_2 = 0.8\pi^2 f N_c^2 \times 10^{-8} \left(\frac{j}{R_e}\right) \tag{4-21}$$

The value of $\boldsymbol{\phi}_o$ is given from the addition of Eqs. (4-13), (4-14), and (4-15).

$$\boldsymbol{\phi}_o = H_0 \left[\left(\frac{k_r \rho_c \, \delta_c}{2} + \mu_w A_w P + Ag \right) - j \left(\frac{k_r \rho_c \, \delta_c}{2} + \mu_w A_w Q \right) \right] \tag{4-22}$$

The value of R_e for a cylindrical coil is given approximately by

$$R_e = \frac{0.57}{d_c} \tag{4-23}$$

Substituting Eqs. (4-22) and (4-23) in Eqs. (4-20) and (4-21), and separating out the resistive and reactive terms,

$$Z_1 = (R_w + R_c) + j(X_w + X_c + X_g) \tag{4-24}$$

$$Z_2 = X_e \tag{4-25}$$

Converting the units of length to inches and substituting the necessary conversion factors, the separate terms in Eqs. (4-24) and (4-25) are as follows:

$$\frac{R_w}{N_c^2} = \frac{15.8 f \, d_w^2 \mu_w Q \times 10^{-8}}{l_c} \quad \text{ohm/turn squared} \tag{4-26}$$

$$\frac{X_w}{N_c^2} = \frac{15.8 f \, d_w^2 \mu_w P \times 10^{-8}}{l_c} \quad \text{ohm/turn squared} \tag{4-27}$$

$$\frac{X_c}{N_c^2} = \frac{R_c}{N_c^2} = \frac{k_r 63.2 \, d_c (f\rho_c)^{1/2} \times 10^{-8}}{l_c} \quad \text{ohm/turn squared} \tag{4-28}$$

$$\frac{X_g}{N_c^2} = \frac{20.1 f A_g \times 10^{-8}}{l_c} \quad \text{ohm/turn squared} \tag{4-29}$$

$$\frac{X_e}{N_c^2} = 35.3 f \, d_c \times 10^{-8} \quad \text{ohm/turn squared} \tag{4-30}$$

where R_w = work resistances, ohms
X_w = work reactance, ohms
X_c = coil reactance, ohms
R_c = coil resistance, ohms
X_g = air-gap reactance, ohms
X_e = external flux-path reactance, ohms

These are the equivalent circuit terms; the circuit is shown in Fig. 4-11*A*(*a*). The circuit can be further reduced to Fig. 4-11*A*(*b*), and the values of this circuit are as follows. The units are ohms per turn squared, and the values are therefore independent of coil turns, which can be calculated later.

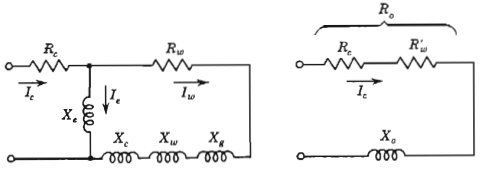

(*a*) Full coil and work equivalent circuit (*b*) Reduced equivalent circuit

FIG. 4-11*A*. Equivalent circuits.

$$\frac{R_w'}{N_c^2} = \frac{(R_w/N_c^2)(X_e/N_c^2)^2}{(Rw/N_c^2)^2 + (X_1/N_c^2 + X_e/N_c^2)^2} \tag{4-31}$$

$$\frac{X_o}{N_c^2} = \frac{(X_e/N_c^2)[(R_w/N_c^2)^2 + (X_1/N_c^2)^2 + (X_e/N_c^2)(X_1/N_c^2)]}{(R_w/N_c^2)^2 + (X_1/N_c^2 + X_e/N_c^2)^2} \tag{4-32}$$

where

$$\frac{X_1}{N_c^2} = \frac{X_w}{N_c^2} + \frac{X_c}{N_c^2} + \frac{X_g}{N_c^2} \tag{4-33}$$

Assuming that

$$\frac{R_o}{N_c^2} = \frac{R_w'}{N_c^2} + \frac{R_c}{N_c^2} \tag{4-34}$$

the major coil properties of efficiency, power factor, power, KVA, volts per turn, and ampere-turns can now be determined, given the required work power.

Coil efficiency:

$$\eta = \frac{R_w'/N_c^2}{R_o/N_c^2} \tag{4-35}$$

Coil power factor:

$$\cos\phi = \frac{R_o/N_c^2}{Z_o/N_c^2} \tag{4-36}$$

where

$$\frac{Z_o}{N_c^2} = \left[\left(\frac{R_o}{N_c^2}\right)^2 + \left(\frac{X_o}{N_c^2}\right)^2\right]^{1/2} \tag{4-37}$$

Coil power and KVA:

$$P_o = \frac{P_w}{\eta} \tag{4-38}$$

$$KVA_c = \frac{P_o}{\cos \phi} \tag{4-39}$$

Coil volts per turn and ampere-turns:

$$\frac{E_c}{N_c} = \left[(KVA_c) \left(\frac{Z_o}{N_c^2} \right) (10^3) \right]^{1/2} \quad \text{volts/turn} \tag{4-40}$$

$$I_c N_c = \left(\frac{KVA_c \times 10^3}{Z_o / N_c^2} \right)^{1/2} \quad \text{amp-turns} \tag{4-41}$$

The actual coil-voltage current and turns are derived in exactly the same way as in the approximate design method of Sec. 4-4. Correction factors can be inserted in Eqs. (4-31) and (4-32) to account for small differences in theoretical and practical results. They are defined as

k_x = reflected coil-reactance correction factor

k_w = reflected work-resistance correction factor

Typical values are shown in Figs. 4-5 to 4-10. These curves have all been derived using the equivalent circuit method, and the correction factors are based on experimental results.

Example 4-7

Design the coil required for the application specifications, derived in Example 4-2, for through-heating steel between 1400 to 2300°F.

1. *Application specifications:*

Total work power, P_w	96 kw
Temperature rise, $\Delta\theta$	1400–2300°F
Work diameter, d_w	2.5 in.
Work resistivity over $\Delta\theta$, ρ_w	117 microhm-cm
Coil length, l_c	33 in.
Coil inner diameter, d_c	5.5 in.
Air gap, x	3.0 in.
Frequency, f	960 cps
Preferred coil voltages, E_c	380 or 760 volts
Work permeability, μ_w	1.0
Coil correction factor, k_r	1.5 (assumed)
Coil resistivity, ρ_c	2.0 microhm-cm

2. *P and Q factors.* The current depth is

$$\delta = \frac{1.98 \times 117^{1/2}}{1^{1/2} \times 960^{1/2}} = 0.69 \text{ in.}$$

from Eq. (1-1) converting to practical units. The ratio d_w/δ is

$$\frac{d_w}{\delta} = \frac{2.5}{0.69} = 3.63$$

P and Q values for this ratio are

$$P = 0.62$$
$$Q = 0.37$$

from Fig. 1-5.

3. *Equivalent circuit components.* Substituting the above values in Eqs. (4-26) to (4-30),

$$\frac{R_w}{N_c^2} = \frac{(15.8)(960)(2.5)^2(1)(0.37)(10^{-8})}{33} = 10.6 \times 10^{-6} \text{ ohm/turn squared}$$

$$\frac{X_w}{N_c^2} = \frac{(15.8)(960)(2.5)^2(1)(0.62)(10^{-8})}{33} = 17.8 \times 10^{-6} \text{ ohm/turn squared}$$

$$\frac{X_c}{N_c^2} = \frac{(1.5)(63.2)(5.5)(960)^{1/4}(2)^{1/4}(10^{-8})}{33} = 6.9 \times 10^{-6} \text{ ohm/turn squared}$$

$$\frac{X_g}{N_c^2} = \frac{(20.1)(960)[(\pi)(2.75)^2 - (\pi)(1.25)^2](10^{-8})}{33}$$

$$= 110 \times 10^{-6} \text{ ohm/turn squared}$$

$$\frac{X_s}{N_c^2} = (35.3)(960)(5.5)(10^{-8}) = 1{,}870 \times 10^{-6} \text{ ohm/turn squared}$$

The reflected components are given in Eqs. (4-31) to (4-34):

$$\frac{X_1}{N_c^2} = (17.8 + 6.9 + 110)(10^{-6}) = 134 \times 10^{-6} \text{ ohm/turn squared}$$

$$\frac{R'_w}{N_c^2} = \frac{(10.6)(1{,}870)^2(10^{-6})}{10.6^2 + 2004.7^2} = 9.2 \times 10^{-6} \text{ ohm/turn squared}$$

$$\frac{X_o}{N_c^2} = \frac{(1{,}870)[(10.6)^2 + (134)^2 + (1{,}870)(134)](10^{-6})}{10.6^2 + 2004.7^2}$$

$$= 125.5 \times 10^{-6} \text{ ohm/turn squared}$$

$$\frac{R_o}{N_c^2} = (9.2 + 6.9)(10^{-6}) = 16.1 \times 10^{-6} \text{ ohm/turn squared}$$

4. *Coil efficiency, power factor, and impedance.* Using Eqs. (4-35) to (4-37),

$$\eta = \frac{9.2 \times 10^{-6}}{16.1 \times 10^{-6}} = 57 \text{ per cent}$$

$$\frac{Z_o}{N_c^2} = (16.1^2 + 125.5^2)^{1/2}(10^{-6}) = 126 \times 10^{-6} \text{ ohm/turn squared}$$

$$\cos\phi = \frac{16.1 \times 10^{-6}}{126 \times 10^{-6}} = 12.8 \text{ per cent}$$

5. *Coil power and KVA.* From Eqs. (4-38) and (4-39),

$$P_o = 96/0.57 = 169 \text{ kw}$$

$$KVA_c = 169/0.128 = 1{,}320 \text{ kva}$$

6. *Coil volts per turn and ampere-turns.* Equations (4-40) and (4-41) give

$$\frac{E_c}{N_c} = [(1{,}320)(126)(10^{-6})(10^3)]^{1/2} = 12.9 \text{ volts/turn}$$

$$I_c N_c = \left(\frac{1{,}320 \times 10^3}{126 \times 10^{-6}}\right)^{1/2} = 102{,}500 \text{ amp-turns}$$

7. *Coil volts, amperes, and turns.* If the preferred coil voltage of 380 volts is selected (the generator voltage of 400 volts less 5 per cent for transmission-line drop), the coil turns are

$$N_c = 380/12.9 = 29.4 \simeq 29 \text{ turns}$$

As the coil length is 33 in., the pitch is

$$\frac{l_c}{N_c} = \frac{33}{29} = 1.135 \text{ in.}$$

It is usual to allow air insulation or spacing in machine-frequency coils; therefore $\frac{3}{4}$-in. tubing can be used, with a $\frac{3}{8}$-in. spacing.

The coil current is

$$I_c = 102{,}500/29 = 3{,}530 \text{ amp}$$

As the depth of current penetration in copper at 960 cps is only 0.09 in., there is no point in using solid copper conductors. Provided the tubing-wall thickness is as close to 0.09 in. as possible, copper losses are minimized.

4-6. SCALE-MODEL ANALOGUE METHODS

An interesting possibility of experimental coil design has been proposed (71) in which the work and coil dimensions are scaled down and the frequency is raised in proportion. The result would enable large and costly coils, drawing very high powers at low frequencies, to be designed from tests using smaller and more economical coils at higher frequencies.

The basis of the method is to reduce all linear dimensions of the coil and load by a convenient ratio, say R. Electrical analogy is then obtained between the required coil and the reduced coil by the following conditions:

1. The frequency is increased by $1/R^2$.
2. The number of coil turns is maintained.
3. The applied voltage is maintained.

The results are listed below:

1. Power factor and efficiency are retained.

2. Coil and work power input and coil loss are reduced by R.
3. Heating pattern is retained.
4. Surface power density is increased by $1/R$.
5. Heating time to a given temperature is reduced in the ratio R^2.

As the only predetermined variable is that of frequency, the ratio R is determined from this. For example, by increasing the frequency from 60 cps to the motor-generator frequency of 3,000 cps, R is given by

$$\frac{1}{R^2} = \frac{3{,}000}{60}$$

Therefore $$R \doteq 1:7$$

A coil 7 in. in diameter, 28 in. long, at 60 cps can be analogued by a coil 1 in. in diameter and 4 in. in length, using 3,000 cps. The coil turns, voltage, power input, etc., are experimentally determined to obtain the required heat pattern and $1/R$ or seven times the required surface power density. The full-scale coil can then be accurately designed using the same voltage and turns as the model.

4-7. MECHANICAL CONSTRUCTION OF COILS

The basic purpose behind most mechanical-coil designs is to couple as closely as possible to the workpiece, consistent with loading and unloading clearances, electrical and thermal insulation, and general industrial ruggedness. Apart from a small percentage of simple, hand-loaded applications, most coils are designed to be integral with work-handling equipment and matching units, such as transformers, power-factor capacitors, etc. Secondary problems, such as stray-field heating, vibration, water and oil effects, must also be considered. Therefore, when the electrical and dimensional parameters have been decided on, the coil must be engineered.

The first items to be considered are the coil windings and the type of conductor. The coil current and turns, together with the frequency, usually determine the type of conductor. High-conductivity copper is always used as the conductor material, and coil losses are high enough for water cooling to be necessary at all times. Silver plating is often added to coils to improve the surface conductivity, particularly at the contact surfaces between the coil and the generator or transformer terminals.

In general, most scanning surface-hardening coils are single-turn and conduct very high currents. These currents may be as high as 20,000 amp, usually at 3 and 10 kc or 500 kc, and therefore bunch around the inner surfaces. Figures 4-12, 4-13, and 4-14 and Fig. 2-18 illustrate typical coils of this type. Construction of the coils usually starts with forging the copper

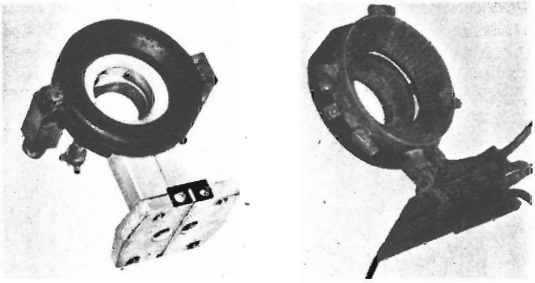

(*a*) (*b*)

FIG. 4-12. Scanning hardening coil and quench assemblies. (*Westinghouse Electric Corp.*)

FIG. 4-13. Various stages in the construction of a combined coil-quench block. (*The Ohio Crankshaft Corp.*)

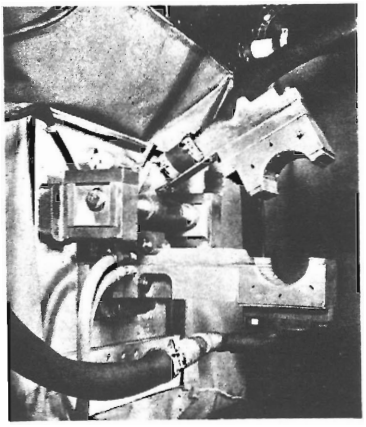

FIG. 4-14. An integral coil-quench block of the split type, which clamps together during heating. (*The Ohio Crankshaft Corp.*)

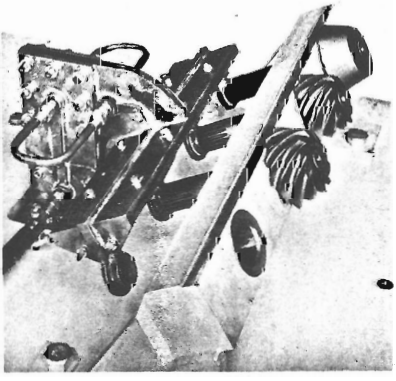

FIG. 4-15. Single turn series r-f annealing coil. (*Westinghouse Electric Corp.*)

shapes from high-conductivity copper or electrolytic tough-pitch copper, such as American Brass Co. 100. Holes of varying diameter are drilled in line with the axis of the work to be scanned and in line with the coil leads. Washers of copper are brazed to the resultant form, and the finished coil is cleaned and silver-plated. Sometimes the quench is built onto the coil, as in Fig. 4-12, and sometimes the coil and quench are one unit, as shown in

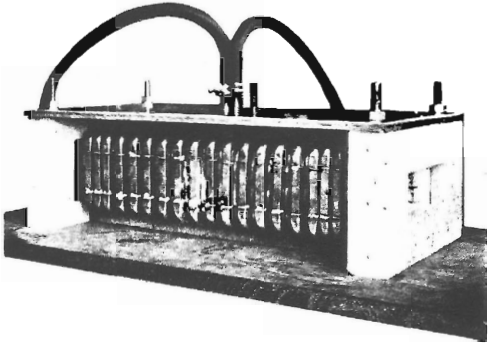

FIG. 4-16. Machine-frequency heating for forging coil. (*Westinghouse Electric Corp.*)

Figs. 4-13 and 4-14. High-temperature solders, such as Sil-Flos, should not be used for construction, as they offer a high resistance to large currents. Joints are brittle and sometimes crack because of thermal expansion on applying current, and they are difficult to rework. Silver solder should always be used.

Figure 4-15 shows four high-current coils used to anneal the threaded ends of automobile pinions at radio frequencies. The coils are all in series.

It is often important to locate high-current coils very firmly in position to prevent the magnetic repulsion between coil and workpiece from damaging and twisting the coil.

Most other types of r-f and machine-frequency coils are constructed from either round or square tubing. The currents in multiturn coils are smaller than those in single-turn coils, and at higher frequencies they tend to concentrate on the shallow surface areas of the tubing. Usually the current concentrates on the side of the tubing nearest the work if it is nonmagnetic (copper, brass, steel above Curie point) and furthest away if it is highly magnetic (steel below Curie point, powdered iron, etc.).

Occasionally it is more economical to construct these types of coils from elbow pieces and straight tubing, particularly where the conductor is square in cross section. However, for r-f heating, continuous tubing is

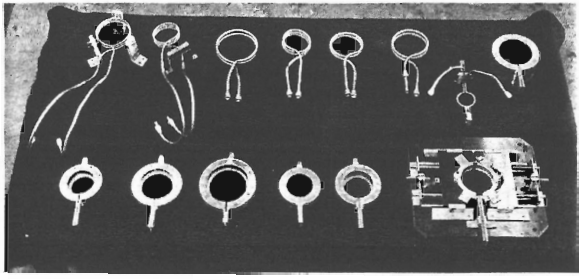

FIG. 4-17. Typical r-f coils and quenches for single-shot hardening and brazing. (*Westinghouse Electric Corp.*)

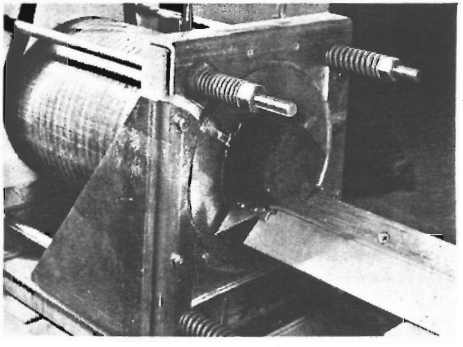

FIG. 4-18. Multilayer hollow-tubing 60-cycle coil used for magnetic steel through-heating. (*Westinghouse Electric Corp.*)

nearly always used. Figure 4-17 shows typical r-f coils designed for a variety of applications.

In supply-frequency through-heating for forging, forming, extruding, annealing, etc., it is usual to use solid copper conductors, water-cooled.

The exception is heating steel up to Curie temperature, when the currents are smaller and conventional round tubing is wound in several layers. Figure 4-18 illustrates such a coil, wound of two layers of ½-in. OD copper tubing.

Figure 4-19 shows various types of fabricated conductors used in the majority of nonferrous and nonmagnetic steel-heating 60-cps coils. The most widely used construction is shown in Fig. 4-19*a*. The depth of the conductor is usually ½ in., as the depth of current penetration in copper at 60 cps is approximately ⅓ in. As the currents carried and the coil-conductor copper losses are usually high, the heat transfer to the cooling

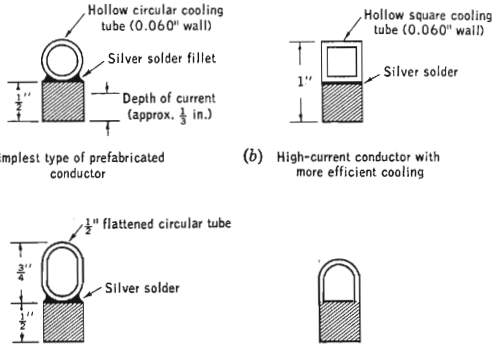

FIG. 4-19. Sixty-cycle heating-coil conductors.

water should be as efficient as possible. Silver-solder fillets are usually built up as shown to assist heat transfer.

If the circular cooling tube is insufficient to carry the flow required, square section tubing is used, as shown in Fig. 4-19*b*. This is more costly; square tubing may be as much as 50 per cent higher in cost per foot. To achieve greater cooling with circular tubing, the tubing can be flattened, as in Fig. 4-19*c*. In certain cases where the number of coils is large, with the same conductor width, it may be more economical to use an extruded section, shown in Fig. 4-19*d*.

The usual method of coil construction consists in first brazing the solid bar and the cooling tube together. The fabricated conductor is then wound onto a wooden mandrel, using a large lathe. These two operations are often

combined into one continuous process. After winding has been completed, the coil is acid-dipped, cleaned, and covered with braided Fiberglas sleeving, usually of 0.060-in. wall thickness. The total coil length is made up of several sections of smaller length in order to simplify construction, especially the process of fitting the sleeving over the conductor. Coils with windings of hollow tube only are constructed in a similar manner, except that the various layers are built up coaxially.

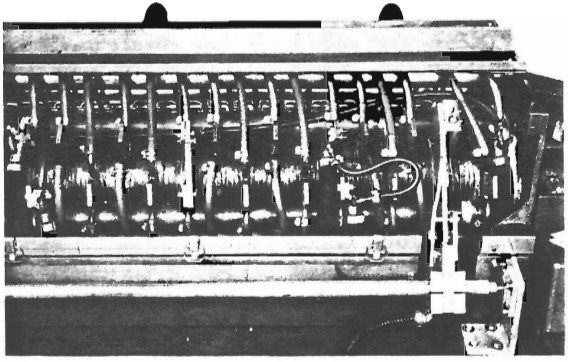

FIG. 4-20. Typical 60-cycle single-layer nonferrous heating coil. (*Westinghouse Electric Corp.*)

The coil sections are fitted with the necessary terminal lugs and cooling leads and are then vacuum-impregnated and baked with conventional organic transformer varnish. The impregnation and baking procedure is usually repeated two to three times to obtain the necessary electrical insulation between turns. Figure 4-20 illustrates a completed coil, constructed with this technique. Coil taps have been provided along every six turns to enable various heat patterns to be obtained in the load.

Machine-frequency coils consist of a small number of turns, usually separated, with air spacing as insulation between turns. Figure 4-16 illustrates this type of construction; the turns are spaced with notched insulating spacers.

Nearly all through-heating coils utilize thermal insulation between coil windings and the workpiece. This is necessary both to protect the windings and varnish from radiant heat and to act as a muffle on the load. Figure 4-21

illustrates some typical insulation methods used in through-heating coil construction for 60 cps and 1, 3, and 10 kc. Stainless steel liners can be used only in 60-cps coils, as higher-frequency induction heats the liner. A lengthwise split of about ½ in. is required to prevent 60-cps heating of the liner. The refractory may be asbestos millboard up to a billet temperature of 1400°F, but over this temperature high-temperature refractory felt, such as Johns Mansville Thermaflex RF 300, must be used. Replaceable stainless steel wear plates are used to reduce wear on the liner.

At higher frequencies and temperatures, only refractory materials can be used. The liners are either extruded to the required shape, as in Fig. 4-21*b* and *c*, or rammed or cast, as in Fig. 4-21*d*. Skid rails, usually made of water-cooled stainless steel tubing, are built into the refractory liners, which have grooves recessed for this purpose. When extruded or prefabricated liners are used they are limited in thickness, because of potential thermal and mechanical shock. Refractory felt is usually required to bring the total insulation up to the necessary thickness and to act as a shock absorber between the liner and the coil, which may be vibrating. An alternative method is to use semicircular or circular firebrick sections of only a few inches in length and grooved to hold the rails (25). These sections are coated on the inside with refractory cement and appear to combine the advantages of the rammed and extruded constructions. The bricks are not so fragile as the extruded liners and can be obtained with thicker walls. Silicon carbide can also be used in place of firebrick. The wear properties of silicon carbide are such that no stainless steel rails are needed. However, it is more brittle than firebrick and will not easily stand excessive mechanical shock.

Cast or rammed refractory coils are often constructed by using a mixture of mica, epoxy resin, and polysulfide resin. The coil is molded directly into its housing; the method enables the coil to be rigidly held and to be protected from industrial atmospheres. A wear plate of ⅛-in. Transite backed by 0.020 in. of aluminum oxide can be used to protect the refractory surface.

Figure 4-21*c* illustrates a type of support suitable for square and heavy billets. The rails, supported by radial supports through the coil turns and liners, are independent of the inner refractory liner. If the coil is to be used for 60-cps heating of square billets, the cross section can be square, with a water-cooled stainless steel liner.

The coil windings and the thermal insulation are usually clamped together between end plates, built up of Transite and steel. Figures 4-16, 4-18, 4-20, and 4-22 illustrate the various housing and clamping methods used in through-heating coils. High-current leads and water connections are clearly visible in Fig. 4-23.

All machine-frequency coils are single-phase, but most 60-cps coils have to be three-phase because of the high loads presented to the supply. In

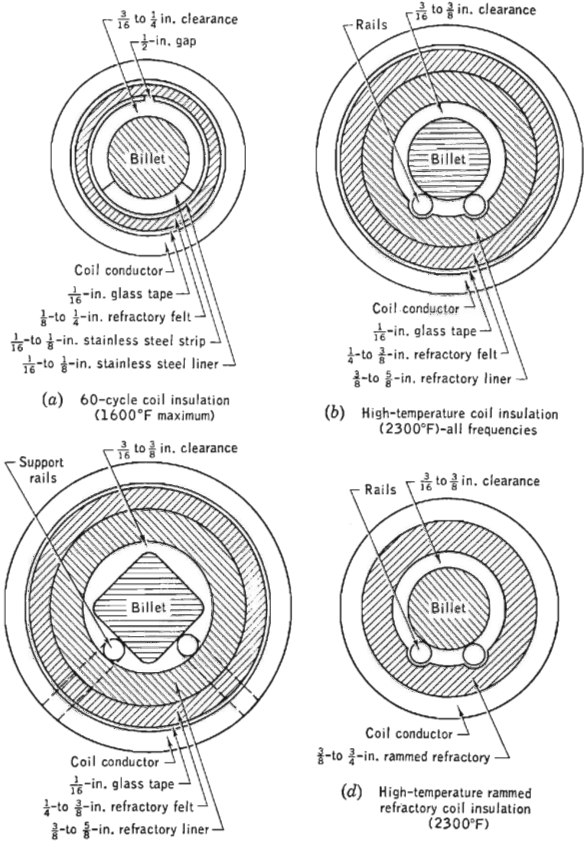

(*a*) 60-cycle coil insulation (1600°F maximum)

(*b*) High-temperature coil insulation (2300°F)-all frequencies

(*c*) Heavy-billet and round cornered square-billet coil insulation (2300°F)

(*d*) High-temperature rammed refractory coil insulation (2300°F)

FIG. 4-21. Through-heating coil construction.

general, the phases are split along the coil to minimize interphase flux cancellation, caused by the phase angle of 60° between the two magnetic fluxes at the junction of the phases. The flux intensity is slightly less, and

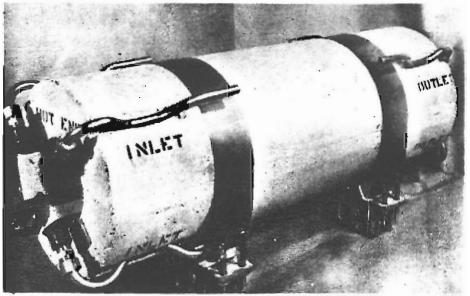

FIG. 4-22. Typical machine-frequency coil. (*The Ohio Crankshaft Co.*)

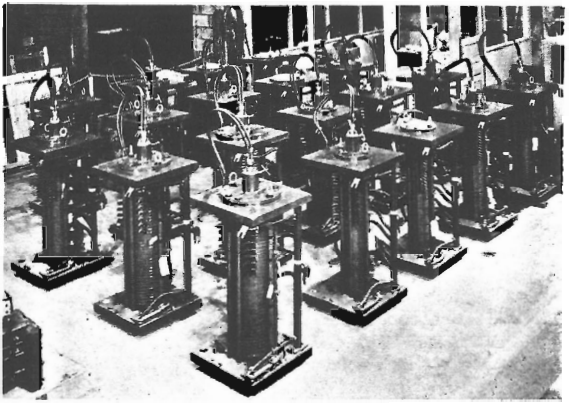

FIG. 4-23. Typical 60-cycle coils. (*Magnathermic Corp.*)

the heating effect and billet temperature both fall off slightly. One method used to reduce this effect is to split the coil into six sections to alternate the phases in each section (54). This spreads out the phase junctions along the

coil and tends to reduce the "cold spots." Another method is to interleave the end windings of each section with the adjacent section. This lengthens the area of phase junction but reduces its intensity. Some billet heaters include two transformers, which are Scott-connected so that the output is two-phase, with a phase-angle difference of 90°. The coil is then wound, with alternate turns fed by each of the two phases. Although this equalizes the flux differences, the power-transfer efficiency is low and the method is not widely used.

CHAPTER 5

RADIO-FREQUENCY SYSTEMS

5-1. THE BASIS OF THE RADIO-FREQUENCY GENERATOR

The major purpose of frequency conversion from supply-line frequencies of 50 and 60 cps to radio frequencies of 200 kc and upwards is to obtain currents with very shallow skin depths. Most generators are used for surface hardening and localized heating, and shallow skin-depth currents are ideally suited for these types of induction heating. A second purpose is to obtain greater power loading. Equation (1-67) shows that power input is directly related to frequency; in fact greater surface power densities are usually obtained at radio frequencies. This property is useful when the coupling between coil and work has to be very poor, as when the work is surrounded by a protective atmosphere and its container. The effective coil power factor is then very low and considerable kilovolt-amperage (KVA) is necessary to supply the kilowatts required. Using radio frequencies, the KVA is readily available and the power or kilowatt can be easily loaded into the work. Figure 2-16 illustrates that higher-power loadings are obtainable at radio frequencies.

All r-f generators consist of certain conversion stages; Fig. 5-1 illustrates a typical generator. Starting at the output end, the coil and workpiece present a power factor of 20 per cent or less to the output terminals. This factor is usually inverted and the value expressed as a Q factor. Figure 5-2 shows the derivation and definition of a circuit Q for a resistive inductance, such as a work coil. The subscript $_o$ used in Fig. 5-2*b* represents the loaded coil as seen by the generator terminals, and includes coil and work losses and inductance. Most r-f-loaded work coils have Q values between 5 to 15 for ferrous loads and 10 to 25 for nonferrous loads, the values occasionally rising to 100 or more for very loosely coupled nonferrous loads.

Now if the definition of circuit Q is modified by the square of the current, a new definition is possible.

$$Q_o = \frac{wL_o}{R_o} = \frac{I_o^2 wL_o}{I_o^2 R_o} = \frac{KVA_o}{P_o} \tag{5-1}$$

From Eq. (5-1), it is seen that the power required P_o has to be multiplied by Q_o to obtain the generator output KVA.

In Fig. 5-1, it may be seen that the source of r-f coil power is the tank and oscillator-tube circuit. The tank circuit is simply a parallel circuit tuned to the required frequency, with the tank capacitor storing energy in the form

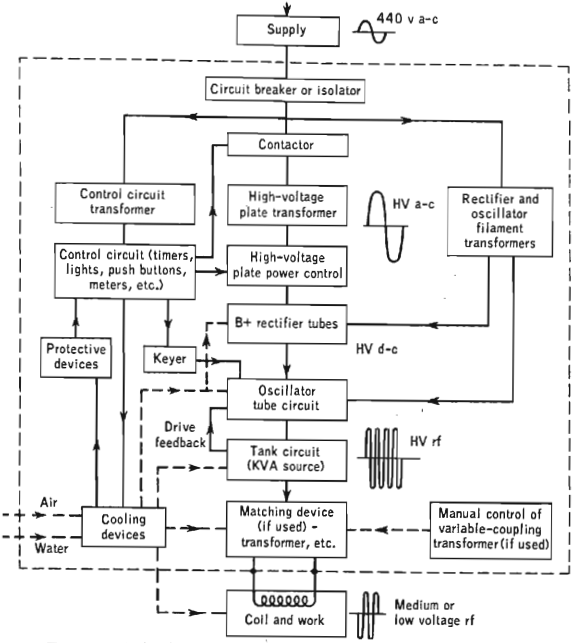

FIG. 5-1. Block schematic diagram of a r-f induction heating generator.

of kilovolt-amperes and then discharging it across the tank coil. The work coil can be either part or all of the tank coil, or it can be the secondary of an r-f transformer. Figure 5-3 shows the basic tank circuits used in most generators. The symbols are as follows:

v_T = tank voltage

z_T = dynamic tank-circuit impedance

FIG. 5-1A. Typical modern 10-kw 450-kc r-f induction heating generator. (*Westinghouse Electric Corp.*)

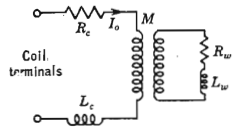

(*a*) Actual coil circuit

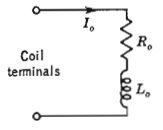

(*b*) Equivalent circuit

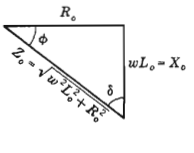

(*c*) Accurate vector diagram of (*b*)

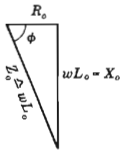

(*d*) Approximation of (*b*) for $\phi \gg \delta$ at high frequencies

$$\cos \phi = \frac{R_o}{Z_o}$$

$$\tan \delta = \frac{R_o}{wL_o}$$

$$\therefore Q_o = \frac{wL_o}{R_o} = \frac{1}{\tan \delta}$$

$$\cos \phi \triangleq \frac{R_o}{wL_o}$$

$$\therefore Q_o \triangleq \frac{1}{\cos \phi}$$

FIG. 5-2. Definition of coil or circuit Q at high frequencies.

I_{a1} = fundamental component of tube r-f current, rms
I_T = tank circulating current
C_T = tank capacitor, source of tank kilovolt-amperes
L'_T = total effective tank inductance, including strays
R'_T = total effective tank resistance, including strays
L_T = tank-coil inductance, including strays
R_T = tank-coil resistance, including strays
L_o = effective work-coil inductance with load
R_o = effective work-coil resistance with load
I_o = coil current
v_o = coil voltage
C_p = coil-boosting or power-factor correction capacitor
L_p = transformer primary-winding inductance
R_p = transformer primary-winding resistance
M = mutual transformer inductance

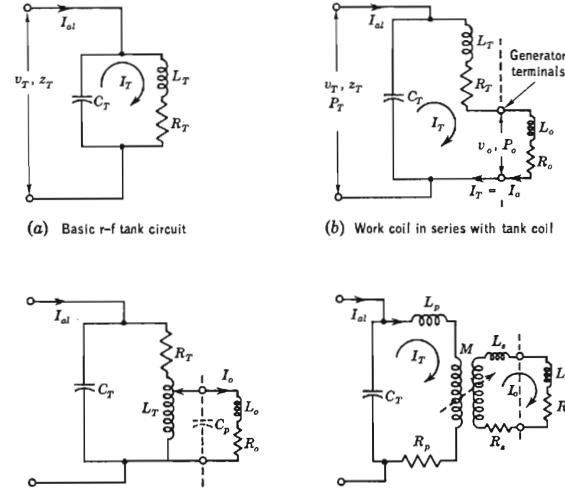

(*a*) Basic r-f tank circuit

(*b*) Work coil in series with tank coil

(*c*) Work coil tapped off tank coil (autotransformer)

(*d*) Work coil coupled to tank coil (r-f transformer)

FIG. 5-3. Radio-frequency induction heating tank circuits.

L_s = transformer secondary-winding inductance
P_T = power into tank circuit (from tube)
Q_T = effective tank circuit Q with loaded work coil
R_s = coupled transformer secondary-winding resistance

In general, stray-lead inductances and resistances are kept small on most tank circuits, at induction radio frequencies (200 kc to 5 Mc) and are no more than 5 per cent of the tank-coil or work-coil inductance and resistance. Booster capacitors are needed only when the coupling to the work is very low and the normal coil current and KVA are insufficient.

The dynamic impedance of a parallel-turned r-f circuit is given by

$$Z_T = \frac{L'_T}{R'_T C_T} = \frac{Q_T}{wC_T} = Q_T w L'_T \tag{5-2}$$

where $w = 2f$
f = tuned frequency of the tank circuit

The mutual inductance of the coupled transformer is given by

$$M = k\sqrt{L_p L_s} \tag{5-3}$$

where k = coefficient of coupling between primary and secondary

Most variable-coupling air-cored r-f transformers have k values up to 0.75, but fixed-coupling transformers, using oil dielectric or ferrite cores, can have k values up to 0.85 to 0.9.

The type of tank circuit used depends on the range of generator applications. Where the loads and coils may vary considerably, but work coupling is not very low and Q_o values are not excessive, the coupled transformer circuit of Fig. 5-3*d* is most suitable. Variable coupling is used if the work-coil impedance varies considerably; it is used mostly in general-purpose sets. The work-coil impedance is usually low, with a low Q value. This means a high value of I_o, usually higher than I_T, but from Eq. (5-1) it can be seen that the coil kilovolt-amperes (KVA_o) need not be excessive. This type of generator output is described as low-impedance or low-KVA. Its main disadvantage is that the transformer KVA losses vary between 75 to 85 per cent (variable coupling) and 60 to 75 per cent (fixed coupling).

When the work-coil impedance and Q values are high and many coil turns are required, the split tank-coil circuit of Fig. 5-3*b* can be used. It provides the higher coil KVA required; in fact the work coil can be the complete tank coil if necessary. This type of generator output is called high-impedance or high-KVA. It is used in cases of poor work coupling, such as semiconductor or nonferrous heating, especially with protective atmospheres. The current values are not usually so high as those in the coupled circuits.

The circuit in Fig. 5-3*c* is a compromise between the high- and low-impedance circuits. It has an advantage where automatic impedance

matching is required. If the work characteristics change abruptly, as in steel passing through Curie point, the tap point on the autotransformer can be switched by relays. Figure 5-3*A* illustrates this circuit as used in the generator shown in Fig. 5-1*A*.

Power losses vary according to the Q of the loaded work coil, the coupling coefficient of the transformer if used, and the stray losses. A well-designed, coupled circuit of the type shown in Fig. 5-3*d* may be between 75 and 80 per cent efficient for a coil Q of 5 to 10, dropping to about 65 to 70 per cent for a Q value between 15 and 20. The high-KVA series circuit of Fig. 5-3*b*

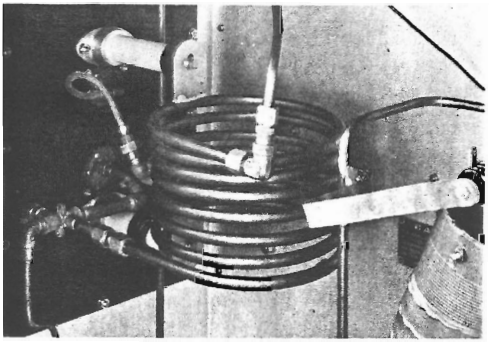

FIG. 5-3*A*. Tapped autotransformer output circuit in a 10-kw r-f generator. (*Westinghouse Electric Corp.*)

usually has to work into a high Q coil and this counteracts the lower circuit losses. The net result is usually a power efficiency of about 70 to 80 per cent.

Coil leads are very important in all these circuits; owing to the high KVA usually required, and the radio frequencies employed, the inductance of coil leads can cause a considerable KVA loss. This reduces the effective value of coil KVA and power. Coil leads should always be kept to a minimum length.

If there were no resistive losses in the tank circuit, it would continue oscillating indefinitely once it started ringing. As this is both undesirable, as the work to be heated is resistive, and impossible to achieve practically, a power source must be available to maintain oscillation. This is the purpose of the oscillator tube. It converts a d-c source of power from the power supply, to r-f power, in conjunction with the tank circuit. The tank-circuit

oscillations are maintained by utilizing a small percentage of the total tank voltage as a feedback to the grid of the tube. The voltage is phase-reversed by 180° and is then used to drive or excite the triode into oscillation; the amplified voltage in turn feeds the tank circuit. This circuit is known as a "self-excited oscillator"; the theory behind its operation is fully described

FIG. 5-3*B*. Interior view of a water-cooled 25-kw 450-kc generator showing the oscillator on the left and the power supply on the right. (*General Electric Corp.*)

in basic r-f heating textbooks (66, 72). In essence, it maintains the tank-circuit oscillations by supplying the power for all the resistive losses and the work. Typical generators are shown in Figs. 5-3*B* and 5-3*C*.

These self-excited oscillator circuits form the basis of nearly all induction heating r-f generators. They are shown in Fig. 5-4, together with the basic feed-back principle of oscillation. The reverse feed-back coupled circuit of Fig. 5-4*b* obtains grid drive from the secondary L_{gs} of the excitation transformer. An advantage of this circuit is that it can provide continuously

variable coupling and therefore drive control by a simple variable r-f transformer. The primary L_{gp} is sometimes part of the effective tank coil L'_T. As in the other circuits, C_{pb} is the plate blocking capacitor. Its purpose is to prevent the plate d-c voltages (the plate power supply) from being applied to the tank circuit and shorted to ground via the d-c short circuit. The grid bias is provided by the d-c component of the grid current and the bias resistor R_b. To prevent r-f current from being passed through the bias resistor, the grid capacitor C_g is chosen to provide a low-reactance path to ground, shunting R_b. Figure 5-3*A* shows the layout of this circuit in the 10-kw 450-kc induction heating generator, with the variable-coupling reverse feed-back transformer at the top of the cubicle.

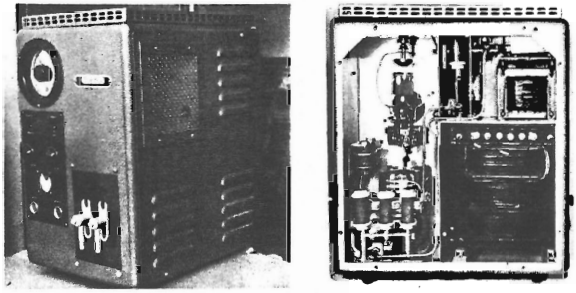

(*a*) (*b*)

FIG. 5-3*C*. Compact 1-kw induction heating generator. (*Reoifon, Ltd., England.*)

The Hartley circuit shown in Fig. 5-4*c* is probably the most utilized oscillator circuit in induction heating. The grid drive is tapped off the tank coil and is phase-inverted. Provided the taps are correctly chosen, it should never be possible to underdrive or overdrive the tube. As the grid is connected directly to the tank circuit, and not coupled as in the reverse feedback circuit, a blocking capacitor C_{gb} is introduced. The bias is produced as a result of the d-c component of grid current through R_b, as above. The r-f component is excluded from R_b by a choke L_b, designed to prevent a high reactance to the grid voltage v_g at the operating frequency. The Hartley circuit is most economical up to 30 Mc.

The third oscillator circuit is the Colpitts, shown in Fig. 5-4*d*. This circuit obtains grid drive by using a capacitance voltage divider instead of an inductance divider, as in the Hartley circuit. Its chief disadvantage is that

two tank capacitors C_{pt} and C_{gt} are required, as opposed to one in the Hartley and reverse feed-back circuits. It is used generally at frequencies above 5 Mc and has the advantage that the phase reversal is exactly 180°; it is not so exact in the other two cases. Parasitic oscillations, caused by stray-lead

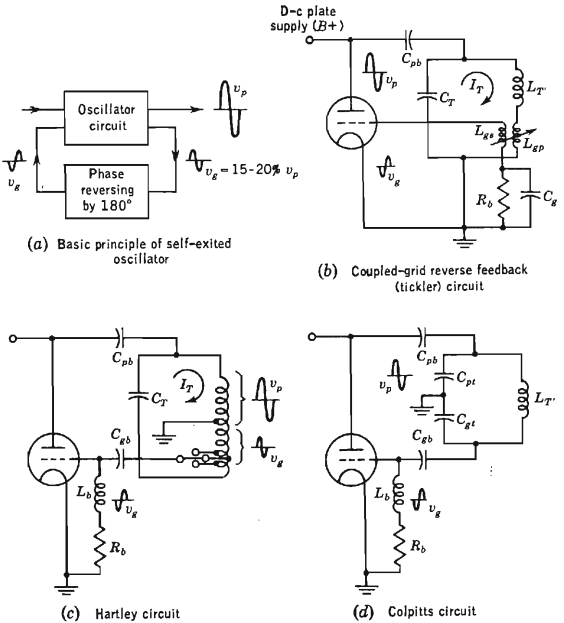

FIG. 5-4. Induction heating; oscillator circuits.

inductances resonating with the valve interelectrode capacitances, are less likely to occur in the Colpitts circuit.

The effects of the interelectrode capacitances are shown in Fig. 5-5. The capacitance between plate and filament may be between 0.1 and 2.0 $\mu\mu$f, and the capacitances between plate and grid, and filament and grid, may be between 10 and 80 $\mu\mu$f. The various stray-lead inductances (L_{ps}, L_{cs}, L_{fs}, and L_{gs}) may resonate with these capacitances at frequencies above 30 Mc.

At these frequencies the tank inductance L_T appears as an open circuit and the tank capacitance C_T as a short circuit. The net result is shown in Fig. 5-5*b*. Carbon-type parasitic suppressor resistors R_{ps} and R_{gs} are sometimes introduced into the plate and grid circuits. These are of low-resistance values (10 to 50 ohms) and are designed to damp out parasitic oscillations.

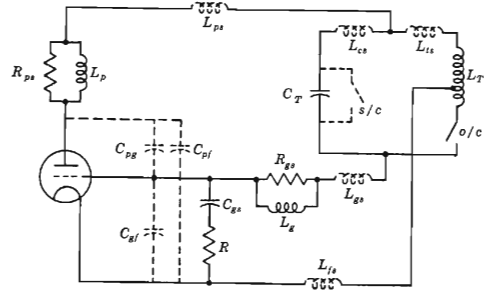

(*a*) Stray capacitances and inductances in an oscillator circuit

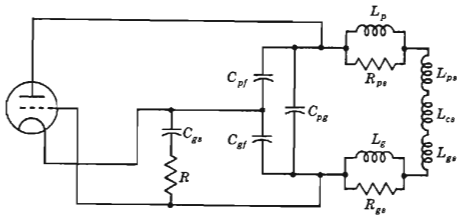

(*b*) Effect of stray elements at high frequencies

FIG. 5-5. Parasitic effects.

Occasionally chokes, such as L_p, are added in parallel to the resistors to act as high reactances to the parasitic frequencies and low d-c resistance paths, bypassing the parasitic resistors. Another method is to bypass the grid-filament interelectrode capacitance by one of larger value (100 $\mu\mu$f), such as C_g, which stops the tube from oscillating at parasitic frequencies by reducing the drive. These parasitic currents can often damage the filament and grid structures and the seals of the tube, as well as the tank capacitance.

5-2. INDUSTRIAL R-F HEATING OSCILLATOR TUBES

The essential purpose of the tube in these circuits is to provide a high-impedance, constant-current source of power. The tube has to match into widely varying loads under extreme industrial conditions; it is usually designed primarily for industrial purposes. The basic design principles are the same as those for any triode.

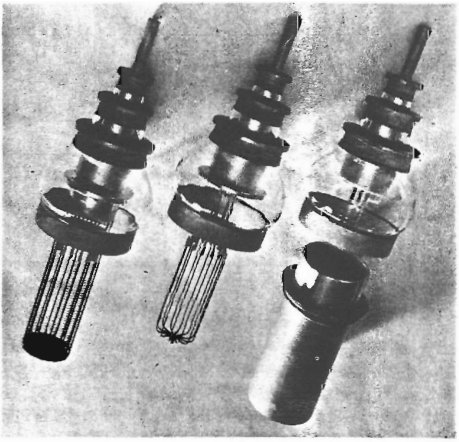

FIG. 5-5*A*. Grid, filament, and plate construction of a water-cooled industrial triode. (*Machlett Laboratories, Inc.*)

The filament, or cathode, acts as a source of electrons as a result of being heated to 1650 to 2200°C. The glass envelope is evacuated almost completely to prevent ionization, and the electrons cluster around the cathode as a space charge. The plate, or anode, is built around the cathode, and attracts the space charge by virtue of the high potential of the plate voltage. The result is a stream of electrons forming the plate current. This is controlled by placing a wire-mesh grid between the plate and cathode. The grid has a voltage applied to it which is negative with respect to the cathode (the grid bias). As this becomes more negative, the electron flow, or plate current, decreases. The reverse occurs if the grid is made less negative (or more positive). Figure 5-5*A* illustrates this construction.

The cathode is usually made of thoriated tungsten, heated between 1600

and 1700°C, or pure tungsten, heated between 2100 and 2200°C. Pure-tungsten filaments tend to be more rugged than thoriated-tungsten filaments but require considerably more heating power to obtain the same emission. Thoriated-tungsten filaments tend to be more easily damaged by ionic bombardment and are more unstable; therefore they are built with a

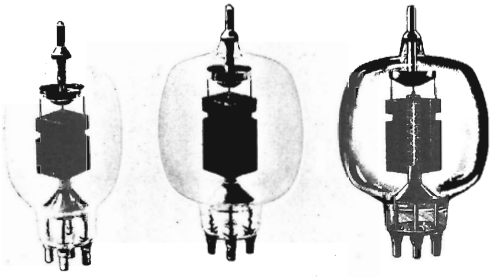

(*a*) (*b*) (*c*)

FIG. 5-5*B*. Radiation-cooled low-power industrial triodes: (*a*) TY5-500, (*b*) TY6-800, (*c*) sectional view of TY6-800. (*Mullard Valve Co., Ltd., England.*)

higher peak emission capability. Most modern high-vacuum r-f heating tubes utilize thoriated-tungsten filaments with high emission and long life.

The plate is usually constructed of molybdenum and tantalum, although carbon is sometimes used for the smaller tubes (Fig. 5-5*B*). Zirconium coating is sometimes used with molybdenum to improve radiation properties and minimize primary and secondary emission. Owing to the high velocity of electron flow or plate current from cathode to plate, the plate and grid are continually bombarded. Heat is dissipated; the losses are known as the plate and grid dissipation losses. Most triodes operating in class C conditions of oscillation are 70 to 80 per cent efficient, which means that between 30 and 20 per cent of the power input is dissipated in the plate and grid. Most of the loss (about 95 per cent) occurs in the plate.

The grid is usually a mesh of copper wire or rod and can be coated with zirconium.

The four methods used to cool high-power industrial oscillator tubes are:

1. Radiation
2. Forced-air
3. Water
4. Water-vapor

Radiation cooling is used for tubes dissipating up to about 3 kw at the plate. Figure 5-5*B* shows two typical triodes with graphite plates, suitable for radiation cooling. The TY5-500 has a maximum continuous plate dissipation of 500 watts, and the TY6-800 can dissipate up to 800 watts. The envelopes are designed to allow maximum convection-cooling effect.

Some tubes are constructed for radiation cooling with silica envelopes. These tubes will stand up to higher envelope temperatures than glass.

Forced-air cooling is used for most modern tubes where the use of water is a disadvantage. Often water is costly to use and may require special filtering. While most induction heating generators use water-cooled tank and work coils, the water requirements are small and the water can run to waste. Conventional tube water-cooling requirements are much higher, and some form of closed water system usually has to be used.

The cooling is assisted by copper fins attached radially to the plate. This method is used in conjunction with a glass or ceramic mounting which insulates the plate from the air-cooling duct and mounting bracket.

Air-flow requirements usually vary according to the plate dissipation at maximum power output of the generator, and the air inlet temperature to the cooling fins. At 70°F inlet temperature, the flow should be at least 40 to 60 cfm per kw of plate dissipation. If the temperature is 120°F, the flow should be at a minimum of 60 to 80 cfm per kw. Centrifugal fans are normally used, as the pressure required is usually at least 1 to 2 in. of water.

Air pressure or flow switches in the ducting ensure that plate power cannot be applied unless the minimum required pressure and flow are present. Air filters are necessary at the entrance to the generator to prevent dust build-up inside the generator, on high-voltage insulators. These are usually of the viscous-coated, Fiberglas type, replaceable after several months' service, or the wire-brush type. Porous-layer filters, which lengthen and break up the air path, are also used.

Water cooling is used when a more compact oscillator installation is required. The water tubing occupies a smaller space than air-cooling fans and ducting. Water is easier to check and monitor for pressure or flow, and temperature can also be used as a monitor. Flow or pressure switches and temperature switches are usually located in the plate power-contactor coil circuit. In the event of excessive plate outlet temperature or low flow, the plate power supply is shut off.

The flow requirements depend on the water inlet temperature, as the heat-exchange efficiency drops with rising temperature. With a temperature at the water jacket inlet of 70°F, the flow should be at least $\frac{1}{3}$ gal min^{-1} kw^{-1} of plate dissipation. At 120°F inlet, the flow should be raised to about $\frac{1}{2}$ gal min^{-1} kw^{-1} maximum dissipation.

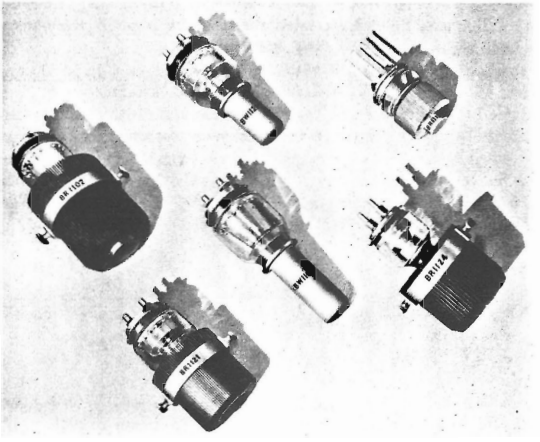

FIG. 5-5C. Typical modern forced-air and water-cooled triodes used in r-f heating. (*The English Electric Co. Ltd., England.*)

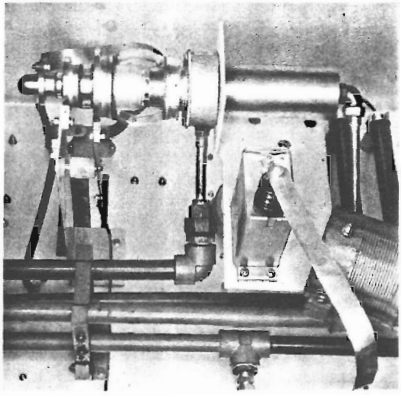

FIG. 5-5D. ML-6420 oscillator tube mounted in a 10-kw r-f generator. (*Westinghouse Electric Corp.*)

Figure 5-5*C* shows a selection of some typical free-air and water-cooled industrial triodes. The BW1102 can dissipate up to 20 kw at the plate, and the BW1121 has a maximum plate dissipation of 15 kw. The plate is usually

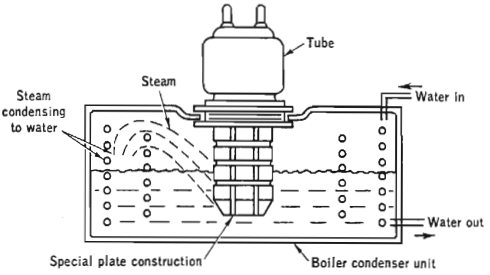

FIG. 5-5*E*. Principle of the vapor-cooled tube.

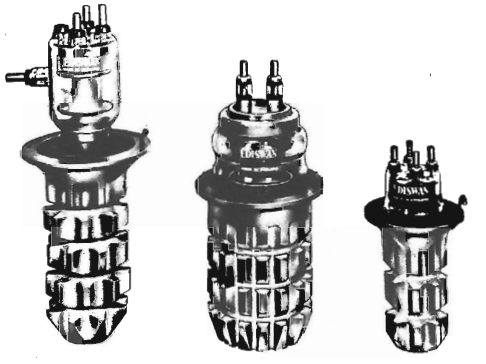

FIG. 5-5*F*. Three vapor-cooled tubes showing special plate construction. (*Edison Swan Ltd., England.*)

constructed of heavy-walled copper, lengthened to allow efficient heat transfer to the water. The air-cooled types Br 1102, 1115, 1121, and 1124 can dissipate 20, 3, 15, and 10 kw, respectively.

Figure 5-5*D* illustrates a smaller water-cooled tube, the ML-6420, located in a 10-kw 450-kc generator. The inlet and outlet water paths are of prefabricated insulating material.

A new cooling method, recently developed in France, involves the principle of latent heat transfer when water is converted to steam. This is illustrated in Fig. 5-5*E*, which shows a specially designed plate construction that presents a large surface area to distilled water. The plate construction is seen in detail in Fig. 5-5*F*. The water is allowed to boil, effecting an efficient latent heat transfer between plate and water. The vapor is cooled by condenser coils and condenses back into the water reservoir. Only a small amount of water is required in the condenser coils, in general about one-fifth of the flow needed in conventional types.

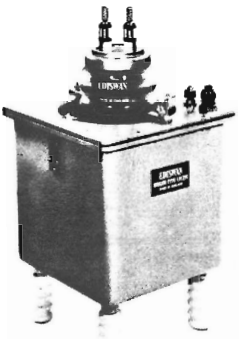

Figure 5-5*G* illustrates a tube complete with condenser box.

FIG. 5-5*G*. Vapor-cooled tube and condenser box. (*Edison Swan Ltd., England.*)

5-3. CLASS C OSCILLATOR DESIGN

The tube operating conditions must be derived to permit selection of the best tube for the circuit, and the optimum circuit components. Various methods of class C analysis have been described in the literature (66, 72, 75, 76), each involving detailed mathematical or graphical procedures. The following analysis is a first approximation and assumes the plate-current angle of flow to be 140° and the grid-current angle of flow to be 120°. These conditions cover most industrial r-f oscillator circuits, and the results can be used to within 5 per cent accuracy.

Figure 5-6 illustrates the major relationships between the grid and plate voltages and their currents during a cycle in the oscillations. Figure 5-4 shows the various methods to achieve reverse feedback of the grid voltage.

The symbols used are as follows:

E_a = instantaneous plate voltage
E_{adc} = d-c plate voltage
$E_{a.\,min}$ = minimum plate voltage
E_g = instantaneous grid voltage
E_b = grid-bias d-c voltage

$E_{g,\max}$ = peak positive grid excursion
v_a = instantaneous plate voltage (E_{adc} reference)
v_g = instantaneous grid voltage (E_b reference)
v_{ap} = peak plate swing
v_{gp} = peak grid swing
I_a = instantaneous plate current
I_{ap} = peak plate current
I_{adc} = d-c component of plate current I_a (average value over θ_a)

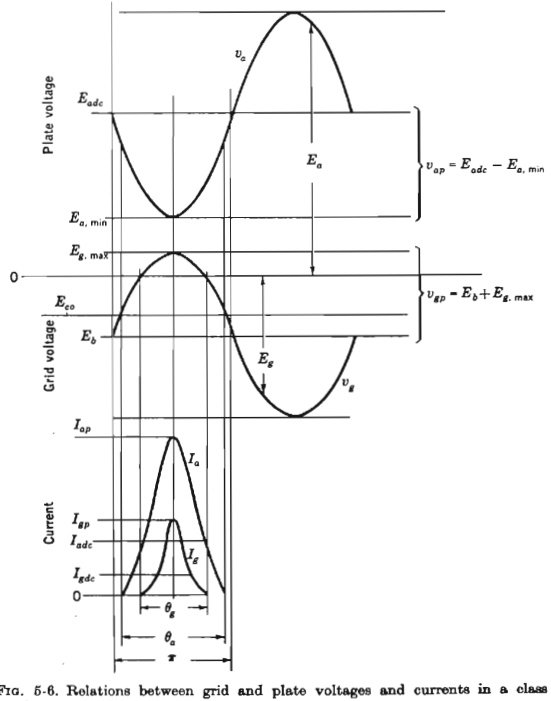

FIG. 5-6. Relations between grid and plate voltages and currents in a class C oscillator.

I_{a1p} = peak fundamental component of plate current I_a
I_g = instantaneous grid current
I_{gp} = peak grid current
I_{gdc} = d-c component of grid current (average value over θ_g)
I_{g1p} = fundamental component of grid currents
I_k = peak space current or cathode emission
P_a = plate input power
P_T = plate output power into tank circuit
P_d = plate dissipation
P_g = grid drive input power
P_{gb} = grid-bias-resistor dissipation
P_{gd} = grid dissipation
z_a = plate impedance
θ_a = angle of plate-current flow
θ_g = angle of grid-current flow
v_f = filament voltage
I_f = filament current

Most tube manufacturers state maximum values of plate and grid dissipations and peak space current. Maximum plate voltage is also specified for various types of power-supply circuits. In general these maximum values allow for 10 per cent regulation from full-load to no-load conditions and therefore include a reasonable safety factor. Standard practice is to work near to the maximum plate voltage, as this helps to produce maximum tube efficiency.

The required power output of the generator to be designed is usually specified, and the transfer efficiency from tube output to generator output can be calculated (see further on). Therefore the tube output is known.

The first stage in designing an oscillator circuit is to consider the power and type of output required. This establishes the frequency and power required at the tank, together with the KVA. In general the frequency is between 400 and 490 kc, for economy and for practical reasons.

The output-circuit design will be outlined in a later section and is assumed to be known at this stage.

The next stage involves choosing an oscillator tube to give the required power output at a convenient plate voltage and current combination.

Most tubes are about 70 to 80 per cent efficient, so that the power of the plate supply can be calculated. Generators of up to 15-kw power output usually utilize between 5- and 9-kv plate voltage. Above 15- to 20-kw power output, plate voltages up to 12 kv are commonly used. Another design guide for selecting an oscillator tube is the impedance of the output circuit. A high-impedance output would require a high plate voltage and low

current. Most induction heating circuits tend to require low-impedance circuits, so that the tube with the highest plate current is preferable. The alternative cooling methods available also guide the selection.

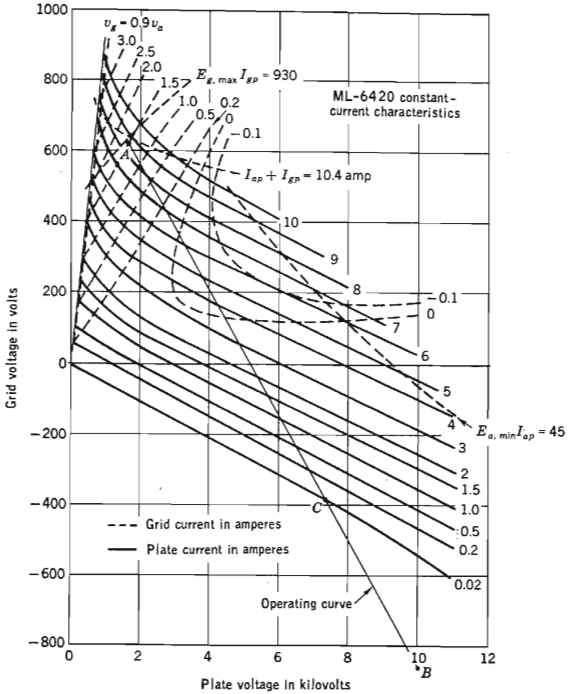

FIG. 5-7. Constant-current characteristics and operating conditions.

Given the oscillator tube with its maximum values of plate dissipation and voltage, grid-dissipation voltage, and peak space current, the operating conditions are now determined from the characteristics curves. Figure 5-7 shows the curves for the ML-6420, a typical 10-kw generator oscillator tube. The first step involves defining the maximum operating curves in terms of

maximum grid and plate dissipations, maximum peak space current, and required power output. The equations used are as follows:

$$v_g = 0.9E_a \tag{5-4}$$

$$I_k = I_{ap} + I_{gp} \tag{5-5}$$

$$E_{g.\,\max} = \frac{P_g}{0.16} \times \frac{1}{I_{gp}} \tag{5-6}$$

$$E_{a.\,\min} = \frac{P_d - 0.15P_T}{0.23I_{ap}} \tag{5-7}$$

If I_k is not given directly it can be estimated approximately from

$$I_k = 17.5 \text{ ma/watt of heater power}$$

for a thoriated-tungsten heater.

The maximum values for the ML-6420 tube are listed below:

Maximum power at plate, P_a ..... 20 kw
Maximum plate dissipation, P_d ..... 12.5 kw
Maximum grid dissipation, P_g ..... 150 watts
Filament voltage, v_f ..... 7.0 volts
Filament current, I_f ..... 85 amp
Peak space current, $I_k = (17.5)(7.0)(85)$ ..... 10.4 amp
Maximum plate voltage, E_{adc} ..... 10.0 kv
Maximum plate current, I_{adc} ..... 2.2 amp
Maximum grid current, I_{gdc} ..... 0.4 amp
Amplification factor, μ 20

At this stage an example of a generator specification for which this value is suitable will be helpful.

Required generator output power, P_o ..... 10 kw
Assumed output-circuit efficiency, η_T ..... 70 per cent
Required tube output power, P_T ..... 14.3 kw
Available power-supply voltage, E_{adc} ..... 10 kv

Using the given maximum values of P_g and P_d, and the given values of I_k and P_T, the four equations (5-4) to (5-7) reduce as follows:

$$v_g = 0.9E_a \qquad \text{volts}$$

$$10.4 = I_{ap} + I_{gp} \qquad \text{amp}$$

$$E_{g.\,\max} = \frac{930}{I_{gp}} \qquad \text{volts}$$

$$E_{a.\,\min} = \frac{12.5 - 0.15 \times 14.3}{0.23I_{ap}} = \frac{45}{I_{ap}} \qquad \text{kv}$$

These curves are reproduced in Fig. 5-7; the limiting area is seen to be under the last three curves. Now what is most desired in the class C operation of a triode tube for industrial heating is the most efficient use of the tube. Distortion, of the type normally considered important in audio work, is completely disregarded in order to produce maximum output power. To achieve this, the bias voltage is selected to produce an angle of anode current flow of almost 140° (Fig. 5-6).

The operating conditions are first chosen on the characteristics curves based on the highest values of plate and grid currents (I_{a_p} and I_{g_p}) within the three limiting curves. This determines the values of maximum grid voltage ($E_{g,\,\max}$) and minimum plate voltage ($E_{a,\,\min}$). The d-c and peak fundamental components of plate and grid currents are then approximated from the following equations, assuming an angle of anode current flow of 140° and grid-current flow of approximately 120°.

$$I_{a_{dc}} = 0.23I_{a_p} \tag{5-8}$$

$$I_{a_{1p}} = 0.4I_{a_p} \tag{5-9}$$

$$= 1.75I_{a_{dc}} \tag{5-10}$$

$$I_{g_{dc}} = 0.17I_{g_p} \tag{5-11}$$

$$I_{g_{1p}} = 0.32I_{g_p} \tag{5-12}$$

$$= 1.88I_{g_{dc}} \tag{5-13}$$

In the example given on the ML-6420 tube, values of plate and grid peak currents are first chosen at 8.5 and 1.5 amp, respectively. It is always desirable to work as close to the diode line ($v_g = v_a$) as possible consistent with keeping underneath the maximum grid-dissipation and peak space–current curves. From Eqs. (5-8) to (5-13),

$$I_{a_{dc}} = 0.23 \times 8.5 = 1.95 \text{ amp}$$

$$I_{a_{1p}} = 0.4 \times 8.5 = 3.40 \text{ amp}$$

$$I_{g_{dc}} = 0.17 \times 1.5 = 0.255 \text{ amp}$$

$$I_{g_{1p}} = 0.32 \times 1.5 = 0.48 \text{ amp}$$

The next step is to see if these values give the required output power P_T with the chosen d-c plate voltage. The equation is

$$P_T = \frac{v_{a_p} I_{a_{1p}}}{2} \tag{5-14}$$

The peak plate voltage swing v_{a_p} is obtained from the d-c plate voltage and the minimum plate voltage, using the following relation:

$$v_{a_p} = E_{a_{dc}} - E_{a,\,\min} \tag{5-15}$$

Using Fig. 5-7, the peak current operating point results in a value of 1,600 volts for $E_a$min. With the plate voltage of 10,000 volts, the peak voltage is

$$v_{ap} = 10{,}000 - 1{,}600 = 8{,}400 \text{ volts}$$

One important point to remember is that the plate-voltage swing above d-c plate voltage is often 10 per cent greater than the swing below the d-c value. Therefore the tank peak voltage should include this factor, and the tank root mean square (rms) voltage should be increased by about 7 per cent in selecting the tank capacitor.

Using Eq. (5-14), the tube output power to the tank circuit P_T is

$$P_T = 8{,}400 \times 3.4/2 = 14.3 \text{ kw}$$

As this is the value required, and as both plate and grid d-c currents are within the rated maximum values, the operating point can be considered satisfactory. The plate dissipation P_d and input power P_a can be checked from

$$P_d = 0.15P_T + 0.23\, E_{a.\,\min}\, I_{ap} \tag{5-16}$$

and

$$P_a = E_{adc}I_{adc} \tag{5-17}$$

Therefore $P_d = (0.15)(14.3) + (0.23)(1.6)(8.5) = 5.29$ kw

and $P_a = 10 \times 1.95 = 19.5$ kw

These values are both less than the tube maximum values. It should be remembered that these equations are only first approximations, to 5 per cent accuracy, which accounts for the slight difference between input power and the sum of the dissipation and output power.

The grid-bias voltage E_b, peak swing v_{gp}, and dissipation P_g are all obtained from

$$E_b = \frac{E_{adc}}{\mu} - 0.52\left(E_{g.\,\max} + \frac{E_{a.\,\min}}{\mu}\right) \tag{5-18}$$

and

$$v_{gp} = -E_b + E_{g.\,\max}$$

and Eq. (5-6). These result in the following values:

$$E_b = (10{,}000/20) - 0.52 \times 700 = -864 \text{ volts}$$

$$v_{gp} = 864 + 620 = 1{,}484 \text{ volts}$$

$$P_g = (0.16)(620)(1.5) = 149 \text{ watts}$$

In general the bias approximates to one and one-half times cutoff voltage.

It is now possible to draw the operating load line AB on the constant-current curves of Fig. 5-7. The lower point B corresponding to E_{adc} and E_b (10,000 and -864 volts) is connected to the peak-current operating point A. This illustrates the values of the voltage and current of both grid and plate

for the conducting half of the cycle. By referring to the first 180° of the cycle shown in Fig. 5-6, it can be seen that the curves can be derived completely from the load line of Fig. 5-7.

A more detailed and accurate analysis of the various currents and voltages is obtainable from the load line, but it is rarely necessary to go beyond the first approximations. Any adjustments can usually be carried out during tests.

The grid angle of current flow θ_g and drive power P_{gd} are given by

$$\theta_g = 2 \cos^{-1} \frac{E_b}{v_{gp}} \tag{5-19}$$

and

$$P_{gd} = \frac{v_{gp} I_{g1p}}{2} \tag{5-20}$$

Therefore $\theta_g = 2 \cos^{-1} (864/1{,}484) = 110°$

and $P_{gd} = 1{,}484 \times 0.48/2 = 357$ watts

The grid angle of current flow is lower than the 120° assumed, but the resultant errors are relatively small. The grid-bias resistor and the power lost in the resistor are given by

$$R_{gb} = \frac{E_b}{I_{gdc}} \tag{5-21}$$

and

$$P_{gb} = E_b I_{gdc} \tag{5-22}$$

Therefore $R_{gb} = 864/0.255 = 3{,}400$ ohms

and $P_{gb} = 864 \times 0.255 = 221$ watts

The grid drive can be checked from

$$\begin{aligned} P_{gd} &= P_{gb} + P_g \\ &= 221 + 149 = 370 \text{ watts} \end{aligned} \tag{5-23}$$

This is within 5 per cent of the result obtained from Eq. (5-20).

Lastly, the angle of plate current flow θ_a, the plate impedance z_a, and the tube efficiency η_v can be checked from

$$\theta_a = 2 \cos^{-1} \left(\frac{-\mu E_b - E_{adc}}{\mu v_{gp} - v_{ap}} \right)^\circ \tag{5-24}$$

$$z_a = \frac{v_{ap}}{I_{a1p}} \tag{5-25}$$

$$\eta_v = \frac{P_T}{P_a} \tag{5-26}$$

Therefore $$\theta_a = 2 \cos^{-1} \left(\frac{20 \times 864 - 10{,}000}{20 \times 1{,}484 - 8{,}400} \right) = 141°$$

$$z_a = 8{,}400/3.4 = 2{,}424 \text{ ohms}$$

$$\eta_v = 14.3/19.5 = 73 \text{ per cent}$$

The plate angle of conduction can be checked from the load line AB. Point C represents the cutoff point, at $E = 7{,}200$ volts and $E_g = -370$ volts.

Therefore θ_a is given by

$$\theta_a = 2 \cos^{-1} \left(\frac{10{,}000 - 7{,}200}{10{,}000 - 1{,}600} \right) = 2 \cos^{-1} \frac{2{,}800}{8{,}400}$$

$$= 141°$$

5-4. GENERATOR-TUBE POWER SUPPLIES

The tube plate power supply is a source of d-c voltage, usually between 3,000 and 12,000 volts, and is capable of giving a d-c plate current which may be anywhere between 500 ma and 20 amp, depending on the tube power requirements. Most power circuits include a high-voltage transformer and rectifiers; Fig. 5-8 shows the four circuits most commonly used. For sets up to about 3-kw r-f output, the single-phase circuits in Fig. 5-8*a* and *b* can be utilized. The single-phase, full-wave circuit is more economical. Smoothing is usually required in these circuits, as the peak ripple voltage can be 67 per cent of the d-c value. The maximum tube plate voltage is usually based on 5 per cent ripple; any excess of this means that the plate d-c voltage has to be decreased, decreasing the maximum available output power. A series choke with an inductance value in henrys approximately equal to the load resistance in kilohms is satisfactory. The tube load resistance is taken as the plate voltage divided by the plate current at maximum load. This is followed by a parallel capacitor chosen to resonate with the choke at a frequency at least one-third of the input frequency, which is 120 cps in the case of single-phase circuits.

For generators above 3 kw, the three-phase circuits in Fig. 5-8*c* and *d* are usually used. They present a balanced load to the supply line; the full-wave circuit of Fig. 5-8*d* has less than 5 per cent peak ripple voltage and so requires no smoothing circuit.

Nearly all power-supply circuits utilize hot-cathode mercury-vapor rectifier tubes, but xenon tubes have recently gained favor. The mercury-vapor tubes have to be heated for some 30 sec at the beginning of each operating period or each day, prior to application of plate voltage. This is necessary in order to vaporize fully all the mercury and to prevent excessive ionic

bombardment of the filament, and its consequent destruction. Mercury-vapor tubes are also sensitive to ambient temperature, as the vapor pressure varies with the ambient conditions. Temperatures much above 60°C tend

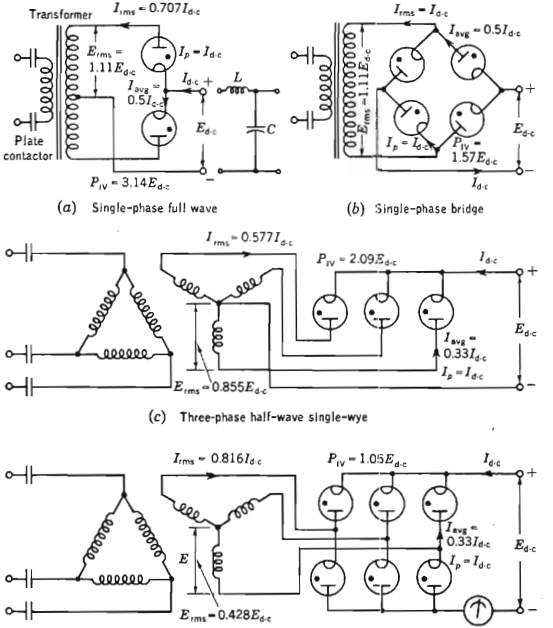

FIG. 5-8. Power-supply rectifier circuits for r-f induction heating oscillators.

to drop the safe peak inverse voltage capabilities, while temperatures below 25°C cause insufficient mercury ionization and filament damage.

Figure 5-8*A* shows a typical three-phase full-wave power supply, installed in the 10-kw generator, for which the oscillator was designed in the previous section. The six tubes are each mounted on separate filament transformers, which are high-voltage insulated.

Xenon rectifiers are not temperature-sensitive and do not require a 30-sec heating period. Older tubes tended to go soft after a long period of service, but modern xenon tubes can give up to 10,000 hr of service.

For average rectifier currents of 3 amp or more, mercury-pool rectifiers, or ignitrons, are often used. They contain a pool of mercury as the cathode, and an arc is struck at the beginning of each cycle from the pool to a starter,

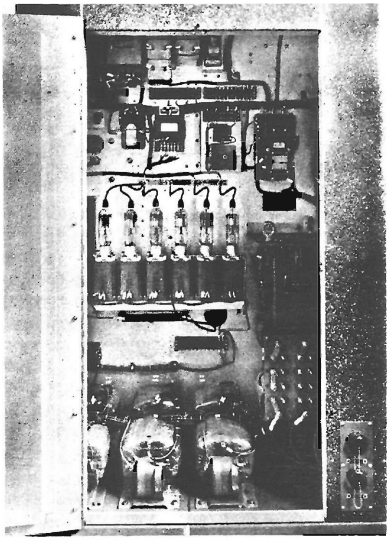

FIG. 5-8A. Power supply and control circuit for the 10-kw 450-kc r-f generator. (*Westinghouse Electric Corp.*)

which is a thin rod. Pool-type rectifiers are used in generators having an r-f output power of 70 kw or more. Exitrons are a type of mercury-pool rectifier in which the arc is struck by a movable arm, raised from outside the envelope by a solenoid.

The utilization factor of the plate supply transformer is also affected by the type of rectifier circuit. This is defined as the ratio of output d-c power to a-c power dissipated directly by the transformer windings in a resistance for equal transformer losses. It is obviously desirable to have this as near

100 per cent as possible, otherwise the KVA requirements of the transformer windings will be excessively greater than the d-c power required. The factors are given below, together with the ratio of windings KVA to d-c power.

From Table 5-1, the minimum transformer KVA is obtained with the three-phase full-wave circuit.

TABLE 5-1. UTILIZATION FACTORS OF HIGH-VOLTAGE TRANSFORMERS

Ratio	Type of circuit			
	Single-phase		Three-phase	
	Full-wave	Bridge	Half-wave	Full-wave
Primary utilization factor.....	0.900	0.900	0.827	0.955
Secondary utilization factor.....	0.637	0.900	0.675	0.955
Primary KVA d-c output, kw...	1.1	1.11	1.21	1.05
Secondary KVA d-c output, kw...	1.57	1.11	1.48	1.05

Figure 5-8 also gives the various voltages and currents in the circuit compared with the required d-c output voltage and current. From this it is seen that the highest value of d-c output voltage for a given rectifier maximum-peak inverse voltage is obtained from the three-phase full-wave circuit. This circuit is used in most generators and has proved to be the most economical design.

Recent developments in semiconductor rectifiers have enabled their use in low-power generators utilizing oscillator tubes with plate voltages of 1,000 volts or less. It is possible to double or quadruple the supply-line voltage and rectify the result to achieve up to 1,000 volts, dispensing with plate transformers.

5-5. GENERATOR CONTROL CIRCUITS

The next major item in the basic generator is the control circuit, which provides the switching and indicating means for the various power stages and can be described in stages.

Most generators are designed with either a circuit breaker or an isolating switch/fuse combination to isolate the generator from the main supply. The plate power is switched electromagnetically by the plate contactor, which is

usually in the primary side of the plate power transformer. This is usually identical to the motor-starter type, with a hold-on contact. Application of plate power produces r-f power, and the plate contactor is switched by the R-F ON push button. This controls the voltage applied to the plate contactor operating coil. The contactor can also be controlled by an external circuit.

Before application of plate power, the various protective devices have to be operated. The rectifier tubes have to be warmed up during a minimum time cycle of 30 sec. The oscillator-tube cooling water or air has to be more than the minimum flow and less than the maximum temperature; other parts of the circuit similarly cooled, such as tank coil, capacitors, etc., have to be protected by flow switches. Current-overload relays which may be in the grid and anode circuits have to be reset. Doors and removable panels usually have to be provided with microswitches which prevent plate power application when they open; such switches have to be closed.

FIG. 5-9. Radio-frequency power process timer unit. (*Automatic Temperature Control Co.*)

As many applications of r-f power are automatic and time-controlled, accurate process times are usually required. Timer units are usually of the motor-driven clutch-operated type; Fig. 5-9 illustrates a typical unit.

Control-circuit voltages have to be 110 volts, and control transformers are required on all but the smaller single-phase generators.

Tube protection from overloads is usually provided by plate-current overload relays, which trip out if the rated plate current is exceeded. Grid-current overload relays are also included where no-load grid currents are excessive. This can occur with tubes designed to give full-output power at grid currents near the maximum amount. In some circuits the grid current could drop to a value low enough to stop oscillation because of insufficient drive. The standing, or static, plate current under these conditions can often produce excessive plate dissipation, damaging the plate. From Fig. 5-7, it is seen that at a plate voltage of 10 kv, the plate current at zero grid voltage (no oscillations) is 5.6 amp. This power (56 kw) would all be dissipated in the plate, exceeding the maximum value of 12.5 kw. By including an undercurrent relay in the grid circuit, which opens up the plate power contactor, plate damage is prevented.

Oscillator- and rectifier-tube filaments are highly sensitive to voltage variations. Tube manufacturers usually state that filament voltages should be within 1 per cent either side of the nominal value for thoriated-tungsten

filaments in oscillator tubes. The filament voltages should be kept to within 2½ per cent for mercury-vapor rectifiers and 5 per cent for xenon rectifiers, with 6 per cent allowable for short periods.

Voltage-regulated transformers of the self-saturating type, with tuned primary windings, are often used in the filament supplies. It is also important to limit the initial oscillator-tube-filament current to a maximum value of 1.5 times its normal hot value. This is necessary as the cold filament resistance is usually as low as one-tenth its hot value, and the surge currents at switching could damage the filament.

5-6. POWER-CONTROL SYSTEMS

Many applications of induction heating generators require the control of power, either during the heating cycle or to match the generator power output to a variety of loads. The various types of power control are listed below:

1. Variable-coupling r-f output transformer
2. Load-position adjustment in work coil
3. Timer
4. Saturable-reactor system—high-voltage
5. Saturable-reactor system—supply-line voltage
6. Thyratron system
7. Oscillator-tube keying

The r-f output transformer method will be described in a later section on load matching. The variation of the load in the work coil consists of varying the degree of coupling by moving the work in and out of the coil. The method is rarely used in modern applications. Timers are used primarily as pulse controls operated to limit the energy induced into the work. They are not strictly power controls, but energy controls.

Saturable-reactor control systems have recently been used to control the tube plate voltage and therefore the r-f output power. The basic principles are fully explained in the literature (77, 78–80). The saturable reactor usually consists of three windings on a high flux-density core of grain-oriented silica steel which has a narrow, rectangular hysteresis loop (Fig. 5-10*b*). The gate winding is in series with the rectifying diode and acts as a variable impedance, dependent on the amount of core saturation. This is controlled by the control winding, which is supplied with a small, variable d-c signal. Varying this current varies the control-winding ampere-turns and therefore the amount of saturation. With no-control ampere-turns, the gate winding presents maximum impedance and output is reduced to about 10 per cent. With maximum-control ampere-turns, the core is saturated and the gate winding presents minimum impedance, being in effect a closed

switch and allowing full voltage across the diode and full output. Some small voltage drop will occur across the gate winding at full saturation, and therefore the plate-transformer secondary turns should provide approxi-

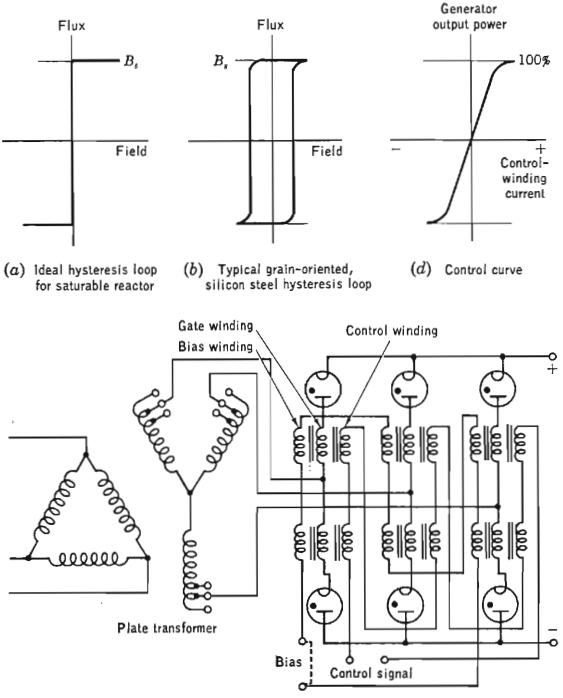

(*a*) Ideal hysteresis loop for saturable reactor (*b*) Typical grain-oriented, silicon steel hysteresis loop (*d*) Control curve

(*c*) Three-phase full-wave high-voltage saturable-reactor power control circuit

FIG. 5-10. High-voltage saturable-reactor control.

mately 10 per cent higher voltage. Earlier designs usually required several secondary taps, as a complete range of power control was not available (78), but later types of reactors resulted in a full range of control on one tap. In

general, this is achieved manually by a simple autotransformer and rectifier circuit with a reversing-polarity switch; the control curve is seen in Fig. 5-10*d*. The circuit is seen in Fig. 5-10*c*, and a typical set of saturable reactors is shown in Fig. 5-11.

When an external signal is used to control power, such as the output from a temperature-control system, the manual control is transferred to the bias winding. The reactors are biased to some point on the control curve, giving

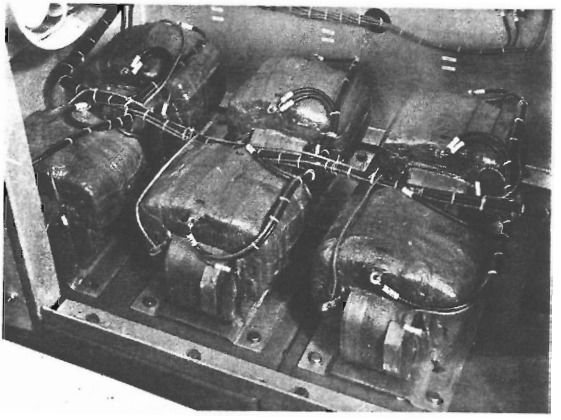

FIG. 5-11. High-voltage, power-control saturable reactors. (*Westinghouse Electric Corp.*)

the steady output power required, and the external signal is fed to the control windings. Work-temperature variations to either side of the fixed set point result in deviations or errors. The current signals at the control windings are proportional to the error, and the reactors are controlled accordingly. A drop in temperature results in greater core saturation and more rectifier voltage, which in turn increases the oscillator plate voltage and the r-f output power, raising the work temperature. This type of system is fully described in Sec. 5-8, External Control Systems.

Experience has shown that when the manual control only is required, the bias windings should be in series and short-circuited (78). This reduces ripple voltages, which may appear across the control d-c supply, and in fact acts as a ripple filter.

Power control may also be achieved by using conventional a-c saturable reactors on the low-voltage side of the plate transformer. Although the voltage insulation required is much less than the high-voltage type, current requirements usually increase the over-all size of the reactors to a larger extent. Also the control-winding ampere-turns would have to be somewhat the same as in the load or gate windings. In the high-voltage units, connecting them in series with the rectifier diodes reduces the control-winding ampere-turns required to about 20 per cent of the load windings (77, 80). However, the low-voltage design enables all the windings to be wound on one three-phase core, which reduces the total volume.

The only disadvantages of saturable reactors are the relatively slow response times, due to the delay in core saturation, and the possibility of drift. Response times may extend to 0.5 sec for from 20 to 100 per cent full load in high-voltage units, but this is not serious for most r-f generator applications. Drift is due to air-gap variations in C-core-type reactors, as the magnetizing current and magnetic reluctance are very sensitive to the air gap. This is a typical problem with most types of C-core magnetic amplifiers and is usually controlled by careful bonding and the use of correct gap cements.

Thyratron power-control systems are also used in induction heating generators. The thyratron is a mercury-vapor rectifier with the addition of a grid which surrounds the anode; it is sometimes known as a grid-controlled rectifier. The main characteristic of the thyratron is that it will not conduct unless the grid voltage is at some value less negative than the critical grid voltage. If a constant d-c bias is applied to the grid and an a-c voltage superimposed on this, as in Fig. 5-12*a*, the thyratron will conduct at the point where the a-c voltage exceeds the critical voltage. As the grid passes a negligible amount of current before conduction, the bias source can be one of high impedance, such as a pentode amplifier. Once the tube has fired it will continue to conduct even when the a-c grid voltage falls below the critical voltage, and will stop conducting only when the plate voltage is less than the cathode voltage. If this a-c grid voltage is made to alter its phase angle with respect to the plate voltage by a phasing network, the firing or conduction angle θ_c will be increased. This results in retarding the plate current and voltage conducting point, as seen in Fig. 5-12*a*. The resultant d-c plate voltage is reduced, together with the d-c plate current, and the total d-c voltage to the oscillator plate is reduced. This in turn reduces the r-f output of the generator.

One disadvantage of the thyratron is that the rise in plate voltage at the firing angle is so steep that it could constitute a voltage impulse or surge, which could damage the rectifier insulation or the plate transformer. Also, the grid circuit could be damaged if arc-backs should occur; it must be insulated to withstand the maximum plate voltage. The thyratron has a

limited life, whereas the saturable reactor lasts indefinitely and is a good deal more rugged for industrial use. The response time of the saturable reactor is slower, but because of this the wavefront at saturation or conduction is less steep and does not constitute a serious impulse effect. Surge-suppression units often have to be used with thyratrons, causing additional

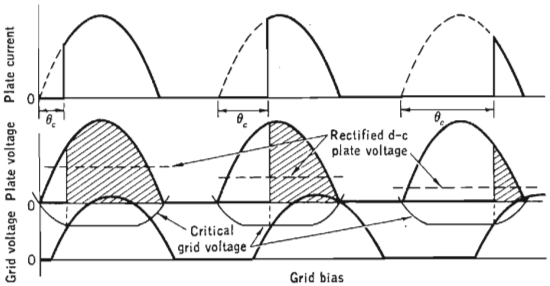

(*a*) Effect of increasing cutoff or phase-back angle θ_c on d-c plate voltage

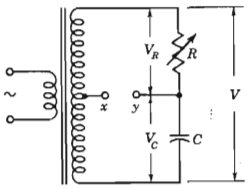

(*b*) Phasing circuit

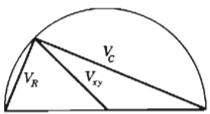

(*c*) Variable-phase grid voltage

FIG. 5-12. The operation of the thyratron.

power losses and unit cost. One advantage of the thyratron is that it does not drift with time in its characteristics, but it is more sensitive to line-voltage variations, which change its critical grid voltage.

Figure 5-12*b* illustrates a typical phasing circuit, the output across x and y being connected across the grid and cathode, with a bias voltage in series with the thyratron.

Mercury-pool rectifier tubes of the ignitron or exitron type often include a grid for grid control. It is likely that these tubes will be utilized for all large power generators where power control is required.

High-speed, pulse-type power control can also be achieved using oscillator-tube keying. The basis of this method is the fast switching of a cutoff bias applied to the tube grid. Figure 5-13 illustrates a relay-operated keying circuit. With the switch open as shown, a negative voltage E_{key} is applied to the oscillator grid, of sufficient value to cut off oscillations, stopping grid current and shutting off r-f output power. When the switch is closed to the RF ON position, the negative voltage is removed as 2-KEY is open and the grid circuit closed via the contact 1-KEY, restoring normal grid bias and oscillation. For faster switching the relay contacts could be replaced by thyratrons.

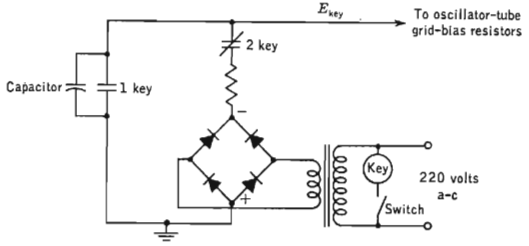

FIG. 5-13. Keying circuit for impulse power control.

Power control is also possible by utilizing variable autotransformers on the primary side of the plate transformer, and varying the high-voltage secondary output. This method is mainly confined to laboratory applications, but by motorizing the autotransformer it can be utilized with a closed-loop system for applications such as semiconductor processing.

5-7. LOAD-MATCHING OUTPUT CIRCUITS

Some indications of the basic problems of matching induction heating loads into tank circuits and tube plate impedances were given in Sec. 5-1. Figure 5-3 shows the major types of matching circuits used in induction generators.

Many induction heating applications utilize low-impedance coils, where the coil voltage is low but the coil current may be high. A typical loaded coil may have an impedance of 5 ohms. The coil has to match up to the dynamic plate impedance of the tube, which could be as high as 5,000 ohms. The essential matching device is an r-f transformer, as shown in Fig. 5-3*c* and *d*.

Figure 5-14 illustrates the equivalent tank circuit with the symbols that were used in Fig. 5-3. Previous references (73) have usually disregarded the primary and secondary resistances, but these are not negligible in the higher-powered generators operating at 500 kc. Variable-coupling transformers, which have relatively low coupling factors, can result in power losses as great as 50 per cent.

Therefore one of the first considerations is the power-transfer efficiency. As this is a very important factor, its derivation, based on certain practical assumptions, is described below.

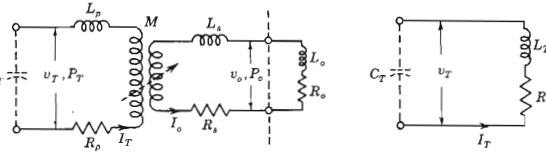

(*a*) R-f transformer (*b*) Equivalent circuit

FIG. 5-14. Radio-frequency transformer equivalent circuit.

Conventional transformer analysis (74) gives the value of the equivalent circuit in Fig. 5-14*b*.

$$R_T' = R_p + (R_s + R_o)\left[\frac{k^2 L_p L_s w^2}{(R_s + R_o)^2 + (L_s + L_o)^2 w^2}\right] \tag{5-27}$$

$$L_T' = L_p - (L_s + L_o)\left[\frac{k^2 L_p L_s w^2}{(R_s + R_o)^2 + (L_s + L_o)^2 w^2}\right] \tag{5-28}$$

It is possible to measure the coupling factor k by obtaining the resonant frequency of the tank circuit with the secondary short-circuited and open-circuited.

$$k = \sqrt{1 - \frac{f_{oc}^2}{f_{sc}^2}} \tag{5-29}$$

where f_{oc} = tank-circuit frequency, open-circuit secondary
f_{sc} = tank-circuit frequency, short-circuit secondary

The power-transfer efficiency is defined as

$$\eta_T = \frac{P_o}{P_T} = \frac{I_o^2 R_o}{I_T^2 R_T'} \tag{5-30}$$

Circuit analysis of Fig. 5-14*a* gives

$$\frac{I_o}{I_T} = \frac{wk\sqrt{L_p L_s}}{\sqrt{(R_s + R_o)^2 + w^2(L_s + L_o)^2}} \tag{5-31}$$

Combining Eqs. (5-30) and (5-31),

$$\eta_T = \frac{Q_p}{Q_p + \dfrac{Q_p R_s}{R_o} + \dfrac{1}{k^2}\left[\dfrac{(R_s + R_o)^2 + w^2(L_s + L_o)^2}{wL_s R_o}\right]} \tag{5-32}$$

where

$$Q_p = \frac{wL_p}{R_p} \tag{5-33}$$

Equation (5-32) represents the accurate expressions for power-transfer efficiency. As it is often difficult to measure accurately the various resistances and reactances, the equation can be simplified to

$$\eta_T = \frac{P_o}{P_T} = \frac{1}{1 + \dfrac{Q_o}{Q_s}\dfrac{1}{x} + \dfrac{Q_o}{Q_p k^2}\dfrac{(1+x)^2}{x}} \tag{5-34}$$

where

$$Q_s = \frac{wL_s}{R_s} \tag{5-35}$$

$$Q_o = \frac{wL_o}{R_o} \tag{5-36}$$

$$x = \frac{L_o}{L_s} \tag{5-37}$$

The value of x, or L_o/L_s, for maximum power transfer is obtained by differentiating Eq. (5-34) and equating the result to zero. The result is

$$x_{\eta_T \max} = \frac{L_o}{L_{s(\eta_T \max)}} = \sqrt{1 + \frac{k^2 Q_p}{Q_s}} \tag{5-38}$$

In the case of a fixed-coupling transformer at high frequencies, the secondary often consists of a single-current sheet of high Q. Therefore Eq. (5-38) reduces to

$$\frac{L_o}{L_{s(\eta_T \max)}} = 1 \tag{5-39}$$

and the loaded work-coil inductance should equal that of the secondary.

The only assumption in Eq. (5-34) is that Q_{s+o} is large, where

$$Q_{s+o} = \frac{w(L_s + L_o)}{R_s + R_o} \tag{5-40}$$

Figure 5-15 represents Eq. (5-34) in the form of curves for typical values of Q_s and Q_p. The drop in efficiency is marked with a rise in the work-coil loaded $Q(Q_o)$. The value of 5 might represent a tightly coupled steel load, while the value of 20 could be a nonferrous load.

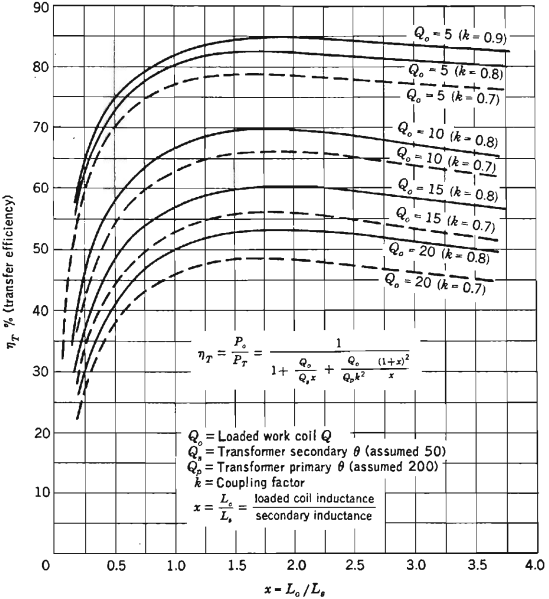

FIG. 5-15. Power-transfer efficiency curves.

The second important factor is the KVA-transfer efficiency. This determines the tank KVA and the value of the tank capacitor. It is defined as

$$\epsilon_T = \frac{KVA_o}{KVA_T} = \frac{k^2 x}{(1+x)^2 - k^2(1+x)} \tag{5-41}$$

where $KVA_o = v_o I_o$, loaded-coil KVA
$KVA_T = v_T I_T$, tank KVA

The effective tank circuit is

$$Q_T = \frac{KVA_T}{P_T} \tag{5-42}$$

The expression can be derived in exactly the same way as the power-transfer efficiency, by circuit analysis of the equivalent circuits in Fig. 5-14.

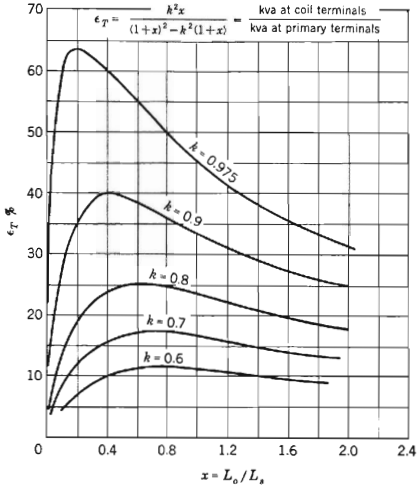

FIG. 5-16. KVA transfer efficiency for transformer as a function of loaded coil inductance and secondary inductance.

If Eq. (5-41) is differentiated and the result equated to zero, the value of x for maximum KVA transfer is obtained.

$$x_{\epsilon_T \max} = \frac{L_o}{L_{s(\epsilon_T \max)}} = \sqrt{1 - k^2} \tag{5-43}$$

Curves of ϵ_T for various values of the coupling factor k are shown in Fig. 5-16. The effect of improving the coupling factor is significant. The majority of r-f transformers vary between k values of 0.65 and 0.9, and the KVA transfer can be improved from 15 to 40 per cent within this range.

The value of $\epsilon_T \max$ is obtained by substituting Eq. (5-43) in Eq. (5-41),

and is plotted in Fig. 5-17, together with the corresponding curve for the coil-to-secondary inductance ratio.

The ratio of secondary-to-primary currents may be approximated from Eq. (5-31) by the following expression:

$$\frac{I_o}{I_T} = \frac{kN_p/N_s}{1 + L_o/L_s} \tag{5-43a}$$

This assumes that Q^2_{s+o} is large, and that inductance is proportional to the square of the turns. This equation is plotted in Fig. 5-17 for $k = 0.8$ and $N_p/N_s = 8$.

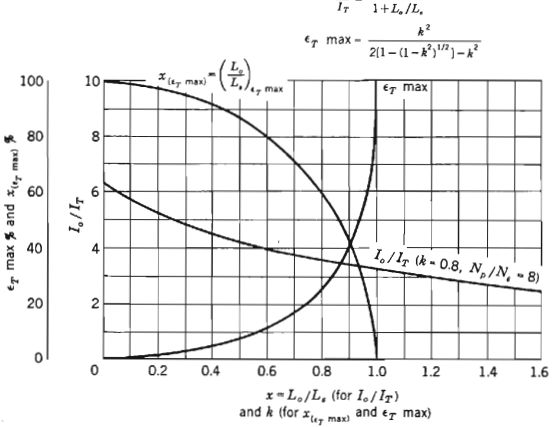

FIG. 5-17. Maximum KVA transfer and primary-to-secondary inductance ratio for maximum KVA transfer as a function of coupling factor.

From the curves in Figs. 5-15 to 5-17, the following factors are apparent:

1. Efficiency of power transfer and of KVA transfer improves with increased coupling.

2. Efficiency of KVA transfer is greatly affected by a change of k value from 0.8 to 0.9, but this change has little effect on power transfer.

3. For a typical k value of 0.8, maximum KVA transfer occurs at a loaded coil-to-secondary inductance ratio of 0.6.

4. With a coil Q of 10, a k value of 0.8 results in maximum power transfer at a coil-to-secondary inductance ratio of 1.8.

5. From (3) and (4), it is obvious that the coil-to-secondary inductance ratio depends on whether coil power or KVA is primarily required.

A simple transformer design and tank circuit are illustrated by an example on a reverse feed-back circuit.

Example 5-1

Calculate the tank-circuit power or tube-output power P_T, tank capacitance C_T, tank current I_T, tank KVA KVA_T, primary inductance L_p, and secondary inductance L_s of an r-f transformer with the following specifications:

Power output, P_o ..... 10 kw
Work-coil loaded Q, Q_o 10
Work-coil loaded inductance, L_o ..... 1.5 microhenrys
Tube plate impedance, z_a ..... 2,500 ohms
Frequency, f ..... 450 kc
Tube plate voltage, peak, v_{ap} ..... 8,400 volts

As the power output is given rather than the KVA, it can be assumed that maximum power transfer is required consistent with as much KVA as is possible. Assume typical Q values for primary and secondary turns of 200 and 50, and a k value of 0.8. From Fig. 5-15, the curve of $Q_o = 10$ and $k = 0.8$ gives a maximum transfer efficiency of 70 per cent.

The tank-circuit power is

$$P_T = \frac{P_o}{\eta_T} = \frac{10}{0.7} = 14.3 \text{ kw}$$

As the oscillator circuit is a reverse feed-back type, the plate impedance to ground z_a will be the same as the tank dynamic impedance z_T (Fig. 5-4*b*).

The ratio of secondary-to-coil inductance x for this maximum power transfer is approximately 1.5. From Fig. 5-16, the curve of $k = 0.8$ peaks at a value of $x = 0.7$. The efficiency of KVA transfer at this ratio, from Fig. 5-16, is 20 per cent. The tank KVA is

$$KVA_T = \frac{P_o Q_o}{\epsilon_T}$$

$$= \frac{10 \times 10}{0.2} = 500 \text{ kva} \qquad (5\text{-}43b)$$

The effective tank circuit Q is

$$Q_T = \frac{KVA_T}{P_T}$$

$$= 500/10 = 50 \qquad (5\text{-}44)$$

It is now possible to derive the tank capacitance required, using Eq. (5-2).

$$C_T = \frac{(50)(10^6)}{(2)(\pi)(450)(10^3)(2{,}500)} = 0.007\ \mu\text{f}$$

Using the ratio of 1.5 for the secondary-to-coil inductance, the secondary inductance is

$$L_s = L_o x = 1.5 \times 1.5 = 2.25 \text{ microhenrys}$$

The *effective* primary inductance of the transformer L'_T is given by

$$L'_T = \frac{1}{w^2 C_T}$$

$$= \frac{(10^6)}{(2)^2(\pi)^2(450)^2(10^6)(0.007)(10^{-6})} = 17.8 \text{ microhenrys} \qquad (5\text{-}45)$$

The actual primary inductance L_p is given in terms of the effective inductance L'_T by

$$L_p = \frac{1}{1 - \dfrac{k^2}{1 + L_o/L_s}}$$

$$= \frac{1}{1 - \dfrac{0.8^2}{1 + 1.5}} = 13.5 \text{ microhenrys} \qquad (5\text{-}46)$$

By using the curve of I_o/I_T in Fig. 5-17, the coil current can be derived, given the tank current. The tank current in turn is given from the tank KVA, if the root mean square (rms) tank voltage is known. If the 10-kw oscillator derived in Sec. 5-3 is coupled to the above transformer in a reverse feed-back circuit, the peak plate voltage can be taken as the tank voltage, with a 10 per cent factor added because of the increased positive swing.

$$v_{Tp} = v_{ap} + \tfrac{1}{10} v_{ap} = 8{,}400 + 840 = 9{,}240 \text{ volts}$$

The tank current is given from

$$I_T = \frac{\sqrt{2} KVA_T}{v_{Tp}} = \frac{\sqrt{2} \times 500}{9{,}240} = 76.5 \text{ amp}$$

Figure 5-17 indicates that for the coil-to-secondary inductance ratio x of 1.5, the coil-to-primary current ratio I_o/I_T is 2.5. This gives a work-coil current of

$$I_o = 2.5 \times 76.5 = 190 \text{ amp}$$

If more current is required, Fig. 5-17 shows that if the value of x, or L_o/L_s, is decreased, in other words if the coil inductance is decreased, the current will increase. This is achieved at the expense of power-transfer efficiency, as is seen from Fig. 5-15.

The curves in Fig. 5-15 are typical for a variable-coupling transformer

suitable for work coils of several turns. Single-turn work coils of very low impedance (less than 0.5 ohms) are usually matched to single-turn secondary transformers with fixed coupling. Here the secondary $Q(Q_s)$ is high and the power transfer efficiency greater. This results in higher coil currents for no greater loss in the transformer. The disadvantage is that with fixed coupling the range of coil inductances and Q factors that can be matched to the generator is very limited. The variable-coupling transformer, although less

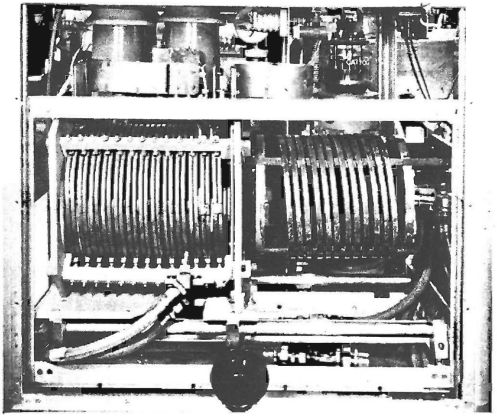

FIG. 5-17*A*. Variable coupling r-f current transformer. (*Redifon, Ltd., England.*)

efficient, also provides a good power control. Decoupling by moving the primary with respect to the secondary lowers the value of the coupling factor k and the efficiency of KVA transfer. Equation (5-43*a*) shows that this decreases the secondary or coil current, decreasing the power into the work and therefore the generator power.

Figure 5-17*A* illustrates a typical variable coupling r-f transformer.

5-8. EXTERNAL CONTROL SYSTEMS

Section 5-6 covered most of the available methods of power control of r-f generators that are built into the generator itself. Many automatic processes use some external signal to trigger these power-control devices, such as functions of time or temperature of the workpiece. These systems are usually of the closed-loop type and in fact form a type of servounit.

The majority of r-f heating applications are controlled by timers, situated either in the generator or in external work-handling equipment. Automatic processes are usually continuous, the completion of one cycle triggering off the next. Figure 5-18 illustrates a typical process. Rocker arm shafts are fed on a conveyor into a coil powered by a 50-kw 350-kc r-f generator. When in position, the shaft triggers off a timer, applying r-f power and hardening the shaft. The timer shuts off power when it has timed out, and the hardened

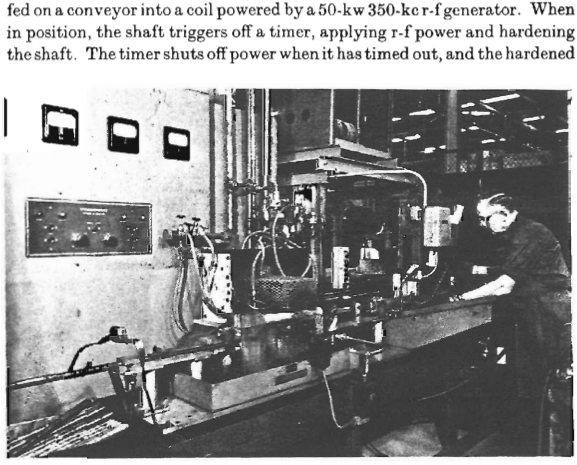

FIG. 5-18. Automatic time-controlled r-f heating process. (*Westinghouse Electric Corp.*)

shaft is ejected, simultaneously initiating a new cycle. In this particular equipment a small photocell, located in front of the coil, checks for temperature variations and rejects shafts when the temperature has varied by more than a preset amount.

Temperature is not used so often as time as a control in the normal processes of hardening, brazing, soldering, etc. In the more recent applications of semiconductor processing, the times are sufficiently long to warrant the use of temperature control. Figure 3-41 shows a number of r-f generators using thyratrons for power control in crystal growing; Fig. 5-18*A* illustrates a typical crystal-growing installation.

The principles of crystal production are complex and are covered by existing references (82). The material (either silicon or germanium) must first be refined to remove as much impurity as possible. This is usually done in the case of silicon by the zone-refining method shown in Fig. 5-19*b* (81).

Melted zones are caused to move down the material in a carbon boat, and the impurities are carried with them to the end of the boat. The temperature of melting is about 950°C. As molten silicon has a great affinity for most crucible materials, the levitation method, illustrated in Fig. 5-19*b*, is used. In this method, a rod of silicon, while being rotated, is raised and lowered

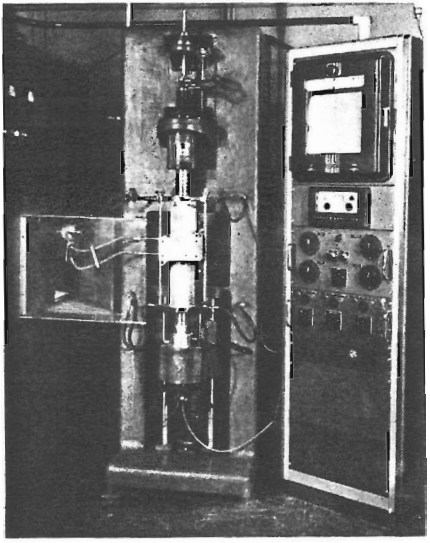

FIG. 5-18*A*. Crystal-growing system. (*Leeds and Northrup Company.*)

through a coil. The small molten zone, heated to 1400°C, has enough surface tension to keep the rod in one section. The impurities are carried to either end of the rod in the same way as in the germanium method.

After refining, the semiconductor material must be a single crystal and must have a strictly controlled amount of impurity added for transistor action. Three methods of crystal growing are used (81): the crystal-pulling, the zone-leveling, and the levitation methods. Crystal pulling, the most widely used, is shown in Fig. 5-19*c*. A small seed, containing the necessary degree of impurity, is dipped into the molten material and then pulled up

by a rotating rod. The crystal is shown growing as the rod is raised. Sometimes the crucible is also rotated to ensure uniformity. This method is used for silicon and germanium.

Germanium crystals can also be grown by the zone-leveling method. This consists essentially of the same equipment as in germanium zone refining

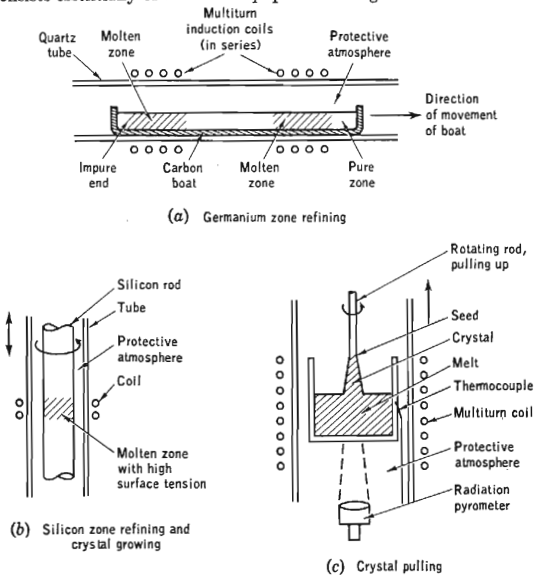

FIG. 5-19. Semiconductor processing.

with the addition of a single, oriented impure seed added at one end of the boat. The rest of the boat contains purified germanium; as the boat is pulled through the coils, a single crystal containing the required impurity is formed.

The levitation method of silicon zone refining can also be used for crystal growing if one end of the rod is formed of a single, oriented crystal. Continuous passage of the rod up and down through the coil coarsens the structure until it is a solid crystal.

With all these methods, very accurate temperature and power control is

required to maintain the highly critical impurity density and crystal growth rate. A typical system is shown in Fig. 5-20 for crystal growing. The temperature is measured either by direct sighting of a radiation pyrometer or by a sapphire rod. The advantage of the rod is that it acts as an infrared transmission line and the end can be placed very near the crucible. In certain cases a platinum–platinum-rhodium thermocouple, located in the crucible side, can be used.

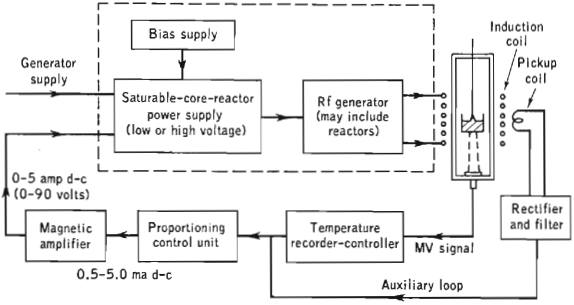

FIG. 5-20. Semiconductor temperature-control system—power-proportioning.

The millivoltage output is fed to a potentiometer type of temperature recorder-controller, usually of the strip-chart type. This is fitted with a span of approximately 100°C, and is suppressed to allow the lower end of the span to be preset at any desired temperature. The mid-point is usually the required melt temperature.

Any deviation from this set point results in a signal proportional to the deviation. The signal is fed to a proportioning control unit, where it is amplified and the result fed to a magnetic amplifier. The milliampere signal is amplified to about 0 to 5 amp, required to drive the saturable reactors controlling the generator. These reactors are biased back to some optimum power point sufficient to supply all heat losses in the melt and maintain the temperature constant. Therefore, any temperature change results in a small amount of correction to the power level to eliminate the error.

Programming is often used, as the temperature of the interface between crystal and melt varies even though the crucible temperature is kept constant. Usually the set point on the controller is automatically lowered by the control unit to counteract the rise of the interface as the process develops.

The saturable reactors can be of the high-voltage type shown in Fig. 5-10c, or they can be inserted in the low-voltage supply to the generator. Alternatively, thyratrons can be used, in which case the magnetic amplifier output signal controls a phasing network at the grids.

A linearizing auxiliary loop is often added, as shown in Fig. 5-20. This provides a correction signal in the event of mains fluctuations causing a temperature variation. It consists of an r-f rectifier and filter which is fed from a pickup coil near the main heating coil. The loop will oscillate at about 10 cps (81), by combining the signal with that from the recorder.

Most processes involve high-impedance, multiturn coils heating large crucibles. In the levitation method, a narrow zone is heated by a low-impedance coil. One method to accomplish this combines an r-f transformer and a complete tank circuit in a small single unit. This is then capable of scanning up and down the vertical rod, with only low-current leads feeding back to the generator.

5-9. RADIO-FREQUENCY–GENERATOR CIRCUIT METERING

The most important quantity measured in r-f generators is the plate direct current. This is used as an indication of generator loading in the heating processes and gives a direct measurement of the efficiency of the coil and the power output of the generator. If the plate d-c voltage is known, the product of the difference between the no-load and full-load plate current values and the plate voltage gives a good approximation to the power loading into the work. The current is usually measured in the ground lead of the power supply, as shown in Fig. 5-8*d*. To prevent stray r-f current from damaging the instrument, especially the torque springs, a bypass capacitor is usually placed across the terminals. For ½-Mc frequencies, a value of 0.01 μf is sufficient. The maximum safe value is usually indicated in red on the meter, as currents above this value can damage the tube.

Grid-current metering is often incorporated in larger generators; it can give a good indication of the correct operating condition of the oscillator tube. If oscillation of the tank circuit fails, the grid-current meter will read zero and the plate voltage should be immediately removed. The reasons were outlined in Sec. 5-3. Also it may be possible to damage the grid by excessive grid current (the maximum safe value is often indicated on the meter). Radio-frequency bypassing capacitors are used in the same way as on the plate-current meter. The meter is usually located in the ground return lead of the d-c grid circuit. In smaller generators, a link is provided in this position which enables an external meter to be inserted during tests.

Plate d-c voltage can be measured directly between ground and the output of the power supply. A standard multiplier resistor and milliammeter is

conventionally used. Again, this is usually located in the circuit only in the larger generators.

Filament voltage is sometimes measured when the supply voltage variations are excessive and could cause filament damage, particularly in large expensive tubes. This method, when combined with voltage control, is often more economical than a constant-voltage transformer.

High-frequency measurements are not easy to carry out at the power levels associated with most induction heating generators. The circulating current is the most useful indication of power loading; it can be measured by use of either a simple pickup loop or a toroid type of current transformer. Ring dust-cores are often used for the transformer core, and the current ratio is approximately equal to the number of turns when the toroid is coupled to a tank-circuit lead, as shown in Fig. 5-21*a*. The meter is usually of the thermocouple type. Pickup loops are often coupled into the tank coil, but in general the accuracy is not so high as that of the toroidal transformer. Thermocouple meters can also be connected straight into the lead at a point where the lead temperature is a function of current. This is usually confined to small-power generators.

High-frequency voltages are usually measured by rectifying to direct current and then measuring the peak voltage across an electrostatic voltmeter (Fig. 5-21*c*). For high voltages, a capacitance divider can also be used, as shown in Fig. 5-21*b*. The ratio of C_1 to C_2 gives a voltage ratio of about 200:1. D_1 is a crystal diode. C_2 charges up when the r-f voltage is positive, then discharges during the negative cycle, through R_1 or R_2. These give different voltage ranges, as the current through them and the milliammeter M_1 is a function of the resistance values. This procedure also measures peak voltages. The time content R_1C_2 or R_2C_2 is large compared with one cycle of the r-f voltage, so that the voltage across C_2 is steady.

Radio-frequency power is rarely measured directly and is difficult to meter accurately. By measuring the power input into a calorimeter, such as shown in Fig. 5-21*a*, and calibrating this against either r-f tank current or d-c plate voltage, a reasonably accurate indirect indication can be achieved. The calorimeter usually consists of a steel cylinder with a water inlet and outlet, arranged to give maximum heat exchange from the heated cylinder to the water. Temperature is measured at inlet and outlet points. The power transferred (and assumed loaded into the cylinder walls) is given by Eq. (4-12).

Frequency is usually measured by a simple tuned circuit and current indicator. The basis of all frequency measurements of generators is shown in Fig. 5-21*e*. The current, when the circuit is tuned to resonate with the signal, can be indicated by the lamp as shown, or by a meter measuring

the rectified current. Very accurate frequency checks are possible using a heterodyne frequency meter. Signals from the meter are compared with those from the source and the results indicated audibly, either via head-

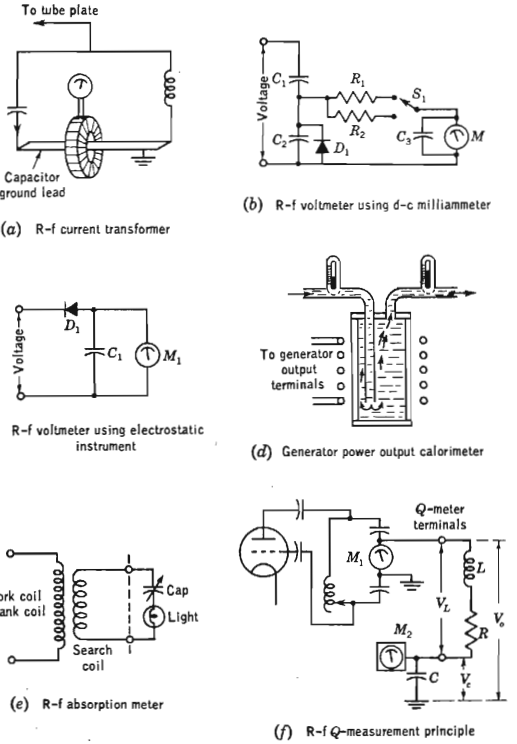

FIG. 5·21. Measurements at radio frequencies.

phones or an amplifier and loud-speaker. When the local oscillator frequency is the same as that of the signal, the zero beat point can be picked up as a null point or dip in the audible frequencies.

The frequency of a tuned circuit is usually determined by a grid-dip oscillator (GDO). This consists of an oscillator circuit, usually a Colpitts type, as shown in Fig. 5-22. The inductance is external to the unit and is of the plug-in type, to enable a range of frequencies to be covered. It is coupled to the tuned circuit to be measured, and the capacitance is varied until the oscillator and tuned-circuit frequencies are identical. The oscillator tube is then loaded and the grid current dips, as indicated on the grid-current meter.

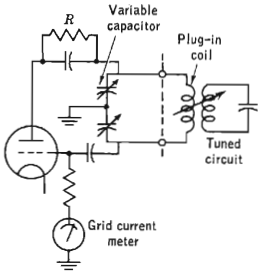

FIG. 5-22. Grid-dip oscillator.

The GDO can also be used as a frequency wavemeter by removing the plate voltage and coupling to the oscillating circuit to be measured. The tube acts as a diode, and the point of maximum current on the meter indicates the external frequency of the measured oscillator.

The only other variable that is usually measured in r-f work is the Q of the various inductances, such as tank coils, work coils, etc. The principle of a Q meter is shown in Fig. 5-21. The definition of Q given in Eq. (5-1) can be enlarged as follows:

$$Q = \frac{wL}{R} = \frac{v_L}{v_o} = \frac{1}{wcR} = \frac{V_c}{v_o} \tag{5-47}$$

In other words, a series resonant circuit has a voltage developed across the inductor or capacitance of Q times that across the circuit. By applying a known voltage v_o from a variable-tuned oscillator, and measuring the voltage across the capacitor v_c with a valve voltmeter, the voltmeter (M_2) scale can be calibrated directly in values of Q. This is true provided that the capacitor has a low loss factor. The variable inductor is tuned until the voltmeter on the oscillator circuit (M_1) is at a maximum.

Two other conditions are necessary: the source impedance of the applied voltage V_o should be low and the admittance of the valve voltmeter measuring the magnified voltage V_c should also be low. The meter M_1 serves to standardize the injected or applied voltage.

The values of inductance, capacitance, and effective resistance of components at radio frequencies can be measured by the Q-meter method or by a variety of alternative circuits (83). Transmission-line characteristics can also be determined.

5-10. STRAY-FIELD RADIATION

One of the most important factors in r-f heating generator and system design is the elimination of stray-field radiation. In general, radiation increases in field strength with increase in frequency and effective external coil length. It is also a function of equipment height above ground level and of the effective screening of the cubicle.

The basis of the Federal Communications Commission's regulations (84) is as follows:

1. The specific frequency assignments for r-f heating equipment are 13.56, 27.12, 40.62, and 2,450 Mc.

2. Equipments outside these bands are to be limited to a maximum field strength of 10 μv per meter at 1 mile from the equipment.

3. Any interference with radio, television, or communications is to be corrected, whether the frequency is within the assigned bands or not.

4. Regulation violations will result in making further operations unlawful unless a station licence is issued.

Induction heating generators are usually certified by the manufacturer with a typical coil and lead attachment. On smaller attachments, the generator is mounted on a rotating trolley and is operated with a coil at no-load and maximum plate voltage. This usually results in maximum radiation. The field strength is checked at some distance from the generator (usually several hundred feet) and the trolley rotated by about 15° intervals. The results are plotted on a polar diagram. The angles of the maximum lobes are determined, and further measurements are taken along these lobes up to 1 mile. An attenuation law is derived for distance against field strength. If the strength at 1 mile is less than 10 μv per meter, the equipment can be safely certified. Larger equipments are checked by taking measurements at convenient points around the generator at several hundred feet away.

If the field strength at 1 mile is greater than 10 μv per meter, the causes of excessive radiations are investigated. They are likely to be included in the following:

1. Poor metallic contact between doors or panels and the frame
2. Excessive ventilation openings
3. Large coils, leads, and transmission lines
4. Poor shielding of coils and leads
5. Reradiation from r-f currents in the power lines
6. Bad grounding of the generator or shields
7. Harmonics of the fundamental oscillations
8. Reradiation from reflecting "antennas," such as nearby power lines.

Most of these causes can be reduced or eliminated by good engineering

practice in design construction and installation of the r-f equipment. Particular attention should be paid to the contact surfaces between doors and movable panels, both on generators and on associated equipment. This bonding of joints should utilize low-resistivity metals and tight contact. Theoretically, if no openings existed in the equipment, shielding would be perfect and radiation would be eliminated.

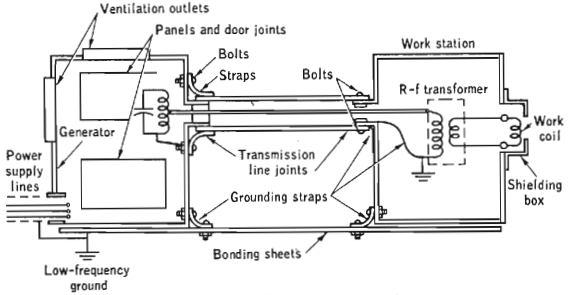

FIG. 5-23. Sources of r-f radiation and correcting measures.

Figure 5-23 illustrates a typical system, with possible sources of radiation. Ventilating outlets should be kept to a minimum and should be covered by metallic grills. Joints should be generously overlapped, and bolts should be reasonably closely spaced, up to approximately 6 in. This is particularly important where return currents pass across joints, as in the case of transmission-line shields. Copper and aluminum, either in sheet or grill form, or sprayed onto steel, are the best metals for shielding or contact joints (85). Brass hardware should always be used. Beryllium-copper weather stripping should be used for panels or doors, and piano-type continuous hinges utilized on doors.

Earth straps should be used across joints, such as the ends of transmission lines. Work coils are not usually shielded because of application work handling, but r-f transformers and switches should be mounted in well-shielded cubicles. Grounding should be used with caution; only one low-frequency ground should be used on the whole equipment. The floor should be aluminum or copper if possible, and all parts of the system should be well bonded to it. Alternatively, one section of the transmission line between two units can be widened as much as possible to act as a common ground or low-impedance bond between the units. Long grounding straps should

never be used, and the low-frequency ground should be tied in with the incoming power supply.

In any continuous process involving a conveyor system, the coil and leads may have to be shielded in the case of higher frequencies (5 to 10 Mc). The aperture into the shielding should not be wider than about 12 ft.

The generator design should include an oscillator compartment shielded and separate from the power supply. It may also be necessary to use LC filters in the power supply lines. Both these measures prevent r-f currents from entering the supply lines and being reradiated. Any interunit control wiring in a system should pass through conduit. Items such as meters, relays, lamps, etc., should have small bypass capacitors across them. Values such as 0.01 μf, 300 volts working direct current should be used.

All units in system installations should be located as close together as possible. Conduits, water points, air ducting, etc., should all enter the generator as closely together as is practical. Power lines should be brought up in conduit, which should run underground for about 50 ft.

The International Distress Band of 490 to 510 kc is completely barred for industrial equipment.

CHAPTER 6

MACHINE-FREQUENCY HEATING SYSTEMS

6-1. PRINCIPLES OF THE MOTOR-GENERATOR SYSTEM

The ideal requirement of a machine-frequency supply for induction heating is a constant-voltage power source. The load usually varies over a wide range of lagging power factors, and is corrected to as near unity power factor

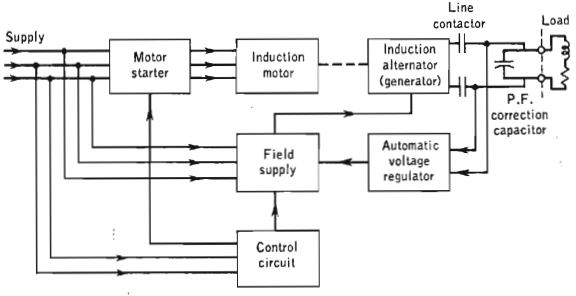

FIG. 6-1. Machine-frequency system.

as possible. Figure 6-1 shows the basic system used for most induction heating loads at machine frequencies. If an automatic voltage regulator and power-factor correction capacitors are used, the supply to the load can be made relatively voltage-constant.

The principle of operation of the high-frequency alternator differs from that of the standard supply-frequency alternator in the location of the field windings. In the higher-frequency alternator these windings are located on the stator, together with the armature windings. Figure 6-2 shows the cross section of a typical large induction alternator. The field-windings flux follows a path through both sets of rotor and stator teeth, the air gaps between teeth, the rotor shaft, and the yoke around the windings. The construction of this type of alternator is illustrated in Figs. 6-3 and 6-4.

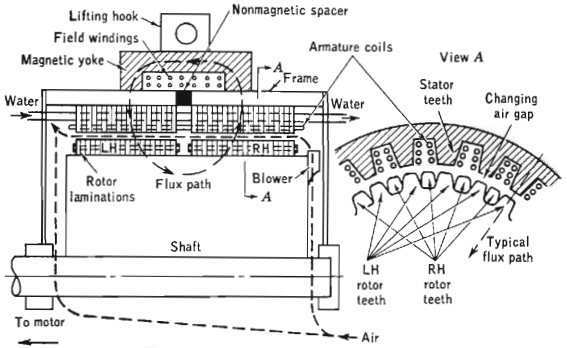

FIG. 6-2. Typical induction alternator.

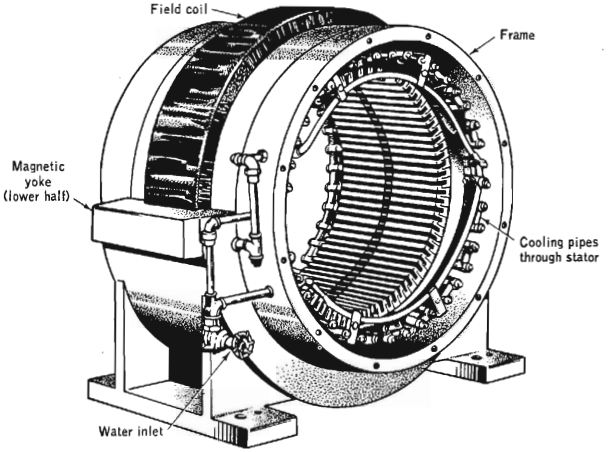

FIG. 6-3. High-frequency generator stator without armature windings (upper half of yoke removed). (*Westinghouse Electric Corp.*)

It is seen that the teeth in each half of the stator are in straight rows, but the rotor teeth are 180 electrical degrees out of phase. This accounts for the appearance of view *A* in Fig. 6-2. There are twice as many stator as rotor teeth in each half.

As the rotor turns, the reluctance of the air gap between rotor and stator teeth changes from a minimum to a maximum. The magnetizing force resulting from the field coil is constant (for a constant field current); therefore the flux in each stator tooth varies with the reluctance. As the rotor

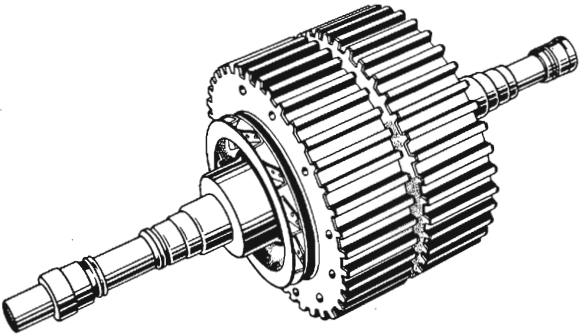

FIG. 6-4. High-frequency inductor-type generator rotor with blower. (*Westinghouse Electric Corp.*)

turns, the change in flux linking the two halves of each armature coil (left half and right half) is such that it induces a voltage in the same direction in each half. These voltages add, and all the coil voltages can be connected in series or parallel. In general, the coils are arranged so that there are two output voltages which can be in series or parallel, depending on the load impedance.

The generator frequency is given by

$$f = \frac{RPM}{60} N_R \quad \text{cps} \tag{6-1}$$

where RPM = rotor revolution per min
N_R = number of rotor teeth

A typical motor may drive the generator at 1,800 rpm and with each half

of the generator containing 100 rotor teeth and 200 stator teeth, the frequency is

$$f = 1{,}800 \times 100/60 = 3{,}000 \text{ cps}$$

Frequencies most commonly used are 960, 3,000, and 9,600 cycles.

The yoke and frame shown in Fig. 6-3 are made of heavy steel, the yoke being split to allow removal of the field coil. The frame is made up from two rolled steel rings separated by a nonmagnetic spacer. The spacer ensures that most of the flux passes across the air gap. The stator core is usually constructed from laminations of silicon steel, rigidly bolted together.

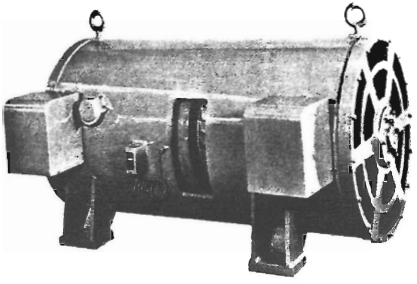

FIG. 6-5. Air-cooled motor-generator set. (*Westinghouse Electric Corp.*)

The rotor consists of silicon steel laminations built up onto a steel shaft. Occasionally, large rotors are forged. Teeth are punched in the outer surface. Air gaps between rotor and stator teeth are kept as small as possible; therefore the rotor bearings and the rotor are usually heavier than in low-frequency generators.

The motors in most motor-generator sets are of the conventional inductance type. The coupling between motor and alternator is usually flexible.

Cooling is usually carried out by air, water, or hydrogen. The actual method depends on the generator rating and its location in operation. A dirt-laden atmosphere such as that in a forge shop, will require total enclosure of the set and a water-to-air heat exchanger. The generator room should also be adequately ventilated, and the room temperature rise due to the set should be kept to 10°F maximum.

Small sets are usually either open and air-cooled or totally enclosed and water-cooled. Figure 6-5 shows a typical open, air-cooled set, with the motor and generator built into one frame. This type can be operated at

960, 3,000, and 10,000 cycles, up to 250-kw output power at $^{220}/_{440}$ or $^{400}/_{800}$ volts. By the addition of water-to-air heat exchangers at each end, the sets can be operated as water-cooled types. An exchanger is shown in Fig. 6-6.

Larger sets are often cooled by both water and air, and the motor and generator are built into separate frames. Figure 6-7 shows a set of this type,

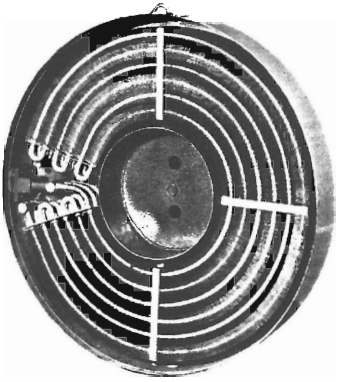

FIG. 6-6. Water-cooled heat exchanger for motor-generator set. (*Westinghouse Electric Corp.*)

with a water cooler built into the stator punchings. Figure 6-4 illustrates this construction. The motor is open and completely air-cooled. An exciter generator is shown built into the motor, for field excitation.

In certain cases, where water or air cooling would be insufficient, hydrogen-to-water heat exchangers are used. The complete set is totally enclosed in a hydrogen atmosphere. Figure 6-8 illustrates a set of this construction, with the heat-exchanger plumbing and pump clearly visible. This set is rated at 3,000 kw at 3,000 cycles.

Vertical sets have certain advantages over the horizontal types described above. Large bearings are possible, and bearing life is improved because of even loading. Floor space is reduced and maintenance is simple owing to easy vertical removal of the rotor. On the other hand, overhead space is higher. Figure 6-9 illustrates a typical vertical construction.

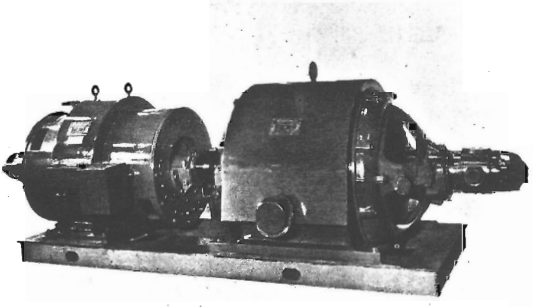

FIG. 6-7. Large water- and air-cooled motor-generator set. (*Westinghouse Electric Corp.*)

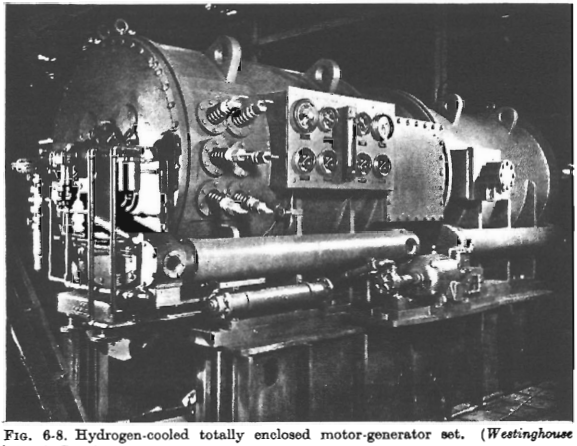

FIG. 6-8. Hydrogen-cooled totally enclosed motor-generator set. (*Westinghouse Electric Corp.*)

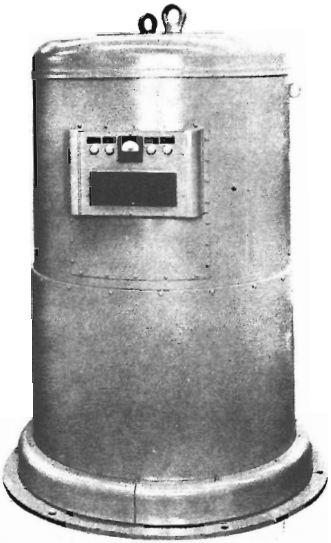

FIG. 6-9. 100-kw vertical-type water-cooled motor-generator set. (*The Ohio Crankshaft Corp.*)

6-2. OPERATING CHARACTERISTICS OF THE GENERATOR

Most generators possess internal reactance and resistance because of the resistance of the windings and the magnetic leakage fluxes. This causes a drop in terminal voltage with increasing load current, and the regulation is therefore similar in effect to that of a transformer.

The internal inductance and impedance are usually determined under load conditions. The open-circuit and short-circuit characteristics are measured and plotted against excitation current, as shown in Fig. 6-10. If N is the normal exciting current under full-load conditions, then the synchronous impedance is the open-circuit voltage divided by the short-circuit current. This is because the whole of the voltage is used to drive the short-circuit current through the armature windings against the internal impedance.

The operating characteristics of the generator are therefore affected by the power factor of the load, and the synchronous impedance could be an important function. Figure 6-11*a* shows a typical vector diagram, where

E_o = armature-induced voltage (terminal voltage at no load)
E = terminal voltage on load
I = load current (output of generator)
R_a = armature resistance
L_a = armature inductance
f = generator frequency
z_a = armature impedance
ϕ = load phase angle
θ = internal generator phase angle

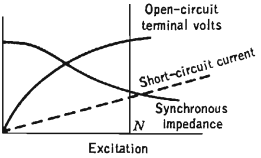

FIG. 6-10. Internal synchronous impedance of a generator.

The synchronous reactance drop ($I2\pi fL_a$) is very nearly the same as the synchronous impedance Iz_a, as R_a is usually small compared with $2\pi fL_a$.

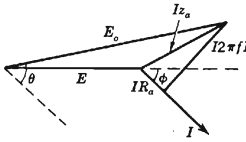

(*a*) Generator vector diagram

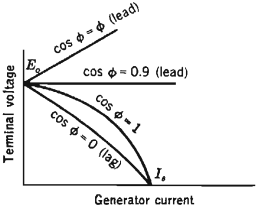

(*b*) Generator characteristics

FIG. 6-11. Generator-voltage current characteristics.

The relation between generator current I and voltage E is given from

$$\left(\frac{E}{E_o}\right)^2 + \frac{2EI}{E_o I_s}\sin\phi + \left(\frac{I}{I_s}\right)^2 = 1 \quad (6\text{-}2)$$

where I_s = short-circuit current at normal excitation.

The curve of Eq. (6-2) is plotted in Fig. 6-11*b* for different values of the power factor. In general, most induction heating loads are inductive, with power factors as low as 0.1 lagging. These are usually corrected by parallel capacitors, and the curves show that the least terminal-voltage drop is obtained with a slightly leading power factor. A value of 0.9 is usually recommended in practice.

Excessive capacitance should be avoided, as the terminal voltage rises with a large leading power factor. In some cases this could lead to voltage breakdown in the armature insulation.

Modern generators are built with a reasonable amount of internal armature reactance, to prevent an excessive short-circuit current which would

damage the windings. The consequence is that voltage regulation, given by

$$\text{Per cent regulation} = \frac{E_o - E}{E} \times 100$$

is often excessive. Automatic regulation, described later, is always required.

Recommended operating and loading conditions include maintenance between 0.9 leading and unity power factor for maximum power loading. It is often possible to exceed the maximum rating by 10 per cent for short periods, and a current overload of 50 per cent can usually be tolerated for 1 min. The internal reactance is often series-tuned with an external capacitance of equal reactance.

The motor-generator sets are usually started by conventional means such as autotransformer, resistance, or star-delta starters. The starting voltages are normally two-thirds-full line voltages, and the initial surge of locked-rotor currents is about five times the steady full-load currents.

Power-efficiency values for most generators vary between 65 and 95 per cent, usually increasing with increase in loading and decrease in frequency. A typical 960-cycle 250-kw generator would be 95 per cent efficient at full load. A 10,000-cycle 350-kw generator at full load may be only 73 per cent efficient, dropping to 64 per cent at one-half load.

Operating two or more sets in parallel on the same busbar is often considered better than operating one large set. Maintenance problems are reduced, the number of sets can be increased if required, cooling can be of the conventional type, and more individual control is possible. The driving motors should have suitably similar characteristics, and it is preferable to utilize induction rather than synchronous motors. The full-load slip on each motor in the combination should decrease in proportion to the increase in set rating. As a precaution, the total rating of a combination of sets should be decreased by between 5 and 10 per cent of the sum of the individual ratings. In general, all sets in a combination should have the same power, frequency, and voltage rating.

Each set in a combination is run up to full speed with no field excitation, then brought onto the busbar and run into synchronism. Field currents are applied and increased to give the rated output voltages.

6-3. LOAD MATCHING AND TUNING

All generators have definite voltage, current, and power-factor ratings for full-load operation. Typical voltages are 220, 400, 440, and 800 volts; the power factor must be maintained between unity and 90 per cent leading. Power ratings can vary between 7½ kw at 10,000 cycles and 10,000 kw at 960 cycles.

All coils have to be power-factor corrected by capacitors, and most hardening and brazing coils require transformers as they are usually of small impedance compared with the generator. Most through-heating coils can be designed with voltage requirements equal to the generator output, eliminating transformers.

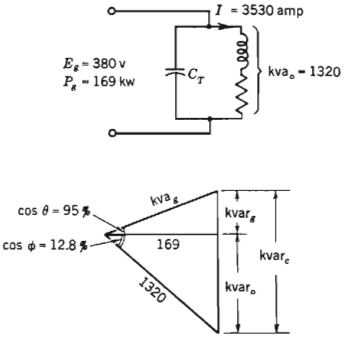

FIG. 6-12. Power-factor correction in a motor-generator set system.

Example 6-1

Derive the power-factor correction capacitance required for the coil designed in Example 4-7 to result in a 95 per cent leading generator power factor.

Figure 6-12 illustrates the circuit and vector diagram of the power, KVA, and KVA relations. The generator KVA and $KVAR$ are given by

$$KVA_g = 169/0.95 = 178 \text{ kva}$$
$$KVAR_g = (178^2 - 169^2)^{1/2} = 56 \text{ kvar}$$
$$KVAR_o = (1{,}320^2 - 169^2)^{1/2} = 1{,}305 \text{ kvar}$$

Therefore the capacitance $KVAR$ is

$$KVAR_c = KVAR_g + KVAR_o = 1{,}305 + 56 = 1{,}361 \text{ kvar}$$

A typical 960-cycle capacitor is rated at 160 kvar at 450 volts. For 380 volts, it has to be derated.

$$KVAR = 160(380^2/450^2) = 115 \text{ kvar}$$

Therefore for the nearest whole number of capacitors required

$$\text{No. of units} = 1{,}361/115 = 11.8 + 0.2 = 12$$

Machine-frequency capacitors are usually constructed of aluminum plates, separated by low-loss paper. Each capacitor is made up of several elements and is water-cooled. The dielectric material is usually a synthetic chlorinated diphenyl oil, and the case either steel and brass or plain brass at higher frequencies. The capacitors can usually be mounted either upright or on their sides. Some high-voltage units must be mounted with the case insulated from ground. Cooling-water requirements vary between 0.2 gpm (water at 5°C) and 1.0 gpm (water at 25°C) for a 300-kvar unit.

Derating is necessary for reduced-voltage and -frequency operation. The $KVAR$ must be reduced by the square of the voltages, as above, or by the direct ratio of the frequencies.

Most continuous through-heating applications maintain a reasonably constant power factor. A large number of single-shot hardening applications present a load with a widely varying power factor. The initial stage of the cycle presents a power factor near unity, but as Curie point is passed, this drops sharply to as much as 10 per cent of unity. In order to maintain the generator as near unity as possible, extra capacitors are often added across the terminals. These are usually switched in automatically via machine-frequency contactors. A multicontact process timer is often used, and one contact is set to energize the contactor coil when the work temperature reaches the Curie point.

The selection of a machine-frequency transformer to match a low-impedance coil to a generator is generally based on experimental tests. It is possible to estimate the approximate ratings required if certain assumptions are made. The basic principles are the same as for an r-f transformer, but the coupling factor is usually improved to 0.9 or more. This is because all machine-frequency transformers are fixed-coupling, with cores of high saturation density, made of grain-oriented silicon steel. Transformer losses are small, usually of the order of 5 per cent, and efficiency of KVA transfer is high (75 per cent).

Using a modification of the previous coil-calculation formulas, based on coils suitable for shaft hardening, it is possible to approximate the coil current from

$$I_o = \frac{2{,}000 P_s^{1/4} l_c}{f^{1/4} N_c} \quad \text{amp} \tag{6-3}$$

where P_s = surface power density on work, watts per sq in.
l_c = coil length, in.
f = frequency, cps
N_c = coil turns

The method to determine the transformer and capacitors required to match a coil to a generator can best be illustrated by an example.

Example 6-2

Derive a suitable transformer and power-factor correction capacitors to match the coil to the generator in Example 4-5.

The generator power per square inch was given at 20 kw per sq in. at 9,600 cps. Most hardening scanning coils are about 50 to 60 per cent efficient; therefore the work-surface power density is given by

$$P_{sw} = (50/100) \times 20 = 10 \text{ kw/sq in.}$$

The coil was 1 in. long. Assume one turn. Therefore the current is

$$I_o = \frac{(2{,}000)(10 \times 10^3)^{1/2}(1)}{(9{,}600)^{1/4}(1)} = 20{,}000 \text{ amp}$$

The generator power in Example 4-5 was 94.4 kw. Allowing 5 per cent transformer and lead loss, the coil power is

$$P_o = (95/100) \times 94.4 = 90 \text{ kw}$$

Assuming a power factor of 35 per cent, the coil KVA is

$$KVA_o = 90/0.35 = 257 \text{ kva}$$

The coil voltage is

$$E_o = \frac{KVA_o}{I_o} = \frac{257{,}000}{20{,}000} = 12.9 \text{ volts}$$

Allow 75 per cent KVA transfer efficiency. The primary KVA will be

$$KVA_p = \frac{KVA_o}{0.75} = \frac{257}{0.75} = 345 \text{ kva}$$

If a generator voltage of 800 volts is assumed, then the primary current is

$$I_p = \frac{KVA_p}{E_g} = \frac{345{,}000}{800} = 430 \text{ amp}$$

The transformer turns ratio is therefore

$$\frac{N_p}{N_s} = \frac{I_s}{I_p} = \frac{I_o}{I_p} = \frac{20{,}000}{430} = 46.5:1$$

Now both the coil current and the turns ratio are excessively high for the coil required. If a two-turn coil is assumed, then the coil current becomes

$$I_o = \frac{(2{,}000)(10^4)^{1/2}(1)}{(9{,}600)^{1/4}(2)} = 10{,}000 \text{ amp}$$

The coil voltage is increased to

$$E_o = 257{,}000/10{,}000 = 25.7 \text{ volts}$$

The turns ratio now becomes

$$\frac{N_p}{N_s} = \frac{10{,}000}{430} = 23.2:1$$

The power factor presented by the primary of the transformer is

$$\cos \phi_p = \frac{P_g}{KVA_p} = \frac{94.4}{345} = 27.4 \text{ per cent lag}$$

In order to present unity power factor, the capacitive $KVAR$ must equal

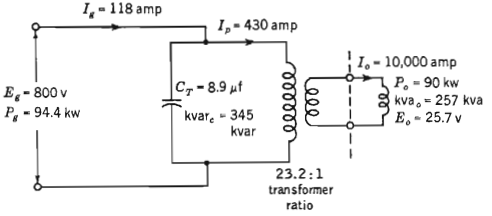

FIG. 6-13. Matching a low-impedance coil to a motor-generator set.

the reactive $KVAR$ presented by the transformer. For approximate calculations, this can be taken as the KVA of the primary.

$$KVAR_c = KVA_p = 345 \text{ kvar}$$

The capacitance is given by

$$C_T = \frac{I_p}{2\pi f E_g} = \frac{(430)(10^6)}{(2)(\pi)(9{,}600)(800)} = 8.9 \ \mu\text{f}$$

The generator line current is

$$I_g = \frac{P_g}{E_g} = \frac{94.4 \times 10^3}{800} = 118 \text{ amp}$$

Figure 6-13 illustrates the system for the low-impedance coil.

A larger current than would result from the coil calculations in Chap. 4 is obtained from Eq. (6-3), because the coils used in hardening are usually short, with a large end effect. The end effect is caused by the relatively large amount of steel entering and leaving the coil in scanning applications.

The impedance of the coil is

$$z_o = \frac{E_o}{I_o} = \frac{25.7}{10{,}000} = 2.57 \times 10^{-3} \text{ ohm}$$

The impedance of the generator is

$$z_g = \frac{E_g}{I_g} = \frac{800}{118} = 6.8 \text{ ohms}$$

The coil impedance in Example 6-1 is given from

$$z_c = 380^2/(1{,}320 \times 10^3) = 0.11 \text{ ohm}$$

and the generator impedance is

$$z_g = 380^2/(178 \times 10^3) = 0.81 \text{ ohm}$$

If these results are compared, it is obvious that the more economical system is one in which the coil impedance is of the same order as that of the

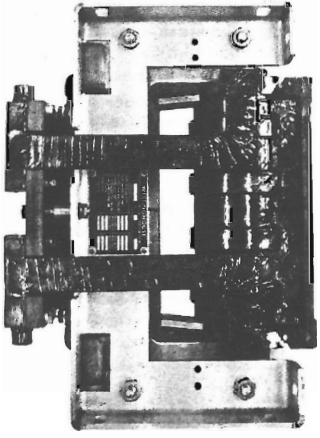

FIG. 6-14. A 3,000/9,600-cycle transformer. (*Westinghouse Electric Corp.*)

generator. A transformer is always more costly than several capacitors. However, most hardening applications require these transformers, which are usually housed in control cubicles.

Figure 6-14 shows a typical water-cooled, 3,000/9,600-cycle transformer. Ratios between 5:1 and 40:1 are usually obtainable, with coil currents up to 20,000 amp. It is recognized that many hardening applications involve a duty cycle of less than 1 min. Therefore the secondary-coil current ratings

can often be increased for these duty cycles. Owing to the high core flux densities, resulting from transformer KVA values as high as 1,000, the cores are usually water-cooled in addition to the windings.

Variable-ratio transformers are also available, for use with more than one type of coil and coil impedance. Occasionally, it is necessary to match a coil with an impedance similar to that of the generator. Autotransformers can be used; their cost is usually less than that of completely isolated secondary types.

6-4. CONTROL SYSTEMS

Some machine-frequency applications, for example, through-heating for annealing, forging, and brazing, involve long-time cycles. Single-shot hardening time cycles are often as short as r-f applications. Therefore both temperature- and time-controlled systems are used. Scanning hardening applications are usually controlled by limit switches, which are actuated by the moving part (coil or workpiece). Manual control is used to a lesser extent than in r-f heating, probably because of the higher power levels and production rates encountered in machine-frequency installations. Automation is more advanced, partly because of the faster production rates, and also because of the need to recover the high initial capital cost of the equipment.

Time-controlled systems usually involve the use of multicontact cam timers, which switch the generator-line machine-frequency contactors in or out. These contactors are basically similar to the supply-line 50-cycle type but are derated below the equivalent 50-cycle rating. Because of the longer arcs produced on breaking the circuit, magnetic or compressed-air blowout systems are used. The magnetic blowout consists of a strong magnetic field, produced by coils, across the arc. This tends to lengthen the arc path and break it, reducing pitting on the contact surfaces. The break speed is also increased, and the arc shields are usually larger than in 60-cycle contactors. Because of the induction heating properties of machine-frequency currents, steel parts are kept to a minimum.

Certain applications require different power levels during the application. An example is the scanning hardening of a shaft of different cross-sectional areas. In such cases, the power is usually adjusted by changing the excitation d-c voltage, which varies the generator output voltage.

Manual power control is achieved by either a rheostat or an autotransformer, which varies the a-c voltage to a bridge rectifier circuit. The smaller generators use this to control the field windings directly. Larger motor-generator sets utilize a small d-c motor-generator set, which is also used as a voltage regulator control.

Temperature control is basically the use of a temperature controller with auxiliary contacts. This controller is similar to the type described in the semiconductor control in Chap. 5. The controller is used to switch off the machine-frequency line contactor at the end of the heating cycle when the required temperature has been reached. Temperature measurements are usually made with radiation-type pyrometers focused on the work. It is not usual to pulse power because of limitations on the high-current contactors.

Protective circuits are mainly used in connection with cooling, generator overloads, and grounding. If the air or water temperature is too high, or the flow too low, the flow and temperature switches open up the main breaker, removing the main driving motor and exciter driving motor from the line. Similarly, if the generator current or field current exceeds the rated value by about 15 per cent, the main breaker or starter is opened. Any resistance of less than about 50 ohms to ground from the generator terminals operates a grounding device. This usually opens the generator-line contactor and removes the field excitation.

6-5. MEASUREMENTS AT MACHINE FREQUENCIES

Nearly all machine-frequency equipment includes instruments for measuring the following variables:

Generator terminal voltage
Generator line current
Generator power output at terminals
Generator power factor or $KVAR$
Field-excitation current

A typical metering system is shown in Fig. 6-15. The voltage is stepped down to one-fourth the terminal voltage by potential transformers. These are shown as T_1 and T_3, and are always fused because of possible meter faults.

Most instruments, except rectifier-type voltmeters, are designed for a specific frequency. Ammeters are of the repulsion iron type, and voltmeters are usually supplied with direct current from a rectifier.

Current transformers, of the iron-cored toroidal type, are used to step line currents down to 5 amp maximum value. These should always be short-circuited when the meters are removed to prevent damage by a switch, such as S_1.

Watts and $KVAR$ or power factor are measured by the utilization of both current and voltage from the two transformers T_1 and T_2. The instruments used are of the standard dynameter type and are represented as W

and VAR on Fig. 6-15. Current practice is to present the variables of voltage, current, power, and $KVAR$ as percentages of the full-load figures. This enables one pair of instruments to be used for a range of different generator power ratings.

Field current is simply the d-c energizing current to the field windings, supplied either by a rectifier or by the exciter motor generator.

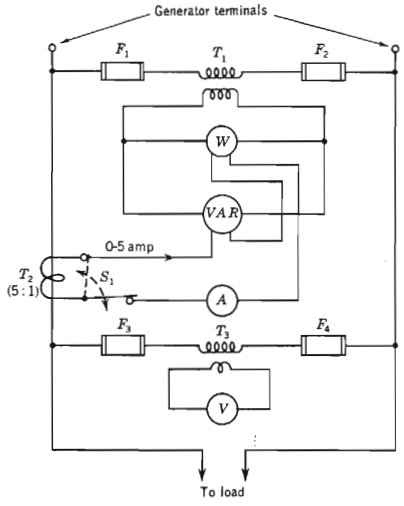

FIG. 6-15. Typical motor-generator metering system.

Most induction heating steel loads are heated in coils which result in flux densities many times those of saturation. Therefore the current waveforms from motor-generator sets are not sinusoidal, but are distorted, with peaks resulting from the drop in impedance at saturation point in the voltage cycle. It is for this reason that all current measurements should be treated with caution.

Any leads to low power-control circuits or temperature-controlling instruments should always be twisted if they run near sources of machine-frequency current. Open loops can easily act as pickup coils, as the magnetic fields near machine-frequency transmission lines, coils, and transformers

are always of high intensity. Temperature controllers should be fitted with filters for the appropriate frequency. These not only protect the instrument but prevent spurious readings.

Current transformers are checked and their characteristics measured using conventional methods. The resistive winding losses are determined by short-circuiting the secondary turns. The water flow and temperature rise in both primary and secondary turns are used to check losses. The open-circuit current determines the excitation and core loss. The core loss is determined by the flow and temperature rise of the water cooling the core.

The calorimetric use of water flow and temperature rise is used extensively to check most of the sources of power losses. Water-cooled capacitors and busbars, as well as coils, can be quite accurately checked for losses. Cylindrical water loads are used to determine loading powers in the same way as in high-frequency power measurements.

6-6. OUTPUT, CONTROL, AND WORK-HANDLING STATIONS

Motor-generator systems usually incorporate three basic groups of controls.

One group contains all the control instruments, indicator lights, protective devices, generator metering, switch gear, and regulators necessary for the motor generator itself. The motor starter and its associated control circuits are usually included in this group.

The second group contains the medium-frequency output controls, such as switch gear, push buttons and lights, capacitors and transformers, protective devices, temperature-measurement instruments (if used), and water control. In the majority of systems the motor generator is located remotely from the application, so that the machine-frequency power at the control station is often metered. Alternatively, the generator-output meters are duplicated in the control station.

The third group contains the work-handling controls. As most systems are automatic or semiautomatic, this group includes timers, limit switches and relays, push buttons and indicator lights, drive motors, water and quench-oil controls.

These groups are nearly always mutually interconnected, and in the case of smaller generators, they are sometimes located together in one unit. Figure 6-16 illustrates such a combination. This is a dual-station installation with two outputs. These can be supplied with transformers for low-impedance coils, or directly connected to the generator output. Power-factor capacitors are also mounted in the top cabinets or work stations. A sink for quenching is built into the top of the main work cabinet, and work-handling mechanisms can be built into this. Water or oil supplies are

usually integral with this type of unit, and various timing circuits are available for work-handling control.

Motor-generator sets up to about 250-kw output power often include the generator controls mounted on the motor generator itself. In this type of packaged control, the unit is complete and requires no extra control circuit, apart from that associated with an output station. The set can be operated

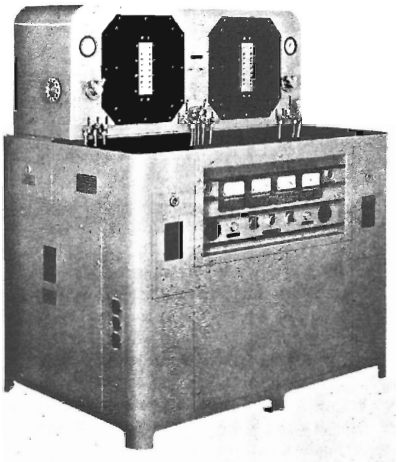

FIG. 6-16. Combined motor-generator set, control circuit, and output station. (*The Ohio Crankshaft Corp.*)

from these controls. A small motor generator at the rear provides field excitation and voltage regulation. The cubicle also contains instrument current and voltage transformers, fuses, supply-line contactor, ground detector, and surge protector unit. This is the complete group of motor-generator set controls.

When the motor-generator set is relatively close to the application or is remotely located but does not require direct control, a remote control panel usually contains the necessary control. A generator line contactor is included so that power can be switched to the remote work station. Meters, meter transformers, push buttons, indicator lights, fuses, and voltage control rheostat are also mounted in the cubicle.

The second group of controls is usually housed, as an output or heating station, in a cubicle located adjacent to the application. It provides the link between the motor-generator controls and the coil and work-handling controls. Figure 6-17 shows the interior of a typical output station. The water-cooled capacitors, shown at the bottom of the cubicle, are linked by water-cooled busbars to the output terminals. The coil current is mainly

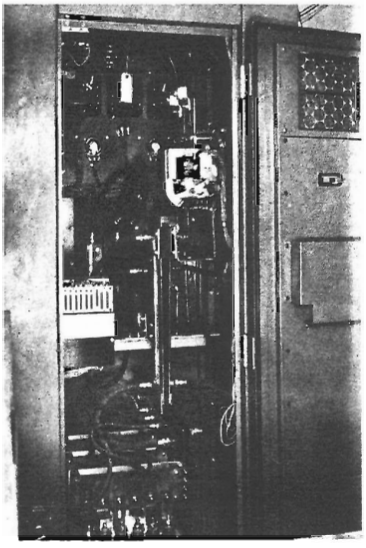

FIG. 6-17. Interior of output station. (*Westinghouse Electric Corp.*)

reactive and is several times the input-line current. The input leads, shown entering the cubicle roof, are connected to the load contactor mounted on the right-hand side. The instruments and their transformers are shown at the top, and an auxiliary timer is added for work-handling control. The cubicle also contains auxiliary contactors, control transformers, rheostats, push buttons, etc. Provision can be made for machine-frequency transformers in this type of station. Figure 6-17*A* shows a portable station.

Work-handling equipment is usually built in cubicle form and always

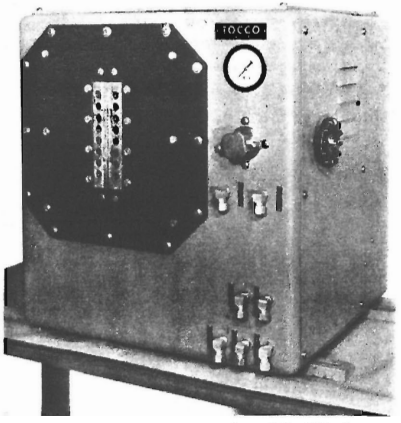

FIG. 6-17*A*. Small portable heating station. (*The Ohio Crankshaft Corp.*)

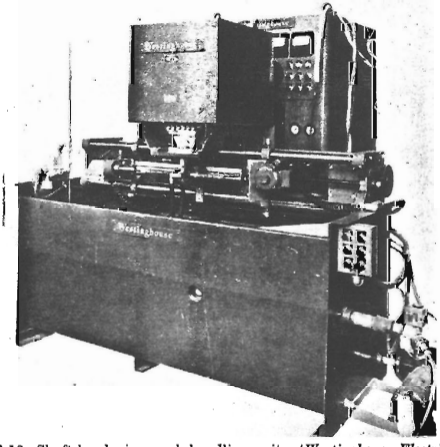

FIG. 6-18. Shaft-hardening work-handling unit. (*Westinghouse Electric Corp.*)

contains a push-button box for initiating or changing the application cycle. Certain applications which occur very frequently in machine-frequency heating, such as scanning, hardening, and billet heating, are usually carried out on standard equipment. A shaft-hardening unit is shown in Fig. 6-18. In this case the transformer is built into the unit, and the power is supplied from the output station illustrated in Fig. 6-17. A variable-speed drive controls the scanning speed, and a fixed-speed motor rotates the shaft.

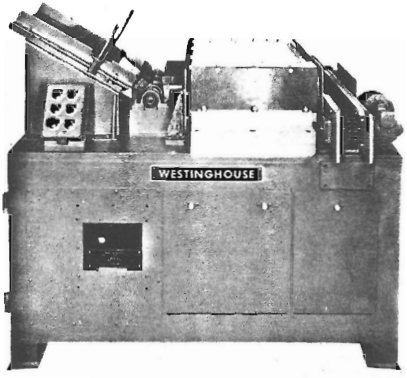

FIG. 6-19. Billet-heating work-handling equipment with controls and capacitors. (*Westinghouse Electric Corp.*)

Multicontact timers enable a complete program of events to be cycled. These include heating and quenching operations for both continuous and intermittent heating. The flexibility in these standard units enables a wide range of shaft diameters, lengths, and shapes to be heat-treated. It is also possible to utilize r-f power from an r-f generator where required.

Several machine-frequency work-handling units with the appropriate controls are illustrated in Chap. 3. In many cases where the weight and nature of the work necessitate large equipment dimensions, the correction capacitors are located in the equipment itself. This is particularly noted in high-impedance billet-heating coils, such as those used in the heaters shown in Figs. 3-1, 3-2, and 6-19.

6-7. COMPLETE SYSTEMS

The combinations of motor generators, motor-generator controls, output stations, work-handling units, and auxiliary equipments are varied and numerous. Unlike r-f generators, which contain most of the r-f system

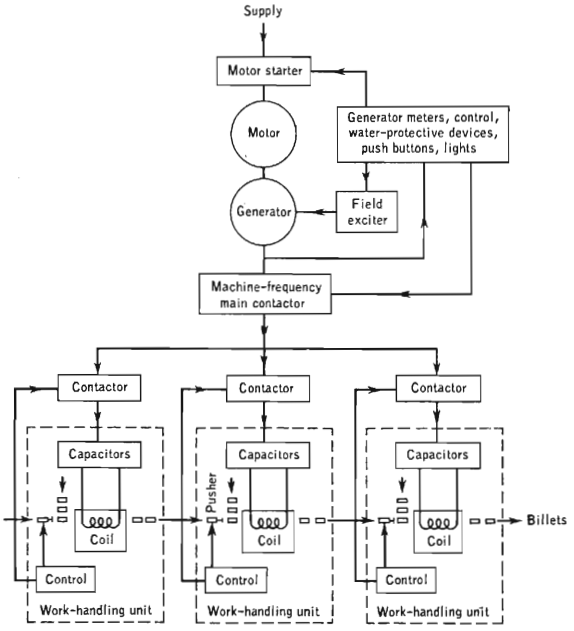

FIG. 6-20. Three-station forging system.

inside the one cubicle, motor-generator-system components are nearly always separate. It is also common practice to supply several output stations or work-handling equipments from one or more generators. This permits the system to grow with the whole plant as the production requirements increase.

A typical forging system is outlined in Fig. 6-20. The motor-generator

set is rated at 1,250 kw, 3,000 cycles, 800 volts output, the motor being a 1,950 horsepower induction unit. The set is of the totally enclosed hydrogen-cooled type shown in Fig. 6-8. It is 86 per cent efficient at full load and requires 2.5-kw excitation power and 70 gpm of water cooling. The output is switched by the main contactor suitable for the maximum current of

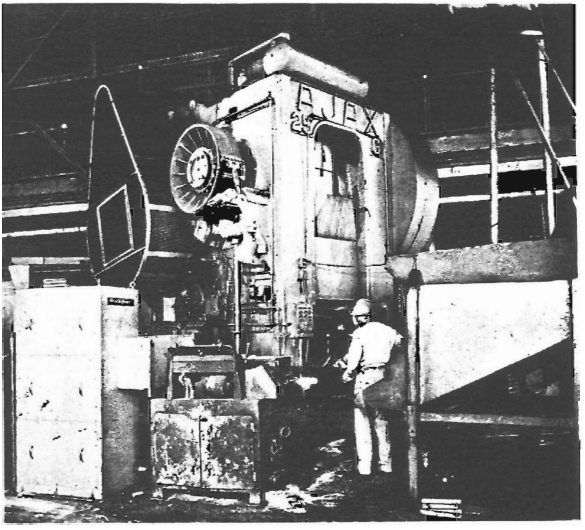

FIG. 6-21. Work-handling unit and contactor from system in Fig. 6-20. (*Westinghouse Electric Corp.*)

1,565 amp. This in turn feeds the main busbar, from which the three work-handling stations are fed via separate smaller contactors. The station, similar to that shown in Fig. 6-19, is seen, together with the contactor, in Fig. 6-21. Each station can heat 300 billets per hr, the billet sizes ranging up to $1\frac{7}{16} \times 1\frac{7}{16} \times 13$ in. long. Forging temperatures of 2250°F are reached. As each billet can weigh up to 7.8 lb, the system pounds per kilowatthour is given for each station as

$$\text{System lb/kwhr} = (7.8 \times 300)/400 = 5.85$$

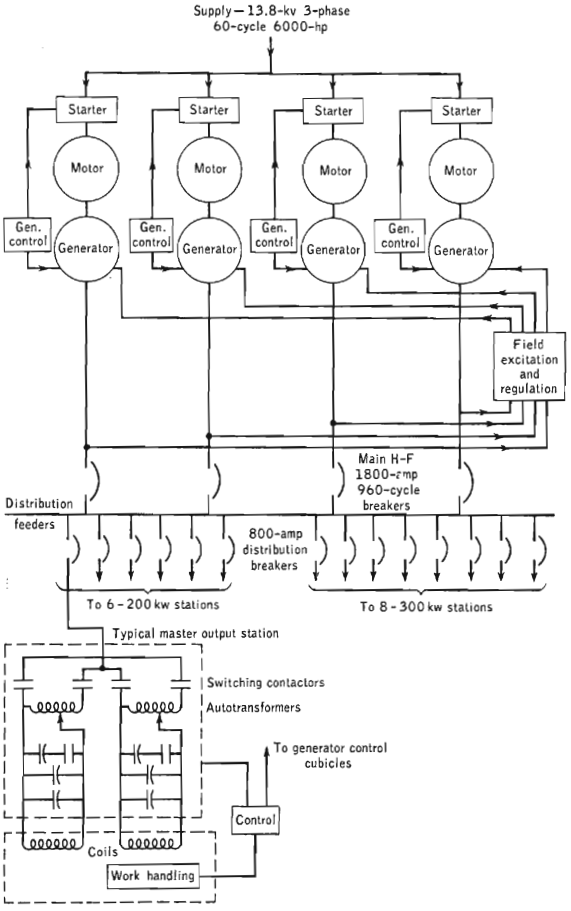

FIG. 6-22. A 5,000-kw 960-cycle system for annealing shell-nose ends.

This figure falls within the range 5 to 8 lb per kwhr expected in forging heating.

Another interesting system is shown in Fig. 6-22. This is one of the largest single induction heating systems in the world (33). The application, illustrated in Fig. 3-4, is for through-heating the nose ends of 8-in. and 155-mm shells. The power center consists of four 1,250-kw 960-cycle motor-generator sets. Three of these sets are connected in parallel to a common bus or feeder, and the fourth is on stand-by. The sets are totally enclosed and are water-cooled. Each has its own control cubicle, which contains metering indicator lights, push buttons, etc.

The output of each generator is fed via a circuit breaker to the common feeder, and this in turn feeds 14 master output stations. Six of these are 200-kw output for the 8-in. shells, and the remaining eight are 300-kw output for the 155-mm shells. Each station is protected by a breaker and contains two outputs, only one of which is used at any one time. The station is shown in Fig. 6-23; the two switching contactors are seen mounted at the top of the side panels. These are cross-connected so that power is alternated between each coil. The coils are matched to the 800-volts feeder by autotransformers, located at the bottom of the cubicle, on either side. Correction capacitors are in the center, and the capacitor switching contactors are midway up on the side panels. These contactors automatically switch in extra capacitors after the Curie point has been reached; the timers for this are mounted adjacent to the contactors.

Regulation is provided for all the generators in parallel by a master regulator and field-excitation motor-generator set. All the field windings are paralleled, but each can be individually adjusted.

The main breakers open up for a fault in the generator or main feeder to the feeder breakers. The feeder breakers are grouped into three sets, so that if one of the three generator main breakers trips, its group of feeder breakers will also trip. The stand-by generator may be brought onto the main feeder and another removed by the work-handling operator with a minimum of delay.

From these two systems it is seen that a minimum bill of material is necessary for any machine-frequency system. This is usually made up as follows:

1. Motor starter (manual or automatic, full or reduced voltage)
2. Motor-generator set (air-, water-, or hydrogen-cooled)
3. Generator control cubicle (generator- or floor-mounted)
4. Output control station [can be combined with (3)]
5. Work-handling station [can contain items in (4) and (3)]
6. Protective devices
7. Excitation supply

System efficiencies can be averaged from the individual efficiencies of the components.

1. Motor-generator set at full load: 75 to 95 per cent
2. Transformers, capacitors, busbars, and transmission lines: 90 to 95 per cent
3. Coils: 50 to 80 per cent

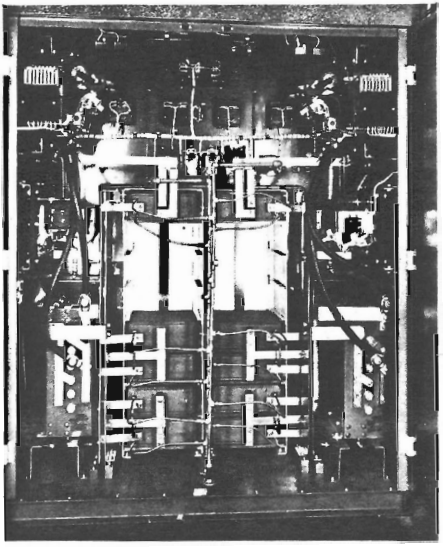

FIG. 6-23. Dual-position master output station. (*Westinghouse Electric Corp.*)

Taking the lowest and highest figures, the over-all, or system, efficiency can vary between 40 and 70 per cent. The lower value represents heating for forging systems with coils having little thermal insulation, and the higher value is for low-temperature annealing systems. A good average range is 50 to 55 per cent from supply line to thermal power in the work. This represents hardening systems.

CHAPTER 7

SUPPLY-FREQUENCY HEATING SYSTEMS

7-1. ADVANTAGES AND LIMITATIONS

The major advantage of this type of system is that there is no frequency conversion. Power losses are reduced and the system is greatly simplified by the lack of either rotating or complex electronic equipment. Maintenance is also reduced, and switchgear, correction capacitors, control circuits, etc., can be selected from standard ranges. Secondary problems, such as radiation losses, stray-field heating, and unwanted high-frequency induced currents are negligible or nonexistent. Capital cost of the equipment is less than that for either machine-frequency or r-f equipment of the same power level.

The only use of the supply frequency of 60 (or 50) cycles is for through-heating. As most application requirements in through-heating include maximum temperature uniformity, these frequencies are more suitable than the higher values, because, as seen in Chaps. 1 and 3, the greatest current penetration results from the lowest frequency [Eq. (1-1)].

The fundamental disadvantage of low-frequency heating, especially at 60 cycles, is the decrease in power input for a given work shape and coil magnetic intensity. Equation (1-67) showed that power input varied directly as frequency. This disadvantage is partly compensated by the temperature-uniformity factor, as a minimum time is required for heat to soak in from the surface. Surface-power-density figures are usually lower, but workpieces are much larger. Billet diameters often measure 10 to 12 in. or more, and lengths range up to 5 to 6 ft. Therefore coil and system power requirements are very high. A single coil may take 800 kw of power.

Because of the very high power levels involved, balanced three-phase systems are nearly always used. The coils may be either three-phase or equally loaded single-phase types in multiples of three. Owing to the interphase effects described in Sec. 4-7, the three-phase coil results in some degree of temperature unevenness. In general, most nonferrous through-heating is carried out on single-coil heaters of the type shown in Figs. 3-6 and 3-7. These are therefore three-phase coils, which present a reasonably

balanced load provided the coil is filled with billets. If the coil is only partly filled, one phase becomes out of balance. For this reason it is better to avoid a neutral wire in the supply line, which could carry an excessive current.

Most steel-heating systems utilize a continuous flow of work through one or more lines of coils. Often the higher temperatures are obtained by

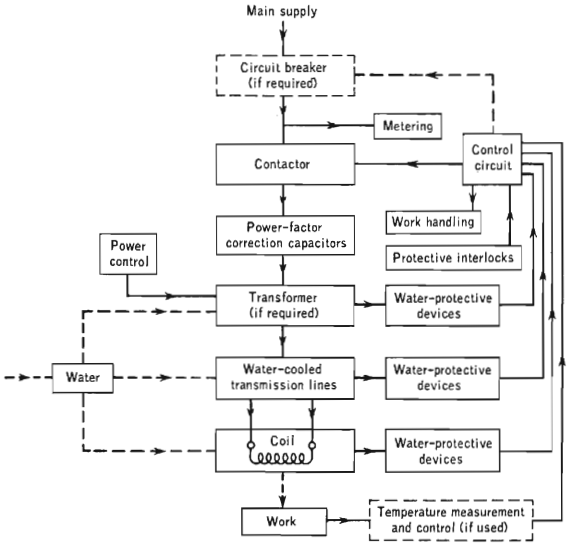

FIG. 7-1. Basic supply-frequency system.

machine-frequency coils, and usually the number of coils is such that each can be single-phase. This enables a well-balanced three-phase load to be presented to the supply.

Figure 7-1 illustrates the major components of a typical supply-frequency system (54). The transformers are usually included for matching low-impedance, low-voltage coils to high-voltage supplies. It is usual for several primary taps to be incorporated both for a variety of coils and for power control. This is the only control available in supply-frequency systems, apart from varying the rate of work throughput and switching or pulsing

the power via temperature control. It is usually utilized in nonferrous, single-shot heating, where the loads vary considerably. Off-load tap changing is necessary, as the currents and voltages involved preclude on-load changing.

As most ferrous heating coils are operated from low-voltage supplies, such as 440 volts, transformers can often be dispensed with. In these installations, the only form of control is time, via the speed of throughput.

Although limited power control is a disadvantage in these systems, it is not so important as in higher-frequency systems, because of the time factor, which is usually much greater at the lower frequencies.

7-2. LOAD MATCHING

Most coils at 60 cycles have relatively high power factors, because of the low frequency. Values usually range from 35 (nonferrous) to 60 per cent (magnetic steel). Impedance and voltage values are often comparable to those of the supply, in the case of steel heating to Curie point. Standard 440-volt, air-cooled capacitors are used.

High-voltage supplies (2,400 and 4,100 volts) are most commonly utilized for nonferrous heaters. As coils at these voltages would require an excessive number of turns and would present formidable insulating problems, transformers are always used. Power-factor correction capacitors are of the standard type, similar to low-voltage capacitors. Chlorinated diphenyl or similar dielectric mediums are used. The electrodes are aluminum foil, separated by impregnated paper. Ratings for each capacitor usually vary between 15 and 50 kvar.

In smaller systems, the individual capacitors are mounted in the work-handling and coil cubicle. Larger systems utilize separate capacitor racks. One such system has a 2,700-kvar rack, which contains a compartment suitable for mounting a circuit breaker, as well as facilities for metering and controlling the breaker. Each capacitor unit is individually fused to the busbars. Safety devices usually include a short-circuit grounding switch. This shorts the main power bus to ground when the compartment door is opened. The doors are also interlocked so that they cannot be opened except by using a special master key. This is obtainable only by removing it from the main breaker, when the breaker is tripped and locked in the open position.

It is also possible to switch in extra capacitors for loads with varying power factors. This is usually accomplished by using the increase in current, and can be used for steel heating. The increased current after Curie point is sufficient to act as a control signal to operate the breaker coil.

Power-control and matching transformers are usually similar to welding

transformers. Current and KVA values are high, and the secondary turns are generally water-cooled. Dry-type distribution transformers are occasionally used for high-power installations, where space is not an important factor.

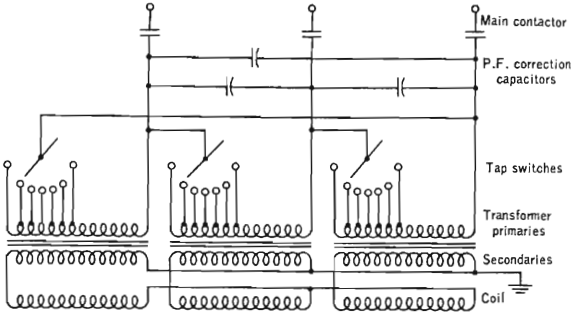

(*a*) Single primary tap-changing system

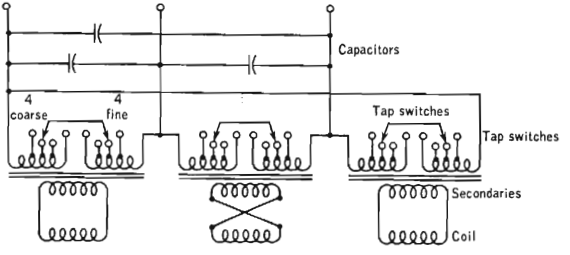

(*b*) Coarse-and-fine tap-changing system

FIG. 7-2. Transformer power-control systems.

In most nonferrous heating systems, it is desirable to keep the volume of the equipment to a minimum. Also coil currents tend to be higher than in ferrous systems. Welding-type transformers, mounted directly below the coil, are utilized. This ensures minimum coil leads and lead losses. The secondary windings are fabricated from solid copper-bar stock, water-cooled

by copper tube brazed on the outer edges. Currents may rise to 10,000 or 15,000 amp, when only water cooling could remove the resistive losses.

The primary windings are of the pancake type, built up of copper strip. Tapping arrangements depend on the requirements. One alternative is shown in Fig. 7-2*a* (20). Each primary winding has seven taps, which can provide seven secondary voltages. The coil can be energized with different combinations of these voltages on each phase. A second method involves transformers having two sets of primary windings. One set is tapped with four coarse taps, and the other with four fine taps. Used in combination with two off-load tap switches connected as shown, 16 different secondary voltages are available on each phase.

Owing to the high currents and flux densities employed, contact thermostats are usually fitted to the secondary turns. These thermostats open if the temperature becomes excessive, opening the main contactor. As most billet heaters are of the type shown in Fig. 3-6, with coils mounted above the transformers, extra precautions have to be taken against damage to the insulation by water. Secondary and primary turns are potted and drip-proof covers added.

7-3. CONTROL AND SWITCHGEAR

Control and switching of supply-frequency systems is inevitably simpler than in higher-frequency circuits. The lack of generators and their associated control and protective circuits is the main reason, but transmission lines, switchgear, metering, etc., all provide a basically simple system.

Where impulse switching is used for power control, motor-starter-type contactors are utilized. A 400-amp 4,160-volt air-break type is shown in Fig. 7-3. For some small nonferrous billet-heating systems, this contactor is mounted in the heater cubicle. Generally, a separate contactor cubicle is provided, often remotely located from the rest of the system.

In most ferrous heating systems, with large production rates, power is not impulse-switched and the main circuit switch is a breaker. Circuit faults are not common in supply-frequency systems, but occasionally a coil breakdown will occur. The usual line-fault protection is incorporated in switchgear. Current limiting fuses in the contactor cubicle give short-circuit protection but allow sustained overloads. Sustained overload protection is provided by thermal switches in the cooling circuits or thermostats on the transformers and coils. Current transformers can be used to provide a step-down signal to open the contactor coil.

As the power levels are very high in many systems, continuous power control using saturable reactors, thyratrons, or autotransformers is uneconomical. Heating cycles are relatively long, and temperature-controlled

impulse power switching is often used. A typical temperature-control panel is shown in Fig. 7-4. The strip chart recorder-controller receives a millivolt signal from the temperature-sensing element. This is usually a twin-prod, chromel-alumel thermocouple embedded in either the side or the end of the billet. Figure 4-20 illustrates a thermocouple in contact with the billet through the side of a coil. Two temperature levels are selected and preset

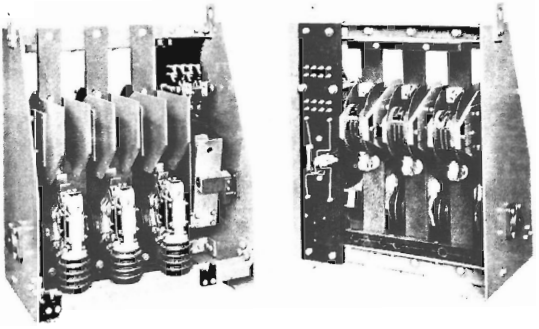

FIG. 7-3. Air-break high-voltage 60-cycle contactor. (*E.C. and M. Co.*)

on the recorder-controller. As the billet is heated and the temperature rises these two positions are passed. Two mercury-switch contacts close at each position, the second contact opening the operating-coil circuit in the main contactor. The contactor opens, shutting off power and allowing the temperature to fall. When the temperature reaches the lower setting, the contactor is switched on and power is restored. This cycling process maintains the billet at a mean temperature until it is required for the extrusion operation. On the panel shown in Fig. 7-4, a small auxiliary controller was added. This was used to monitor the billet after it had left the heater but before it was loaded into the extrusion press. By adding a set of remote-control buttons for the heater, it was possible to convert the panel to a complete control unit, which could be located in the best operating position.

In the case of steel heating for annealing, by the single-shot process, the sensing element is usually a radiation pyrometer. Two types of radiation pyrometer commonly used for temperatures up to 3500°F utilize sensitive

thermopiles which result in small voltages proportional to the temperature. In fully automatic forging induction heating, the production rate is the sole determining factor in the temperature of the billets. Radiation temperature is utilized as a check to reject billets below the required level. The radiation pyrometers shown at the end of the heating line in Fig. 3-1 are used in this way.

An interesting possibility is that of differential temperature control. Chapter 2 emphasized the importance of temperature distribution in billet heating, and in particular the factors in surface-to-center temperature differentials.

Two sensing elements, such as prod thermocouples, can be embedded in the end of a billet, one at the outer surface and one at a point near the center. The difference between the two millivoltage signals can be used to shut off power if the differential signal exceeds a certain minimum amount. This means that if the heating rate is too fast and the surface temperature is likely to melt or burn the metal, the excessive differential will cause power to pulse on and off. During the off periods the differential will tend to equalize, and the over-all billet temperature rises over the heating part of the cycle. Although this method has not yet gained wide acceptance, it promises to provide a much closer control over the heating and metallurgical effects of induction through-heating.

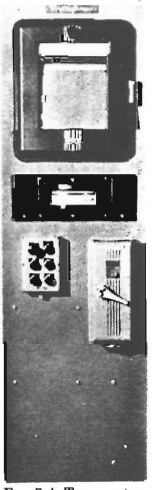

FIG. 7-4. Temperature-control panel for nonferrous 60-cycle heating. (*Westinghouse Electric Corp.*)

7-4. MEASUREMENTS AT SUPPLY FREQUENCY

Monitoring is usually limited to the current, voltage, power, and power factor of the incoming supply. Instruments used are of the standard 60-cycle type, and a high degree of accuracy is not considered necessary. Five per cent full-scale accuracy is generally sufficient for most systems.

In many nonferrous-billets heater systems, measurements are not considered necessary at all, as the temperature-control equipment determines whether the heating rate is sufficient.

Occasional coil-current measurements are made in order to prevent excessive currents and unbalancing in the phases. Clip-on ammeters are useful for these checks.

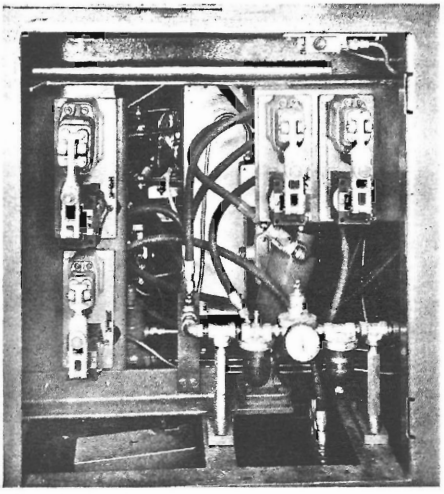

FIG. 7-5. Solenoid-operated air valves in a 60-cycle billet heater. (*Westinghouse Electric Corp.*)

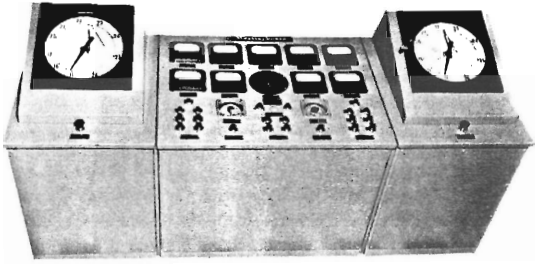

FIG. 7-6. Operator's control pulpit for a large-scale 60-cycle ferrous heating installation. (*Westinghouse Electric Corp.*)

7-5. BILLET HEATERS AND WORK-HANDLING EQUIPMENT

Various work-handling equipments and billet heaters were shown in Figs. 3-1 and 3-4 to 3-7. The work-handling part of supply-frequency systems is nearly always simple but rugged. Feed-through mechanisms are generally of the pneumatic or hydraulic type, and the work is pushed through the coils in a horizontal plane. In some instances, the work is raised and lowered in and out of the coil, as in Fig. 3-4.

Pusher mechanisms are shown on the large aluminum billet heaters in Fig. 3-7. These have to overcome the considerable friction of the wear plates and accumulated metal shavings, as well as the weight of the billet. Three- or four-in.-bore air cylinders, supplied with air at pressures of 80 to 100 psi, are most commonly used. Adjustable restrictions in the air paths provide a speed control on the pusher rod. Heavy-duty, solenoid-operated air valves are utilized to provide electrical control; Fig. 7-5 illustrates these valves used in the heater shown in Fig. 3-6. An oil filter and air-pressure gauge are also included for cleaning and metering the air supply.

In large ferrous heating installations the work-handling mechanism is controlled from an operator's pulpit. This contains all push buttons and lights controlling and metering the process, as well as meters, timers, etc. Figure 7-6 shows the control pulpit used for the system in Fig. 3-1; it contains, in addition, temperature indicators monitoring the output temperature. As this system was powered by both 60- and 960-cycle supplies, the pulpit contains controls for both frequencies.

Outfeed mechanisms depend on the further processing of the billets. Roller mechanisms are usual for the large, nonferrous billets. The smaller steel billets are often moved on conveyor belts.

7-6. COMPLETE SYSTEM

The selection of the parts of a supply-frequency system can often be directly guided by the heating requirements. In r-f and machine-frequency systems, available generators often dictate the selection, but at 60 cycles the exact power can be calculated to close approximations. Also, the fact that in through-heating the power in to the work can be closely estimated helps determine the over-all power. Coil losses can be theoretically calculated, and losses in the remainder of the system are usually small.

The best way to illustrate the system design is to relate the theoretical calculations of a coil with selection of components.

Example 7-1

Design coils based on the application requirements shown on page 246.

Requirements	Aluminum	Steel (0.44C)
Temperature range, θ_o–θ, °F	70–950	70–1400
Temperature rise, $\Delta\theta$, °F	880	1330
Production rate, lb per hr	5,000	1,900
Maximum surface-to-center temperature differential, θ_s–θ_c, °F	100	200
Mass per billet, M, lb	55	5.28
Length per billet, l'_w, in.	20	3.75
Diameter of billet, d_w, in.	6	2.5
Radius of billet, a, in.	3	1.25
Metal density, γ, lb per cu in.	0.097	0.283

The coil requirements can now be calculated in some detail, using the methods and examples described in Chaps. 1, 2, and 4.

Requirements	Aluminum	Steel (0.44C)
Average resistivity over $\Delta\theta$, ρ_w, microhm-cm	5.45 (Fig. 2-3)	54 (Fig. 2-2)
Pounds per kilowatthour over $\Delta\theta$, lb per kwhr	16.2 (Fig. 2-8)	16 (Appendix)
Thermal conductivity over $\Delta\theta$, k_c, cal cm^{-1} sec^{-1} $°C^{-1}$	0.38	0.11 (Fig. 2-4)
Surface radiation loss in coil, P_r, watts per sq in.	6	20
Thermal power, P_t, kw	308.6 (Eq. 2-3a)	120 (Eq. 2-3a)
Specific heat, s cal gm^{-1} sec^{-1} $°C^{-1}$	0.247 (Appendix)	0.16 (Appendix)
Assumed ratio of net to total power-input density, P_n/P_a	0.9	0.9
Assumed power-density input for steel, P_a, watts per sq in.	...	500
Permeability, μ_w	1.0	13 (Fig. 1-9)
Current depth, δ_w, in.	0.6 (Fig. 2-1a)	0.55 (Fig. 2-1a)
Ratio a/δ_w	5.0	2.27
Radiation correction factor $F(P_a/P_n, k_2)$	0.75 (Fig. 2-13)	0.51 (Fig. 2-13)
Net surface power density, P_n, watts per sq in.	200 (Eq. 4-3)	410 (Eq. 4-3)
Corrected permeability (steel), μ_w	...	15 (Fig. 1-9)
Corrected current depth (steel), δ_w, in.	...	0.5 (Fig. 2-1a)
Ratio a/δ_w (steel)	...	2.5
Corrected radiation factor, $F(P_a/P_n, k_2)$	...	0.54 (Fig. 2-13)
Corrected net surface power density, P_n, watts per sq in.	...	390 (Eq. 4-3)

Requirements	Aluminum	Steel (0.44C)
Calculated minimum surface area heated, A_s, sq in.	1,543 (Eq. 4-4)	307 (Eq. 4-4)
Calculated minimum length, l_w, in.	82 (Eq. 4-5)	39 (Eq. 4-5)
Selected work length, l_w, in.	80 (4 billets)	37.5 (10 billets)
Selected surface area heated, A_s, sq in.	1,500	295
Net surface power density, P_n, watts per sq in.	206	406
Total surface power density, P_a, watts per sq in.	$206 + 5 = 211$	$406 + 20 = 426$
Work power, P_w, kw	$(211)(1{,}500 \times 10^{-3}) = 316$	$(426)(295 \times 10^{-3}) = 126$
Coil length, selected, l_c, in.	$80 + 2 = 82$	37.5
Coil diameter, selected, d_c, in.	$6 + 1 = 7$	$2.5 + 1.5 = 4.0$
Billets per hour	$5{,}000/(4 \times 55) = 22.5$	$1{,}900/(10 \times 5.28) = 36$
Time per billet in coil, min	$60/22.5 = 2.67$	$60/36 = 1.67$

The coil itself can now be calculated. Steel heating below Curie is usually carried out in a two- or three-layer coil, because of the greater power-loading capabilities of magnetic material. The line voltage is used in this case. For aluminum, a single-layer coil has to be used to minimize coil losses. A coil wound of the minimum practical number of turns consistent with transformer voltages is used.

The coil is designed using the approximate method described in Sec. 4-4. Efficiency, power factor, and impedance in Chap. 4 are used. Values are approximated from the nearest lengths, permeabilities, etc.

Requirements	Aluminum	Steel
Coil efficiency, η_c, per cent	53 (Fig. 4-5)	65 (Fig. 4-6)
Coil power factor, $\cos\phi$, per cent	42 (Fig. 4-7)	55 (Fig. 4-8)
Coil impedance per turns squared, Z'/N_c^2, ohms per turn squared	3.5×10^{-6} (Fig. 4-10)	10^{-5} (Fig. 4-9)
Coil power, P_c, kw (Eq. 4-8)	$316/0.53 = 595$	$126/0.65 = 194$
Coil kilovolt-amperes, KVA_c, kva (Eq. 4-9)	$595/0.42 = 1{,}420$	$194/0.55 = 353$
Coil volts per turn, E_c/N_c (Eq. 4-10)	$[(3.5)(10^{-6})(1{,}420)(10^3)]^{1/2} = 2.2$	$[(10^{-5})(353)(10^3)]^{1/2} = 1.88$
Coil ampere-turns, I_cN_c (Eq. 4-10)	$\left(\frac{1{,}420 \times 10^3}{3.5 \times 10^{-6}}\right)^{1/2} = 635{,}000$	$\left(\frac{353 \times 10^3}{10^{-5}}\right)^{1/2} = 188{,}000$
Coil volts, E_c, volts (approx.)	$120 \times 2.2 = 264$ (assuming 120 turns)	440 (assuming line voltage)
Coil turns, N_c (approx.)	120 (assuming $\frac{5}{8}$-in.-wide copper strip and 0.060-in. insulation)	$440/1.95 = 225$ (3 layers of 0.5-in.-diameter copper tube)
Coil current, I_c, amp	$635{,}000/120 = 5{,}300$	$188{,}000/225 = 835$
Coil copper loss, P_c, kw (Eq. 4-11)	$595 - 316 = 279$	$194 - 126 = 68$
Coil cooling water, GPM_c, gpm (Eq. 4-12)	$279/(0.147 \times 40) = 47.2$	$68/(0.147 \times 40) = 11.6$

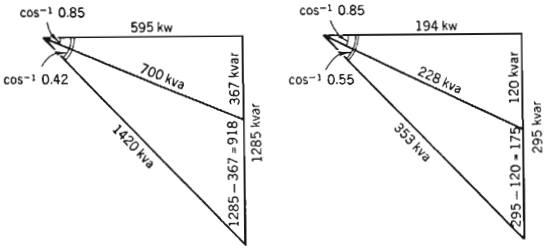

FIG. 7-7. Vector diagrams of aluminum and steel 60-cycle coils.

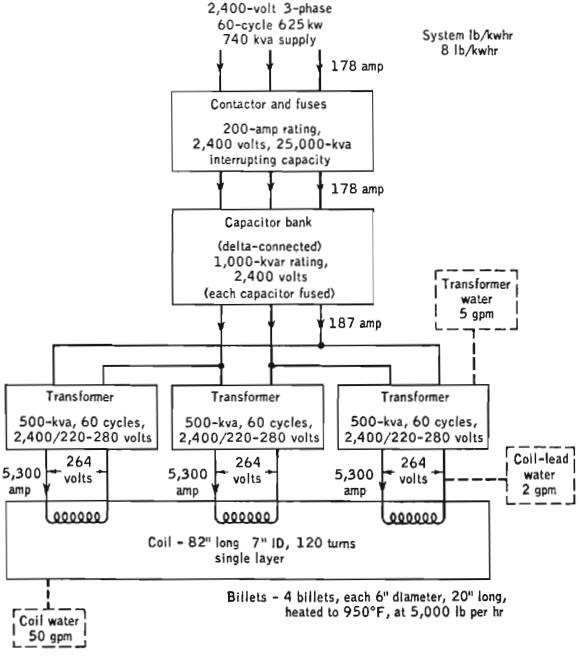

FIG. 7-8. Typical aluminum supply-frequency heating system.

The coils are constructed along the lines outlined in Sec. 4-7. Each of the two systems can be built up from the vector diagrams of Fig. 7-7. Supply-line power factors vary from 75 to 90 per cent lag, depending on the local tariffs.

Figure 7-8 shows a typical aluminum heating system designed in Example 7-1. A factor of 5 per cent has been allowed in the ratings of the contactor, capacitors, and transformers. This allows for losses in the system, mainly in the transformers and coil leads. The capacitor bank would be too large to mount on the heater unit and would be contained in a special rack.

The contactor would be uprated to 200 amp, a convenient manufacturers' rating. The fuses would depend on the interrupting capacity of the main supply breaker. A typical rating is 25,000 kva, which would deal with most fault conditions. The system is usually protected against overloading by thermal overloads in the contactor control circuit.

Transformers would be mounted inside the heater cubicle. The tap arrangement of Fig. 7-2*b* would be ideal for the required voltage range of 220 to 280. The heater would be similar to those shown in Figs. 3-6 and 3-7. The work handling depends primarily on the further processing of the billets. Other heaters of the nonferrous type are shown in Fig. 3-8.

Figure 7-9 outlines the 60-cycle section for steel heating designed above, incorporated in a dual-frequency installation. Example 4-2 gives the application specifications. One of the billet heaters is shown in Fig. 7-10. It includes both 60- and 960-cycle coils, as well as 960-cycle capacitors (22), work-handling gear, and controls. In this particular system, four heaters of this type are supplied from a 1,600-kw 60-cycle 440-volt 3-phase power supply. The 960-cycle power is supplied by four 175-kw 800-volt motor-generator sets. The 60-cycle capacitors are separately mounted in racks, and the controls are also separately located.

Final surface-to-center temperature differentials are usually between 50 and 150°F. A large differential can be tolerated in the 60-cycle section because the 960-cycle coil temperature is sufficient to nearly equalize the differential. In practice it is difficult to calculate length of the 60-cycle coil purely on temperature differential. Coils are designed as in Chap. 4, on the basis of the nonmagnetic state of steel and the final forging temperature differentials. The 60- and 960-cycle coils are usually of approximately the same length and power requirements.

Figure 3-1 shows the heater arrangement of another dual-frequency (60- and 960-cycle power) system. Here, two lines of coils are mounted on one heater. The supply-frequency coils are fed from a Scott-connected transformer, with a primary line voltage of 6,900 and two secondary voltages of 480. Each of these 480-volt lines feeds two of the four 60-cycle coils in

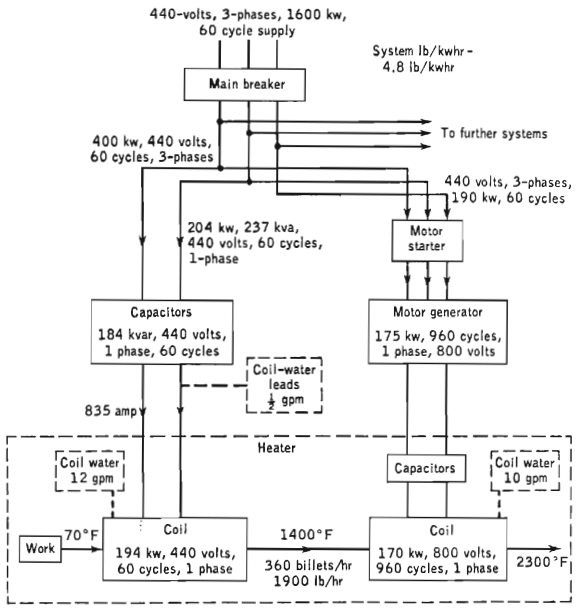

FIG. 7-9. Typical steel heating for forging dual-frequency heating system.

parallel, and a 1,000-kw 960-cycle motor-generator set supplies the four 960-cycle coils in parallel.

In general, most supply-frequency systems, or the supply-frequency section of dual-frequency systems, require the following bill of material:

1. Main breaker if system is large
2. Contactor and fuses (temperature-controlled systems)
3. Capacitor bank
4. Transformers (tapped primaries in nonferrous heating)
5. Work-handling equipment
6. Protective devices
7. Coil or coils
8. Heater cubicle (usually contains some or all of items 3, 4, 5, 6, and 7)

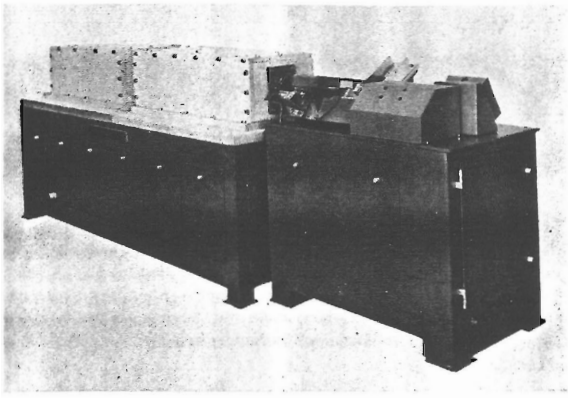

Fig. 7-10. Dual-frequency billet heater (see Fig. 7-9). (*Westinghouse Electric Corp.*)

System efficiencies vary mainly according to the metal heated and the billet diameters. The breakdown can be approximated as follows:

1. Transformer, leads, transmission lines, etc.: 90 to 95 per cent
2. Coils: 60 to 90 per cent (steel), 40 to 60 per cent (nonferrous metals)

A good over-all figure would be 70 per cent (steel to Curie point), and 45 per cent (nonferrous metals).

CHAPTER 8

AUXILIARY AND CONTROL EQUIPMENT

8-1. TRANSMISSION LINES: THEORY

The theoretical aspect of transmission lines becomes more complex as the frequency of the transmitted power increases. This is because of the decreasing wavelength, which approaches the physical dimensions of the line. At these small wavelengths or high frequencies, the characteristics of the line, based on its series resistance and inductance, and shunt capacitance and conductance, become important.

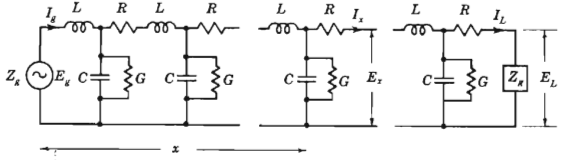

FIG. 8-1. Basic transmission line at radio frequencies.

This can be seen from the basic transmission-line equations:

$$E_x = E_L \cosh \gamma x + I_L Z_o \sinh \gamma x \tag{8-1}$$

and

$$I_x = I_L \cosh \gamma x + \frac{E_x}{Z_o} \sinh \gamma x \tag{8-2}$$

where E_x = voltage across line at x feet from termination end, volts
I_x = current through line at x feet from termination end, amp
E_L = termination-end voltage, volts
I_L = termination-end current, amp
Z_o = line characteristic impedance, ohms
γ = propagation constant

The line is represented in Fig. 8-1, with the characteristics lumped as shown. The propagation constant is given by

$$\gamma = \sqrt{(R + jwL)(G + jwC)} \tag{8-3}$$

where the constants are for unit length of line. Equation (8-3) is often written

$$\gamma = \alpha + j\beta \tag{8-4}$$

where α = attenuation constant
β = phase constant
β is given by

$$\beta = \frac{2\pi}{\lambda} = \frac{2\pi f\sqrt{k}}{984} \quad \text{radians per unit length} \tag{8-5}$$

where f = frequency, Mc
k = dielectric constant between two conductors
λ = wavelength, ft

At an induction heating frequency of 1 Mc, and assuming the dielectric is air ($k \simeq 1$), β would be

$$\beta = \frac{(2)(\pi)(1)(1)^{1/2}}{984} = 0.0064 \text{ radians per ft}$$

In a well-designed transmission line at 1 Mc the attenuation constant α, which indicates the energy dissipated in the line, is usually small compared with β. Therefore, by substituting the value of β above in Eq. (8-1), for a distance of 10 ft of transmission line,

$$\begin{aligned} E_{10} &= E_L \cosh 0.064 + I_L Z_o \sinh 0.064 \\ &= E_L 1.002 + I_L Z_o 0.064 \end{aligned}$$

The characteristic impedance Z_o is given approximately by

$$Z_o = \sqrt{\frac{L}{C}} \quad \text{ohms} \tag{8-6}$$

where L = inductance per ft of line, henrys
C = capacitance per ft of line, farads

If the line is assumed to consist of two parallel bars of 2-in. width, separated by ½ in., the inductance can be approximated as 6.5×10^{-8} henry per ft (Fig. 8-5). The capacitance is approximately 11.0×10^{-12} farad per ft. This results in a characteristic impedance of

$$Z_o = \sqrt{\frac{6.5 \times 10^{-8}}{11.0 \times 10^{-12}}} = 77 \text{ ohm}$$

Therefore the voltage at a point 10 ft from the termination of the line is

$$E_{10} = E_L 1.002 + I_L 4.9$$

A typical termination voltage might be 5,000 volts, with a line current of 100 amp. This results in

$$E_{10} = 5{,}010 + 490 = 5{,}500 \text{ volts}$$

This illustrates clearly that the effects of frequency, and of line capacitance and inductance, are relatively small at induction heating frequencies up to 1 Mc. The voltage drop is 500, which results in a KVA drop of

$$KVA_{10} = 500 \times 100/10^3 = 50 \text{ kva}$$

If the frequency is 5 Mc, β becomes

$$\beta = 5 \times 0.0064 = 0.032 \text{ radians per ft}$$

Substituting this in Eq. (8-1), together with the same line dimensions, current, and voltage as in the above example,

$$E_{10} = (5{,}000)(1.05) + (100)(47)(0.33)$$

$$= 5{,}250 + 1{,}550 = 6{,}800 \text{ volts}$$

This indicates a voltage drop of 1,800, and a KVA drop of

$$KVA_{10} = 1{,}800 \times 100/10^3 = 180 \text{ kva}$$

The theory of transmission lines, particularly at high frequencies, is complex and has been described elsewhere (86). But as KVA losses are not negligible even at 1 Mc or less, lines should be carefully designed and should be as short as possible. Maximum power-transfer efficiency is achieved by satisfying two conditions:

1. The impedance presented to the generator by the line and load should be equal in magnitude and opposite in phase to the internal impedance of the generator.
2. The load impedance at the line termination should equal the characteristic impedance of the line.

In practice, if a line is less than one-eighth of a wavelength long, a mismatch at the receiving end is not considered serious. At 1 Mc, any length of line less than 120 ft does not need termination matching devices. But at 5 Mc, this length is reduced to 25 ft, and standing waves may occur with longer lengths.

Standing waves result if the load impedance is mismatched to the characteristic impedance of the line. The impedance along the line is no longer purely resistive, and reflected waves appear. The voltage and current along the line become the sum of the forward and reflected waves. These contribute to the losses in the line and reduce the power-transfer efficiency.

The ratio of maximum to minimum voltage, or current values, along a line is known as the standing-wave ratio. Ratios of 1.1 or less result in negligible power loss, and higher ratios can often be tolerated from an efficiency consideration (86). But as high standing-wave ratio values cause corona and insulation breakdown, excessive local heating, and radiation, it is always good practice to keep them as low as possible.

(*a*) 10 kc (*b*) 3 kc (*c*) 1 kc

FIG. 8-2. Current depths in a copper conductor at 85°C.

Various matching devices can be used on lines longer than $\lambda/8$, such as variable-load coupling, quarter-wave transformers, and matching stubs. In general, however, good transmission-line design, preferably using coaxial cable, and keeping the lengths to a minimum, make these devices unnecessary at induction radio frequencies.

At machine and supply-line frequencies, the wavelengths involved are so long that most of the r-f line theory does not apply. Lines usually consist of multistranded cable, although solid rectangular busbars are sometimes used for shorter runs. Resistance and reactance are the components which most affect power transfer and kva losses.

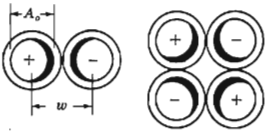

FIG. 8-3. Current distribution in grouped-conductor cable.

The effective resistance and reactance of conductors will be increased with higher frequencies owing to the skin effect. Figure 8-2, shows the actual depths of penetration in an isolated copper conductor at 85°C at different motor-generator-set frequencies. The proximity effect of one conductor or another also varies the current path and therefore the resistance and reactance. In Fig. 8-3, two and four cable groups are shown as they affect current distribution.

The resistance and reactance per unit length of two conductors are given by (87)

$$R_e = 0.354 \times 10^{-6} \frac{\rho_e}{A_o d} \frac{M_o(A_o/\sqrt{2}\,d)}{M_1(A_o/\sqrt{2}\,d)} \cos\left[\frac{3\pi}{4} - (\theta_1 - \theta_o)\right] x \times \frac{1}{\sqrt{1 - (A_o/W')^2}} \quad \text{ohms/in.} \quad (8\text{-}7)$$

where R_e = effective a-c resistance per unit length, ohms per in.
ρ_e = effective resistivity of conductor material, microhm-cm
A_o = diameter of cable, in.
M_o, M_1, θ_o, θ_1 = Bessel functions (88)
f = frequency, cps
$d = 1.98\sqrt{\rho/f}$ in. (current depth)
W' = distance between centers, in.

and

$$X_e = R_e \tan\left[\frac{3\pi}{4} - (\theta_1 - \theta_o)\right] \quad \text{ohms/in.} \quad (8\text{-}8)$$

where X_e = effective a-c reactance per unit length.

The external reactance is

$$X_o = 8\pi f\, 2.54 \times 10^{-9} \cosh^{-1} \frac{W'}{A_o} \quad \text{ohms/in.} \quad (8\text{-}9)$$

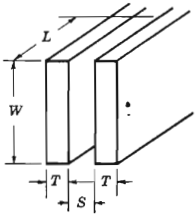

FIG. 8-4. Solid busbar transmission line for machine- and radio-frequency power.

Solid busbars of the type shown in Fig. 8-4 are sometimes used for machine-frequency power transmission. The resistance and reactance per unit length are given by (89)

$$R_1 = \frac{2\rho}{Wd} F \quad \text{ohms/in.} \quad (8\text{-}10)$$

$$X_1 = \frac{0.8\rho}{Wd} G + 0.2f \frac{S}{W} J \quad \text{microhms/in.} \quad (8\text{-}11)$$

where $d = 1.98\sqrt{\rho/f}$ in.
ρ = conductor resistivity, microhm-cm
W = height of conductor
f = frequency, cps
S = spacing between conductors, in.
F, G = functions of T/d
J = function of S/W

Equation (8-11) is plotted in Fig. 8-5 as inductance per inch.

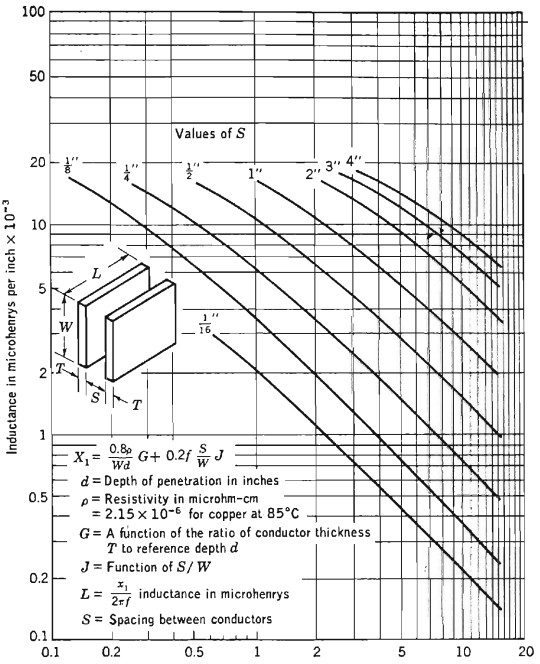

FIG. 8-5. Inductance of a parallel-bar transmission line.

8-2. PRACTICAL TRANSMISSION LINES

Practical lines can be designed on the basis of the above theory and good engineering practice.

Radio-frequency lines are usually either air-spaced parallel bars or tubes, or coaxial conductors. Figure 8-6 shows a typical r-f transmission-line system. The copper conductors should be spaced at 0.1 in. per 1,000 volts. Both conductors must be insulated from the shield by good-quality insulators, which should be ½ in. for every thousand volts.

The line drop should be no more than 500 volts. If the line is terminated in an r-f transformer as shown and the secondary grounded, the insulation should be capable of withstanding this voltage. The work station should never be separately grounded but should be well bonded to the line shielding, and this should be used as a ground to the generator.

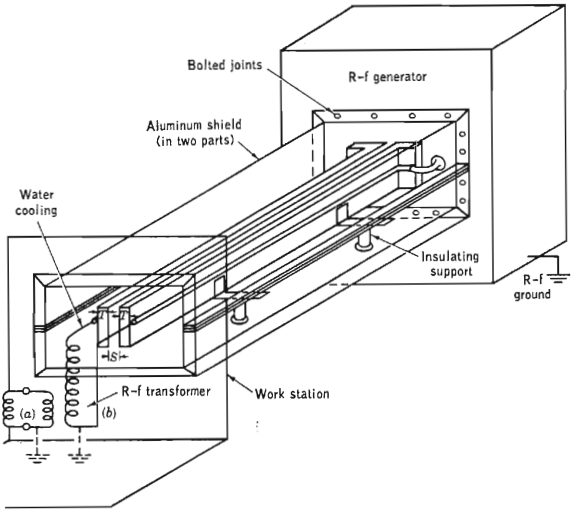

FIG. 8-6. Radio-frequency transmission-line design.

Example 8-1

Design a transmission line based on the following requirements:

Length of line, l	10 ft
Line current, I_L	200 amp
Frequency, f	450 kc
Maximum r-f voltage	6,000 volts

Assuming 500 volts maximum line drop and a negligible resistance, the maximum line reactance X_1 should be

$$X_1 = 500/200 = 2.5 \text{ ohms}$$

This results in a line inductance of

$$L = \frac{(2.5)(10^6)}{(2)(\pi)(450)(10^3)} = 0.88 \text{ microhenry}$$

As the line voltage is 6,000, allow a spacing of $\frac{3}{4}$ in. between conductors. As the line is 10 ft, the maximum inductance per inch is $0.88/120 = 7.35 \times 10^{-3}$. From Fig. 8-5, the minimum recommended width is seen to be 2.5 in.

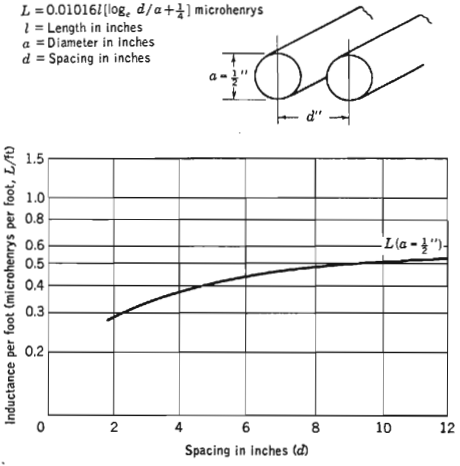

FIG. 8-7. Inductance of a primary transmission line of two parallel tubes.

The conductors should be made of copper, water-cooled and supported by 3-in. insulators. At least 1 in. should separate the line from the shield. Brass hardware must always be used, and the precautions against radiation outlined in Chap. 5 should be observed.

Figure 8-7 shows the inductance per unit length of parallel tubes.

Machine-frequency lines usually consist of two, four, or multiples of two cables. The cables are the conventional multistrand, varnished cambric, extraflexible type, suitable for copper temperatures up to 85°C. They are arranged with polarities as in Fig. 8-3, and are either side by side or spaced 1 in. apart. Most cables are between 250 and 500 circular mils.

Example 8-2

Determine the resistance, reactance, and impedance per foot length, and current-carrying capacity of the following transmission line:

Frequency of power, f ..... 10,000 cps
Cable size ..... 350,000 circular mils
No. of cables ..... 2, side by side
Resistivity of copper at 85°C, ρ ..... 2.17 microhm-cm
Distance between cable centers, W' ..... 1.07 in.

The *effective* diameter is given by converting the circular mils to inches:

$$A_e = 10^{-3}\sqrt{373{,}300} = 0.611 \text{ in.}$$

As the *actual* diameter of the stranded cable (less sheath) is $A_o = 0.80$ in., the effective resistivity is assumed to be

$$\rho_e = 2.17 \times (0.80/0.611)^2 = 3.7 \text{ microhm-cm}$$

The current depth is

$$d = 1.98\sqrt{\frac{\rho_e}{f}} = 1.98\sqrt{\frac{3.7}{10^4}} = 0.038 \text{ in.}$$

Substituting these values, together with the Bessel functions (88), into Eqs. (8-7) and (8-8), and multiplying by 12 for 1-ft length,

$$R_e = 0.354 \times 10^{-6} \frac{3.7}{0.8 \times 0.038} \times \frac{M_o(0.80/\sqrt{2} \times 0.38)}{M_1(0.80/\sqrt{2} \times 0.38)}$$

$$\times \cos\left[\frac{3\pi}{4} - (\theta_1 - \theta_o)\right] \times \frac{1}{\sqrt{1 - (0.8/1.07)^2}} \times 12$$

$$= 43 \times 10^{-6} \times 1.02 \times 0.73 \times 1.505 \times 12 = 575 \times 10^{-6} \text{ ohm/ft}$$

$$X_e = 575 \times 10^{-6} \times \tan 43.6 = 550 \times 10^{-6} \text{ ohm/ft}$$

From Eq. (8-9), the external reactance is

$$X_o = (8)(\pi)(10^4)(10^{-8})(2.54)(12) \cosh^{-1}(1.07/0.8)$$

$$= 6{,}150 \times 10^{-6} \text{ ohm/ft}$$

Therefore the impedance per foot length is

$$Z_e = \sqrt{R_e^2 + (X_e + X_o)^2} = 6{,}710 \times 10^{-6} \text{ ohm/ft}$$

Assuming a maximum power dissipation of 19.5 watts per foot, the current capacity is

$$I_L = \sqrt{\frac{W}{R_e}} = \sqrt{\frac{19.5}{575 \times 10^{-6}}} = 184 \text{ amp}$$

The following table is based on the above type of calculations. The figures are within 10 per cent of measured results (87).

TABLE 8-1. RESISTANCE, IMPEDANCE, WATTS, AND CURRENT-CARRYING CAPACITIES OF CABLE IN FREE AIR, 30°C AMBIENT, 85°C MAXIMUM COPPER TEMPERATURE (87)

Cable size, circular mils	Two cables—side by side				Four cables—similar polarities opposite			
	Watts per ft of run	Current rating, amp	Resistance, milliohms per ft	Impedance, milliohms per ft	Watts per ft of run	Current rating, amp	Resistance, milliohms per ft	Impedance, milliohms per ft
Frequency of current in line—10,000 cps								
250	17.2	162	0.655	7.57	22.2	292	0.262	3.03
350	19.5	184	0.575	6.71	25.3	332	0.230	2.69
500	21.2	208	0.480	6.41	27.1	375	0.192	2.56
Frequency of current in line—3,000 cps								
250	17.2	211	0.384	2.38	22.5	382	0.154	0.95
350	18.2	236	0.325	2.17	23.5	425	0.130	0.87
500	20.8	278	0.270	2.04	27.0	500	0.108	0.82
Frequency of current in line—1,000 cps								
250	16.9	270	0.234	0.890	22.1	487	0.093	0.356
350	18.9	305	0.203	0.816	24.6	550	0.081	0.326
500	20.6	358	0.160	0.752	26.6	645	0.064	0.301

Experimentally determined figures for parallel busbars at machine frequencies are given in Table 8-2. The results are very similar to those calculated from Eqs. (8-10) and (8-11).

TABLE 8-2. RESISTANCE REACTANCE, WATTS LOSS, AND CURRENT-CARRYING CAPACITIES OF AIR-COOLED COPPER BUSBARS AT MACHINE FREQUENCIES (89)

Width W, in.	Spacing S, in.	Watts loss per in. of run for 50°C rise	10,000 cps			3,000 cps			1,000 cps		
			Microhms per in. of run		Rated amperes	Microhms per in. of run		Rated amperes	Microhms per in. of run		Rated amperes
			R_1	X_1	I_L	R_1	X_1	I_L	R_1	X_1	I_L
2	⅛	1.81	29	88	250	16	23.8	338	9.2	15.1	444
	¼	3.45	29	415	345	16	132	466	9.2	47.8	613
	1	3.67	29	682	355	16	211	480	9.2	74.5	631
3	⅛	2.52	19.5	60	360	10.7	22.7	487	6.2	10.2	639
	¼	4.88	19.5	294	500	10.7	93	676	6.2	33.6	888
	1	5.58	19.5	501	535	10.7	155	723	6.2	54	950
4	⅛	3.44	14.6	45	485	8.0	17.2	655	4.6	7.7	861
	¼	5.72	14.6	229	625	8.0	72	844	4.6	26	1,110
	1	7.37	14.6	401	710	8.0	124	960	4.6	43	1,260
6	⅛	4.42	9.7	37.5	675	5.3	13.6	913	3.1	5.9	1,200
	¼	6.82	9.7	159	840	5.3	50	1,200	3.1	18.0	1,490
	1	9.30	9.7	284	980	5.3	88	1,410	3.1	30.5	1,740
8	⅛	5.41	7.3	22.9	860	4.0	8.7	1,160	2.3	3.9	1,530
	¼	8.20	7.3	121	1,060	4.0	38.2	1,430	2.3	13.7	1,880
	1	10.7	7.3	221	1,210	4.0	68	1,630	2.3	23.7	2,150

In general, these values apply when the thickness of the busbar is at least $\frac{1}{8}$ in.

Summarizing machine-frequency cables and busbars, the following practices should be carried out in good designs:

1. Standard stranded cable can be used at machine frequencies, with reduced ratings.
2. The best arrangement for cables is four conductors with staggered polarities.
3. Contact between strands varies current-carrying capacities of cables.
4. Calculated and experimental values of characteristics for cable and busbar agree closely.
5. The thickness of busbars should be at least $1.2\,d$, where d is the current depth.
6. Maximum current can be carried in busbars when the width is vertical, the spacing greater than $\frac{1}{4}$ of the width, and the bars painted black.
7. Water cooling can increase the current-carrying capacities of cable and busbars.
8. Spacing between bars should be approximately $\frac{1}{2}$ in. for 440- or 220-volt lines, and $\frac{3}{4}$ in. for 800-volt lines.

8-3. R-F TRANSFER SWITCHES

Many applications of r-f power require the maximum use of the generator. One of the best ways to achieve this is by using two work positions with one generator, and transferring power by an r-f switch.

Figures 8-8 and 8-9 illustrate a 400-amp switch designed for 500-kc operation at up to 8,000 volts. The main features of these switches are heavy contacts, with water cooling, rugged construction, and large solenoids. These solenoids pull the contact arm through a small arc (approximately 15°), and interlocks remove r-f power during switching.

The switches can usually be bolted to the face of the generator over the output terminals. Auxiliary circuits can be interconnected with external work-handling equipment.

8-4. NEW SOURCES OF INDUCTION HEATING POWER

The inherent disadvantages and maintenance problems of rotary and r-f generators have led to experiments with several alternative sources of power.

One type of frequency converter is that using mercury-arc rectifiers. Experimental work has been carried out over a number of years (90); a recent installation appears to have good practical possibilities (91).

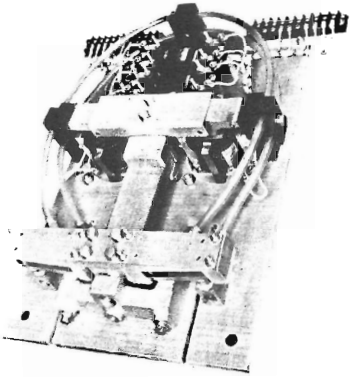

FIG. 8-8. A 400-amp r-f transfer switch. (*Westinghouse Electric Corp.*)

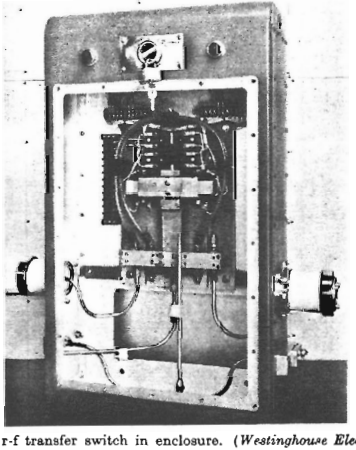

FIG. 8-9. A r-f transfer switch in enclosure. (*Westinghouse Electric Corp.*)

The advantages of the inverter are that it is more efficient than a motor-generator set, it is static, and its output frequency may be varied. The major drawbacks are the difficulty of obtaining suitable rectifier tubes, the design of control circuits, and starting conditions.

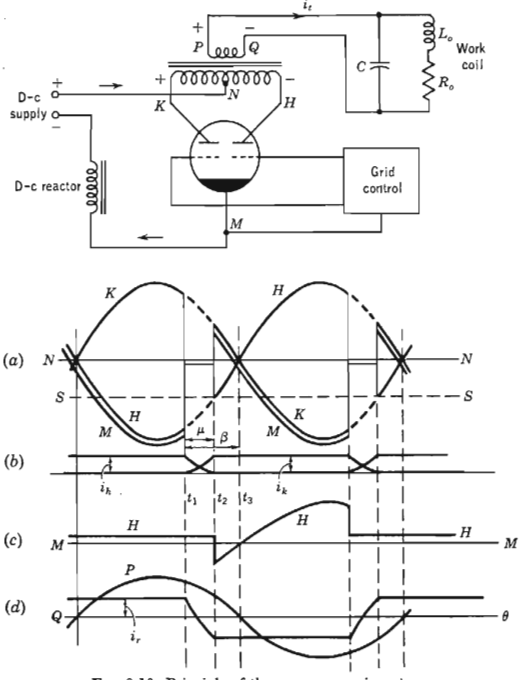

FIG. 8-10. Principle of the mercury-arc inverter.

Figure 8-10 shows the basic principles of the inverter: (*a*) curves of the plate and cathode voltage with respect to the neutral N; (*b*) plate currents; (*c*) plate-to-cathode potential of one plate; (*d*) output voltage and current.

The circuit is shown with H firing first, producing a plate current i_h and a positive half-cycle of output voltage across the transformer secondary. Grid control prevents plate K from firing until time t_1, when the current

commutes from plate H to plate K in the phase angle time of t_2. This assumes that a sinusoidal voltage is maintained by the tuned load circuit. After t_2, all the current is taken by K in the form of i_k. The output voltage and current swing in the opposite direction, because of the winding arrangement of the transformer.

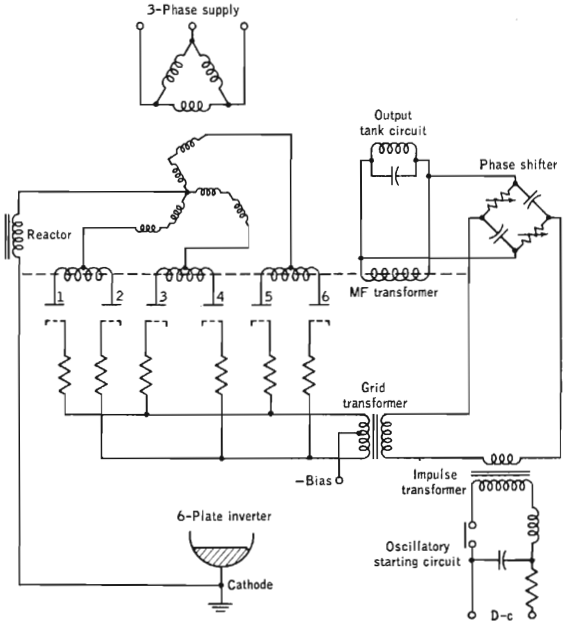

FIG. 8-11. Medium-frequency cycloinverter.

The output voltage QP varies in proportion to the d-c input voltage, with a fixed firing angle and load impedance. Alternatively the firing angle can be varied to give different output voltages. The ripple voltage MS is absorbed by the d-c reactor.

Practical inverters usually consist of a large three-phase, full-wave, grid-controlled mercury-pool rectifier fed directly from a three-phase supply.

The grids are self-excited from the output circuit. This circuit, known as a cycloinverter, is shown in Fig. 8-11. The average output voltage can be controlled by the use of a phase shifter in the same way as in thyratron operation. The reactor is again used to suppress the third harmonic ripple current.

Starting problems are generally overcome by arranging the grid control circuit to provide an early firing angle β during the first few cycles. This prevents inverter action, and the first two plates (1 and 2 in Fig. 8-11) carry both currents in parallel. The reactor prevents this current from rising to full load. The next pair of plates takes over the current and after this the action is normal.

Figure 8-10*d* shows that the output current is an approximate square wave. This means that the inverter works at a slightly higher frequency than the tuned output circuit. Increasing the firing angle β increases the output-circuit frequency. Also the harmonic content of this current increases the capacitor rms current. In general, the capacitor requirements can be calculated on the basis of a sinusoidal voltage, with little inaccuracy.

At full power output, inverter efficiencies may be as high as 85 per cent. Frequencies vary between 1 and 1.5 kc.

8-5. MAGNETIC MULTIPLIERS

Reference has already been made to frequency triplers. The principle of the magnetic multiplier is based on the summation of pulses obtained from saturable reactors (92). Figure 8-12 shows the waveforms resulting from a tripler. Each phase voltage is applied to its own reactor and the load in series. As explained in Chap. 5, the reactor drops nearly all the voltage until it saturates at the critical or firing angle θ_f. By adding the pulses produced in this way, a 60-cycle supply can be multiplied to 180 cps. Obviously, the critical angle must not exceed 60°, to prevent simultaneous saturation of two reactors and a line-to-line short circuit.

If phase-changing transformers are included in the circuit to provide multiphase star outputs, any number of multiplications is possible. In practice, nine or eleven times appears to be a reasonable limit to any one stage. The output can of course be fed to another stage.

This principle, known for many years, was utilized for early radio transmitters. Limitations in core materials resulted in low power efficiencies and large sizes for these early attempts at multiplication. Recently, vast improvements have been made in the quality of rectangular-loop magnetic materials. Saturation flux densities of 14,000 to 16,000 gauss or more are possible; materials such as Deltamax are used. As a result, multipliers have been designed for computers, motor control, and aircraft equipment with

high degrees of multiplication. Square-loop hysteresis curves can be shown to produce considerable harmonics. This factor, together with the use of phase-changing transformers and several stages of multiplication, could result in frequencies of 1,000 cycles.

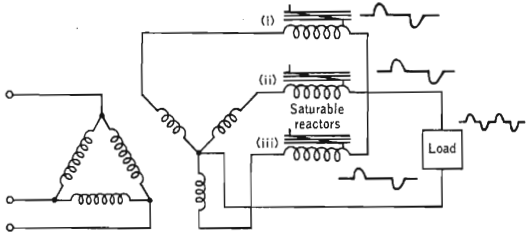

(*a*) Frequency tripler

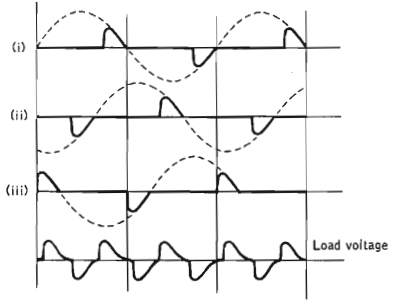

(*b*) Waveforms

FIG. 8-12. Principle of the magnetic multiplier.

At present, the size of a multiplier is greater than that of the equivalent motor-generator set, and the efficiency tends to be somewhat lower (50 to 90 per cent) (92). However, the inherent advantages of simplicity, low maintenance cost, ruggedness, and static operation appear to make the use of higher-powered multipliers very desirable for low-frequency induction through-heating. In addition, the saturable reactors can be controlled as to firing angle by a bias supply. This provides a good power control for the power output.

A two-stage multiplier is shown in Fig. 8-13, with power control available

by an adjustable bias at the second stage (93). This circuit is essentially a tripler followed by a doubler. The capacitor C is used to improve the power factor of the doubler stage. It is claimed that the regulation of this type of two-stage unit is improved over that of a single-stage sextupler.

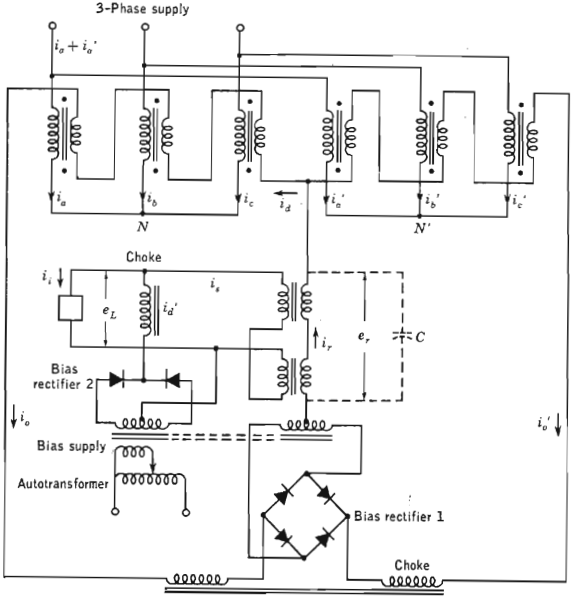

FIG. 8-13. Two-stage magnetic-frequency sextupler.

The efficiency of the doubler stage can be made very high. Values as high as 98 per cent have been quoted (94).

The other major disadvantage of the magnetic multiplier is its inherently low-input power factor. This requires considerable correction, as values for triplers may be as low as 30 per cent (93). Regulation tends to be high because of inherent leakage inductance and aftersaturation inductance, but this can be improved by tuning the load with a series capacitor.

Although the magnetic multiplier has several disadvantages, its potentialities for low-frequency induction heating are good. Provided the size can

be reduced and the efficiency and input power factor increased, it could offer serious competition to the motor generator at through-heating frequencies.

8-6. TRANSISTOR INVERTERS

With the recent introductions of high-power transistors, it is now possible to design switching circuits converting d-c to a-c power of the order of several thousand watts. The basic principle of the circuit is shown in Fig. 8-14. It was developed primarily as a source of d-c to a-c conversion (95).

A junction transistor can conveniently be considered as a relay or controlled switch. A typical set of collector voltage-current curves is shown in Fig. 8-14*b*. If the base is zero, or slightly positive, the collector current (in this case supplied by the battery) is practically zero. The transistor is therefore an open switch with a very small leakage current. This is the point 0. By suddenly changing the base voltage to a suitable negative value, the transistor is saturated and carries a large collector current I_c. The emitter-to-collector voltage is practically zero; the transistor is therefore a closed switch. This is the point *c*, and the current is the result of the battery voltage E_c across the load resistance R_L. In both instances the dissipation resulting from the collector current and voltage is below the maximum allowed. But the power switched is E_cI_c, many times the maximum dissipation, and the base current and voltage are very low. Commercial transistors are now available which are theoretically capable of switching almost 1 kw of power using 1 watt of base power.

Two of these power transistors are shown connected to a transformer with an idealized rectangular hysteresis loop, as in Fig. 8-14*c*. The inverter action can be explained by assuming that transistor *A* is conducting or closed and *B* is cut off or open. The battery is now across winding 2 of the transformer, with the polarity as shown. Voltages of the same polarity are induced in the other windings; this results in a negative base voltage at *A* and a positive base voltage at *B*. This maintains *A* conducting and *B* cutoff.

The battery voltage *E* across winding 2 produces an increase of flux in the core until the core saturates. This is represented by the path *a-b-c* in Fig. 8-14*c*. At saturation the current in winding 2 rapidly rises and the reactance drops, causing the voltages in the remaining windings to disappear. The negative base drive is removed from transistor *A*, so that it is nonconductive and acts as an open switch. The current of the winding is then zero, and the flux drops to *d* (Fig. 8-14*c*). The flux change from *c* to *d* induces voltages in the windings, opposite in polarity to the previous condition. This causes transistor *B* to conduct (switch closed) and transistor *A*

is maintained cutoff (switch open). Battery voltage E is now across winding 3, and the cycle repeats in the reverse direction. The output voltage E_o is obviously a square wave with a frequency and amplitude as functions of the turns and saturation flux of the transformers.

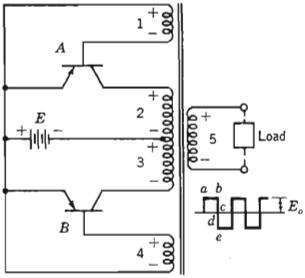

(a) D-c to a-c converter

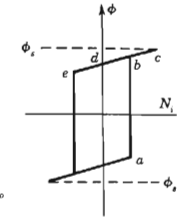

(c) Ideal rectangular loop

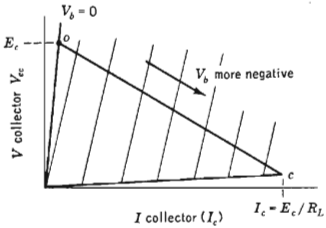

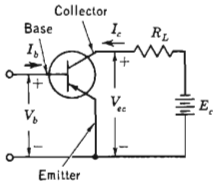

(b) Switching action of a transistor

FIG. 8-14. Transistor inverter.

The relationships are

$$f = \frac{E}{4N_2\phi_s} \quad \text{cps} \tag{8-12}$$

and

$$E_o \doteq \frac{N_5}{N_2} E \quad \text{volts} \tag{8-13}$$

where E = battery voltage, volts
N_2 = primary turns
N_5 = secondary turns
ϕ_s = saturation flux density

Frequencies as high as 12 kc have been reported (95), and it is possible that higher frequencies could be achieved with improved transistors. Power ratings can be increased by utilizing transistors in series, enabling a higher input voltage to be used. Even with transistors available at present, an inverter of several kilowatts at 10 kc and 300 to 500 volts is a practical possibility. Efficiencies of these inverters are very high (95 per cent), and the future potentialities of combining them with high-efficiency silicon diode d-c power supplies are very great. The weight and cost would be low, and the variable-frequency factor of transistor inverters gives them a great advantage over rotary equipment.

APPENDIX A

TABLES OF BER AND BEI, KER AND KEI FUNCTIONS

TABLES OF $X(x)$, $V(x)$, and $Z(x)$*

$X(x) = \text{ber}^2 x + \text{bei}^2 x$, $V(x) = \text{ber}'^2 x + \text{bei}'^2 x$,
and $Z(x) = \text{ber}\, x\, \text{ber}'\, x + \text{bei}\, x\, \text{bei}'\, x$

x	$X(x)$	$V(x)$	$Z(x)$	x	$X(x)$	$V(x)$	$Z(x)$
0	1.000	0.000	0.000	16	6.752×10^{7}	6.461×10^{7}	4.561×10^{7}
1	1.031	2.513×10^{-1}	6.266×10^{-2}	17	2.612×10^{8}	2.506×10^{8}	1.770×10^{8}
2	1.510	1.084	5.209×10^{-1}	18	1.014×10^{9}	9.752×10^{8}	6.887×10^{8}
3	3.803	3.240	2.054	19	3.950×10^{9}	3.806×10^{9}	2.688×10^{9}
4	1.183×10	1.007×10	6.909	20	1.543×10^{10}	1.489×10^{10}	1.052×10^{10}
5	3.883×10	3.375×10	2.345×10	21	6.041×10^{10}	5.842×10^{10}	4.127×10^{10}
6	1.323×10^{2}	1.177×10^{2}	8.215×10	22	2.371×10^{11}	2.296×10^{11}	1.622×10^{11}
7	4.643×10^{2}	4.203×10^{2}	2.943×10^{2}	23	9.326×10^{11}	9.044×10^{11}	6.390×10^{11}
8	1.636×10^{3}	1.526×10^{3}	1.072×10^{3}	24	3.675×10^{12}	3.568×10^{12}	2.521×10^{12}
9	6.077×10^{3}	5.621×10^{3}	3.953×10^{3}	25	1.451×10^{13}	1.410×10^{13}	9.966×10^{12}
10	2.245×10^{4}	2.093×10^{4}	1.474×10^{4}	26	5.736×10^{13}	5.582×10^{13}	3.945×10^{13}
11	8.383×10^{4}	7.863×10^{4}	5.541×10^{4}	27	2.271×10^{14}	2.213×10^{14}	1.564×10^{14}
12	3.167×10^{5}	2.977×10^{5}	2.099×10^{5}	28	9.007×10^{14}	8.783×10^{14}	6.207×10^{14}
13	1.197×10^{6}	1.134×10^{6}	7.999×10^{5}	29	3.576×10^{15}	3.490×10^{15}	2.467×10^{15}
14	4.568×10^{6}	4.344×10^{6}	3.065×10^{6}	30	1.422×10^{16}	1.389×10^{16}	9.799×10^{15}
15	1.752×10^{7}	1.672×10^{7}	1.180×10^{7}	∞	∞	∞	∞

* Data obtained from Reference 4.

TABLES OF BER x, BEI x, KER x, AND KEI x*

If $J_s(x)$ and $Y_s(x)$ are the Bessel's functions of the first and second kinds of zero order, we have

$$J_s(jx\sqrt{j}) = I_s(x\sqrt{j}) = \text{ber } x + j \text{ bei } x$$

and

$$Y_s(jx\sqrt{j}) = K_s(x\sqrt{j}) = \text{ker } x + j \text{ kei } x$$

x	ber x	bei x	ker x	kei x
0	1	0	∞	-0.7854
1	9.844×10^{-1}	2.496×10^{-1}	2.867×10^{-1}	-4.950×10^{-1}
2	7.517×10^{-1}	9.723×10^{-1}	-4.166×10^{-2}	-2.024×10^{-1}
3	-2.214×10^{-1}	1.938	-6.703×10^{-2}	-5.112×10^{-2}
4	-2.563	2.293	-3.618×10^{-2}	2.198×10^{-3}
5	-6.230	1.160×10^{-1}	-1.151×10^{-3}	1.119×10^{-3}
6	-8.858	-7.335	-6.531×10^{-4}	7.216×10^{-3}
7	-3.633	-2.124×10	1.922×10^{-3}	2.700×10^{-3}
8	2.097×10	-3.502×10	1.486×10^{-3}	3.696×10^{-4}
9	7.394×10	-2.471×10	6.372×10^{-4}	-3.192×10^{-4}
10	1.388×10^{2}	5.637×10	1.295×10^{-4}	-3.075×10^{-4}
11	1.330×10^{2}	2.572×10^{2}	-4.779×10^{-5}	-1.495×10^{-4}
12	-1.285×10^{2}	5.470×10^{2}	-6.308×10^{-5}	-3.899×10^{-5}
13	-8.827×10^{2}	6.466×10^{2}	-3.474×10^{-5}	5.387×10^{-6}
14	-2.131×10^{3}	-1.609×10^{2}	-1.088×10^{-5}	1.268×10^{-5}
15	-2.987×10^{3}	-2.953×10^{2}	-1.514×10^{-6}	7.963×10^{-6}
16	-6.595×10^{2}	-8.191×10^{2}	2.466×10^{-6}	2.895×10^{-6}
17	9.484×10^{2}	-1.309×10^{4}	1.797×10^{-6}	2.861×10^{-7}
18	3.096×10^{4}	-7.454×10^{3}	7.438×10^{-7}	-4.555×10^{-7}
19	5.625×10^{4}	2.804×10^{4}	1.293×10^{-7}	-3.982×10^{-7}
20	4.749×10^{4}	1.148×10^{5}	-7.715×10^{-8}	-1.859×10^{-7}
21	-7.616×10^{4}	2.337×10^{5}	-8.636×10^{-8}	-4.388×10^{-8}
22	-4.155×10^{5}	2.539×10^{5}	-4.535×10^{-8}	1.097×10^{-8}

* Data obtained from Reference 4.

APPENDIX B

CHARTS: INTEGRATED RESISTIVITY VS. TEMPERATURE; RESISTIVITY VS. TEMPERATURE; THERMAL POUNDS PER KILOWATTHOUR VS. TEMPERATURE

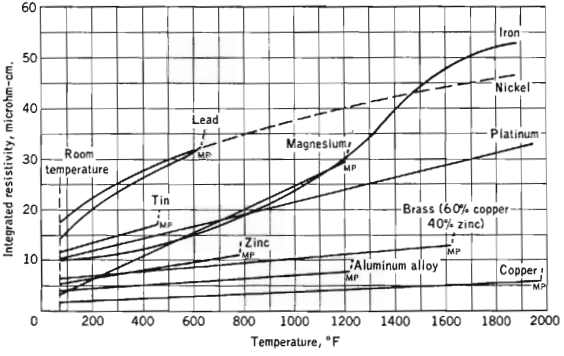

FIG. B-1.

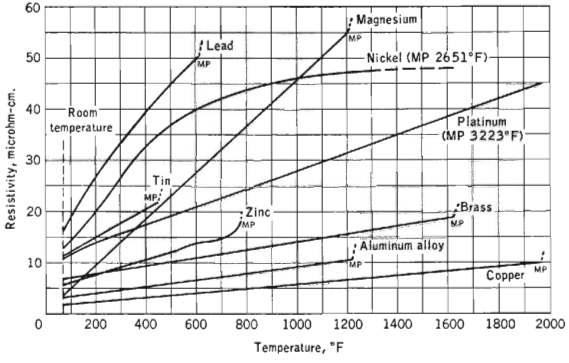
Resistivity, microhm-cm.
Temperature, °F
Room temperature
Magnesium
MP
Lead
MP
Nickel (MP 2651°F)
Platinum (MP 3223°F)
Tin
MP
Zinc
MP
Brass
MP
Aluminum alloy
MP
Copper
MP

FIG. B-2.

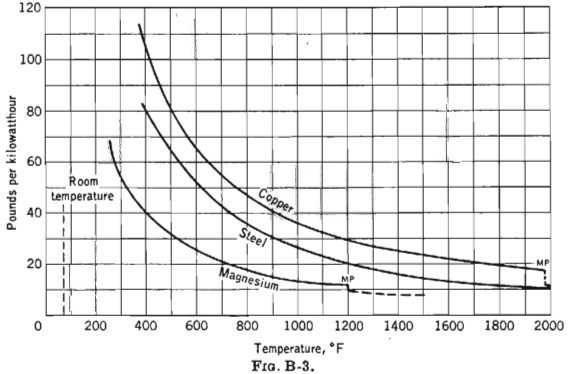
Pounds per kilowatthour
Temperature, °F
Room temperature
Copper
Steel
Magnesium
MP
MP

FIG. B-3.

APPENDIX C

CONVERSION TABLE; CONVERSION FACTORS

CONVERSION TABLE

To convert	Into	Multiply by	Conversely, multiply by
Watts	Joules/sec	1	1
Amp-turns	Gilberts	1.257	0.7958
Amp-turns/in.	Gilberts/cm	0.495	2.021
Btu	Joules	1050	9.48×10^{-4}
Centigrade	Fahrenheit	(°C × 9/5) + 32	(°F − 32) × 5/9
Cu in.	Cu cm	16.39	6.102×10^{-2}
Cu in.	Gal (water)	4.329×10^{-3}	231
Erg	Joule	10^{-7}	10^{7}
Gauss	Lines/sq in.	6.452	0.1550
Gm/cc	Lb/cu in.	0.03613	27.68
Gm	Lb	2.205×10^{-3}	453.6
In.	Cm	2.54	0.3937
Btu	Cal	252	3.968×10^{-3}
Liters	Cu cm	10^{3}	10^{-3}
Liters	Gal	0.26418	3.783
Sq in.	Cir mils	1.273×10^{6}	7.854×10^{-7}
Sq in.	Sq cm	6.452	0.155
Watts	Btu/min	0.05688	17.58
Watts	Cal/sec	0.2389	4.185
Watts	Ergs/sec	10^{7}	10^{-7}
Meters	Ft	3.281	0.3048
Kwhr	Btu	3413	2.93×10^{-4}
Cal sec^{-1} cm^{-1} $°C^{-1}$	Btu hr^{-1} ft^{-1} $°F^{-1}$	242	0.00413
Watts/sq in.	Cal sec^{-1} sq cm^{-1}	0.0371	26.9
U.S. gal	Lb	0.2	8.32
Cu ft	U.S. gal	7.5	0.133
Btu-ft sq ft^{-1} hr^{-1} $°F^{-1}$	Cal cm^{-1} sec^{-1} $°C^{-1}$	4.12×10^{-3}	243
Kwhr	Cal	8.1×10^{5}	1.235×10^{-6}
Gal/gm	Kwhr/lb	5.27×10^{-4}	1900

Conversion Factors

Thermal conductivity coefficient*

	Cal sec^{-1} cm^{-1} $°C^{-1}$	Watts cm^{-1} $°C^{-1}$	Watts $in.^{-1}$ $°C^{-1}$	Cal hr^{-1} cm^{-1} $°C^{-1}$	WE st^{-1} m^{-1} $°C^{-1}$	Btu hr^{-1} sq ft^{-1} $°F^{-1}$	Btu day^{-1} sq ft^{-1} $°F^{-1}$
1 cal sec^{-1} cm^{-1} $°C^{-1}$	1	4.183	10.62	3600.0	360	2903.0	69670.0
1 watt cm^{-1} $°C^{-1}$	2.39×10^{-1}	1	2.540	860.6	86.06	694.0	16655.0
1 watt $in.^{-1}$ $°C^{-1}$	9.413×10^{-2}	3.937×10^{-1}	1	338.7	33.87	273.2	6557.0
1 cal hr^{-1} cm^{-1} $°C^{-1}$	2.778×10^{-4}	1.162×10^{-3}	2.951×10^{-3}	1	0.1	0.8064	19.35
1 WE st^{-1} m^{-1} $°C^{-1}$	2.778×10^{-3}	1.162×10^{-2}	2.951×10^{-2}	10	1.0	8.064	193.5
1 Btu hr^{-1} sq ft^{-1} $°F^{-1}$	3.445×10^{-4}	1.441×10^{-3}	3.660×10^{-3}	1.240	1.240×10^{-1}	1	21.0
1 Btu day^{-1} sq ft^{-1} $°F^{-1}$	1.435×10^{-5}	6.004×10^{-5}	1.525×10^{-4}	5.167×10^{-2}	5.167×10^{-3}	4.167×10^{-2}	1.0

Surface heat-transfer coefficient*

	Cal sec^{-1} sq cm^{-1} $°C^{-1}$	Watts sq cm^{-1} $°C^{-1}$	Watts sq $in.^{-1}$ $°C^{-1}$	Cal hr^{-1} sq cm^{-1} $°C^{-1}$	WE st^{-1} sq m^{-1} $°C^{-1}$	Btu hr^{-1} sq ft^{-1} $°F^{-1}$	Btu day^{-1} sq ft^{-1} $°F^{-1}$
1 cal sec^{-1} sq cm^{-1} $°C^{-1}$	1	4.183	26.99	3600.0	36000	7373.0	176960.0
1 watt sq cm^{-1} $°C^{-1}$	2.391×10^{-1}	1	6.452	860.6	8606	1763.0	42304.0
1 watt sq $in.^{-1}$ $°C^{-1}$	3.706×10^{-2}	1.550×10^{-1}	1	133.4	1334	273.2	6557.0
1 cal hr^{-1} sq cm^{-1} $°C^{-1}$	2.778×10^{-4}	1.162×10^{-3}	7.497×10^{-3}	1	10	2.048	49.16
1 WE st^{-1} sq m^{-1} $°C^{-1}$	2.778×10^{-5}	1.162×10^{-4}	7.497×10^{-4}	1×10^{-1}	1	0.2048	4.916
1 Btu hr^{-1} sq ft^{-1} $°F^{-1}$	1.356×10^{-4}	5.673×10^{-4}	3.660×10^{-3}	4.882×10^{-1}	4.882	1	24.0
1 Btu day^{-1} sq ft^{-1} $°F^{-1}$	5.651×10^{-6}	2.364×10^{-5}	1.525×10^{-4}	2.034×10^{-2}	2.034×10^{-1}	4.167×10^{-2}	1

* These tables are modifications of U.S. Bureau of Standards tables.

CONVERSION FACTORS

Length	Area	Volume
1 cm = 3.937×10^{-1} in.	1 sq cm = 1.550×10^{-1} sq in.	1 l = 2.642×10^{-1} gal
1 m = 3.281 ft	1 sq m = 10.764 sq ft	1 cu cm = 6.102×10^{-2} cu in.
1 in. = 2.540 cm	1 sq in. = 6.452 sq cm	1 cu m = 35.314 cu ft
1 ft = 3.048×10^{-1} m	1 sq ft = 9.290×10^{-2} sq m	1 gal = 3.785 l
		1 cu in. = 16.387 cu cm
		1 cu ft = 2.832×10^{-2} cu m

Mass and density

1 gm = 3.527×10^{-2} oz (avdp)		1 oz (avdp) = 28.350	gm
1 kg = 2.205	lb (avdp)	1 lb (avdp) = 4.536	kg
Standard gravity = 32.174	ft per sq sec	Standard gravity = 980.665	cm per sq sec
Density Hg = 4.911×10^{-1}	lb per sq in.	Density H_g = 13.595	gm per cu cm (at 0°C)
1 gm per cu cm = 62.428	lb per cu ft	1 lb per cu ft = 1.602×10^{-2}	gm per cu cm

Conversion Factors

Pressure

Units	Atm	Kg per sq cm	Lb per sq in.	M Hg 0°C*	Megabar	In. Hg 0°C*
1 atm	1	1.033†	14.696	7.600×10^{-1}†	1.013	29.921†
1 kg per sq cm	9.678×10^{-1}	1	14.223	7.355×10^{-1}	9.807×10^{-1}†	28.959
1 lb per sq in.	6.804×10^{-2}	7.031×10^{-2}	1	5.171×10^{-2}	6.895×10^{-2}	2.036
1 m Hg 0°C*	1.316	1.360†	19.337	1	1.333	39.37†
1 megabar	9.869×10^{-1}	1.020	14.504	7.501×10^{-1}	1	29.530
1 in. Hg 0°C*	3.342×10^{-2}	3.453×10^{-2}	4.911×10^{-1}	2.540×10^{-2}	3.386×10^{-2}	1

* Based on density Hg = 13.5951 gm per cu cm. † Exact by definition.

Power

	Ft-lb per min	Watts*	Cal per sec	Btu per min	Horsepower
1 ft-lb per min	1	2.260×10^{-2}	5.402×10^{-3}	1.286×10^{-3}	3.030×10^{-5}
1 watt	44.254	1	2.391×10^{-1}	5.692×10^{-2}	1.341×10^{-3}
1 cal per sec	185.113	4.183†	1	2.381×10^{-1}	5.609×10^{-3}
1 Btu per min	777.461	17.568	4.200	1	2.356×10^{-2}
1 horsepower	33,000†	745.701	178.269	42.446	1

* Absolute units. † Exact value by definition.

Conversion Factors

Velocity*

	Cm sec^{-1}	Km hr^{-1}	Ft sec^{-1}	Ft min^{-1}	Mile hr^{-1}	Yd sec^{-1}
1 cm sec^{-1}	1	3.6×10^{-2}	3.281×10^{-2}	1.968	2.237×10^{-2}	1.094×10^{-2}
1 km hr^{-1}	27.778	1	9.113×10^{-1}	54.680	6.214×10^{-1}	3.038×10^{-1}
1 ft sec^{-1}	30.480	1.097	1	60	6.818×10^{-1}	3.333×10^{-1}
1 ft min^{-1}	5.080×10^{-1}	1.829×10^{-2}	1.667×10^{-2}	1	1.136×10^{-2}	5.555×10^{-3}
1 mile hr^{-1}	44.704	1.609	1.467	88	1	4.889×10^{-1}
1 yd sec^{-1}	91.440	3.292	3	180	2.045	1

* This table is a modification of U.S. Bureau of Standards tables.

Heat flow

	Cal sec^{-1} sq cm^{-1}	Watt sq cm^{-1}	Cal hr^{-1} sq cm^{-1}	WE st^{-1} sq m^{-1}	Btu hr^{-1} sq ft^{-1}	Btu day^{-1} sq ft^{-1}
1 cal sec^{-1} sq cm^{-1}	1	4.183	3600	36000	13272	318530
1 Watt sq cm^{-1}	2.391×10^{-1}	1	8.606	8606	3173	76147
1 cal hr^{-1} sq cm^{-1}	2.778×10^{-4}	1.162×10^{-3}	1	10	3.687	88.48
1 WE st^{-1} sq m^{-1}	2.778×10^{-5}	1.162×10^{-4}	1.0×10^{-1}	1	3.687×10^{-1}	8.848
1 Btu hr^{-1} sq ft^{-1}	7.534×10^{-5}	3.152×10^{-4}	2.712×10^{-1}	2.712	1	24
1 Btu day^{-1} sq ft^{-1}	3.139×10^{-6}	1.313×10^{-5}	1.130×10^{-2}	1.130×10^{-1}	4.167×10^{-2}	1

Conversion Factors

Energy

	Joule*	Gm-cal$_{20°}$	L-atm	Kg-m	Watt-hr*	Btu (68°)	Ft-lb	Hp-hr	Ton ref
Joule	1	2.391×10^{-1}	9.869×10^{-3}	1.020×10^{-1}	2.778×10^{-4}	9.488×10^{-4}	7.376×10^{-1}	3.725×10^{-7}	3.294×10^{-9}
Gm-cal$_{20°}$	4.183†	1	4.128×10^{-2}	4.265×10^{-1}	1.162×10^{-3}	3.968×10^{-3}	3.085	1.558×10^{-6}	1.378×10^{-8}
L-atm	101.325	24.223	1	10.332	2.814×10^{-2}	9.612×10^{-2}	74.733	3.774×10^{-5}	3.338×10^{-7}
Kg-m	9.806†	2.344	9.678×10^{-2}	1	2.724×10^{-3}	9.303×10^{-3}	7.233	3.653×10^{-6}	3.230×10^{-8}
Watt-hr*	3600†	860.626	35.529	367.098	1	3.415	2655.218	1.341×10^{-3}	1.186×10^{-5}
Btu (68°)	1054.098	251.996	10.403	107.488	2.928×10^{-1}	1	777.461	3.926×10^{-4}	3.472×10^{-6}
Ft-lb	1.356	3.241×10^{-1}	1.338×10^{-2}	1.382×10^{-1}	3.766×10^{-4}	1.286×10^{-3}	1	5.050×10^{-7}	4.466×10^{-9}
Hp-hr	2.684×10^{6}	641770	26494	273745	745.701	2547	1.98×10^{6}	1	8.843×10^{-3}
Ton ref	3.036×10^{8}	7.257×10^{7}	2.996×10^{6}	3.095×10^{7}	84328	288000†	2.239×10^{8}	113.085	1

* Based on the relation 1 gm-cal$_{20°}$ = 4.183 joules (abs) ± absolute unit. 1 International Joule = 1.00034 abs joule. † Exact by definition.

APPENDIX D

ZONE REFINING BY R-F HEATING

The basic purpose of zone refining is to remove impurities in a material by passing a molten zone from one end of a suitably shaped charge to the other. A very high degree of purity is achieved by successive passages; it is also possible to add an accurately controlled amount of impurity by a method of refining known as zone leveling or levitation (99).

Zone refining is based on the principle that the concentration of impurities at the interface between the molten and just-frozen material depends on the effect of the impurities on the melting point of the pure material. If the impurities lower the melting point of the pure material, their concentration in the molten zone is increased. If the melting point of the pure material is raised, the concentration of impurities in the molten zone is lower. Therefore the molten zone, which is caused to travel along the rod of material, can build up impurities, which are then left at one end. The degree of refining and purification is a function of the number of passages made along the rod by the molten zone, but it has a practical limit. Figures of 1 part per billion of electrically active impurities in silicon have been quoted (96).

Most applications of zone refining to date appear to be in the semiconductor field. Germanium is usually refined as indicated in Chap. 5, with the powder or crystal drawn in boats through a series of induction heating coils (Fig. 5-19a). Silicon cannot be treated so easily in this way as it is highly reactive with most boat materials.

The floating-zone method is preferable, as it involves no boats but uses the surface tension of the molten zone to hold it in place in a vertical rod (Fig. 5-19b). Rods of up to 1 in. or more can be refined, by the use of the principle of levitation. This levitational force results from the action between the induced and the induction currents. The number of passes required for silicon is higher than that needed for germanium, as the distribution of impurities is less favorable.

The basic requirements for floating-zone refining are an r-f heater, an accurate mechanical variable-speed vertical drive for the rod, an automatic recycling mechanism, and possibly a means of temperature control. In general, the r-f power output is time-controlled via a variable plate voltage by a programmed sequence. It has sometimes been necessary to preheat the rod by resistance heating in order to lower its resistivity sufficiently so that the r-f power can be loaded into the material. If a frequency of 3 to 5 Mc is selected instead of the conventional 450 kc, the loading problem is easier and the preheating can often be eliminated. The higher frequencies also result in a reduction of mechanical oscillation in the zone, caused by the generator-power supply ripple (usually 360 cps, 6 to 10 per cent) modulating the radio frequency (96). In general, most levitation processes involve the use of a controlled atmosphere or a vacuum, so that the rod is surrounded by a tube to contain the necessary gas or vacuum. This results in a loosely coupled high Q coil, requiring fairly high r-f current and voltage. The higher-frequency range is more suitable for this type of coil.

It is extremely important to maintain the length of the zone and therefore the power input constant during zone refining. Variations in the power supply to the oscillator are usually controlled by stabilizing circuits. Variations in the tank-circuit transfer efficiency, and therefore in output power, can result from loaded work-coil impedance changes. In Fig. 5-15, these changes are shown as functions of work-coil inductance L_o and of coil $Q(Q_o)$. Although most zone-refining tank circuits are of the split tank-coil type, as in Fig. 5-3*b*, the power output curves are similar in shape to those in Fig. 5-15. The peak power is at the point where the total tank impedance z_T is the same as the tube plate impedance z_a.

If the zone length increases, the total loaded work-coil resistance and impedance z_o decreases, decreasing the total tank impedance z_T, and therefore the output power. This in turn reduces the amount of melting and decreases the zone length, increasing the work-coil and tank-coil impedance and bringing back the operating point on the power curve to the original point. The opposite occurs for a decrease in zone length. The whole system is self-stabilizing, and an optimum sensitivity should be achieved, theoretically, if the work coil were the complete tank coil. In practice, the zone length is very difficult to control because of the large inductance required, and a compromise is achieved by using coils of approximately ¼ to ½ microhenry inductance.

The maximum zone length that can be supported by its own tension is a function of the ratio of the surface tension of the material to its density (98) when it is molten. Silicon and aluminum (also iron and titanium) are highly suitable to the process, because of the combination of their properties.

In general, power efficiencies of the tank circuit used are very low (20 per cent or less). Although a few hundred watts are sufficient for the molten zone, generator-power ratings of 5 to 10 kw are usually required (98).

REFERENCES

1. Warren, A. G.: "Mathematics Applied to Electrical Engineering," Chapman & Hall, Ltd., London, 1949.
2. Dwight, H. B.: A Precise Method of Calculation of Skin Effect in Isolated Tubes, *Trans. AIEE*, vol. 42, no. 8, p. 829, 1923.
3. Jahnke, E., and F. Emde: "Tables of Functions with Formulae and Curves," p. 131, Stechert-Hafner, Inc., New York, 1948.
4. Savidge, H. G.: Tables of Ber and Bei, Ker and Kei Functions with Further Formulae for Their Computation, *Phil. Mag.*, vol. 19, pp. 49–58, 1910.
5. Brown, H. G., C. N. Hoyler, and R. A. Bierwirth: "Radio Frequency Heating," D. Van Nostrand Company, Inc., Princeton, N.J., 1947.

5a. Baker, R. M.: Design and Calculation of Induction Heating Coils, AIEE paper 57-4, Oct. 18, 1956; paper 29, March, 1957.

6. Clamer, G. H.: The Development of the Coreless Induction Furnace, *Metals & Alloys*, vol. 6, p. 119, 1935.
7. Losinsky, M.: The Continuous Progressive Surface Hardening of Steel Using High-frequency Current, *Vestnik Metalloprom.*, no. 3, pp. 50–60, 1940.
8. Babat, G., and M. Losinsky: Heat Treatment of Steel by High Frequency Currents, *JIEE*, vol. 86, p. 161, 1940.
9. Vologdin, V. P.: Hardening the Ends of Rails by High-frequency Current, *Stahl u. Eisen*, nos. 8 and 9, p. 47, 1938.
10. Vologdin, V. P.: Induction Heating of Surfaces, *Vestnik Metalloprom.*, no. 3, p. 37, 1940.
11. Seulen, G., and H. Voss: Surface Hardening Induction Heating at Medium Frequencies, *Iron and Steel*, October, 1945, vol. 18, no. 11, p. 445.
12. Brown, R. J.: *Sheet Metal Inds.*, March, 1947.
13. Riegal, G. C.: Case Hardening of Large Gears with High Frequency Current, *Metal Progr.*, vol. 44, p. 78, 1943.
14. Curtis, F. W.: "High-frequency Induction Heating," 2d ed., pp. 226–246, McGraw-Hill Book Company, Inc., New York, 1950.
15. Knowlton, H. B.: Induction Hardening of Gears, *SAE Journal*, vol. 58, pp. 54–58, 1950.
16. Induction and Dielectric Heating—A Survey of Industrial Applications, *Electrified Industry*, June, 1956.
17. Brown, D. W.: High Frequency Heating, *Machinist*, vol. 96, pp. 1369–1376, 1952.
18. Buhler, H.: Induction Surface Hardening, *Werkstatt u. Betrieb*, vol. 83, p. 26, 1950.

19. Kegel, K.: Surface Treatment of Steel by Means of H.F. Heating, *Electrotechnik (Berlin)*, vol. 2, pp. 285–291, 1948.
20. Logan, J. A.: 60-cycle Induction for Forging and Extrusion, *Ind. Heating*, pp. 282–294, 423–446, 1955.
21. Hrovath, J. W.: 60-cycle Induction Heating of Aluminum, AIEE Conference paper, pp. 18–22, 1954.
22. Bernhardt, C. P.: Dual Frequency Heating for Hot Forging, *Metal Progr.*, December, 1954.
23. Induction Heating, *Iron Age*, pp. 115–128, Nov. 10, 1955.
24. Hartwig, C. H.: Sixty Cycle Induction Heating of Large Steel Sections, paper presented at ASME Semi-annual Meeting, June 21, 1954. Also *Ind. Heating*, September and December, 1954, and January, May, and June, 1955.
25. Walter, R. C.: Induction Heating for Forging of Transmission Gears, paper presented at AIEE Conference, Cleveland, Ohio, Feb. 19, 1952.
26. Miller, J. L.: "Modern Assembly Processes," Chapman & Hall, Ltd., London, 1946.
27. Taylor, J. P.: High Speed Soldering with R.F. Power, *Electronics*, February, 1944.
28. Benninghoff, W. E.: Look at Induction Heating, *Steel Processing*, pp. 133–136, March, 1949.
29. Kuchli, G.: Soldering, Annealing, Melting and Sintering with Radio Frequency Heating Equipment, *Brown Boveri Rev.*, vol. 38, pp. 339–43, 1951.
30. Baker, R. M.: Manufacture of Seam-welded Tubes by Low Frequency Induction, U.S. Patent No. 2,647,982.
31. Blakeslie, D. W.: Method of Electric Welding, U.S. Patent No. 1,915,047.
32. Sessions: Apparatus for Electric Welding, U.S. Patent No. 2,086,305.
33. Landsman H. J., and A. F. Lattauzeo: High Powered Induction Heating in Shell Forging, *Steel Processing*, pp. 453–456, July, 1955.
34. Low Frequency Induction Heating of Small Parts at Mullins Plant, *Ind. Heating*, pp. 1782, 1784, and 1924, September, 1955.
35. Which Frequency Do You Choose? *Steel*, pp. 126–130, May 2, 1955.
36. McArthur, B. E.: Sixty Cycle Heating of Ferrous Metals, AIEE Publication 5–74, April, 1955.
37. Kugler, A. N.: Brazed Joints, *Machine Design*, pp. 116–121, Feb. 23, 1956.
38. "Procedure Handbook of Arc Welding Design and Practice," Lincoln Electric Company, Cleveland, 1942.
39. Warburton-Brown, D.: "Induction Heating Practice," Odhams Press Ltd,, London, 1956.
40. Warburton-Brown, D.: Brazing by Induction, *Welding and Metal Fabrication*, July-August, 1953.
41. Baffrey, A. R.: Welding Tubes by Induction, Report on IIId Congress Internationale d'Electrothermie, sec. 2, no. 202, Paris, 1953.
42. Williamson, J. W.: Apparatus for Electric Welding, U.S. Patent No. 2,678,368, 1951.
43. Osborn, H. B.: Induction Heat Treating, *Metal Progr.*, pp. 125–128, November, 1954.
44. Chesnut, F. T.: Melting by Induction, *Ind. Heating*, pp. 1377–1382, July, 1956.
45. Vacuum Melting Catches On, *Steel*, p. 32, December, 1956.

46. Constant Vacuum Unit Tightens Melting Schedules, *Iron Age*, pp. 98–100, September, 1956.
47. Induction Stirrers Upgrade Cast Steel, *Steel*, pp. 132–133, September, 1956.
48. Pieri, C. DI.: Special Developments in the Field of Low Frequency Smelting Ovens, *Ruin. Ass. Elettrotec.* (Italy), RC. 52, 1951. (In Italian.)
49. Induction Hardening of Axle Housing Increases Fatigue Life, *Ind. Heating*, pp. 2468–2470, December, 1955.
50. Paul, M. E.: Surface Hardening by Induction and Improvement of the Fatigue Resistance of Steel by Repeated Stresses, IIId Congress Internationale d'Electrothermie, sec. 2, no. 210, Paris, 1953.
51. Baker, R. M.: Transverse Flux Induction Heating of Continuous Heat Treatment of Non-ferrous Strip, paper presented to AIEE Heating Conference, May, 1953.
52. Baker, R. M.: Transverse Flux Induction Heating, AIEE paper, April, 1950.
53. Baker, R. M.: Induction Heating of Moving Magnetic Strip, AIEE paper, December, 1944.
54. Hatchard, D. G., P. G. Simpson, and L. B. Kimbrough: New 60-cycle Aluminium Billet Heater for Continuous Extrusion Process, *Ind. Heating*, pp. 295–302, February, 1957.
55. Hopkinson, J.: *Phil. Trans., A.*, vol. 180, no. 1, p. 443, 1889.
56. Curie, P.: *Compt. rend.*, vol. 118, pp. 726, 859, 1134.
57. Koebel, N. K.: Fundamentals of Metallurgy Involved in the Heating of Metals, Both Ferrous and Non-ferrous, paper presented at AIEE Electrical Heating Conference, Chicago, May, 1955.
58. Longevin, P.: *Compt. rend.*, vol. 140, p. 1171, 1905.
59. Ewing, J. A.: "Magnetic Induction in Iron and Other Metals," The Electrician Printing and Publishing Co., Ltd., London, 1900.
60. Stansel, N. R.: "Induction Heating," McGraw-Hill, New York, 1949.
61. Kaye, G. W. C., and T. H. Laby: "Physical and Chemical Constants," 11th ed., Longmans, Green & Co., Inc., New York, 1956.
62. Carslaw, H. S., and J. C. Jaeger: "Conduction of Heat in Solids," Oxford University Press, New York, 1947.
63. Baker, R. M.: Classical Heat Flow Problems Applied to Induction Billet Heating, *Trans. AIEE*, vol. 77, pp. 106–112, 1958.
64. Eilender, W., and L. Mintrop: Influence of Rate on Heating Steel on the Pearlite-Austenite Transformation, with Special Reference to Surface Hardening, *Stahl u. Eisen*, vol. 68, p. 83, 1948.
65. "Metals Handbook, 1955 Supplement," pp. 107–123, ASM.
66. May, E.: "Industrial High Frequency Electric Power," Chapman & Hall, Ltd., London, 1949.
67. Sauveur, Albert: "The Metallography and Heat Treatment of Iron and Steel," 4th ed., McGraw-Hill Book Company, Inc., New York, 1935.
68. Davenport, E. S., and E. C. Bain: Transformation of Austenite at Constant Sub-critical Temperature, *Trans. AIME*, vol. 90, p. 117, 1930.
69. Brooker, H. R., and E. V. Beatson: "Industrial Brazing," Iliffe & Sons, Ltd., London, 1953.
70. Templin, A. T., and H. S. Peterson: Induction Brazing, *Machine Design*, Mar. 21, 1957.
71. Baker, R. M.: Scale Model Testing as Applied to Induction Heating, AIEE paper, May, 1955.

72. Langton, L. L.: "Radio-frequency Heating Equipment," Sir Isaac Pitman & Sons, Ltd., London, 1949.
73. Roberds, Wesley M.: Problems in the Design of High-frequency Heating Equipment, *Proc. IRE* (*Inst. Radio Engrs.*), pp. 489–500, July, 1946.
74. Cotton, H.: "Electrical Technology," p. 305, Sir Isaac Pitman & Sons, Ltd., London, 1950.
75. Terman, F. E.: "Radio Engineers' Handbook," McGraw-Hill Book Company, Inc., New York, 1943.
76. "Reference Data for Radio Engineers," 4th ed., International Telephone and Telegraph Corp., New York, 1956.
77. Domhoefer, Warren J., and V. H. Krummenacher: Applying Magnetic Amplifiers, *Elec. Mfg.*, August, 1950, to September, 1951.
78. Mohr, G. R., and Ruben Lee: Magnetic Amplifier Control of Radio-frequency Generators, AIEE paper 54-377, Aug. 16, 1954.
79. Johnson, W. C.: The Magnetic Amplifier, *Trans. AIEE*, July, 1953.
80. Lamm, A. Uno: Some Fundamentals of the Transductor or Magnetic Amplifier, *Trans. AIEE*, vol. 66, pp. 1078–85, 1947.
81. Nylander, G. A.: The Applications of Induction Heating to the Manufacture of Semi-conductors, paper presented at AIEE Conference of Electric Heating, Toledo, Ohio, Apr. 23–24, 1957.
82. Pfann, W. G.: Principles of Zone Melting, *J. Metals*, vol. 194, p. 147, 1952.
83. Owen, David: "Alternating Current Measurements," Methuen & Co., Ltd., London, 1950.
84. Federal Communications Commission's Rules and Regulations, Relating to Industrial, Scientific and Medical Services, part 18, secs. 18.21 and 18.24, U.S. Government Printing Office, 1947.
85. Klingman, G. W.: Reduction of Interference from R.F. Heating Equipment, *Trans. AIEE*, vol. 68, part I, pp. 718–724, 1949.
86. Jackson, Willis: "High Frequency Transmission Lines," Methuen & Co., Ltd., London, 1947.
87. Sabol, J. T.: Characteristics of Single Conductor Electric Cable at High Frequency, AIEE paper 55-679, July 17, 1955.
88. McLachlan, N. W.: "Bessel Functions for Engineers," Oxford University Press, New York, 1934.
89. Williamson, J. W.: Bus Bar Design for High Frequency Induction Heating, AIEE paper 52-68, Dec. 14, 1951.
90. Durard, S. R., and J. B. Rice: Mercury Arc Furnace Converter for Induction Heating of Metals, AIEE technical paper 48-287, September, 1948.
91. Smart, D. L., and J. J. L. Weaver: The Use of Steel Tank Mercury Arc Inverters for Generating Medium Frequencies for Induction Heating, *Proc. IEE* (*London*), vol. 105, part A, 1958.
92. Johnson, L. J., and S. E. Rauch: Magnetic Frequency Multipliers, *Trans. AIEE*, paper 54-248, May, 1954.
93. McMurray, W.: Magnetic Frequency Multipliers and Their Ratings, parts 1 and 2, *Trans. AIEE*, papers 56-229 and 57-91, 1956.
94. Beringer, C. P.: Design of the Resistively Loaded Static Frequency Doubler, *Trans. AIEE*, paper 56-88, November, 1955.
95. Bright, R. Louis, G. Frank Pittman, and G. H. Royer: Transistors as On-Off Switches in Saturable Core Circuits, *Elec. Mfg.*, December, 1954.

96. Pfann, W. G.: "Zone Melting," John Wiley & Sons, Inc., New York, 1958.
97. Buehler, E.: Contribution to the Floating Zone Refining of Silicon, *Rev. Sci. Instr.*, vol. 28, no. 6, June, 1957.
98. Bardsley, W.: The Floating Zone Process, *Research*, April, 1959.
99. Harris, B., and A. E. Jenkins: Controlled Atmosphere Levitation System, *J. Sci. Instr.*, vol. 30, May, 1959.

INDEX